5-3-2019 10:00 AM

Fabrication and Characterization of Collagen-Polypyrrole Constructs Using Direct-Ink Write Additive Manufacturing

Rooshan Arshad
The University of Western Ontario

Supervisor
Aaron David Price
The University of Western Ontario

Graduate Program in Biomedical Engineering
A thesis submitted in partial fulfillment of the requirements for the degree in Master of Engineering Science

Abstract

Current efforts in the tissue engineering field are being directed towards the creation of platforms which will facilitate in instructing cells towards biologically relevant outcomes such as stem cell differentiation and disease pathophysiology. Traditional fabrication methods serve as a limiting factor for the production of such platforms as they lack feature and geometric complexity. Additive Manufacturing (AM) offers advantage over said methods by affording designers creative freedom and great control over printed constructs. Such constructs can then be used to create appropriate models for studying a plethora of tissues and structures. An AM methodology for Direct-Ink Write (DIW) printing of conjugated polymer-based constructs using collagen-polypyrrole (Col-PPy) is presented. Potential for Col-PPy constructs as electro-conductive and electro-active platforms is evaluated through electrical conductivity and ionic conductivity characterization, and demonstrated through bilayer performance and spectrometry evaluations. Finally, degree of polymerization and topography are reported using optical and SEM imaging.

Keywords: Tissue engineering, 3D printing, Conjugated Polymers, Polypyrrole, Collagen

Summary for Lay Audience

The cellular micro-environment is known to be complex, three-dimensional and intricate in its ability to instruct cells through an interplay of electrical, chemical, biochemical and/or mechanical stimulation. Each cell type of interest to tissue engineers is known to be housed in its tissue-specific niche, with unique composition and consequent properties. Although researchers have successfully devised many platforms and mechanisms to achieve said stimulations in isolation or in *in vitro* settings, they remain challenged to reproduce these complexities in 3D cell culture settings, for extended periods of time and in a combinatory manner.

Conjugated polymer (CP) materials, such as Polypyrrole (PPy), are a branch of smart materials that are capable of emulating said unique properties of native cell micro-environments whilst retaining the tailorability of these properties familiar to tissue engineering researchers. However, to date, no platform reminiscent of the native cellular micro-environment capable of imparting combined electrochemomechanical stimulation to instruct cells towards biologically relevant outcomes has been developed. This has been largely because traditional fabrication methods for CPs serve as a limiting factor for the production of such platforms, where produced structures lack feature and geometric complexity inherent to native cell micro-environments.

Additive Manufacturing (AM) offers advantage over said methods by affording designers creative freedom and great control over printed constructs, which can then be used to create appropriate models for studying a plethora of tissues and structures. Presented in this thesis is a novel AM methodology for creating CP-based constructs. Specifically, a Direct-Ink Write (DIW) printing methodology for creating collagen-polypyrrole (Col-PPy) constructs is presented. This dissertation explores the design-ability inherent to AM processes and retention of favourable properties inherent to CP-based structures. Investigations to this end demonstrate 3D printed Col-PPy constructs to be electro-

conductive, electro-active and cyto-compatible, while the degree of response from these constructs is open to modulation. Essentially, researchers armed with such a platform are now capable of modulating the morphology and geometry, electro-conductive and electro-active properties of their 3D printed constructs in 3D cell culture settings, for extended periods of time and in a combinatory manner.

It is strange that only extraordinary men make the discoveries, which later appear so easy and simple.

– G. C. Lichtenberg

Professor of Physics

University of Göttingen, 1769–99

Dedication

Dedicated to everyone.

Acknowledgements

Financial support for my studies was generously provided by the Natural Sciences and Engineering Research Council of Canada (NSERC) and the University of Western Ontario.

Thanks to the members of my Examination Committee. Thanks to the members of my Advisory Committee, to Prof. Cheryle Séguin for providing access to her lab facilities, her insightful and measured guidance throughout the duration of the project, to Prof. Kibret Mequanint for providing astute critique and equipoise to ambitions I set at the inception of this project. Thanks to Courtney Brooks for her time and effort in providing assistance with my cyto-compatibility evaluations of the hybrid polypyrrole constructs. Thanks to Dr. Taylor Martino for facilitating my explorations on the electro-active properties of the hybrid polypyrrole constructs. Thanks to Karen Nygard and Ivan Barker for their SEM and confocal microscopy imaging support.

Special thanks to my thesis supervisor Prof. Aaron Price for giving me the opportunity to become a part of his research family, for his continued support and commitment to my project and my professional development. Thank you to my past and present learned colleagues in the Organic Mechatronics and Smart Materials Laboratory, my dearest friends, and my family, for their advice, support, and ready ear. I owe gratitude to all those who directly or indirectly influenced my pursuits and learnings as a Masters graduate student at University of Western Ontario. I remain forever grateful.

Contents

List of Tables

List of Figures

List of Acronyms and Symbols

Acronyms

β-TCP	β-tricalcium phosphate
2D	2-dimensional
3D	3-dimensional
ABS	Acrylonitrile butadiene styrene
AC	Alternating current
AFM	Atomic force microscopy
AM	Additive manufacturing
AQSA	9,10-anthraquinone-2-sulfonic acid
ASTM	American Section of the International Association for Testing Materials
ATP	Adenosine triphosphate
CAD	computer-aided design
CE	Counter electrode
CLSM	Confocal laser scanning microscopy
CNF	Carbon nanofibers
CNT	Carbon nanotubes
Col-PPy	Collagen-Polypyrrole
Col-Py	Collagen-Pyrrole
CP	Conjugated polymer
CS	Chondroitin sulfate

CT	Computed tomography (X-ray)
CV	Cyclic voltammetry
DBSA	dodecylbenzenesulfonic acid
DBS	dodecylbenzenesulphonate
DC	Direct current
dECM	decellularized extracellular matrix
DIW	Direct-ink write
DMA	Dynamic mechanical analysis
DMEM	Dulbecco's modified Eagle's medium
DMF	Dimethyl formamide
DMSO	Dimethyl sulfoxide
EAP	Electro-active polymer
ECM	Extracellular matrix
EDAX	Energy Dispersive Analysis X-Ray
EtOH	Ethanol
GAG	Glycosaminoglycan
GO	Graphite oxide
HA	Hyaluronic acid
HEMA	2-Hydroxy-ethylmethacrylate
LED	Light-emitting diode
MB	Methylene blue
PEG	Polyethylene glycol
MSC	Mesenchymal stem cells
MTGase	Microbial transglutaminase
NGF	Nerve growth factor
NMP	N-Methyl-2-pyrrolidone
NT-3	neurotrophin-3

PAni	Polyaniline
PBP	poly(2,2-bithiophene)
PBS	Phosphate buffer saline
PCL	poly-(ϵ-caprolactone)
PDMS	Polydimethylsiloxane
PEDOT:PSS	Poly(3,4-ethylenedioxythiophene):polystyrene sulfonate
PGA	Polyglycolic acid
PLA	Polylactic acid
PLGA	Poly(lactic-coglycolic) acid
PLLA	Poly-L-lactic acid
PPy	Polypyrrole
PVA	Polyvinyl alcohol
Py	Pyrrole
RE	Reference electrode
rGO	Reduced graphite oxide
SEM	Scanning electron microscopy
SLA	Stereolithography
SLS	Selective laser sintering
STL	Stereolithography file format
TFSI	Bis(trifluoromethane)sulfonimide
UTS	Ultimate tensile strength
UV	Ultraviolet
WE	Working electrode

Greek symbols

ε	mechanical strain
ε_x	Molecular extinction coefficient
η	apparent viscosity

η_0	consistency constant
$\dot{\gamma}$	shear rate
ρ	resistivity
σ_c	conductivity
σ	mechanical stress

Latin symbols

C_f	correction factor
D	nozzle diameter
d	extruded track width
ΔP	gauge pressure
E	Young's modulus
L	nozzle length
l	strain sensor length
n	power law index
R	electrical resistance
r^2	coefficient of determination
v	end effector travel speed

Chapter 1

Introduction

3D printing, also known as additive manufacturing (AM), enables designers the ability to manipulate computer aided designs (CAD) and produce structures with various geometric and feature complexities, namely: internal and bulk morphology at the macroscopic to microscopic level. AM enables designers with the ability to produce said structures quickly, efficiently and with a high degree of uniformity (Atala et al., 2012; Kang et al., 2016). Past researchers have been successful in 3D printing scaffolds of pure inks or composites of alginate, collagen, chitosan, extracellular matrix proteins, etc. for tissue engineering and biomedical applications (Johnson et al., 2015; Pati et al., 2015; Jose et al., 2016; Donderwinkel et al., 2017). AM fabrication of biomimetic scaffolds or constructs using these biomaterials is of specific interest, for it allows researchers the ability to design and better replicate tissue-based complexities, such as layering and orientation inherent to physiological micro-environment, in accordance with the application at hand (Zhu et al., 2016; Guillemot et al., 2010; Catros et al., 2011; Jia et al., 2016).

Cells are as much of a product of their environment as their environment is a product of cellular activity. The extracellular matrix (ECM) constitutes the native cellular micro-environment. The ECM is a complex network of proteins, glycoproteins, and

polysaccharides; it provides structure and is essential for healthy tissue function as it surrounds all cells (Hubbell, 1995; Watt and Hogan, 2000; Fuchs, 2009). The ECM as the integral component of the native cellular micro-environment influences cell behaviour. Each ECM is tissue specific; differing in porosity, shape, topography, mechanical properties (stiffness and elasticity), bioactivity and electro-conductivity that define and modulate cellular structure and activity (Akhmanova et al., 2015; McBeath et al., 2004; Holst et al., 2010). The ECM in concert with biochemical and biophysical factors works to impart mechanical, electrical and biochemical signals to cells by mediating external environmental stimuli and by holding signal molecules in reserve for later release to cells during specific events such as wound healing, tissue regeneration or bacterial infection (Lane et al., 2014; Katayama et al., 2006; Rosso et al., 2004). Despite extensive work done on elucidating the mechanisms behind cell-ECM interactions and how these interactions dictate cell behaviour, researchers are challenged to replicate the functional aspects of the cellular micro-environment's physical parameters such as mechanotransduction, electrical and biochemical activity in a combinatory manner to assess their influence on cells, tissues, and disease pathophysiology (Iskratsch et al., 2014; Gattazzo et al., 2014).

This gap in knowledge is vital to the current state of tissue engineering research. Researchers have a need to elucidate the workings of the cellular micro-environment, whilst simultaneously maintaining control over the scale, repeatability and morphology of constructs used in evaluations. Maintaining such control over the constructs is vital to understand under which conditions cell behaviour can be influenced towards biologically relevant outcomes. This need could be addressed by utilizing substrates capable of an amalgamated, complex approach of stimulating cells and emulating the cellular micro-environment. One route to achieving this would require using AM technology where researchers may be able to exercise acute control over the physical properties and uniformity of their constructs. The second component of such a platform capable of

an amalgamated, complex approach needed to address said gap in knowledge requires the ability to modulate cell behaviour in a controlled manner.

Electro-active polymer (EAP) materials exhibit direct physical responses such as change in volume, colour or shape in response to external stimuli, such as electrical current or applied potential (Bar-Cohen et al., 2007). Conjugated polymer (CP) materials are a subtype of EAPs. CPs are intrinsically conductive, repeating monomers capable of conformational change, i.e. deformation or expansion, when electrically stimulated at low voltages (Guiseppi-Elie, 2010; Bar-Cohen et al., 2007). These CPs, including polyaniline (PAni), polypyrrole (PPy), etc. have been used in the past for soft robotics, artificial muscles, lab-on-a-chip applications, as drug delivery/release systems, as well as hydrogels, biosensors and neural interface electrodes (Ates, 2013; Guiseppi-Elie, 2010; Trivedi et al., 2008; Svennersten et al., 2011; Berti et al., 2017). In addition to their electro-active characteristics which have inspired investigations into actuator and drug delivery/release system applications, CPs are electrically conductive. These properties of CPs makes them highly attractive candidates for studying the effects of mechanotransduction, electrical and biochemical stimulation in an amalgamated manner. Although several CP-natural/synthetic-based composites capable of imparting electrochemomechanical stimulation on to cells exist in literature, produced structures are greatly limited in feature, size and geometric complexity.

By harnessing AM techniques and the associated properties of CPs, such as PPy, structures with design-ability inherent to AM processes and the electro-active properties inherent to CP-based structures can be produced. Essentially, researchers armed with such a platform would be capable of modulating the morphology, electro-conductive and electro-active properties of their 3D printed constructs, in a 3D cell-culture setting. This notion, however, remains largely uncharted territory in literature. The work presented in this thesis investigates the feasibility of applying an AM technique towards producing CP-based structures, which hold potential for simulating and stimulating *in vivo* complexities

in a combined manner. To this end, a collagen-pyrrole (Col-Py) blend is used to develop novel DIW PPy-based structures. The retention of the favourable properties associated with PPy in the produced constructs are subsequently evaluated.

1.1 Objectives

This research project aims to explore the electromechanical properties associated with PPy by developing innovative AM engineered materials and assessing their potential for biomedical and tissue engineering applications. These goals are embodied by the following research objectives:

- *Investigate methods for 3D printing Col-PPy constructs.* The first objective is towards combining a CP, i.e. PPy, with a scaffolding biomaterial, i.e. collagen, to assess the feasibility of applying DIW AM technology for the production of CP-based structures. The characteristics of the printing ink will be assessed using rheological characterization. Control over the internal morphology of the structures produced with the developed AM methodology will be evaluated using optical imaging and SEM.

- *Demonstrate the application of 3D printed PPy-based constructs.* The second objective will build on the outcomes of the first objective and evaluate the efficacy of the 3D printed Col-PPy structures for retention of favourable properties prevalent in tissue engineering research tradition. Specifically, electro-activity, actuation and electrical conductivity properties of DIW printed constructs will be assessed following direct electrical stimulation. Additionally, cyto-compatibility will be evaluated via cell culture experiments to provide insight to the potential utility of 3D printed collagen-PPy constructs as means for studying cellular behaviour, in a 3D cell culture *in vitro* environment.

1.2 Major contributions

This thesis conveys the following major contributions to the scientific body of knowledge:

- *A Direct-ink write fabrication methodology for the production of collagen-polypyrrole structures.* The first-ever study to establish a DIW fabrication protocol for collagen-PPy structures is presented. This work developed a novel AM methodology for creating designable Col-PPy structures of geometric and feature complexities. The developed Col-PPy fabrication methodology involves the use of a hydrogel scaffolding, i.e. collagen, in concert with PPy to create novel, 3D printable PPy-based hydrogel structures. This thesis demonstrated the effect of increasing PPy concentration on the rheological properties and DIW printability of the DIW ink. Differences in construct porosity, morphology, and topography of the 3D printed constructs were evaluated using optical and SEM imaging. Elemental mapping is performed to evaluate the elemental composition of 3D printed Col-PPy constructs.

- *A novel electro-conductive, electro-active, cyto-compatible, 3D printed collagen-polypyrrole construct.* The retention of favourable properties associated with the developed 3D printed electro-active and electro-conductive PPy-based hydrogel constructs is evaluated. Electro-conductivity, electro-activity and actuation properties of 3D printed structures are reported in this thesis. Cyto-compatibility is qualitatively established for the 3D printed collagen-PPy constructs by culturing human BJ fibroblast cells for 7 days. This thesis offers an upgrade on traditional fabrication methodologies for PPy-based structures and establishes potential utility of DIW PPy-based structures for better emulating *in vivo* complexities *in vitro*.

- *A platform for potentially studying cellular behaviour, stem cell differentiation and disease pathophysiology in response to stimulation via novel 3D DIW printed collagen-polypyrrole constructs established.* The potential of DIW Col-PPy constructs as an instructive substrate capable of imparting electro-conductive stim-

ulation and potential of DIW Col-PPy constructs as electro-active constructs as drug delivery/release systems was established and is discussed in Chapter 4 and Chapter 5.

1.3 Organization of the thesis

The following chapter, Chapter 2, *Background* offers a brief introduction in conventional AM techniques. The chapter then summarizes the fundamental knowledge in the usage and choices for scaffolding biomaterials for tissue engineering applications, properties of the ECM and current state of the art dedicated to replicating said properties *in vitro*. The chapter then summarizes usage of PPy and its electrochemistry, characteristics, synthesis techniques for biomedical applications. Subsequently, the current state of the art for PPy-based structures, followed by a survey on the potential utility of using collagen and PPy in concert, opposed to standalone constructs, is discussed.

In accordance with the aforementioned objectives, the remainder of the thesis is organized as follows: Chapter 3, *Materials and Methods for the Direct-Ink Write Additive Manufacturing of Col-PPy constructs*, details the experimental methodology adopted which lead to the development of an AM fabrication protocol which blends a CP with an ECM protein to create the first-ever DIW printed PPy-based structures, as well as preliminary investigations and the development of a freeze-drying apparatus. Included in this chapter is the methodology adopted for characterization of the physical and functional properties of the novel DIW printed PPy-based structures. Chapter 4, *Characterization of DIW Col-PPy constructs: Part 1*, includes the first half of results from evaluations on the physical and functional properties of the 3D printed constructs, namely: rheology, optical imaging, electro-conductivity and electro-activity via cyclic voltammetry and spectrometry. Results from the second half of aforementioned characterizations are included in Chapter 5, *Characterization of DIW Col-PPy constructs: Part 2*. Namely, actuation,

SEM and tensile evaluations, as well as cell culture experiments and topographical characterization using CLSM. Lastly, Chapter 6, *Concluding Remarks*, summarizes the conclusions of the work, reaffirms the major contributions to knowledge and postulates recommendations for future research using the AM fabrication methodology developed in this thesis.

List of references

Akhmanova, M., Osidak, E., Domogatsky, S., Rodin, S. and Domogatskaya, A. (2015), 'Physical, spatial, and molecular aspects of extracellular matrix of in vivo niches and artificial scaffolds relevant to stem cells research', *Stem Cells International* pp. 1–35.

Atala, A., Kasper, F. K. and Mikos, A. G. (2012), 'Engineering complex tissues.', *Science Translational Medicine* **4**(160), 160rv12–160rv12.

Ates, M. (2013), 'A review study of (bio)sensor systems based on conducting polymers', *Materials Science & Engineering C* **33**(4), 1853–1859.

Bar-Cohen, Y., Kim, K. J., Choi, H. R. and Madden, J. D. W. (2007), 'Electroactive polymer materials', *Smart Materials and Structures* **16**(2), 1–3.

Berti, F. V., Srisuk, P., da Silva, L. P., Marques, A. P., Reis, R. L. and Correlo, V. M. (2017), 'Synthesis and Characterization of Electroactive Gellan Gum Spongy-Like Hydrogels for Skeletal Muscle Tissue Engineering Applications', *Tissue Engineering Part A* **23**(17-18), 968–979.

Catros, S., Fricain, J.-C., Guillotin, B., Pippenger, B., Bareille, R., Remy, M., Lebraud, E., Desbat, B., Amédée, J. and Guillemot, F. (2011), 'Laser-assisted bioprinting for creating on-demand patterns of human osteoprogenitor cells and nano-hydroxyapatite', *Biofabrication* **3**(2), 025001–11.

Donderwinkel, I., van Hest, J. C. M. and Cameron, N. R. (2017), 'Bio-inks for 3D bioprinting: recent advances and future prospects', *Polymer Chemistry* **8**(31), 4451–4471.

Fuchs, E. (2009), 'Finding One•s Niche in the Skin', *Stem Cell* **4**(6), 499–502.

Gattazzo, F., Urciuolo, A. and Bonaldo, P. (2014), 'Extracellular matrix: A dynamic microenvironment for stem cell niche', *BBA - General Subjects* **1840**(8), 2506–2519.

Guillemot, F., Mironov, V. and Nakamura, M. (2010), 'Bioprinting is coming of age: report from the International Conference on Bioprinting and Biofabrication in Bordeaux (3B'09)', *Biofabrication* **2**(1), 010201–7.

Guiseppi-Elie, A. (2010), 'Electroconductive hydrogels: Synthesis, characterization and biomedical applications', *Biomaterials* **31**(10), 2701–2716.

Holst, J., Watson, S., Lord, M. S., Eamegdool, S. S., Bax, D. V., Nivison-Smith, L. B., Kondyurin, A., Ma, L., Oberhauser, A. F., Weiss, A. S. and Rasko, J. E. J. (2010), 'Substrate elasticity provides mechanical signals for the expansion of hemopoietic stem and progenitor cells', *Nature Biotechnology* **28**(10), 1123–1128.

Hubbell, J. (1995), 'Biomaterials in tissue engineering', *Nature Biotechnology* **13**(6), 565–576.

Iskratsch, T., Wolfenson, H. and Sheetz, M. P. (2014), 'Appreciating force and shape-the rise of mechanotransduction in cell biology', *Nature Reviews Molecular Cell Biology* **15**(12), 825–833.

Jia, W., Gungor-Ozkerim, P. S., Zhang, Y. S., Yue, K., Zhu, K., Liu, W., Pi, Q., Byambaa, B., Dokmeci, M. R., Shin, S. R. and Khademhosseini, A. (2016), 'Direct 3D bioprinting of perfusable vascular constructs using a blend bioink', *Biomaterials* **106**(C), 58–68.

Johnson, B. N., Lancaster, K. Z., Zhen, G., He, J., Gupta, M. K., Kong, Y. L., Engel, E. A., Krick, K. D., Ju, A., Meng, F., Enquist, L. W., Jia, X. and McAlpine, M. C. (2015), '3D Printed Anatomical Nerve Regeneration Pathways', *Advanced Functional Materials* **25**(39), 6205–6217.

Jose, R. R., Rodriguez, M. J., Dixon, T. A., Omenetto, F. and Kaplan, D. L. (2016), 'Evolution of Bioinks and Additive Manufacturing Technologies for 3D Bioprinting', *ACS Biomaterials Science & Engineering* **2**(10), 1662–1678.

Kang, H. W., Lee, S. J., Ko, I. K., Kengla, C., Yoo, J. J. and Atala, A. (2016), 'A 3D bioprinting system to produce human-scale tissue constructs with structural integrity', *Nature Biotechnology* **34**(3), 312–319.

Katayama, Y., Battista, M., Kao, W.-M., Hidalgo, A., Peired, A. J., Thomas, S. A. and Frenette, P. S. (2006), 'Signals from the Sympathetic Nervous System Regulate Hematopoietic Stem Cell Egress from Bone Marrow', *Cell* **124**(2), 407–421.

Lane, S. W., Williams, D. A. and Watt, F. M. (2014), 'Modulating the stem cell niche for tissue regeneration', *Nature Biotechnology* **32**(8), 795–803.

McBeath, R., Pirone, D., Nelson, C., Bhadriraju, K. and Chen, C. (2004), 'Cell shape, cytoskeletal tension, and rhoa regulate stem cell lineage commitment', *Developmental Cell* **6**(4), 483–495.

Pati, F., Ha, D.-H., Jang, J., Han, H. H., Rhie, J.-W. and Cho, D.-W. (2015), 'Biomimetic 3D tissue printing for soft tissue regeneration', *Biomaterials* **62**(C), 164–175.

Rosso, F., Giordano, A., Barbarisi, M. and Barbarisi, A. (2004), 'From cell-ecm interactions to tissue engineering', *Journal of Cellular Physiology* **199**(2), 174–180.

Svennersten, K., Berggren, M., Richter-Dahlfors, A. and Jager, E. W. H. (2011), 'Me-

chanical stimulation of epithelial cells using polypyrrole microactuators', *Lab on a Chip* **11**(19), 3287–7.

Trivedi, D., Rahn, C. D., Kier, W. M. and Walker, I. D. (2008), 'Soft robotics: Biological inspiration, state of the art, and future research', *Applied Bionics and Biomechanics* **5**(3), 99–117.

Watt, F. and Hogan, B. (2000), 'Out of eden: Stem cells and their niches', *Science* **287**(5457), 1427–1430.

Zhu, W., Ma, X., Gou, M., Mei, D., Zhang, K. and Chen, S. (2016), 'ScienceDirect 3D printing of functional biomaterials for tissue engineering', *Current Opinion in Biotechnology* **40**, 103–112.

Chapter 2

Background and State of the Art

This chapter will summarize the relevant background information on the AM technique utilized in this thesis, similarities between the native cellular micro-environment and intrinsic properties of PPy-based constructs which will orient the reader on the motivation for this thesis. Various AM techniques are briefly discussed, with associated advantages and disadvantages of each technique. Then, background knowledge on the ECM which constitutes the structural environment of cells, as well as major biochemical and biophysical properties associated with the ECM that govern cell behaviour, tissue-level remodelling and regeneration are discussed. Additionally, current state of the art regarding investigations which aspire to emulate said properties are reviewed, with a focus on collagen-based and PPy-based constructs. Finally, the electrochemistry and functional characteristics, synthesis techniques, and applications of PPy, in terms of tissue engineering applications, are discussed.

2.1 Review of Additive Manufacturing Technology

The main technology involved in this thesis is AM. In recent decades, there has been great interest in developing this technology for industrial, biomedical, and lab-on-a-chip

applications (Kang et al., 2016; Ngo et al., 2018; Wallin et al., 2018; Carrow et al., 2015; Wang et al., 2017; Ambrosi and Pumera, 2016). AM is a rapid prototyping technique that involves laying down successive layers, one on top of the other, that is, in an additive manner to produce structures in accordance with a predetermined CAD model (ASTM Standard ASTM52900 - 15, 2015). The CAD model is easy to manipulate and subsequent versions are easily revised. 3D printing is of high utility because of the creative freedom it affords the designer. The designer is able to produce 3D constructs efficiently and with extreme precision over the structure at the micro- and macroscopic level (Melchels et al., 2012). In addition to control of scale, the designer is capable of controlling internal morphology and geometric complexity of the printed construct. Geometry plays an important role in dictating form, which in certain cases dictates function.

Another advantage inherent to many 3D printing methods is reduced waste, meaning that only material required to build the final 3D object is consumed during the fabrication process. AM techniques have been traditionally divided according to their fabrication principles, namely: photopolymerization, powder based fusion, sheet lamination and extrusion-based (Ambrosi and Pumera, 2016). AM techniques shown in Figure 2.1 and Figure 2.2 are currently being employed towards generating novel implants, devices, substrates, scaffolds and structures from various build materials, for industries ranging from automotive to architecture to medicine (Ambrosi and Pumera, 2016; Ozbolat and Hospodiuk, 2016).

Extrusion-based printing methods involve deposition of material from a nozzle, after the material has undergone prior liquefaction treatment, where the movements of the nozzle reflect the CAD model. The most common method associated with this process is called Fused Deposition Modelling (FDM). FDM represents the conventional form of 3D printing method most recognized (Figure 2.2 (A)). 3D objects are produced when the thermoplastic (e.g. polylactic acid (PLA), acrylonitrile butadiene styrene (ABS),

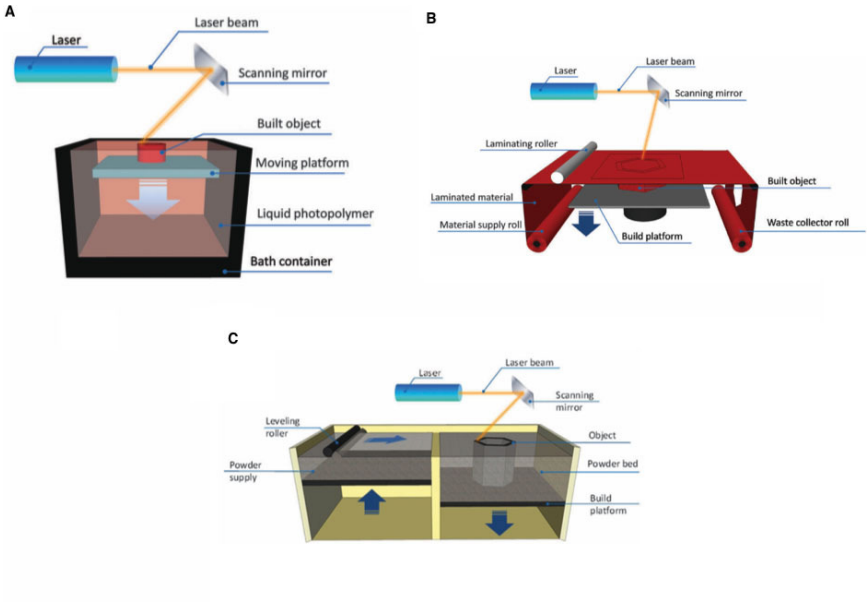

Figure 2.1: The AM techniques (A) Stereolithography (SLA), (B) Lamination object manufacturing, (C) Selective Laser Sintering (SLS) (Ambrosi et al., 2016, included with permission)

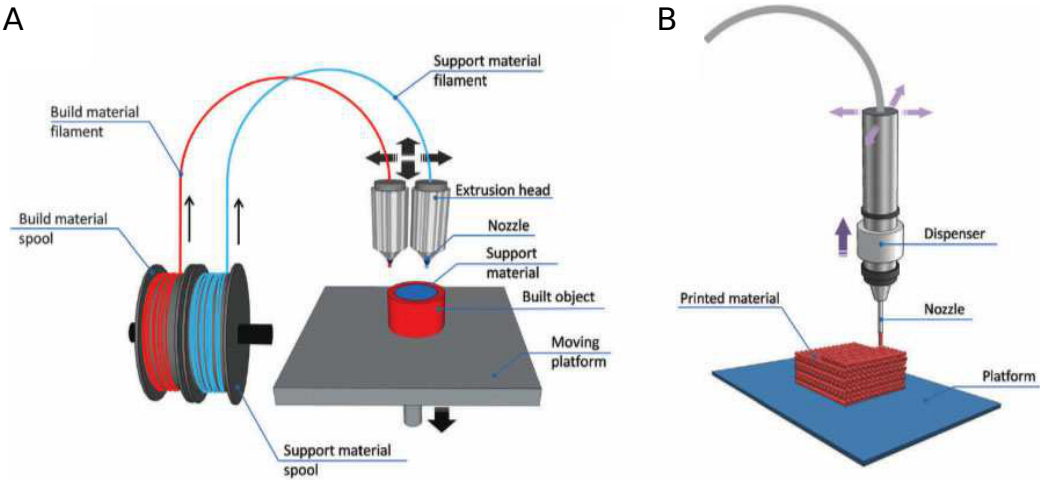

Figure 2.2: The AM techniques (A) Fused Deposition Modelling (FDM), (B) Direct-ink Write (DIW) (Ambrosi et al., 2016, included with permission).

polyvinyl alcohol (PVA), etc.) material is deposited in a semi-molten state from a heated nozzle. The deposited material solidifies as it cools, and subsequent layers are added as additional material is deposited on top of the previous. Although FDM doesn't allow for much variety in applications as the material is restricted to thermoplastics and the resolution is limited by nozzle diameter. However, anyone armed with a computer and a FDM-based 3D printer can produce 3D, complex structures at high speed and low cost due to its simplicity and commercial availability (Hutmacher et al., 2001; Zein et al., 2002).

Another type of extrusion-based printing method commonly employed is called direct-ink write (DIW), shown in Figure 2.2 (B). This method was pioneered by researchers at the Freiburg Materials Research Center, Freiburg, Germany, circa 2000 (Landers et al., 2002). In DIW, a viscous liquid in the form of a paste, dispersion or solution, typically contained in a syringe is connected to a pneumatic dispensing system, is forced through a nozzle and continuously deposited to produce a 3D structure (Landers et al., 2002; Hinton et al., 2015). This technique's main advantage lies in the array of materials that can be used as inks, including: ceramics, hydrogels, reactive polymers and their composites, ECM-derived proteins (Chia and Wu, 2015; Pati, Ha, Jang, Han, Rhie and Cho, 2015; Hinton et al., 2015). For tissue engineers, prior to the development of this AM method, scaffolds and structures were manufactured as sheets, in bulky casts or by employing moulds. This limits the applications of constructs, as interior porosity and morphology is limited to material properties, chemical or physical post-fabrication treatments and not directly tuneable. The utility of these constructs, for instance as cell-delivery platforms, is limited by size as larger scaffolds cannot receive sufficient diffusion of nutrients, leading to local cell death (Galban and Locke, 1997; Fedorovich et al., 2011). A major challenge for DIW printed structures remains the deposited ink's 'bleeding effect'. This effect manifests as 3D printed extruded widths of low viscosity materials are unable to maintain their geometry as extruded. Inadequate mechanical integrity is associated

with the fluid state of these low viscosity print materials, which in turn leads to limitations on size, resolution, complexity and geometric features producible (Ambrosi and Pumera, 2016; Chia and Wu, 2015). However, due to contemporaneous research and advances in DIW printing technology, hydrogel inks such as gelatin, agar, alginate, fibrin, silk, and collagen have been successfully 3D printed, only after print parameters were optimized and matched to the viscosity of the ink, or by the inclusion of sacrificial support materials such as PVA, a water dissolvable polymer, and then processed post-printing for gelation (Kang et al., 2016; Fedorovich et al., 2008; Woodfield et al., 2009). DIW printing is highly advantageous for it allows the designer to produce structures quickly, efficiently and en masse (Chia and Wu, 2015).

Recently, DIW techniques have been furthered developed to incorporate cells into the fluid-material to create bio-inks. This development inspired a new avenue of research which is of great interest to tissue engineering and biomedical applications called bioprinting (Chia and Wu, 2015; Jose et al., 2016). Bioprinting has been used in the past few years to facilitate research in developmental biology, stem cells and materials sciences (Donderwinkel et al., 2017; Bajaj et al., 2014; Murphy and Atala, 2014). It has been successfully used for printing biomaterial composites ladened with cells to create a layer-by-layer assembly of CAD models extracted from MRI or CT, or designed from scratch. With the aim of replicating native biological environments *in vitro*, miniature tissue models, organs-on-a-chip, 2D and 3D structures have been produced via pneumatic or mechanical extrusion of bio-inks using both natural and synthetic hydrogel polymers, such as ECM proteins, gelatin, silk, elastin, hyaluronic acid (HA) and polyethylene glycol (PEG) (Donderwinkel et al., 2017; Park et al., 2015; Gudapati et al., 2016; Kim et al., 2016). However, this technique holds certain limitations. Similar to DIW, the properties and specific print parameters vary from material to material, and must be properly evaluated prior to printing. Properties such as viscosity, porosity, track-width, nozzle diameter, nozzle height, shear thinning and the curing method must be taken

into account and adjusted for accordingly in order to not initiate cell death or apoptosis during the AM process. Another disadvantage associated with the optimization process is the amount of time consumed whilst optimizing the print parameters for each material. However, once this process is optimized, a researcher can begin to fabricate complex structures, and is limited only by components of the 3D printer itself.

Another limitation associated with structures produced using bioprinting is that final products, typically hydrogels, exist in their gel state which exhibit unsuitable mechanical properties for *in vivo* applications (Fedorovich et al., 2008). The poor mechanical stability of these 3D structures is regarded as a critical drawback of current bioprinting technology. Despite the variety of bio-inks investigated, scaffold-free scale-ups of organs has been difficult to achieve primarily due to the copious variations of tissue-specific properties and a lack of complete understanding of the complex interactions between cells and ECM structural properties, which dictate cell behaviour, tissue elasticity and flexibility, as well as disease pathophysiology (Pati, Song, Rijal, Jang, Kim and Cho, 2015; Tzu and Marinkovich, 2008; Chen and Liu, 2016; Jenniskens et al., 2005; Perris, 1997). Another apparent limitation of this technique is the enforcement of a sterile environment due to the incorporation of cells, which needs to be maintained constantly throughout the fabrication process, as well as post-print cross-linking or gelation processes typical for hydrogels may lead to local or general cell death; further limiting the library of materials viable for adaptation with this AM technique Donderwinkel et al. (2017); Guillemot et al. (2010); Jose et al. (2016); Murphy and Atala (2014).

Therefore, for the primary objective of this thesis, a conventional FDM printer previously modified for DIW printing was utilized. Cells were not incorporated into the printing ink for reasons aforementioned. DIW techniques are of interest because they allow researchers to exercise control over the internal morphology and geometry of their printed constructs, which can be based on the microstructure of tissues they aspire to replicate or mimic. Further aspects of the AM technique employed in this thesis are discussed

in Chapter 3, *Materials and Methods for the Direct-Ink Write Additive Manufacturing of Col-PPy constructs* including: configuration, software, model preparation, and relevant process matters.

2.2 Scaffolds in tissue engineering

Tissue engineering and regenerative medicine bodies of work have had an underlying, unifying theme which has been to understand how cells of interest work *in vivo* and how knowledge ascertained from *in vitro* investigations can be used to improve tissue function, decrease immune reaction to allogenic or xenogeneic transplants by developing therapeutic strategies, and to address the scarcity of tissue and organ donors. Regenerative medicine efforts have worked to understand or develop therapeutic strategies in cases where natural processes of regeneration falter, whereas tissue engineering approaches have typically aimed to augment damaged or diseased tissue by either replacing, repairing, and regenerating it. Early on, it became established that cells do not respond or behave in the same manner in a 2D cell culture setting as they would in a 3D environment, for the native cell environment is a complex combination of chemical, biochemical and 3D mechanical cues (Duval et al., 2017; Edmondson et al., 2014). Tissue engineers, thus, have aimed to produce 3D scaffolds, which served as temporary substrates that cells would adhere to, degrade and remodel by depositing their own extracellular proteins. This lead to the advent of tissue-specific engineering approaches, where researchers worked to produce scaffolds that closely mimicked the native cellular micro-environment in hopes of providing an instructive micro-environment for the cells or biologically relevant outcomes at hand.

Although a complete replication of complexities of the native ECM remains a distant promise, much progress has been made towards this end. Researchers have been able to produce an array of cell-delivery platforms from various natural and synthetic

materials, and shown to observe similar physical properties to that of target tissues and degrade at a rate that matches neo-tissue development. At present, research efforts being done in tissue engineering are towards improving *scaffold-guided* tissue regeneration *in vivo*, and improving *cell-guided* tissue regeneration. Scaffold-guided tissue regeneration relies on invasion of neighbouring cells at the state of implantation. This is a well-established, clinically used technique where scaffolds are treated with growth factors and biochemical cues that promote migration into the scaffold post-implantation, usually implanted at a wound site or where repair is the desired outcome. The second approach involves harvesting cells from the patient, loading their cells onto a scaffold prior to implantation, allowing the cells to mature *in vitro*. Afterwards, the cell-laden scaffolds can be implanted into the host to promote *in vivo* regeneration, repair or remodelling at the implant site and integration with surrounding ECM. These paradigms have been dogmatic and motivated researchers to continually add to the library of scaffolds, hydrogels, blends and composites available for achieving biologically relevant outcomes such as cell proliferation or tissue maturation, typically in a static manner; that is, as a static cell-delivery or material-induced cell response platform. Few have ventured to go further.

Incorporation of AM technology with established tissue engineering techniques has allowed researchers and clinicians the ability to personalize their constructs with designed intricacies. Although, scale-ups and uniformity from print-to-print have not yet been achieved to an absolute degree, much progress has been made in the context of applying AM techniques to the fabrication of constructs and scaffolds from a range of conventional biomaterials. These incorporations have led to expansion in the range of complex structures researchers could produce, as well as greater control over their construct's properties, specifically: composition, biomolecule entrapment, size, porosity, morphology, geometry and structural orientation (Pishko and Amirpour, 1998). Tissue engineers, having introduced AM technology into their fabrication protocols, have pro-

duced 3D scaffolds that better reflect the physiological environment; advances from these investigations have further informed researchers of standards and requirements necessary to qualify a successful scaffold before moving onto the final stage of testing, that is, host implantation. Of these requirements, the most important one to show is cyto-compatibility and/or biocompatibility.

Traditionally, these scaffolds have been primarily static systems designed for simple degradation and integration by the host; however, human physiology is more complex, heterogenous and dynamic. Recent years have seen a trend towards the development of scaffolds and substrates that are capable of instructing cells or modulating the vicinity of implant site towards biologically relevant outcomes such as regeneration, specifically without scar formation, fibrosis, or immune rejection, via incorporation of drugs/bioactive molecules or functionalization of the construct itself via incorporation of electro-active, conductive or shape memory polymers (Burdick and Murphy, 2012; Bakarich et al., 2015; Nadgorny et al., 2016; Zhang and Khademhosseini, 2017).

2.3 The ECM

The native cellular micro-environment, i.e. the ECM, is essential for healthy tissues as it surrounds all cells. It consists of tissue specific niches that differ in their biochemical and mechanical attributes (Lane et al., 2014). The ECM is a complex, interconnected meshwork of proteins, glycoproteins and polysaccharides (Lane et al., 2014; Choi et al., 2014). There are two classifications of ECM, namely: the basal lamina and connective tissue ECM. The basal lamina, or the basement membrane, is a thin sheet substrate that contributes to tissue structure and stability (Yurchenco and Patton, 2009; Sannes and Wang, 2009). It serves as the interface between epithelia, neural cells, or muscles cells, and their surrounding tissue and connective tissue ECMs, in addition to serving as physical support and providing boundary constraints (McMillan et al.,

2003). Connective tissue ECM is enriched in insoluble proteins and it forms the basic 3D structure of tissues. Connective tissue ECM plays a major role in regulating cell function as it directs interactions between neighbouring cells and secreted factors, inflammation factors, chemical cues such as hypoxia and glucose, as well as mechanosensory cues that stimulate resident cells (Streuli, 1999; Ngan F Huang and Li, 2017; Hubmacher and Apte, 2013). Each ECM is tissue-specific due to the ECM's intricate protein-polysaccharide network compositions; differing in macromolecule concentration, physical and biomechanical factors such as hydrophilicity, elasticity, stiffness, shear forces, porosity, 3D architecture and topography that hold influence over cellular structure and cell behaviour (Moore and Lemischka, 2006; Scadden, 2006; Yin and Li, 2006; Singh et al., 2015; Crapo et al., 2011).

Secreted by the cells, the main macromolecules within the matrix that contribute to the complex tissue specific 3D architecture consist of the following: fibrous proteins that include collagen and elastin, glycosaminoglycans (GAGs), proteoglycans, and glycoproteins. Collagen is the most abundant protein in mammals, as well as in any ECM. In the human body, it serves as the main structural protein found in bone, cartilage, tendons and ligaments (Gelse, 2003). The collagen family of proteins includes 28 subtypes. Collagens include fibrillar, network forming, anchoring fibril proteins that have been extensively studied and shown to provide structural integrity and stability to the ECM (Aziz et al., 2016; Ekblom, 1995). Further aspects of collagen are discussed in section 2.4.2 of this chapter, including: properties, past investigations as a tissue engineering scaffold, integrations with PPy, and scaffold synthesis techniques.

The diversity seen across tissues in their ECM is characterized by the varying concentrations of these aforementioned macromolecules, the manner in which the macromolecules are organized, in addition to any specialized macromolecules present specific to that tissue and/or ECM (Rosso et al., 2004; Hynes and Naba, 2012). This diversity makes it challenging to adopt one, ideal hydrogel or scaffold due to the distinct

characteristics and features of tissue-specific ECMs. During development, cells secrete the macromolecules that form the ECM. These macromolecules are organized into tissue-specific structures dependent on the function, needs and stresses experienced by said tissue. Afterwards, cells begin to respond to the deposited ECM, as it begins to influence and modulate cellular behaviours such as attachment, gene expression, survivals, proliferation, migration, anoikis, orientation, differentiation, as well as apoptosis via ECM-cell interactions involving bioactive molecules, electrical and biomechanical signals (Lu et al., 2012). This feedback and reciprocal relationship of ECM-cell interactions is one that researchers must account for when designing tissue engineering approaches and therapeutic strategies.

2.3.1 Bioactivity

The ECM is "bioactive" in the sense that there is no free diffusion between the cells (other than through gap junctions), so most extracellular factors interact with the ECM prior to interacting with the cells. The availability, mobility and distribution of these factors can therefore be regulated by the micro-environment via mediation of biochemical, mechanical and electrical signals *in vitro* to study cellular response and behaviour as a result of variable stimulation. The ECM controls signalling by influencing receptor-ligand binding and by holding signal molecules in reserve until specific events trigger their release to cells in the near vicinity (Ngan F Huang and Li, 2017; Hubmacher and Apte, 2013). These specific events include wound healing and bacterial infection. One instance of this phenomena is in the case of chondrogenic cells in articulating cartilages, where diffusivity of nutrients and oxygen is controlled by the stiffness and porosity of the ECM which influences chondrocyte turnover.

Although the cellular responses to chemical and biochemical cues such as toxins, growth factors, hormones, steroids and ischemia have been scrupulously investigated by researchers, other critical aspects of the cellular micro-environment have been difficult

to employ simultaneously in a controlled manner. Specifically, biophysical components such as mechanotransduction, bioactivity and electrical conductivity that operate in concert in the cellular 3D micro-environment have been a challenge for researchers to replicate *in vitro*. Therefore, there is a need to improve our understanding of the ECM niche by investigating how select cells behave when subjected to a range of combined electrical, biochemical and mechanical stimulation, in a 3D cell culture environment. A designable, electrically conductive, electro-active, mechanically active scaffold tailorable to the outcomes of clinical relevance would address this need, and vastly transform the current state of tissue engineering and regenerative medicine. Such a platform would allow researchers the ability to investigate the extent to which mechanotransduction, bioactivity and electro-conductivity effects — in a combinatory or isolated manner — play a role in tissue repair and regeneration, in stem cell differentiation, as well as in pathogenic events such as fibrosis, cancer and tumour development (Kim et al., 2018; Kessenbrock et al., 2010; Desmouliere et al., 2014; Maller et al., 2010; Guarino et al., 2007). Furthermore, a biomimetic scaffold that allows timed release of soluble factors such as growth factors or drugs would enhance therapeutic efficiency of regenerative medicine applications, improve drug testing efforts, and provide edification on tissue engineering strategies (Tandon et al., 2018). The project presented in this thesis works to investigate one potential avenue towards addressing that need.

2.3.2 Mechanotransduction effects

The prevalent motivation behind current tissue engineering research studies is to learn to modulate the processes that lead to disease progression, wound healing, and scarring, with focus towards developing therapeutic strategies and scaffolds for tissue engineering purposes that directly instruct cell behaviour towards promoting tissue regeneration (Humphrey et al., 2014; Bonnans et al., 2014). With the aim of developing tissue regeneration strategies, researchers have worked to relate biological relevance to the

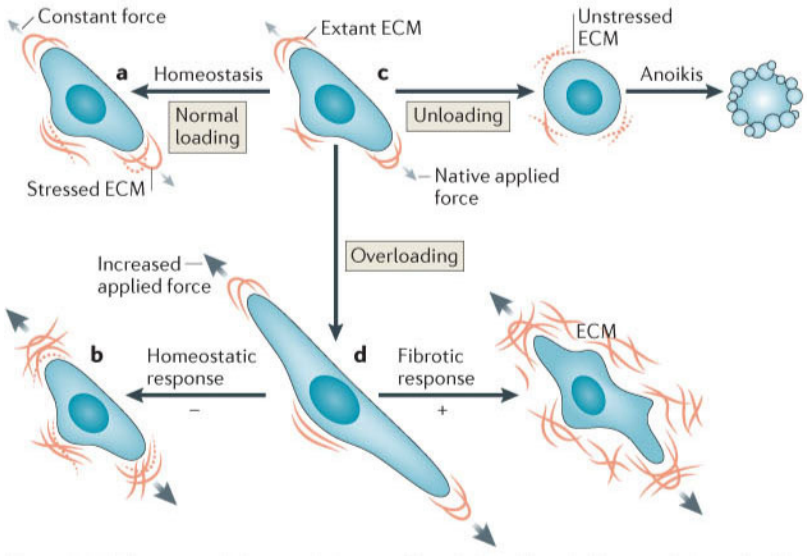

Figure 2.3: Illustration of ECM homeostasis and cellular response to mechanotransduction effects shows a fibrotic cellular response is resultant from tissue stiffening (Humphrey et al., 2014, included with permission).

ECM's transference of external cues to elicit specific cell behaviour and response (Atala et al., 2012; Butler et al., 2009). The activation of these behaviours works to inform the development of therapeutic strategies for meeting clinical needs in the future. Substrates and scaffolds that held a mismatch of ECM physical factors, such as stiffness/elasticity, porosity or stresses (tensile and/or shear), to those of target cells/tissue observed activation of non-relevant behavioural patterns such as apoptosis, loss of cell phenotype or transformation (Akhmanova et al., 2015; Marastoni et al., 2008). The ECM is dynamic in the sense that the ECM undergoes constant remodelling as needs of the tissue change. In normal physiology, mechanosensory cues from the ECM direct cells to secrete ECM remodelling factors which are kept in a balanced, homeostatic standing. For instance, in the biomechanics of lung parenchyma, bone cell differentiation, cartilage hydrophilicity, muscle growth and adaptation, as well as in fibrosis pathogenesis of the heart, lung, skin, and blood vessel tissue (Suki et al., 2005; Mullender et al., 2004; Tidball, 2005; Hinz, 2009). However, in a disease model, these same mechanosensory cues can lead to tissue degradation due to a mismatch in production of anabolic and

catabolic factors (Humphrey et al., 2014; Bonnans et al., 2014; Schuppan et al., 2001). Another clear instance to the extent to which mechanotransduction effects influence cellular behaviour is demonstrated by Wolff's law, at the organ level: bone cells respond to mechanical forces by remodelling bone structure, that is, by resorption or formation of bone, according to the stresses and strains experienced by the tissue (Frost, 1994). More so, at the cellular level, mechanotransduction causes changes in the cytoskeleton that stimulate alignment or polarity, growth factor secretion and/or proliferation (Hamill and Martinac, 2001; Jansen et al., 2017). For instance, tissue stiffening is a predominant feature of fibrosis and it obstructs organs whose mechanical properties are important for their function (Humphrey et al., 2014). Additionally, enzymatic degradation of the ECM and protein unfolding as a function of mechanotransduction has also been implicated in tumour formation and cancer development (Westermarck and Kähäri, 1999; Kessenbrock et al., 2010). Although methods for measuring physical characteristics of extracellular matrices and tissues have been developed, researchers remain challenged in replicating mechanotransduction effects and observing consequent cellular behaviour in 3D cell culture settings for extended time periods.

It is important to note that the forces acting on tissues are not always directly perceived by the cells, but rather stimuli is transmitted through the ECM unto the cells since tissues undergo constant turnover and since tissue/ECM remodelling can sometimes lead to changes in the stiffness of the ECM. As Figure 2.3 shows cells must be able to assess the physical properties of their surrounding ECM and consequently, maintain or remodel the ECM accordingly lest dysregulation in homeostasis leads to fibrotic pathogenesis and disease onset (Wells, 2008). The significance of elucidating mechanotransduction effects is also observed in the context of stem cells, where construct stiffness has also been demonstrated to play an important role in their differentiation (Maller et al., 2010; Kim et al., 2018; Lo et al., 2000; Skardal et al., 2012). In a study by Engler et al. (2006), the relationship between substrate elasticity and bone

marrow-derived mesenchymal stem cells (MSC) committing to lineages and exhibiting corresponding phenotypes was investigated. Researchers found that MSCs, with extreme sensitivity, probe their micro-environments for elasticity and undergo elasticity-directed lineage specification. A platform that could emulate or impart mechanical stimulation to cultured cells holds grave implications for investigations in regenerative medicine and tissue engineering.

Currently, *in vitro* models that postulate to learn of the mechanobiology of cell types typically isolate and plate cells onto thin gel layer materials (e.g. acrylamide or silicone), which can vary in stiffness upon changing concentrations or layer thickness, however, nonetheless show typical linear mechanical response. In contrast, native ECM is capable of withstanding a range of strains and demonstrates viscoelasticity/non-linear mechanical response (Mammoto and Ingber, 2010; Fung, 1983; Storm et al., 2005). Additionally, different methods and devices used for evaluating Young's modulus or complex modulus give different results for the same tissue (Humphrey et al., 2014; Akhmanova et al., 2015). This demonstrates a disparity between current means for studying mechanotransduction effects *in vitro*, and a need for an upgrade. Table 2.1 showcases key aspects of techniques employed to study mechanotransduction effects *in vitro*, and the limited edification they provide. The project presented in this thesis works to investigate a potential route for directing elasticity of the cellular micro-environment and studying consequent cellular response.

2.3.3 Electrical Stimulation

In addition to experiencing mechanical stresses and strains, cells experience electric cues that play a vital role in the development and regeneration of tissue by regulating proliferation, maturation, polarity, and differentiation (Shi et al., 2014, 2016; Uz et al., 2018). In mature tissue, these electrical cues are perceived via direct connectivity to ion channels at the cell membrane. Since no free electrons are available to serve as

Table 2.1: Table of experimental methods used to study physical properties of substrates, tissues and cells *in vitro* (Akhmanova et al., 2015).

Method	**Properties measured**	**Scale**	**Description**
Atomic Force Microscopy (AFM)	Young's modulus	nm	A nanoindenter measures the force-indentation displacement profile
Dynamic Mechanical Analysis (DMA)	Viscoelasticity, Young's modulus, storage and loss modulus	Macroscopic	A sinusoidal stress is applied and the strain in the material is profiled
Rheology	Shear storage modulus, loss modulus, and viscosity	Macroscopic	Viscoelasticity of materials is determined by imparting shear stress and measuring material response
Magnetic Resonance Elastography	Shear stiffness	μm	Shear waves are propogated on the surface of samples to assess shear stiffness response
SEM/Confocal Imaging	Porosity and pore size	nm	Samples are directly imaged and assessed

charge carriers in physiological solutions, differential concentrations of charged ions such as Na^+ , K^+ and Cl^- establish an electrochemical gradient on the two sides of the membrane, creating a measurable membrane potential and current flow. As cells couple together, a resistive barrier forms at the tissue level leading to measurable, endogenous electric fields existing across epithelial tissue like skin and cornea (McCaig et al., 2005).

More than a century ago, pioneering works in electrophysiology by Galvani, Matteucci and Du-Bois Reymond demonstrated that injury caused a disruption in the electric fields across these epithelial layers (Roth, 1994). With advancements in technology, researchers learnt that wound-induced electric fields controlled cell orientation and proliferation near the edge of the wound (Song et al., 2002). This phenomena motivated tissue engineers to investigate the extent to which electrical conductivity plays a role in mediating cellular behaviours as a function of temporal ionic current changes in the cellular micro-environment; leading to the development of electro-conductive biomaterials, substrates and scaffolds capable of stimulating cells *in vitro*. These substrates have been typically produced via inclusion of conductive materials, such as CPs, carbon nanotubes (CNT), carbon nanofibers (CNF), graphene, graphite oxide (GO), reduced (rGO), etc. as stand-alone constructs or as composites blended with natural and/or synthetic polymers (Thompson et al., 2015; Stejskal, 2017; Ganji et al., 2016; Rowlands et al., 2007; Huang et al., 2017; Mihic et al., 2015).

Despite the diversity of materials available for creating electro-conductive composites, methods for producing these scaffolds has been limited to 2D films, electro-spun fibres or mould casting and hydrogel fabrication techniques. Electro-spinning methods produce high quality and robust fibres for various biomaterials which can be controlled for porosity, orientations, diameter and scale. Although tuning the process and ambient factors (such as shape of collector, spin speed, applied voltage, humidity and temperature) have allowed researchers to produce a range of fibrous and patterned scaffolds, the technique is limited to the production of thin fibres, making it difficult to produce complex structures

where effective control over the internal morphology and assembly of complex structures can be achieved (Wang et al., 2013; Prabhakaran et al., 2011). For the same reason of lacking of effective control over the internal morphology and inability to produce complex structures, 2D films and mould casts are greatly limited in the range of their application.

The electro-conductive scaffold serves to regulate cell-cell and cell-ECM interactions by mimicking the native micro-environment and electrical signal propagation, in addition to providing sufficient biochemical and biomechanical factors necessary for keeping cells happy. Of the aforementioned materials used to create electro-conductive scaffolds, electro-conductive hydrogels have emerged as a promising candidate for tissue engineering applications. The typical limitations associated with hydrogels such as unsuitable mechanical properties, potential immunogenicity or uncontrolled degradation can be addressed by incorporation of biodegradable constituents and adopting fabrication methods which eliminate or overcome said limitations. Conductive additives such as carbon-based nanomaterials (e.g. CNFs, CNTs, graphene, and rGO) produce highly conductive scaffolds even if present at low concentrations (0.003–0.01 $S \cdot cm^{-1}$); however, potential toxicity associated with these carbon-based nanomaterials and challenges in creating uniform dispersion in hydrogels has hindered clinical applications (Firme III and Bandaru, 2010; Kunzmann et al., 2011; Gurunathan and Kim, 2016). Another set of conductive biomaterials that have been successfully incorporated with hydrogels concern CPs. Further aspects are discussed in section 2.5. The project presented in this thesis works to investigate the retention of electro-conductivity of PPy as a means for route for electrically stimulating cells and studying consequent cellular response.

2.4 Review of Scaffolding Biomaterials for Tissue Engineering

2.4.1 dECM

Currently, research efforts in tissue engineering and regenerative medicine are directed towards designing and investigating biomimetic scaffolds in order to find biomaterials that closely resemble tissue-specific ECMs, producing well-defined 3D constructs viable for intended regenerative capacity and improving physiological relevance of engineered human tissues (Tzu and Marinkovich, 2008; Chen and Liu, 2016; Jenniskens et al., 2005; Ventre and Netti, 2016). Naturally-derived materials, especially those containing ECM components, have shown great promise and hold an upper hand to alternative biomaterials, which have shown difficulty in demonstrating long-term retention after host implantation and sufficient biodegradability (Asti and Gioglio, 2014). Of these naturally-derived materials, collagen or decellularized ECM (dECM) and other ECM components have been explored.

At present, researchers have been able to DIW print as well as bioprint dECMs of adipose, skin, cartilage, liver and bone origin. Although dECMs of autologous or xenogeneic source, once deprived of their antigenic components, have been successfully used as biological scaffolding materials and cell delivery systems even with traditional fabrication methods, it is not without its limitations. Decellularization protocols typically involve exposure to detergents, harsh enzymes and physical forces that cause disruption of the ECM components (Crapo et al., 2011). This can lead to loss of GAG protein content in the dECM, which necessitates changes in the physical properties of the scaffold which may lead to complications in the long-term, such as implant rejection. Substrates or scaffolds that held a mismatch in physical factors and mechanical properties have been observed to result in activation of non-relevant behavioural patterns such

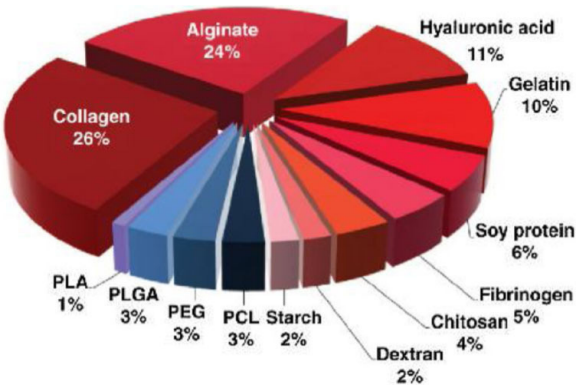

Figure 2.4: A chart illustrating the distribution of natural (red) and synthetic (blue) polymers use as DIW ink (Carrow et al., 2015, included with permission).

as apoptosis, loss of phenotype or phenotype transformation (Akhmanova et al., 2015).

Even though detergent-free protocols have been developed, which diminish the cytotoxicity effect seen from detergent residuals, the efficacy of these dECM in terms of *in vivo* response to implantation is still not quantitively standardized. Due to the advantage of already present complex cues and 3D architecture inherent to native ECM, the acellular and biodegradable nature of these ECM-rich scaffolds makes them promising platforms for promoting tissue regeneration at the implantation site as viable cell delivery systems. However, dECM scaffold biomechanical properties and micro-geometry effects on cell function have not been well-studied to date. Researchers studying decellularization protocols involving a trypsinization step observed a drastic loss in mechanical stiffness of the dECMs due to collapse of collagen architecture and decrease in porosity in post-trypsinized dECM (Singh et al., 2015). Although this field of study is still in its infancy, most dECM scaffolds do not possess the desired mechanical properties, which makes it difficult to attribute any consequent cell behaviour and modulation as a function of dECM content or concentration as viable means for studying cellular response by modulating their micro-environment properties (Donderwinkel et al., 2017; Singh et al., 2015; Jang et al., 2016).

2.4.2 Collagen as Scaffolding Biomaterial for Tissue Engineering

Alternatively, instead of using dECM as the scaffolding source, researchers have instead opted to use a more accessible and naturally-derived polymers as the scaffolding base component for biomedical applications involving cell-culture platforms and tissue-engineering scaffolds. Furthermore, after the marriage of AM technology and tissue engineering techniques, 3D printed scaffolds consisting of biologically derived materials (Figure 2.4) such as collagen, elastin, silk, dECM, HA, chitosan, alginate, gelatin, etc. have been the focus of extended research as they have been shown to establish a micro-environment that can be attuned to represent target ECM, to promote extended cell viability, and for feasibility as a vehicles of realizing tissue engineering prospects (Donderwinkel et al., 2017; Wang et al., 2017; Rhee et al., 2016; Bajaj et al., 2014; Patra and Young, 2016; Dong and Lv, 2016). A large amount of work has been dedicated for investigating these biomaterials and their derivatives for drug delivery, wound healing, tissue engineering and regenerative goals. For the purposes of the work presented in this thesis, review is limited to investigations of collagen and collagen-composite constructs.

Collagens are a major family of ECM proteins that characteristically form a triple helix structure of three polypeptide chain repeats. 28 different collagen proteins have been identified to date; each hallmarked by long, repetitive protein sequences of glycine-X-Y, stabilized by hydrogen bonding. These proteins all impart structure, strength and resilience to tissues, adding to the complexity and diversity of ECMs. Fibrillar, meaning fibril forming, collagen types I, II, III, V and XI are predominant in many human tissues and of interest to researchers because of their association with extracellular matrix scaffolding and high structural stability due to covalent cross-links between fibrils and self-aggregation (Dong and Lv, 2016; Gelse, 2003; Mouw et al., 2014).

Collagen is a ubiquitous protein in mammals. It constitutes the majority of soft and hard tissues. It can be extracted from bone, cartilage, tendon, ligament, blood vessels,

and skin. Collagen's obtainability and excellent biological characteristics motivated researchers to look at medical applications of collagen as a biomaterial, including: nerve and ligament repair implants, bone regeneration, skin regeneration, tendon regeneration, cornea regeneration, wound healing, drug delivery and as gene therapy vehicles (Sarker et al., 2015; Rieu et al., 2017; Chattopadhyay and Raines, 2014; Cen et al., 2008). Standalone collagen scaffolds have been developed by freeze-drying and electro-spinning methods, captillazing on the self-aggregating properties of fibrillar collagen. Investigations by Barnes and Bowlin (2007) showed that electro-spun collagen fibres produced patterning similar to native collagen ECM and supported adequate cell proliferation. Offeddu et al. (2015) showed that mechanical properties of freeze-dried collagen scaffolds was dependent on the initial collagen slurry concentration, and this relationship could be benefited from matching target tissue mechanical properties with implanted scaffolds. Despite the attractive biomaterial properties of collagen such as low immunogenicity, a porous structure, and biocompatibility, it lacks the mechanical and structural integrity to be used as a standalone scaffold in aqueous conditions (Chevallay and Herbage, 2000; Gelse, 2003). However, chemical treatments such as genipin, transglutaminase, and physical treatments such as critical point drying, freeze-drying and UV irradiation have shown great success in cross-linking collagens and increasing scaffold mechanical strength (Offeddu et al., 2015; Yeong et al., 2007).

One reason collagen has emerged as a widely studied biomaterial in tissue engineering research, in addition to its ubiquity and favourable properties, is the ability to culture almost any cell type on collagen based scaffolds. Collagen-based scaffolds have been evaluated for their suitability as platforms capable of achieving nerve tissue, tendon/ligament, skin, bone and cartilage tissue regeneration and repair (Koopmans et al., 2009; Meimandi-Parizi et al., 2013; Friess, 1998; Chevallay and Herbage, 2000). Another common investigation has been vascular grafting (Lee et al., 2008). Tendons and ligament predominantly (70–80%) comprise of collagen (Rieu et al., 2017). Similarly,

skin also predominantly consists of collagen (Chattopadhyay and Raines, 2014; Aziz et al., 2016). Collagen-based scaffolds have shown great success where autologous skin grafts and allogenous skin grafts have been associated with poor long-term retention and donor-site morbidity (Hanasono et al., 2010).

Although pure scaffolds have been used in skin regeneration and repair tissue engineering applications, they are limited as the mechanical properties of the scaffold do not completely reflect the *in vivo* complexity of ECM mechanics of organs other than skin or tendon. Therefore, researchers have opted to using collagenous scaffolds in concert with other biomaterials which allows certain advantages and room for manipulation for biomedical applications of interest. For instance, collagen has been combined with hyaluronic acid (HA) to create scaffolds that showed enhanced differentiation of rat bone marrow-derived MSCs towards chondrogenesis, *in vitro*, under ischemic conditions (Bornes et al., 2015). Collagen has also been combined with silk-fibroin, a protein obtained from silk glands of spiders, silkworms, scorpions, mites or flies, to increase mechanical integrity of the collagen-based scaffold whilst simultaneously improving cell adhesion and proliferation of human corneal epithelial cells (Long et al., 2015; Rockwood et al., 2011). Collagen has also been investigated as a blend with chitosan, a well-known derivative of insect exoskeleton aminopolysaccharide chitin that holds advantageous properties such as biocompatibility, biodegradability, and non-toxicity (Elieh-Ali-Komi and Hamblin, 2016; Ahmed and Ikram, 2016). Sun et al. (2015) reported better porosity, water absorption rate, higher elasticity modulus, higher metabolism and proliferation of rat bone marrow-derived MSCs in silk-fibroin-collagen scaffolds compared to silk-fibroin-chitosan scaffolds. Another route undertaken by researchers is to combine collagen with synthetic materials to create hybrid blends and improve their performance. In this approach, the synthetic polymer becomes the supporting material, i.e. it provides the bulk of mechanical support for the structure, while collagen serves as a surface-active protein to provide cells better adhesion via topography and recognition

signals (Gordon and Hahn, 2010). Investigations of collagen with synthetic polymers, such as poly-(ϵ-caprolactone) (PCL), PLA, PVA, PEG, PGA, and PLGA, have shown great potential for applications in vascular tissue engineering, nerve repair, and bone and liver regeneration (Dong and Lv, 2016). Collagen and inorganic blends have also been investigated to create composite scaffolds to suit various clinical requirements. Their performance has been evaluated in terms of control of morphology, elasticity, stiffness, and degradation. Major attention has been given to ceramic/inorganic polymers like hydroxyapatite and β-tricalcium phosphate (β-TCP). Essentially, these investigations show the benefits associated with collagenous constructs and collagen-blends are vast in terms of tissue regeneration and repair strategies, even as an additive.

Utility of collagen has been demonstrated in multiple arenas of tissue engineering, as previously mentioned, however, the most important reason for its inclusion in this thesis project is due to the fact that it has been previously 3D printed using DIW systems (Kontturi et al., 2014; Haaparanta et al., 2014; Jia et al., 2013; Lee et al., 2008). Collagen has been 3D printed as a standalone ink, as a bio-ink using bioprinting systems, as well as printed in concert with bioactive components as a composite, including: collagen-calcium phosphate, collagen-HA and collagen-alginate (Park et al., 2014; Inzana et al., 2014; Rhee et al., 2016; Yang et al., 2018; Nocera et al., 2018). The rheological properties of collagen were evaluated and found to be indicative of shear thinning behaviour that is particular to inks for DIW printing or bioprinting viability. These investigations collectively suggest that incorporation of bioactive components into collagen-based scaffolds retains its biologically relevant properties and holds potential for personalized and designed therapeutic strategies for tissue regeneration, such as bone or nerve repair. Although the synergy between a multitude of scaffolding components and AM technology has allowed researchers with an expansive ability to produce multitude of substrates similar to patterning of the ECM as delivery systems capable of modulating cellular behaviour, most of these exists as static substrates.

There exists a need for further investigations that facilitate scale-ups of existing tissue engineering approaches to the organ scale. For the sake of achieving tissue engineering and clinically relevant outcomes, investigations that will allow us to profile cell behaviour under stimulated conditions will improve our understanding of how changes in the native cellular micro-environment influence cell phenotype, behaviours and consequent function.

2.5 Review of Conjugated polymers

Conjugated polymer (CP) materials are a branch of electro-active polymer (EAP) materials. EAPs are materials that exhibit physical responses such as change in volume, colour or shape in response to external stimuli such as electrical current or applied potential. CPs are characterized by alternating single and double bonds along the polymer backbone, a process known as conjugation, which allows charge delocalization and enables CPs their electro-conductive properties (Smela, 2003; Spinks et al., 2009).

Another interesting property of CPs is that they undergo conformational change when the oxidation state of the CP backbone is changed, in response to electrochemical switching (Jager et al., 1999*a*; Wang, Shapiro and Smela, 2004; Wang et al., 2008). As potential is applied, bond re-orientation causes the formation of charges along the backbone which are balanced by ionic ingress or egress, resulting in volume change (Spinks et al., 2009; Otero and Martinez, 2016; Otero, 2018). This qualifies the CP construct as an actuator capable of performing mechanical work, or a biosensor, or a drug delivery release system. CP-based constructs are superior to inert scaffolds or substrates in the sense that traditional constructs serve only as cell delivery or molecule entrapment platforms, whereas CP-based constructs offer a multifaceted stimulation afforded by the unique properties of CPs, namely the dopant-dependent topographical, electro-active, chemical and electrical properties (Seil and Webster, 2010). Due to

these advantageous properties, CPs have been used in the past for applications in soft robotics, artificial muscles, lab-on-a-chip, hydrogels, biosensors and neural interface electrodes (Ates, 2013; Guiseppi-Elie, 2010; Trivedi et al., 2008; Svennersten et al., 2011; Berti et al., 2017).

CP-based structures are of specific interest to tissue engineers because of their ability to mimic critical aspects of the native cellular micro-environment such as electrical conductivity, bioactivity and/or mechanical actuation. Integrations of CPs with naturally-derived and synthetically-derived materials allows functionalization of substrates that would have otherwise remained static in nature. These integrations for tissue engineering purposes has been a field of study since the late 1980s, providing researchers the ability to observe cellular behaviour of different cell types on fabricated substrates, post-electrical stimulation (Ramanavicius et al., 1999; Kontturi et al., 1998; Miller and Zhou, 1987). CPs such as polyaniline (PAni), polypyrrole (PPy), poly(3,4-ethylenedioxythiophene):polystyrene sulfonate (PEDOT:PSS) and poly(2,2-bithiophene) (PBP) have been utilized to generate a multitude of 2D and 3D structures, including: films, powders, membranes, aerogel and hydrogel scaffolds, nanofibers, as well as linear, tubular, and bending actuators (Huang et al., 1986; Mattioli-Belmonte et al., 2003; Wang, Shapiro and Smela, 2004; George et al., 2005; Bhadra et al., 2009; Asplund et al., 2009; Farajollahi et al., 2016; Khaldi et al., 2016; Yan et al., 2017).

Despite the variety in the amount of structures formed, the polymerization processes associated with creating CP-based constructs has made it challenging for researchers to incorporate AM technology. Another limitation of unmodified CPs, *in vivo* and *in vitro*, is their lack of biodegradability. To address these limitations, researchers have combined CPs with a range of biologically-derived materials, that are inherently biodegradable, as well as with biologically active molecules which act as surface proteins or cell adhesion molecules to promote degradation *in vivo* and *in vitro* (Ismail et al., 2011; Leonavicius et al., 2011; Shi et al., 2014; Mihic et al., 2015; Shin et al., 2017).

2.5.1 Polypyrrole as the CP of choice

Of the aforementioned CPs, PPy and PPy composites have been by far the most extensively studied. This is primarily due to its high electrical conductivity, biocompatibility, commercial availability and ability to operate in physiological conditions (Jager, 2013; Stejskal, 2017; Ouyang, 2018; Tandon et al., 2018). Additionally, topographical modification and actuation modulation can be achieved by inclusion of dopant molecules or bioactive molecules during the polymerization step which can influence its ion exchange or electro-active capacity, as well as influence promotion of cell adhesion and proliferation of different cell types; ranging from endothelial cells and nerve cells to osteoblasts (Jayamurgan et al., 2013; Molino et al., 2013; Sharma et al., 2013; Bendrea et al., 2011). Another reason for widespread use of PPy is due to its ease of synthesis. PPy has been successfully integrated with a variety of naturally-derived or synthetically-derived biomaterials and shown to retain favourable properties (Stejskal, 2017; Shin et al., 2017; Ketabat et al., 2017; Tandon et al., 2018). Synthesis parameters such as oxidant, dopant, pH, temperature, substrate and solvent can influence functional properties of PPy constructs. The tailorable manner in which PPy-based scaffolds and constructs can be produced makes PPy an emergent tool for novel applications in tissue engineering (Smela and Gadegaard, 2001; Smela, 2003).

2.5.2 Synthesis and Actuation Mechanism of Polypyrrole

Construct properties such as roughness, thickness, conductivity, volume change/actuation, etc. are influenced by reaction parameters such as pH, solvent, dopant, and temperature, and dependent on the method of PPy's synthesis as shown by an extensive study by Fonner et al. (2008). PPy is typically synthesized via the chemical oxidative polymerization or electrochemical polymerization method. During electrochemical polymerization, monomers deposit onto the surface of the working electrode,

typically platinum or gold, by application of an anodic potential, generating films of modular thickness (Heinze et al., 2010). The reaction proceeds favourably if the chosen solvent is aqueous, ionically conductive and has a large enough potential window to not undergo electrolysis at the applied oxidation potential, that is, to provide a stable solution for the polymerization of pyrrole. As shown in Figure 2.5, the application of the anodic potential generates a radical ion and subsequent resonance structures which react with other monomers to create oligomers, which subsequently react with other monomers/oligomers to create longer oligomers/polymers. At the same time, an anion/dopant/counterion molecule contained in the solution is incorporated into the polymer to maintain a net neutral charge for the polymer as the film forms (Genies et al., 1983). Interestingly, this doping stage can also be introduced after the synthesis of the electrochemically polymerized PPy film has finished (Kupila and Kankare, 1995). This allows great room for modulation of the topographical, electrochemical, mechanical and electrical properties of the end-product.

Additionally, the pH of the polymerizing solution significantly influences the reactivity and conductivity of the polymer. The pH lowers as a new proton is produced from a monomer being added to the polymer backbone. Another factor that influences the kinetics of the polymerization process is temperature, which has been observed to decrease redox properties and conductivity of films if polymerization occurs even at room temperature compared to $-20\ ^{\circ}C$ (Sabouraud et al., 2000). This process has been more popular over the years because it yields films of variable thickness and smoothness on the anode surface, depending on the type and duration of potential applied, but mainly because it provides better control over morphology than traditional chemical polymerization methods (Guimard, 2008; Toshima and Ihata, 1996).

The second method, referred to as chemical oxidative polymerization, concerns the chemical oxidation polymerization of pyrrole in the presence of a catalyst (e.g. an oxidant such as $FeCl_3$), and follows a similar reaction as the mechanism shown in Figure 2.5.

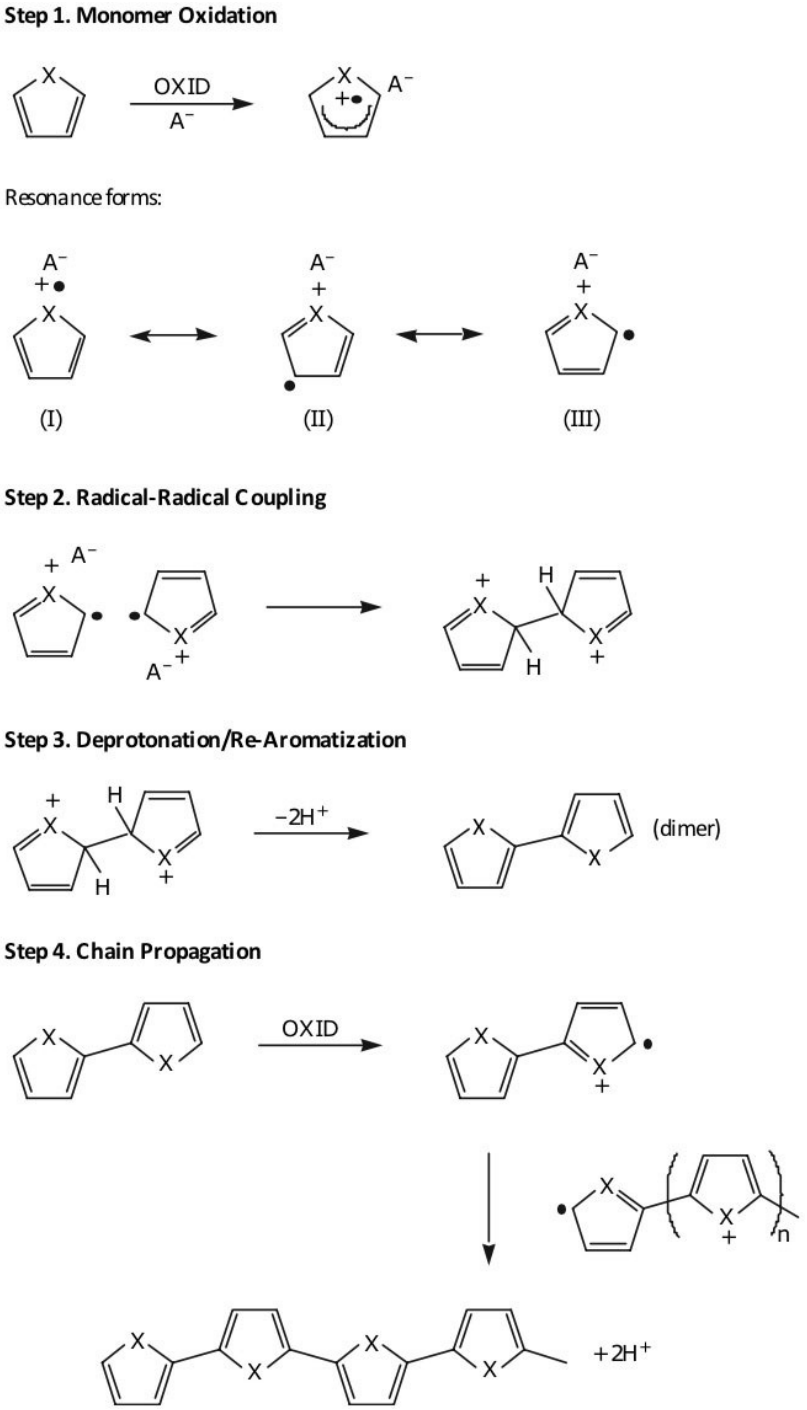

Figure 2.5: The oxidative polymerization reaction that occurs in both electropolymerization and chemical polymerization methods for PPy. The mechanism described in this figure is the commonly accepted polymerization mechanism for PPy (Wallace et al., 2009, included with permission).

Produced constructs have been observed to be powders of nm size, be insulating films, or take on the shape of a mould, if PPy is blended with other materials that fill said mould, as it is polymerized (Pei and Qian, 1991, 1992; Salmón et al., 1982; Yamaura et al., 1991). While electrochemical synthesis of PPy leads to the highest conductivity and the best mechanical properties, other materials can be better incorporated with PPy as blends via chemical oxidation polymerization. As synthesized, PPy exists in its oxidized state as shown by Figure 2.6. The current passing through the polymer in this oxidized state displays better electronic conductivity due to aligned polymer chains (Machida et al., 1989).

The mechanism responsible for the actuation behaviour of PPy results from a change in the oxidation state of the polymer backbone, which results in ingress and egress of ions into the polymer backbone to balance charges, presenting as volumetric change, and inducing surface stress that presents as modular surface elasticity (Spinks et al., 2009). This creates room for harnessing the PPy construct as an actuator capable of performing mechanical work and studying how cells respond to changes in substrate elasticity. On a molecular level, the actuation behaviour is dependent on a series of interconnected phenomena, namely: rate of charging, diffusivity of ions, ion migration rates, ion channels formations during cyclic redox, as well as the interactions between anionic, cationic and solvent species and with the polymer backbone (Madden et al., 2004; Bahrami-Samani et al., 2008; Alici et al., 2008; Shoa et al., 2010; Wang et al., 2008). Despite the complexity of factors governing electro-activity and actuation capability, macroscopic PPy electrochemically polymerized films exhibit large, repeatable volumetric change for extended periods of time (Jager et al., 1999*b*,*a*).

A major advantage of PPy and similar CPs is their versatility in range of functional properties; one that is afforded by the inclusion of dopant molecules. Dopants influence functional, biological activity, as well as physical properties of the CP. Depending on dopant choice, the CP's biodegradability is significantly influenced (Smela, 2003; Otero

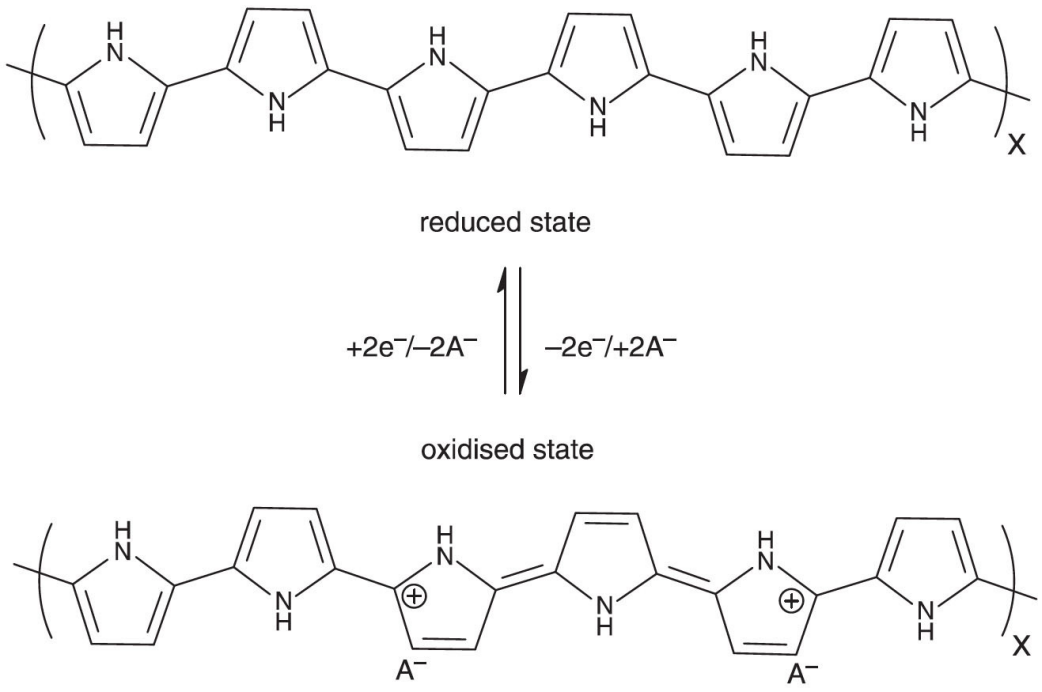

Figure 2.6: The oxidized and reduced states for PPy (Wallace et al., 2009, included with permission).

and Martinez, 2016; Smela and Gadegaard, 2001). Dopants are typically anionic species that can be introduced during or after the synthesis of the PPy to neutralize the charge on the oxidized PPy chains (Kaneto et al., 2012). The criteria involved in selecting dopants is dependent on the construct's application. For biomedical applications, it is necessary that these dopants be biocompatible and cationic species be available in fluids for prompt exchange. Dopants can be as small as monovalent ions such as Cl^-, F^-, I^-, Br^-, PF_6, etc. or large bulky molecules like dodecylbenzenesulfonate (DBS^-), bis-trifluoromethanesulfonimide ($TFSI^-$), etc. The resulting actuation strain for PPy constructs doped with these small ions is typically in the range of 1–3% (Yan et al., 2017; Madden et al., 2004; Smela and Gadegaard, 2001). For applications requiring larger strains, these smaller dopants can be exchanged for larger molecules; however, due to their large size, dopants such as DBS tend to be embedded into the polymer chain during reduction and oxidation processes, making actuation the primarily the function of

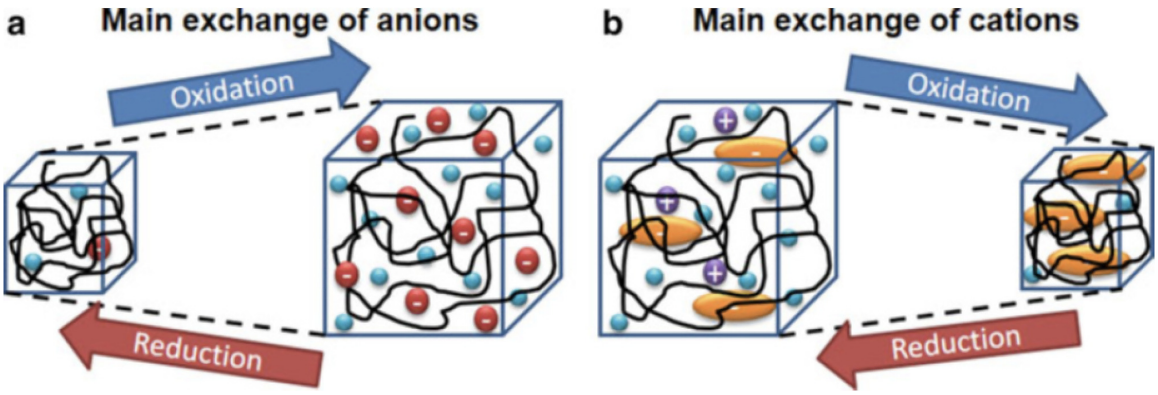

Figure 2.7: The oxidized and reduced states in response to electrochemical switching for PPy constructs (Capri et al., 2016, included with permission).

cation exchange.

Although several theoretical models have been presented to describe the behaviours of PPy-based constructs under different conditions exist, for instance, migration and diffusion models by Posey (1966) and Wang, Shapiro and Smela (2004) or capacitance models by Feldberg (1984), the dominant player has been accepted to be the ion exchange — ingress and egress of ions — occurring between PPy and the electrolyte solution (Otero and Martinez, 2016). Mechanical force is outputted as a consequence of reduction and oxidation of PPy, which leads to solvent molecules being exchanged from the CP. This variation in the concentration of ions inside the polymer and redox electrochemistry presents as expansion/swelling or contraction/shrinking of the PPy structure. Consumed charge determines the number of ions exchanged between the CP and the electrolyte solution, and degree of volume change (Carpi, 2016). The reactions majorly driving actuation for PPy-based constructs can be divided into anion-exchange dependent or cation-exchange dependent, depending on the dopants embedded into the polymer. For PPy constructs that have not been doped with macro-anions (A^-), as large anions can become trapped in the polymer during redox, anion-exchange is dominant. As equation 2.1 shows, oxidation of PPy leads to positive charges existing along the polymer chain (Otero and Martinez, 2016). Oxidized chains force anions from the solvent

to enter the construct and compensate for the charge imbalance. This incorporation causes swelling of the CP; whereas reduction of the polymer chain induces a neutral charge on PPy molecules which leads to expulsion of the anions (a^-) and shrinkage of the construct, assuming the anion is small and mobile. Simply, the anion-exchange dominant construct expands during oxidation and contracts during reduction. Sustained electrochemical switching of the polymer backbone, that is, by application of reducing and oxidizing potentials, presents as reversible volume variation, that is, actuation.

$$PPy^+(a^-)_n + ne^- \underset{\text{Oxidation}}{\overset{\text{Reduction}}{\rightleftharpoons}} PPy^0 + n(a^-) \tag{2.1}$$

$$PPy^0(A^-)_n(c_n^+) \underset{\text{Reduction}}{\overset{\text{Oxidation}}{\rightleftharpoons}} PPy^+(A^-)_n + n(c^+) + ne^- \tag{2.2}$$

In PPy constructs where the polymer is doped with large and immobile anions, i.e. A^-, the actuation mechanism is cation-exchange dependent; assuming the cation (c^+) is small and mobile. Here reduction of the polymer chain causes the PPy molecules to become neutral while the macro-anions that are trapped in the polymer chain force cations to enter the polymer to compensate for the charge imbalance. This influx of ions into the construct causes swelling of the construct; whereas oxidation of the polymer chain causes the macro-anions to reverse back to the PPy molecules which leads to expulsion of the cations due to opposing charges from the polymer chain. This results in shrinkage of the construct. As equation 2.2 shows, the effect seen in anion-exchange and cation-exchange dependent actuation mechanisms is directly opposite, where oxidation and reduction of the PPy backbone leads to opposing results, that is, expansion/contraction, based on the status of polymer doping. This variable response to dopants allows researchers to investigate PPy as an electro-actuator, variably doped and optimized for specific outputs of stress or strain to create volumetric, linear or bending actuators (Smela, 2003; Jager, 2013; Yan et al., 2017). Additionally,

the actuation mechanisms shown in Figure 2.7 are those which allow PPy to be applied as controlled drug release systems, where the dopant is exchanged for molecules of biological relevance, for instance dexamethasone, neural growth factor, etc. (Pillay et al., 2014).

2.5.3 Biomedical applications for Polypyrrole

The bioactuator component comes into play as researchers investigate PPy-based actuators as biomedical micro-devices capable of manipulating aspects of their environments, for instance, micro-robotic arms, or as replacements of skeletal muscle. Mammalian skeletal muscle myofibrils have been evaluated to output large strains (20–40%) but deliver low stresses (0.1–0.5 MPa) while PPy stress and strain outputs can vary with dopant choice (Otero and Boyano, 2003; Madden et al., 2000). For instance, PPy-based films doped with DBS have been reported to impart 0.6 MPa stresses but low strain outputs of 1–12% (Kivilo et al., 2016; Kiefer et al., 2014; Bay et al., 2003). These aforementioned electromechanically active properties along with biocompatibility, low stimulation voltage and low production cost give PPy-based materials potential as artificial muscles. For tissue engineers, PPy-based constructs that can be doped with molecules which result in modular physio-chemical and mechanical properties raise questions for potential in modulating cellular behaviours under specific conditions. For instance, doping of PPy with biomolecules or ECM components that promote tissue growth and maturation, or doped with anionic species such as Cl^- that deter cell attachment can be used as functionalized scaffolds for specific clinical applications and serve as a tissue substitute for important *in vitro* investigations (Yan et al., 2017; Liu et al., 2011; Björninen et al., 2014).

Controlled drug-release using PPy has been demonstrated for a number of drugs and biomolecules such as dexamethasone, adenosine triphosphate (ATP), naproxen, nerve growth factor (NGF), neurotrophin-3 (NT-3) and dopamine (Pernaut and Reynolds,

2000; Kontturi et al., 1998; George et al., 2006; Wadhwa et al., 2006; Jin et al., 2015; Miller and Zhou, 1987). This not only has important implications in tissue engineering where scaffolds can go beyond the usual static-substrate status quo, but by incorporating PPy a complex, dynamic and instructive environment for cells can be fabricated.

PPy's biocompatibility and potential as an 'active' scaffold in promoting neurite growth under electrical stimulation has been demonstrated both *in vivo* and *in vitro* (Kim et al., 2006; Lee et al., 2009; Bendrea et al., 2011; Balint et al., 2013, 2014; Durgam et al., 2012; Stewart et al., 2016; Camci-Unal et al., 2014). For instance, Jin et al. (2015) investigated the potential of using PPy films as an electrochemically controlled growth factor protein release system for NGF and NT-3, and demonstrated a synergistic effect of electro-stimulus and NGF/NT-3 release promoted axon elongation of neural cells. Their work showed potential for using electrochemically controlled release of growth factors from conductive PPy substrates as a means of directing nerve tissue engineering. In the case of PPy/chitosan-based nerve conduits, electrical stimulation enhanced nerve repair compared to control chitosan scaffolds *in vivo* in rats (Huang and Tang, 2012). Researchers also developed PPy-based substrates that were capable of modulating Schwann cell migration, directionality and displacement. Schwann cell migration speed was postulated to be a function of the electro-active property of the PPy films, whereas Schwann cell directionality and displacement was governed by electro-conductivity of the PPy films (Forciniti et al., 2014). Similarly, another group observed that PPy-PLA fibres modulated neurite proliferation, adhesion, alignment and elongation (Zhou et al., 2017). This suggests that similar to fibroblasts, physio-chemical, electrical and mechanical properties of the cellular micro-environment can be designed to influence neural cell phenotype, proliferation and growth; an application that PPy-based constructs are adequately suited for.

Although the mechanisms by which electrical stimulation influences various intracellular signalling pathways involved in proliferation, migration and apoptosis have not been

well-studied, researchers have been able to demonstrate that application of different forms of exogenous electrical stimulation does indeed alter cellular behaviour and is capable of influencing neurite elongation, neurite orientation and stem cell differentiation (McCaig et al., 2005; Love et al., 2018). To this end, various cell types have been cultured on electro-conductive hydrogels and electrical stimulation has been shown to play an important role in both tissue development and maturation. Electro-conductive hydrogels have found a home in cardiac, bone and neural tissue engineering applications as well as these cell types are well-known to respond to external electrical stimulation for development, proliferation and tissue organization (Thrivikraman et al., 2018; Huang et al., 2017).

Hydrogels once integrated with PPy typically via doping, blending or electrochemical polymerization become capable of imparting the unique properties associated with said materials whilst also largely retaining properties typically associated with hydrogels such as biocompatibility, hydrophilicity, porosity, mechanical properties, and biodegradability (Koetting et al., 2015; Wanjare and Huang, 2017; Ahadian et al., 2013; Vunjak-Novakovic et al., 2010; Mihic et al., 2015; Radisic et al., 2004). PPy-based hydrogel substrates have also been investigated for use as electro-conductive substrates that relay a uniform distribution of electrical stimulation throughout the construct, and therefore providing an instructive environment for cell proliferation. One limitation, however, of conjugated polymer based hydrogels is their low electro-conductivity, typically 10 $S \cdot cm^{-1}$), when compared to other conductive materials or stand-alone conjugated polymer based constructs, typically more than 10^3–10^5 $S \cdot cm^{-1}$, (Balint et al., 2013; Mekonnen et al., 2016; Li and Khor, 1994). This decrease is due to the natural impedance imparted by the hydrogel/scaffolding materials. However, this too can be modulated by utilizing differing quantities of dopants, different dopant molecules, as well as by modulating the charge transfer to adjacent molecules and the chain length by utilizing different fabrication conditions. For instance, integration of dopant molecules introduces extra electrons

that carry charge, which imparts an increase in conductivity (Otero and Martinez, 2016; Willerth and Sakiyama-Elbert, 2007). Additionally, researchers have demonstrated the utility of using electro-conductive substrates for facilitating neuronal cell maturation and tissue development, including other tissues such as skeletal muscle (Green et al., 2008; Gilmore et al., 2009; Fattahi et al., 2014; Berti et al., 2017), smooth muscle (Rowlands and Cooper-White, 2008) and bone tissue engineering (Huang et al., 2017; Fahlgren et al., 2015; Hu et al., 2014; Liu et al., 2013; Zhu et al., 2017). These investigations constitute electrical stimulation as emerging and effective tool for directing cell behaviour, one that can be achieved by employing PPy-based hydrogel constructs.

It has been well established that bone undergoes constant remodelling as a function of mechanical loading (Carter and Caler, 1985). This loading effect induces ionic currents that stimulate osteoblast activity (Carvalho et al., 1994; Lindsey et al., 1987; Kohavi et al., 1992). A study by Björninen et al. (2014) compared the effect of HA and chondroitin sulfate (CS), a common GAG protein, doped PPy films on human adipose stem cells, under electrical stimulation. They reported that while both films induced osteogenic differentiation, CS-PPy films supported better stem cell proliferation and higher mineral deposition under electrical stimulation. A study by Fahlgren et al. (2015) looked at the effect of PPy films on human primary osteoblasts. The PPy films were doped with p-toluene sulfonate (PPy-pTS), chondroitin sulfate (PPy-CS), or dodecylbenzenesulfonate (PPy-DBS). PPy-DBS showed the roughest topography, highest number of cells adhered and maintaining morphology, evidenced by organized actin filaments and vinculin attachment points, compared to PPy-pTS or PPy-pCS films. These aforementioned investigations suggest that PPy-based constructs are capable of guiding bone regeneration by electrically stimulation, modulating osteoblast and stem cell activity. Their results also implicate DBSA as an effective dopant for achieving desirable results of cyto-compatibility. Additionally, as previously mentioned, researchers were also able to blend PPy with biologically derived materials to create hybrid hydrogel

constructs, including: PPy-HA, PPy-CS-Collagen, PPy-CS, PPy-Agarose, PPy-silicone, PPy-Alginate, and PPy-collagen, while retaining their advantageous properties such as high ion diffusivity rates, porosity, biocompatibility and successfully producing instructive electro-conductive and/or electro-active scaffolds (Li and Khor, 1994; Hur et al., 2014; Guiseppi-Elie, 2010; Liu et al., 2011; Björninen et al., 2014; Wang, Gu, Yuan et al., 2004; De Giglio et al., 2001). Therefore, the amount of materials that PPy can be blended with is quite expansive. Select samples of this list are included in table 2.2.

Table 2.2: Integrations of PPy with various dopants/hydrogels/substrates have been observed to retain properties intrinsic to PPy and promote favourable tissue engineering outcomes.

Constituents and form	Cells investigated	Time period	Outcome	Reference
PPy-$FeCl_3$ powders and membranes	Rat dorsal root ganglia	24 weeks	Biocompatibility of PPy and greater neurite extension from dorsal root ganglia compared to control (ITO)	Wang, Gu, Yuan et al. (2004)
PPy-Collagen fibrous scaffold	Human MSCs	10 days	Up-regulation of neural markers on hMSCs, adoption of neuronal-like morphology	Yow et al. (2011)
PPy-DBS/ClO_4/TsO/Cl doped films	Rat fetal neural stem cells (NSC)	7 days	Biocompatibility of PPy is dopant-dependent, PPy-DBS best suited for NSC culture	Lundin et al. (2011)
PPy-DBS/pTS/CS doped films	Human primary osteoblasts	3 days	Biocompatibility of PPy-DBS, stable focal adhesions and organized actin filaments structure	Fahlgren et al. (2015)
PPy-CNT-PLLA sputter-coated nanofibers	Rat bone-marrow MSCs	7 days	Time-dependent electrical stimulation of PPy-composites influences osteogenic differentiation of MSCs	Zhu et al. (2017)
Electro-spun PLGA fibres coated with PPy-DBS	Human induced pluripotent stem (iPS) cells	7 days	PLGA-PPy-DBS fibres shown to be cyto-compatible, deliver micro-mechanical stimulation to iPS cells, and electrochemical switching of the fibres increased expression of cardiac markers	Gelmi et al. (2016)
PPy-poly(styrene-4-sulfonate) films	Rat neonatal Schwann cells	20 hours	Schwann cell migration directionality and up-regulation of nerve growth factor affected by electrical stimulation using PPy-based substrate	Forciniti et al. (2014)
PPy-CS/HA doped films	Human adipose stem cells (hASCs)	7 days	Electrically stimulated PPy-CS substrates better suited as osteogenic differentiation than PPy-HA substrates	Björninen et al. (2014)
PPy powder suspended in CS hydrogel	Rat sciatic nerve defect	12 weeks	Electrical environment with ES localized at the conductive scaffold is capable of accelerating axonal regeneration and remyelination of nerve defect	Huang and Tang (2012)

2.6 Review of Collagen and Polypyrrole Integration Investigations

Tissue engineering bodies of work involving PPy typically produced 2D films or layered 3D films via electrochemical polymerization, or fibrous, aerogel or hydrogel constructs via chemical polymerization which took on the shape of the container of polymerization. However, these CP-based structures are known to lack creative design; something that has been a limiting factor for their applications and known for some time now, but left without intervention. Investigations involving Col-PPy integrations began with seminal work done by Li et. al., circa 1994. They were able to successfully create Col-PPy hybrid materials by using $FeCl_3$ as the initiator for chemical oxidation of pyrrole and demonstrate that collagen and PPy existed as a stable blend using amino acid analysis and thermogravimetry, while higher concentrations of collagen served to lower the electrical conductivity of hybrid constructs (Li and Khor, 1994). However, formed PPy was readily precipitated from solution and only larger concentrations of collagen produced fibrous constructs. Li and Khor (1994) attributed this effect to incompatibility between surface energies of PPy and collagen molecules but observed that collagen was difficult to denature using detergents due to entrapment in the hybrid matrix. Later, Ateh et al. (2006) were able to develop Col-PPy 2D thin films using electrochemical polymerization. However, as previously mentioned, cells do not behave the same way in 2D cell culture as they do in 3D, and the 2D nature of these films majorly limits the edification from applying these constructs.

Since the foundational work by Li and Khor (1994) and Ateh et al. (2006), PPy has continued to be combined with a multitude of biomaterials and polymerized using both the chemical and electrochemical routes Khor et al. (1996); Lam et al. (1999); Gilmore et al. (2009); Gangopadhyay and Molla (2011); Rowlands et al. (2007); Gelmi et al. (2016). However, investigations for Col-PPy constructs, or ECM protein-PPy

constructs, have largely remained stagnant. For instance, Liu et al. (2011) evaluated the effects of electrical stimulation of rat pheochromocytoma neural cells using Col-PPy-CS films made by electrochemical polymerization. They demonstrated the superiority of electrically stimulated Col-PPy-CS substrates over static/unstimulated Col-PPy-CS and PPy-CS films, as evidenced by increased neurite outgrowth and proliferation on electrically stimulated Col-PPy-CS substrates. Mekonnen et al. (2016) were able to develop conductive Col-PPy hybrid aerogels from animal skin waste, while Ravichandran et al. (2018) were able to produce PPy-collagen based hydrogel capable of sensing glucose levels that would conform to the tissue by using an injection-casting method as a delivery mechanism. Similarly, Ketabat et al. (2017) developed an injectable conductive hydrogel using a collagen-alginate-PPy blend, with favourable viscosity and potential as DIW ink. Although PPy has been combined with other biomaterials, collagen remains a natural choice for creating hybrid blends as it is the most abundant protein in our bodies, provides the bulk structural support to tissue ECMs, and is recognized by most cell types but also due to its polyvalent electrostatic interactions with ECM-based proteins (Higgins et al., 2012). For this reason, collagen was chosen as the scaffolding base in investigations concerning this thesis.

The modifiability of PPy-based constructs affords researchers freedom of movement which not only facilitates modulation of the fabricated construct's physical and chemical properties, but also the subsequent functionalization of the construct, to serve as a static or dynamic construct. This quality has rendered PPy a promising candidate for the creation of platforms capable of temporal control over cellular behaviour, both as standalone constructs and blends/composites. However, despite being shown to be biocompatible and cyto-compatible, fabricated structures are restricted in feature and geometric complexity (Ramanaviciene et al., 2010; Vaitkuviene et al., 2013, 2014; Castano et al., 2004; Wang, Gu, Yuan et al., 2004).

PPy is considered to be insoluble, infusible, and difficult to disperse or maintain as

a nano-dispersion in most organic solvents (Spinks et al., 2009). This has warded off any pursuits for 3D printing PPy-based constructs. However, researchers have seen success with solubilizing PPy in solvents such as DMF, NMP, DMSO, H_2O_2 and m-cresol (Leonavicius et al., 2011; Lee et al., 1995). These solubilized solutions have then been used to produce 2D films and coatings/substrates via chemical oxidation polymerization and subsequent electro-deposition techniques and shown to be of similar absorbance, electro-conductivity and ionic conductivity properties as their electrochemically polymerized counterparts (Lee et al., 1995). One complication from using these solvents is that the viscosity associated with PPy, even when nano-dispersed, is too low for use as a direct write ink (Lee et al., 1995). Additionally, these aforementioned solvents are highly toxic, which further complicates the fabrication process for constructs destined for *in vivo* implantation experiments or *in vitro* cell culture testing. Therefore, the problems associated with PPy processability indicated that any intervention in the polymerization process or measures taken towards adapting an AM technique would have to be introduced either during or prior to polymerization of PPy, or it must be blended with a material where the blend exists as a stable hybrid.

2.7 Chapter summary

This chapter summarized the necessary background knowledge on AM technique used in this thesis, properties associated with the ECM and the cellular micro-environment which have been difficult to emulate *in vitro* in unison, and justifications behind construct compositional elements utilized in this thesis. This chapter discussed past and present relevant research done with collagen and PPy in the context of tissue engineering applications. This chapter discussed challenges associated with adapting AM methodologies to PPy fabrication protocols and provided edification from the current state of the art which sets PPy-based constructs as potential means of imparting electro-

chemomechanical stimulation to cells and studying *in vivo* complexities of the cellular micro-environment in an amalgamated manner.

List of references

Ahadian, S., Ostrovidov, S., Hosseini, V., Kaji, H., Ramalingam, M., Bae, H. and Khademhosseini, A. (2013), 'Electrical stimulation as a biomimicry tool for regulating muscle cell behavior', *Organogenesis* **9**(2), 87–92.

Ahmed, S. and Ikram, S. (2016), 'Chitosan based scaffolds and their applications in wound healing', *Achievements in the Life Sciences* **10**(1), 27–37.

Akhmanova, M., Osidak, E., Domogatsky, S., Rodin, S. and Domogatskaya, A. (2015), 'Physical, spatial, and molecular aspects of extracellular matrix of in vivo niches and artificial scaffolds relevant to stem cells research', *Stem Cells International* pp. 1–35.

Alici, G., Spinks, G., Madden, J., Wu, Y. and Wallace, G. (2008), 'Response characterization of electroactive polymers as mechanical sensors', *IEEE/ASME Transactions on Mechatronics* **13**(2), 187–196.

Ambrosi, A. and Pumera, M. (2016), '3d-printing technologies for electrochemical applications', *Chemical Society Reviews* **45**(10), 2740–2755.

Asplund, M., Thaning, E., Lundberg, J., Sandberg-Nordqvist, A., Kostyszyn, B., Inganäs, O. and Von Holst, H. (2009), 'Toxicity evaluation of pedot/biomolecular composites intended for neural communication electrodes', *Biomedical Materials* **4**(4).

Asti, A. and Gioglio, L. (2014), 'Natural and synthetic biodegradable polymers: Different scaffolds for cell expansion and tissue formation', *The International Journal of Artificial Organs* **37**(3), 187–205.

ASTM Standard ASTM52900 - 15 (2015), *Terminology for Additive Manufacturing Technologies*, ASTM International, West Conshohocken, PA.

Atala, A., Kasper, F. K. and Mikos, A. G. (2012), 'Engineering complex tissues.', *Science Translational Medicine* **4**(160), 160rv12–160rv12.

Ateh, D. D., Navsaria, H. A. and Vadgama, P. (2006), 'Polypyrrole-based conducting polymers and interactions with biological tissues', *Journal of The Royal Society Interface* **3**(11), 741–752.

Ates, M. (2013), 'A review study of (bio)sensor systems based on conducting polymers', *Materials Science & Engineering C* **33**(4), 1853–1859.

Aziz, J., Shezali, H., Radzi, Z., Yahya, N., Abu Kassim, N., Czernuszka, J. and Rahman, M. (2016), 'Molecular mechanisms of stress-responsive changes in collagen and elastin networks in skin', *Skin Pharmacology and Physiology* **29**(4), 190–203.

Bahrami-Samani, M., Cook, C., Madden, J., Spinks, G. and Whitten, P. (2008), 'Quartz crystal microbalance study of volume changes and modulus shift in electrochemically switched polypyrrole', *Thin Solid Films* **516**(9), 2800–2807.

Bajaj, P., Schweller, R. M., Khademhosseini, A., West, J. L. and Bashir, R. (2014), '3D Biofabrication Strategies for Tissue Engineering and Regenerative Medicine', *Annual Review of Biomedical Engineering* **16**(1), 247–276.

Bakarich, S., Gorkin, R., Panhuis, M. and Spinks, G. (2015), '4d printing with mechanically robust, thermally actuating hydrogels', *Macromolecular Rapid Communications* **36**(12), 1211–1217.

Balint, R., Cassidy, N. J. and Cartmell, S. H. (2013), 'Electrical Stimulation: A Novel Tool for Tissue Engineering', *Tissue Engineering Part B: Reviews* **19**(1), 48–57.

Balint, R., Cassidy, N. J. and Cartmell, S. H. (2014), 'Conductive polymers: Towards a smart biomaterial for tissue engineering', *Acta Biomaterialia* **10**(6), 2341–2353.

Barnes, C. P. and Bowlin, G. L. (2007), 'Cross-linking electrospun type ii collagen tissue engineering scaffolds with carbodiimide in ethanol', *Tissue engineering* **13**(7), 1593–1605.

Bay, L., West, K., Sommer-Larsen, P., Skaarup, S. and Benslimane, M. (2003), 'A conducting polymer artificial muscle with 12% linear strain', *Advanced Materials* **15**(4), 310–313.

Bendrea, A.-D., Cianga, L. and Cianga, I. (2011), 'Review paper: Progress in the Field of Conducting Polymers for Tissue Engineering Applications', *Journal of Biomaterials Applications* **26**(1), 3–84.

Berti, F. V., Srisuk, P., da Silva, L. P., Marques, A. P., Reis, R. L. and Correlo, V. M. (2017), 'Synthesis and Characterization of Electroactive Gellan Gum Spongy-Like Hydrogels for Skeletal Muscle Tissue Engineering Applications', *Tissue Engineering Part A* **23**(17-18), 968–979.

Bhadra, S., Khastgir, D., Singha, N. and Lee, J. (2009), 'Progress in preparation, processing and applications of polyaniline', *Progress in Polymer Science (Oxford)* **34**(8), 783–810.

Björninen, M., Siljander, A., Pelto, J., Hyttinen, J., Kellomäki, M., Miettinen, S., Seppänen, R. and Haimi, S. (2014), 'Comparison of Chondroitin Sulfate and Hyaluronic Acid Doped Conductive Polypyrrole Films for Adipose Stem Cells', *Annals of Biomedical Engineering* **42**(9), 1889–1900.

Bonnans, C., Chou, J. and Werb, Z. (2014), 'Remodelling the extracellular matrix in development and disease', *Nature Reviews Molecular Cell Biology* **15**(12), 786–801.

Bornes, T., Jomha, N., Mulet-Sierra, A. and Adesida, A. (2015), 'Hypoxic culture of bone marrow-derived mesenchymal stromal stem cells differentially enhances in vitro chondrogenesis within cell-seeded collagen and hyaluronic acid porous scaffolds', *Stem Cell Research and Therapy* **6**(1).

Burdick, J. and Murphy, W. (2012), 'Moving from static to dynamic complexity in hydrogel design', *Nature Communications* **3**.

Butler, D., Goldstein, S., Guldberg, R., Guo, X., Kamm, R., Laurencin, C., McIntire, L., Mow, V., Nerem, R., Sah, R., Soslowsky, L., Spilker, R. and Tranquillo, R. (2009), 'The impact of biomechanics in tissue engineering and regenerative medicine', *Tissue Engineering - Part B: Reviews* **15**(4), 477–484.

Camci-Unal, G., Annabi, N., Dokmeci, M. R., Liao, R. and Khademhosseini, A. (2014), 'Hydrogels for cardiac tissue engineering', *NPG Asia Materials* **6**(5), e99–e99.

Carpi, F., ed. (2016), *Electromechanically active polymers*, Springer.

Carrow, J., Kerativitayanan, P., Jaiswal, M., Lokhande, G. and Gaharwar, A. (2015), *Polymers for bioprinting*, Elsevier Inc.

Carter, D. and Caler, W. (1985), 'A cumulative damage model for bone fracture', *Journal of Orthopaedic Research* **3**(1), 84–90.

Carvalho, R., Scott, J., Suga, D. and Yen, E. (1994), 'Stimulation of signal transduction pathways in osteoblasts by mechanical strain potentiated by parathyroid hormone', *Journal of Bone and Mineral Research* **9**(7), 999–1011.

Castano, H., O'Rear, E., McFetridge, P. and Sikavitsas, V. (2004), 'Polypyrrole thin films formed by admicellar polymerization support the osteogenic differentiation of mesenchymal stem cells', *Macromolecular bioscience* **4**(8), 785–794.

Cen, L., Liu, W., Cui, L., Zhang, W. and Cao, Y. (2008), 'Collagen tissue engineering: Development of novel biomaterials and applications', *Pediatric Research* **63**(5), 492–496.

Chattopadhyay, S. and Raines, R. (2014), 'Review collagen-based biomaterials for wound healing', *Biopolymers* **101**(8), 821–833.

Chen, F.-M. and Liu, X. (2016), 'Advancing biomaterials of human origin for tissue engineering', *Progress in Polymer Science* **53**, 86–168.

Chevallay, B. and Herbage, D. (2000), 'Collagen-based biomaterials as 3d scaffold for cell cultures: applications for tissue engineering and gene therapy', *Medical and Biological Engineering and Computing* **38**(2), 211–218.

Chia, H. and Wu, B. (2015), 'Recent advances in 3d printing of biomaterials', *Journal of Biological Engineering* **9**(1).

Choi, Y., Choi, J., Woo, C. and Cho, Y. (2014), 'Stem cell delivery systems inspired by tissue-specific niches', *Journal of Controlled Release* **193**, 42–50.

Crapo, P. M., Gilbert, T. W. and Badylak, S. F. (2011), 'An overview of tissue and whole organ decellularization processes', *Biomaterials* **32**(12), 3233–3243.

De Giglio, E., De Gennaro, L., Sabbatini, L. and Zambonin, G. (2001), 'Analytical characterization of collagen- and/or hydroxyapatite-modified polypyrrole films electrosynthesized on ti-substrates for the development of new bioactive surfaces', *Journal of Biomaterials Science, Polymer Edition* **12**(1), 63–76.

Desmouliere, A., Darby, I. A., Laverdet, B. and Bonté, F. (2014), 'Fibroblasts and myofibroblasts in wound healing', *Clinical, Cosmetic and Investigational Dermatology* pp. 301–11.

Donderwinkel, I., van Hest, J. C. M. and Cameron, N. R. (2017), 'Bio-inks for 3D bioprinting: recent advances and future prospects', *Polymer Chemistry* **8**(31), 4451–4471.

Dong, C. and Lv, Y. (2016), 'Application of collagen scaffold in tissue engineering: Recent advances and new perspectives', *Polymers* **8**(2), 42–20.

Durgam, H., Sapp, S., Deister, C., Khaing, Z., Chang, E., Luebben, S. and Schmidt, C. E. (2012), 'Novel Degradable Co-polymers of Polypyrrole Support Cell Proliferation and Enhance Neurite Out-Growth with Electrical Stimulation', *Journal of Biomaterials Science, Polymer Edition* **21**(10), 1265–1282.

Duval, K., Grover, H., Han, L.-H., Mou, Y., Pegoraro, A., Fredberg, J. and Chen, Z. (2017), 'Modeling physiological events in 2d vs. 3d cell culture', *Physiology* **32**(4), 266–277.

Edmondson, R., Broglie, J., Adcock, A. and Yang, L. (2014), 'Three-dimensional cell culture systems and their applications in drug discovery and cell-based biosensors', *Assay and Drug Development Technologies* **12**(4), 207–218.

Ekblom, P. (1995), 'Role of extracellular matrix in animal development - an introduction', *Experientia* **51**(9-10), 851–852.

Elieh-Ali-Komi, D. and Hamblin, M. R. (2016), 'Chitin and chitosan: Production and application of versatile biomedical nanomaterials.', *Int J Adv Res (Indore)* **4**(3), 411–427.

Engler, A., Sen, S., Sweeney, H. and Discher, D. (2006), 'Matrix elasticity directs stem cell lineage specification', *Cell* **126**(4), 677–689.

Fahlgren, A., Bratengeier, C., Gelmi, A., Semeins, C. M., Klein-Nulend, J., Jager, E. W. H. and Bakker, A. D. (2015), 'Biocompatibility of polypyrrole with human primary osteoblasts and the effect of dopants', *PLoS ONE* **10**(7), e0134023–17.

Farajollahi, M., Woehling, V., Plesse, C., Nguyen, G. T. M., Vidal, F., Sassani, F., Yang, V. X. D. and Madden, J. D. W. (2016), 'Self-contained tubular bending actuator driven by conducting polymers', *Sensors & Actuators: A. Physical* **249**, 45–56.

Fattahi, P., Yang, G., Kim, G. and Abidian, M. (2014), 'A review of organic and inorganic biomaterials for neural interfaces', *Advanced Materials* **26**(12), 1846–1885.

Fedorovich, N., De Wijn, J., Verbout, A., Alblas, J. and Dhert, W. (2008), 'Three-dimensional fiber deposition of cell-laden, viable, patterned constructs for bone tissue printing', *Tissue Engineering - Part A.* **14**(1), 127–133.

Fedorovich, N., Kuipers, E., Gawlitta, D., Dhert, W. and Alblas, J. (2011), 'Scaffold porosity and oxygenation of printed hydrogel constructs affect functionality of embedded osteogenic progenitors', *Tissue Engineering - Part A* **17**(19-20), 2473–2486.

Feldberg, S. (1984), 'Reinterpretation of polypyrrole electrochemistry. consideration of capacitive currents in redox switching of conducting polymers', *Journal of the American Chemical Society* **106**(17), 4671–4674.

Firme III, C. and Bandaru, P. (2010), 'Toxicity issues in the application of carbon nanotubes to biological systems', *Nanomedicine: Nanotechnology, Biology, and Medicine* **6**(2), 245–256.

Fonner, J. M., Forciniti, L., Nguyen, H., Byrne, J. D., Kou, Y.-F., Syeda-Nawaz, J. and Schmidt, C. E. (2008), 'Biocompatibility implications of polypyrrole synthesis techniques', *Biomedical Materials* **3**(3), 034124–13.

Forciniti, L., Ybarra III, J., Zaman, M. H. and Schmidt, C. E. (2014), 'Schwann cell response on polypyrrole substrates upon electrical stimulation', *Acta Biomaterialia* **10**(6), 2423–2433.

Friess, W. (1998), 'Collagen - biomaterial for drug delivery', *European Journal of Pharmaceutics and Biopharmaceutics* **45**(2), 113–136.

Frost, H. (1994), 'Wolff's law and bone's structural adaptations to mechanical usage: an overview for clinicians.', *Angle Orthodontist* **64**(3), 175–188.

Fung, Y. (1983), 'On the foundations of biomechanics', *Journal of Applied Mechanics, Transactions ASME* **50**(4), 1003–1009.

Galban, C. and Locke, B. (1997), 'Analysis of cell growth in a polymer scaffold using a moving boundary approach', *Biotechnology and Bioengineering* **56**(4), 422–432.

Gangopadhyay, R. and Molla, M. R. (2011), 'Polypyrrole-polyvinyl alcohol stable nanodispersion: A prospective conducting black ink', *Journal of Polymer Science Part B: Polymer Physics* **49**(11), 792–800.

Ganji, Y., Li, Q., Quabius, E., Böttner, M., Selhuber-Unkel, C. and Kasra, M. (2016), 'Cardiomyocyte behavior on biodegradable polyurethane/gold nanocomposite scaffolds under electrical stimulation', *Materials Science and Engineering C* **59**, 10–18.

Gelmi, A., Cieslar-Pobuda, A., de Muinck, E., Los, M., Rafat, M. and Jager, E. W. H. (2016), 'Direct Mechanical Stimulation of Stem Cells: A Beating Electromechanically Active Scaffold for Cardiac Tissue Engineering', *Advanced Healthcare Materials* **5**(12), 1471–1480.

Gelse, K. (2003), 'Collagens—structure, function, and biosynthesis', *Advanced Drug Delivery Reviews* **55**(12), 1531–1546.

Genies, E., Bidan, G. and Diaz, A. (1983), 'Spectroelectrochemical study of polypyrrole films', *Journal of Electroanalytical Chemistry* **149**(1-2), 101–113.

George, P., Lavan, D., Burdick, J., Chen, C.-Y., Liang, E. and Langer, R. (2006), 'Electrically controlled drug delivery from biotin-doped conductive polypyrrole', *Advanced Materials* **18**(5), 577–581.

George, P., Lyckman, A., Lavan, D., Hegde, A., Leung, Y., Avasare, R., Testa, C., Alexander, P., Langer, R. and Sur, M. (2005), 'Fabrication and biocompatibility of polypyrrole implants suitable for neural prosthetics', *Biomaterials* **26**(17), 3511–3519.

Gilmore, K. J., Kita, M., Han, Y., Gelmi, A., Higgins, M. J., Moulton, S. E., Clark, G. M., Kapsa, R. and Wallace, G. G. (2009), 'Skeletal muscle cell proliferation and differentiation on polypyrrole substrates doped with extracellular matrix components', *Biomaterials* **30**(29), 5292–5304.

Gordon, M. and Hahn, R. (2010), 'Collagens', *Cell and Tissue Research* **339**(1), 247–257.

Green, R., Lovell, N., Wallace, G. and Poole-Warren, L. (2008), 'Conducting polymers for neural interfaces: Challenges in developing an effective long-term implant', *Biomaterials* **29**(24-25), 3393–3399.

Guarino, V., Causa, F. and Ambrosio, L. (2007), 'Bioactive scaffolds for bone and ligament tissue', *Expert Review of Medical Devices* **4**(3), 405–418.

Gudapati, H., Dey, M. and Ozbolat, I. (2016), 'A comprehensive review on droplet-based bioprinting: Past, present and future', *Biomaterials* **102**, 20–42.

Guillemot, F., Mironov, V. and Nakamura, M. (2010), 'Bioprinting is coming of age: report from the International Conference on Bioprinting and Biofabrication in Bordeaux (3B'09)', *Biofabrication* **2**(1), 010201–7.

Guimard, N. K. (2008), Biodegradable electroactive materials for tissue engineering applications, PhD thesis, The University of Texas at Austin.

Guiseppi-Elie, A. (2010), 'Electroconductive hydrogels: Synthesis, characterization and biomedical applications', *Biomaterials* **31**(10), 2701–2716.

Gurunathan, S. and Kim, J.-H. (2016), 'Synthesis, toxicity, biocompatibility, and biomedical applications of graphene and graphene-related materials', *International Journal of Nanomedicine* **11**, 1927–1945.

Haaparanta, A.-M., Järvinen, E., Cengiz, I., Ellä, V., Kokkonen, H., Kiviranta, I. and Kellomäki, M. (2014), 'Preparation and characterization of collagen/pla, chitosan/pla, and collagen/chitosan/pla hybrid scaffolds for cartilage tissue engineering', *Journal of Materials Science: Materials in Medicine* **25**(4), 1129–1136.

Hamill, O. and Martinac, B. (2001), 'Molecular basis of mechanotransduction in living cells', *Physiological Reviews* **81**(2), 685–740.

Hanasono, M., Skoracki, R. and Yu, P. (2010), 'A prospective study of donor-site morbidity after anterolateral thigh fasciocutaneous and myocutaneous free flap harvest in 220 patients', *Plastic and Reconstructive Surgery* **125**(1), 209–214.

Heinze, J., Frontana-Uribe, B. A. and Ludwigs, S. (2010), 'Electrochemistry of Conducting Polymers—Persistent Models and New Concepts †', *Chemical Reviews* **110**(8), 4724–4771.

Higgins, M., Molino, P., Yue, Z. and Wallace, G. (2012), 'Organic conducting polymer-protein interactions', *Chemistry of Materials* **24**(5), 828–839.

Hinton, T. J., Jallerat, Q., Palchesko, R. N., Park, J. H., Grodzicki, M. S., Shue, H. J., Ramadan, M. H., Hudson, A. R. and Feinberg, A. W. (2015), 'Three-dimensional printing of complex biological structures by freeform reversible embedding of suspended hydrogels', *Science Advances* **1**(9), e1500758–e1500758.

Hinz, B. (2009), 'Tissue stiffness, latent tgf-β1 activation, and mechanical signal transduction: implications for the pathogenesis and treatment of fibrosis', *Current rheumatology reports* **11**(2), 120.

Hu, W.-W., Hsu, Y.-T., Cheng, Y.-C., Li, C., Ruaan, R.-C., Chien, C.-C., Chung, C.-A. and Tsao, C.-W. (2014), 'Electrical stimulation to promote osteogenesis using conductive polypyrrole films', *Materials Science & Engineering C* **37**(C), 28–36.

Huang, G., Li, F., Zhao, X., Ma, Y., Li, Y., Lin, M., Jin, G., Lu, T. J., Genin, G. M. and Xu, F. (2017), 'Functional and Biomimetic Materials for Engineering of the Three-Dimensional Cell Microenvironment', *Chemical Reviews* **117**(20), 12764–12850.

Huang, H.-Y. and Tang, Q.-Q. (2012), *Differentiation of mesenchymal stem cells into adipocyte lineage: Role of cytoskeleton-associated proteins*, Springer Netherlands.

Huang, W., Humphrey, B. and MacDiarmid, A. (1986), 'Polyaniline, a novel conducting polymer. morphology and chemistry of its oxidation and reduction in aqueous electrolytes', *Journal of the Chemical Society, Faraday Transactions 1: Physical Chemistry in Condensed Phases* **82**(8), 2385–2400.

Hubmacher, D. and Apte, S. (2013), 'The biology of the extracellular matrix: Novel insights', *Current Opinion in Rheumatology* **25**(1), 65–70.

Humphrey, J. D., Dufresne, E. R. and Schwartz, M. A. (2014), 'Mechanotransduction and extracellular matrix homeostasis', *Nature Reviews Molecular Cell Biology* **15**(12), 802–812.

Hur, J., Im, K., Kim, S. W., Kim, J., Chung, D.-Y., Kim, T.-H., Jo, K. H., Hahn, J. H., Bao, Z., Hwang, S. and Park, N. (2014), 'Polypyrrole/Agarose-Based Electronically Conductive and Reversibly Restorable Hydrogel', *ACS Nano* **8**(10), 10066–10076.

Hutmacher, D., Schantz, T., Zein, I., Ng, K., Teoh, S. and Tan, K. (2001), 'Mechanical properties and cell cultural response of polycaprolactone scaffolds designed and fabricated via fused deposition modeling', *Journal of Biomedical Materials Research* **55**(2), 203–216.

Hynes, R. and Naba, A. (2012), 'Overview of the matrisome-an inventory of extracellular matrix constituents and functions', *Cold Spring Harbor Perspectives in Biology* **4**(1).

Inzana, J., Olvera, D., Fuller, S., Kelly, J., Graeve, O., Schwarz, E., Kates, S. and Awad, H. (2014), '3d printing of composite calcium phosphate and collagen scaffolds for bone regeneration', *Biomaterials* **35**(13), 4026–4034.

Ismail, Y. A., Martínez, J. G., Harrasi, A. S. A., Kim, S. J. and Otero, T. F. (2011), 'Sensing characteristics of a conducting polymer/hydrogel hybrid microfiber artificial muscle', *Sensors and Actuators B: Chemical* **160**(1), 1180 – 1190.

Jager, E. (2013), Conducting polymer actuators for medical devices and cell mechanotransduction, *in* '2013 IEEE/ASME International Conference on Advanced Intelligent Mechatronics', pp. 1–7.

Jager, E., Smela, E., Inganäs, O. and Lundström, I. (1999*a*), 'Polypyrrole microactuators', *Synthetic Metals* **102**(1-3), 1309–1310.

Jager, E. W., Smela, E., Inganas, O. and Lundstrom, I. (1999*b*), Applications of polypyrrole microactuators, *in* 'Polypyrrole microactuators', Vol. 3669, Society of Photo-Optical Instrumentation Engineers, Bellingham, WA, United States, pp. 377–384.

Jang, J., Kim, T., Kim, B., Kim, S.-W., Kwon, S.-M. and Cho, D.-W. (2016), 'Tailoring mechanical properties of decellularized extracellular matrix bioink by vitamin b2-induced photo-crosslinking', *Acta Biomaterialia* **33**, 88–95.

Jansen, K. A., Atherton, P. and Ballestrem, C. (2017), 'Mechanotransduction at the cell-matrix interface', *Seminars in Cell and Developmental Biology* **71**, 75–83.

Jayamurgan, P., Ponnuswamy, V., Ashokan, S. and Mahalingam, T. (2013), 'The effect of dopant on structural, thermal and morphological properties of DBSA-doped polypyrrole', *Iranian Polymer Journal* **22**(3), 219–225.

Jenniskens, G. J., Veerkamp, J. H. and van Kuppevelt, T. H. (2005), 'Heparan sulfates in skeletal muscle development and physiology', *Journal of Cellular Physiology* **206**(2), 283–294.

Jia, L., Prabhakaran, M., Qin, X. and Ramakrishna, S. (2013), 'Stem cell differentiation on electrospun nanofibrous substrates for vascular tissue engineering', *Materials Science and Engineering C* **33**(8), 4640–4650.

Jin, J., Huang, Z., Yin, G., Yang, A. and Tang, S. (2015), 'Fabrication of polypyrrole/proteins composite film and their electro-controlled release for axons outgrowth', *Electrochimica Acta* **185**(C), 172–177.

Jose, R. R., Rodriguez, M. J., Dixon, T. A., Omenetto, F. and Kaplan, D. L. (2016), 'Evolution of Bioinks and Additive Manufacturing Technologies for 3D Bioprinting', *ACS Biomaterials Science & Engineering* **2**(10), 1662–1678.

Kaneto, K., Takayanagi, K., Tominaga, K. and Takashima, W. (2012), How to improve electrochemomechanical strain in conducting polymers, *in* 'Electroactive Polymer Actuators and Devices (EAPAD)', Vol. 8340, SPIE.

Kang, H. W., Lee, S. J., Ko, I. K., Kengla, C., Yoo, J. J. and Atala, A. (2016), 'A 3D bioprinting system to produce human-scale tissue constructs with structural integrity', *Nature Biotechnology* **34**(3), 312–319.

Kessenbrock, K., Plaks, V. and Werb, Z. (2010), 'Matrix Metalloproteinases: Regulators of the Tumor Microenvironment', *Cell* **141**(1), 52–67.

Ketabat, F., Karkhaneh, A., Aghdam, R. M. and Tafti, S. H. A. (2017), 'Injectable conductive collagen/alginate/ polypyrrole hydrogels as a biocompatible system for biomedical applications', *Journal of Biomaterials Science, Polymer Edition* pp. 0–0.

Khaldi, A., Maziz, A., Alici, G., Spinks, G. M. and Jager, E. W. H. (2016), 'Bottom-up microfabrication process for individually controlled conjugated polymer actuators', *Sensors & Actuators: B. Chemical* **230**, 818–824.

Khor, E., Li, H. and Wee, A. (1996), 'Animal tissue-polypyrrole hybrid biomaterials: Shrinkage temperature evaluation', *Biomaterials* **17**(19), 1877–1879.

Kiefer, R., Temmer, R., Aydemir, N., Travas-Sejdic, J., Aabloo, A. and Tamm, T. (2014), 'Electrochemistry of interlayer supported polypyrrole tri-layer linear actuators', *Electrochimica Acta* **122**, 322–328.

Kim, I. G., Gil, C.-H., Seo, J., Park, S.-J., Subbiah, R., Jung, T.-H., Kim, J. S., Jeong, Y.-H., Chung, H.-M., Lee, J. H., Lee, M. R., Moon, S.-H. and Park, K. (2018), 'Mechanotransduction of human pluripotent stem cells cultivated on tunable cell-derived extracellular matrix', *Biomaterials* **150**, 100–111.

Kim, J., Deshpande, S. D., Yun, S. and Li, Q. (2006), 'A Comparative Study of Conductive Polypyrrole and Polyaniline Coatings on Electro-Active Papers', *Polymer Journal* **38**(7), 659–668.

Kim, J., Kim, S. and Jung, Y. (2016), 'Current status of three-dimensional printing inks for soft tissue regeneration', *Tissue Engineering and Regenerative Medicine* **13**(6), 636–646.

Kivilo, A., Zondaka, Z., Kesküla, A., Rasti, P., Tamm, T. and Kiefer, R. (2016), 'Electro-chemo-mechanical deformation properties of polypyrrole/dodecylbenzenesulfate linear actuators in aqueous and organic electrolyte', *RSC Advances* **6**(99), 96484–96489.

Koetting, M., Peters, J., Steichen, S. and Peppas, N. (2015), 'Stimulus-responsive hydrogels: Theory, modern advances, and applications', *Materials Science and Engineering R: Reports* **93**, 1–49.

Kohavi, D., Pollack, S. and Brighton, C. (1992), 'Short-tern effect of guided bone regeneration and electrical stimulation on bone growth in a surgically modelled resorbed dog mandibular ridge', *Biomaterials, Artificial Cells and Immobilization Biotechnology* **20**(1), 131–138.

Kontturi, K., Pentti, P. and Sundholm, G. (1998), 'Polypyrrole as a model membrane for drug delivery', *Journal of Electroanalytical Chemistry* **453**(1-2), 231–238.

Kontturi, L.-S., Järvinen, E., Muhonen, V., Collin, E., Pandit, A., Kiviranta, I., Yliperttula, M. and Urtti, A. (2014), 'An injectable, in situ forming type ii collagen/hyaluronic acid hydrogel vehicle for chondrocyte delivery in cartilage tissue engineering', *Drug Delivery and Translational Research* **4**(2), 149–158.

Koopmans, G., Hasse, B. and Sinis, N. (2009), 'The role of collagen in peripheral nerve repair', *International review of neurobiology* **87**, 363–379.

Kunzmann, A., Andersson, B., Thurnherr, T., Krug, H., Scheynius, A. and Fadeel, B. (2011), 'Toxicology of engineered nanomaterials: Focus on biocompatibility, biodistribution and biodegradation', *Biochimica et Biophysica Acta - General Subjects* **1810**(3), 361–373.

Kupila, E.-L. and Kankare, J. (1995), 'Influence of electrode pretreatment, counter anions

and additives on the electropolymerization of pyrrole in aqueous solutions', *Synthetic Metals* **74**(3), 241–249.

Lam, Y., Chow, K. and Khor, E. (1999), 'Preparation and characterization of covalently bonded biopolymer-polypyrrole hybrid materials', *Journal of Polymer Research* **6**(4), 203–210.

Landers, R., Hübner, U., Schmelzeisen, R. and Mülhaupt, R. (2002), 'Rapid prototyping of scaffolds derived from thermoreversible hydrogels and tailored for applications in tissue engineering', *Biomaterials* **23**(23), 4437–4447.

Lane, S. W., Williams, D. A. and Watt, F. M. (2014), 'Modulating the stem cell niche for tissue regeneration', *Nature Biotechnology* **32**(8), 795–803.

Lee, J., Kim, D. and Kim, C. (1995), 'Synthesis of soluble polypyrrole of the doped state in organic solvents', *Synthetic Metals* **74**(2), 103–106.

Lee, J. Y., Bashur, C. A., Goldstein, A. S. and Schmidt, C. E. (2009), 'Polypyrrole-coated electrospun PLGA nanofibers for neural tissue applications', *Biomaterials* **30**(26), 4325–4335.

Lee, S., Liu, J., Oh, S., Soker, S., Atala, A. and Yoo, J. (2008), 'Development of a composite vascular scaffolding system that withstands physiological vascular conditions', *Biomaterials* **29**(19), 2891–2898.

Leonavicius, K., Ramanaviciene, A. and Ramanavicius, A. (2011), 'Polymerization model for hydrogen peroxide initiated synthesis of polypyrrole nanoparticles', *Langmuir* **27**(17), 10970–10976.

Li, H. and Khor, E. (1994), 'Interaction of collagen with polypyrrole in the production of hybrid materials', *Polymer International* **35**(1), 53–59.

Lindsey, R., Grobman, J., Leggon, R., Panjabi, M. and Friedlaender, G. (1987), 'Effects of bone graft and electrical stimulation on the strength of healing bony defects in dogs', *Clinical Orthopaedics and Related Research* **222**, 275–280.

Liu, L., Li, P., Zhou, G., Wang, M., Jia, X., Liu, M., Niu, X., Song, W., Liu, H. and Fan, Y. (2013), 'Increased proliferation and differentiation of pre-osteoblasts mc3t3-e1 cells on nanostructured polypyrrole membrane under combined electrical and mechanical stimulation', *Journal of Biomedical Nanotechnology* **9**(9), 1532–1539.

Liu, X., Yue, Z., Higgins, M. J. and Wallace, G. G. (2011), 'Conducting polymers with immobilised fibrillar collagen for enhanced neural interfacing', *Biomaterials* **32**(30), 7309–7317.

Lo, C.-M., Wang, H.-B., Dembo, M. and Wang, Y.-L. (2000), 'Cell movement is guided by the rigidity of the substrate', *Biophysical Journal* **79**(1), 144–152.

Long, K., Liu, Y., Li, W., Wang, L., Liu, S., Wang, Y., Wang, Z. and Ren, L. (2015), 'Improving the mechanical properties of collagen-based membranes using silk fibroin for corneal tissue engineering', *Journal of Biomedical Materials Research - Part A* **103**(3), 1159–1168.

Love, M., Palee, S., Chattipakorn, S. and Chattipakorn, N. (2018), 'Effects of electrical stimulation on cell proliferation and apoptosis', *Journal of Cellular Physiology* **233**(3), 1860–1876.

Lu, P., Weaver, V. and Werb, Z. (2012), 'The extracellular matrix: A dynamic niche in cancer progression', *Journal of Cell Biology* **196**(4), 395–406.

Lundin, V., Herland, A., Berggren, M., Jager, E. W. H. and Teixeira, A. I. (2011), 'Control of Neural Stem Cell Survival by Electroactive Polymer Substrates', *PLoS ONE* **6**(4), e18624–8.

Machida, S., Miyata, S. and Techagumpuch, A. (1989), 'Chemical synthesis of highly electrically conductive polypyrrole', *Synthetic Metals* **31**(3), 311–318.

Madden, J., Cush, R., Kanigan, T. and Hunter, I. (2000), 'Fast contracting polypyrrole actuators', *Synthetic Metals* **113**(1), 185–192.

Madden, P. G. A., Madden, J. D. W., Anquetil, P. A., Vandesteeg, N. A. and Hunter, I. W. (2004), 'The Relation of Conducting Polymer Actuator Material Properties to Performance', *IEEE Journal of Oceanic Engineering* **29**(3), 696–705.

Maller, O., Martinson, H. and Schedin, P. (2010), 'Extracellular Matrix Composition Reveals Complex and Dynamic Stromal-Epithelial Interactions in the Mammary Gland', *Journal of Mammary Gland Biology and Neoplasia* **15**(3), 301–318.

Mammoto, T. and Ingber, D. (2010), 'Mechanical control of tissue and organ development', *Development* **137**(9), 1407–1420.

Marastoni, S., Ligresti, G., Lorenzon, E., Colombatti, A. and Mongiat, M. (2008), 'Extracellular matrix: A matter of life and death', *Connective Tissue Research* **49**(3-4), 203–206.

Mattioli-Belmonte, M., Giavaresi, G., Biagini, G., Virgili, L., Giacomini, M., Fini, M., Giantomassi, F., Natali, D., Torricelli, P. and Giardino, R. (2003), 'Tailoring biomaterial compatibility: In vivo tissue response versus in vitro cell behavior', *International Journal of Artificial Organs* **26**(12), 1077–1085.

McCaig, C., Rajnicek, A., Song, B. and Zhao, M. (2005), 'Controlling cell behavior electrically: Current views and future potential', *Physiological Reviews* **85**(3), 943–978.

McMillan, J. R., Akiyama, M. and Shimizu, H. (2003), 'Epidermal basement membrane

zone components: ultrastructural distribution and molecular interactions', *Journal of Dermatological Science* **31**(3), 169–177.

Meimandi-Parizi, A., Oryan, A. and Moshiri, A. (2013), 'Role of tissue engineered collagen based tridimensional implant on the healing response of the experimentally induced large achilles tendon defect model in rabbits: A long term study with high clinical relevance', *Journal of Biomedical Science* **20**(1).

Mekonnen, B. T., Ragothaman, M., Kalirajan, C. and Palanisamy, T. (2016), 'Conducting collagen-polypyrrole hybrid aerogels made from animal skin waste', *RSC Advances* **6**, 63071–63077.

Melchels, F. P. W., Domingos, M. A. N., Klein, T. J., Malda, J., Bartolo, P. J. and Hutmacher, D. W. (2012), 'Additive manufacturing of tissues and organs', *Progress in Polymer Science* **37**(8), 1079–1104.

Mihic, A., Cui, Z., Wu, J., Vlacic, G., Miyagi, Y., Li, S.-H., Lu, S., Sung, H.-W., Weisel, R. and Li, R.-K. (2015), 'A conductive polymer hydrogel supports cell electrical signaling and improves cardiac function after implantation into myocardial infarct', *Circulation* **132**(8), 772–784.

Miller, L. and Zhou, Q. (1987), 'Poly(n-methylpyrrolylium) poly(styrenesulfonate): A conductive, electrically switchable cation exchanger that cathodically binds and anodically releases dopamine', *Macromolecules* **20**(7), 1594–1597.

Molino, P. J., Zhang, B., Wallace, G. G. and Hanks, T. W. (2013), 'Surface modification of polypyrrole/biopolymer composites for controlled protein and cellular adhesion', *Biofouling* **29**(10), 1155–1167.

Moore, K. and Lemischka, I. (2006), 'Stem cells and their niches', *Science* **311**(5769), 1880–1885.

Mouw, J., Ou, G. and Weaver, V. (2014), 'Extracellular matrix assembly: A multiscale deconstruction', *Nature Reviews Molecular Cell Biology* **15**(12), 771–785.

Mullender, M., El Haj, A. J., Yang, Y., van Duin, M. A., Burger, E. H. and Klein-Nulend, J. (2004), 'Mechanotransduction of bone cells in vitro: Mechanobiology of bone tissue', *Medical and Biological Engineering and Computing* **42**(1), 14–21.

Murphy, S. V. and Atala, A. (2014), '3D bioprinting of tissues and organs', *Nature Publishing Group* **32**(8), 773–785.

Nadgorny, M., Xiao, Z., Chen, C. and Connal, L. (2016), 'Three-dimensional printing of ph-responsive and functional polymers on an affordable desktop printer', *ACS Applied Materials and Interfaces* **8**(42), 28946–28954.

Ngan F Huang, N. L. and Li, S. (2017), *Engineering Stem Cells for Tissue Regeneration*, Vol. 1, 1 edn, World Scientific Publishing Company.

Ngo, T. D., Kashani, A., Imbalzano, G., Nguyen, K. T. Q. and Hui, D. (2018), 'Additive manufacturing (3d printing): A review of materials, methods, applications and challenges', *Composites Part B* **143**, 172–196.

Nocera, A., Comín, R., Salvatierra, N. and Cid, M. (2018), 'Development of 3d printed fibrillar collagen scaffold for tissue engineering', *Biomedical Microdevices* **20**(2).

Offeddu, G., Ashworth, J., Cameron, R. and Oyen, M. (2015), 'Multi-scale mechanical response of freeze-dried collagen scaffolds for tissue engineering applications', *Journal of the Mechanical Behavior of Biomedical Materials* **42**, 19–25.

Otero, T. and Boyano, I. (2003), 'Comparative study of conducting polymers by the escr model', *Journal of Physical Chemistry B* **107**(28), 6730–6738.

Otero, T. F. (2018), 'Artificial muscles driven by the cooperative actuation of electro-chemical molecular machines. Persistent discrepancies and challenges', *International Journal of Smart and Nano Materials* **00**(00), 1–19.

Otero, T. F. and Martinez, J. G. (2016), 'Electro-chemo-biomimetics from conducting polymers: fundamentals, materials, properties and devices', *Journal of Materials Chemistry B* **4**(12), 2069–2085.

Ouyang, J. (2018), 'Recent advances of intrinsically conductive polymers', *Wuli Huaxue Xuebao/ Acta Physico - Chimica Sinica* **34**(11), 1211–1220.

Ozbolat, I. T. and Hospodiuk, M. (2016), 'Current advances and future perspectives in extrusion-based bioprinting', *Biomaterials* **76**, 321–343.

Park, J. Y., Choi, J.-C., Shim, J.-H., Lee, J.-S., Park, H., Kim, S. W., Doh, J. and Cho, D.-W. (2014), 'A comparative study on collagen type I and hyaluronic acid dependent cell behavior for osteochondral tissue bioprinting', *Biofabrication* **6**(3), 035004–12.

Park, S., Kang, Y. J. and Majd, S. (2015), 'A Review of Patterned Organic Bioelectronic Materials and their Biomedical Applications', *Advanced Materials* **27**(46), 7583–7619.

Pati, F., Ha, D.-H., Jang, J., Han, H. H., Rhie, J.-W. and Cho, D.-W. (2015), 'Biomimetic 3D tissue printing for soft tissue regeneration', *Biomaterials* **62**(C), 164–175.

Pati, F., Song, T.-H., Rijal, G., Jang, J., Kim, S. W. and Cho, D.-W. (2015), 'Ornamenting 3D printed scaffolds with cell-laid extracellular matrix for bone tissue regeneration', *Biomaterials* **37**(C), 230–241.

Patra, S. and Young, V. (2016), 'A Review of 3D Printing Techniques and the Future in Biofabrication of Bioprinted Tissue', *Cell Biochemistry and Biophysics* **74**(2), 93–98.

Pei, Q. and Qian, R. (1991), 'Protonation and deprotonation of polypyrrole chain in aqueous solutions', *Synthetic Metals* **45**(1), 35–48.

Pei, Q. and Qian, R. (1992), 'Electrochemical polymerization of pyrrole in aqueous buffer solutions', *Journal of Electroanalytical Chemistry* **322**(1-2), 153–166.

Pernaut, J.-M. and Reynolds, J. (2000), 'Use of conducting electroactive polymers for drug delivery and sensing of bioactive molecules. a redox chemistry approach', *Journal of Physical Chemistry B* **104**(17), 4080–4090.

Perris, R. (1997), 'The extracellular matrix in neural crest-cell migration', *Trends in Neurosciences* **20**(1), 23–31.

Pillay, V., Tsai, T.-S., Choonara, Y., Du Toit, L., Kumar, P., Modi, G., Naidoo, D., Tomar, L., Tyagi, C. and Ndesendo, V. (2014), 'A review of integrating electroactive polymers as responsive systems for specialized drug delivery applications', *Journal of Biomedical Materials Research - Part A* **102**(6), 2039–2054.

Pishko, M. and Amirpour, M. (1998), 'Influence of biomaterial topography on neovascularization of surrounding tissue', *FASEB Journal* **12**(5), A733.

Posey, F. (1966), 'Theory of potentiostatic and galvanostatic charging of the double layer in porous electrodes', *Journal of the Electrochemical Society* **113**(2), 176–184.

Prabhakaran, M., Ghasemi-Mobarakeh, L. and Ramakrishna, S. (2011), 'Electrospun composite nanofibers for tissue regeneration.', *Journal of nanoscience and nanotechnology* **11**(4), 3039–3057.

Radisic, M., Park, H., Shing, H., Consi, T., Schoen, F., Langer, R., Freed, L. and Vunjak-Novakovic, G. (2004), 'Functional assembly of engineered myocardium by electrical stimulation of cardiac myocytes cultured on scaffolds', *Proceedings of the National Academy of Sciences of the United States of America* **101**(52), 18129–18134.

Ramanaviciene, A., Kausaite, A., Tautkus, S. and Ramanavicius, A. (2010), 'Biocom-

patibility of polypyrrole particles: an in-vivo study in mice', *Journal of Pharmacy and Pharmacology* **59**(2), 311–315.

Ramanavicius, A., Habermuller, K., Csöregi, E., Laurinavicius, V. and Schuhmann, W. (1999), 'Polypyrrole-entrapped quinohemoprotein alcohol dehydrogenase. evidence for direct electron transfer via conducting-polymer chains', *Analytical Chemistry* **71**(16), 3581–3586.

Ravichandran, R., Martinez, J., Jager, E., Phopase, J. and Turner, A. (2018), 'Type i collagen-derived injectable conductive hydrogel scaffolds as glucose sensors', *ACS Applied Materials and Interfaces* **10**(19), 16244–16249.

Rhee, S., Puetzer, J. L., Mason, B. N., Reinhart-King, C. A. and Bonassar, L. J. (2016), '3D Bioprinting of Spatially Heterogeneous Collagen Constructs for Cartilage Tissue Engineering', *ACS Biomaterials Science & Engineering* **2**(10), 1800–1805.

Rieu, C., Picaut, L., Mosser, G. and Trichet, L. (2017), 'From tendon injury to collagen-based tendon regeneration: Overview and recent advances', *Current Pharmaceutical Design* **23**(24), 3483–3506.

Rockwood, D., Preda, R., Yücel, T., Wang, X., Lovett, M. and Kaplan, D. (2011), 'Materials fabrication from bombyx mori silk fibroin', *Nature Protocols* **6**(10), 1612–1631.

Rosso, F., Giordano, A., Barbarisi, M. and Barbarisi, A. (2004), 'From cell-ecm interactions to tissue engineering', *Journal of Cellular Physiology* **199**(2), 174–180.

Roth, B. (1994), 'Mechanisms for electrical stimulation of excitable tissue', *Critical Reviews in Biomedical Engineering* **22**(3-4), 253–305.

Rowlands, A., Hudson, J. and Cooper-White, J. (2007), 'From scrawny to brawny:

The quest for neomusculogenesis; smart surfaces and scaffolds for muscle tissue engineering', *Expert Review of Medical Devices* **4**(5), 709–728.

Rowlands, A. S. and Cooper-White, J. J. (2008), 'Directing phenotype of vascular smooth muscle cells using electrically stimulated conducting polymer', *Biomaterials* **29**(34), 4510–4520.

Sabouraud, G., Sadki, S. and Brodie, N. (2000), 'The mechanisms of pyrrole electropolymerization', *Chemical Society Reviews* **29**(5), 283–293.

Salmón, M., Kanazawa, K. K., Diaz, A. F. and Krounbi, M. (1982), 'A chemical route to pyrrole polymer films', *Journal of Polymer Science: Polymer Letters Edition* **20**(3), 187–193.

Sannes, P. L. and Wang, J. (2009), 'Basement Membranes and Pulmonary Development', *Experimental Lung Research* **23**(2), 101–108.

Sarker, B., Hum, J., Nazhat, S. and Boccaccini, A. (2015), 'Combining collagen and bioactive glasses for bone tissue engineering: A review', *Advanced Healthcare Materials* **4**(2), 176–194.

Scadden, D. (2006), 'The stem-cell niche as an entity of action', *Nature* **441**(7097), 1075–1079.

Schuppan, D., Ruehl, M., Somasundaram, R. and Hahn, E. (2001), 'Matrix as a modulator of hepatic fibrogenesis', *Seminars in Liver Disease* **21**(3), 351–372.

Seil, J. and Webster, T. (2010), 'Electrically active nanomaterials as improved neural tissue regeneration scaffolds', *Wiley Interdisciplinary Reviews: Nanomedicine and Nanobiotechnology* **2**(6), 635–647.

Sharma, M., Waterhouse, G. I. N., Loader, S. W. C., Garg, S. and Svirskis, D. (2013),

'High surface area polypyrrole scaffolds for tunable drug delivery', *International Journal of Pharmaceutics* **443**(1-2), 163–168.

Shi, Z., Gao, H., Feng, J., Ding, B., Cao, X., Kuga, S., Wang, Y., Zhang, L. and Cai, J. (2014), 'In situ synthesis of robust conductive cellulose/polypyrrole composite aerogels and their potential application in nerve regeneration', *Angewandte Chemie - International Edition* **53**(21), 5380–5384.

Shi, Z., Gao, X., Ullah, M., Li, S., Wang, Q. and Yang, G. (2016), 'Electroconductive natural polymer-based hydrogels', *Biomaterials* **111**, 40–54.

Shin, J., Choi, E., Cho, J., Cho, A.-N., Jin, Y., Yang, K., Song, C. and Cho, S.-W. (2017), 'Three-dimensional electroconductive hyaluronic acid hydrogels incorporated with carbon nanotubes and polypyrrole by catechol-mediated dispersion enhance neurogenesis of human neural stem cells', *Biomacromolecules* **18**(10), 3060–3072.

Shoa, T., Madden, J., Mirfakhrai, T., Alici, G., Spinks, G. and Wallace, G. (2010), 'Electromechanical coupling in polypyrrole sensors and actuators', *Sensors and Actuators, A: Physical* **161**(1-2), 127–133.

Singh, S., Afara, I. O., Tehrani, A. H. and Oloyede, A. (2015), 'Effect of decellularization on the load-bearing characteristics of articular cartilage matrix', *Tissue Engineering and Regenerative Medicine* **12**(5), 294–305.

Skardal, A., Mack, D., Atala, A. and Sokern, S. (2012), 'Substrate elasticity controls cell proliferation, surface marker expression and motile phenotype in amniotic fluid-derived stem cells', *Journal of the Mechanical Behavior of Biomedical Materials* **17**, 307–316.

Smela, E. (2003), 'Conjugated polymer actuators for biomedical applications', *Advanced Materials* **15**(6), 481–494.

Smela, E. and Gadegaard, N. (2001), 'Volume change in polypyrrole studied by atomic force microscopy', *The Journal of Physical Chemistry B* **105**(39), 9395–9405.

Song, B., Zhao, M., Forrester, J. and McCaig, C. (2002), 'Electrical cues regulate the orientation and frequency of cell division and the rate of wound healing in vivo', *Proceedings of the National Academy of Sciences of the United States of America* **99**(21), 13577–13582.

Spinks, G., Alici, G., Mcgovern, S., Xi, B. and Wallace, G. (2009), *Conjugated Polymer Actuators: Fundamentals*, John Wiley and Sons.

Stejskal, J. (2017), 'Conducting polymer hydrogels', *Chemical Papers* **71**(2), 269–291.

Stewart, E. M., Wu, Z., Huang, X. F., Kapsa, R. M. I. and Wallace, G. G. (2016), 'Use of conducting polymers to facilitate neurite branching in schizophrenia-related neuronal development', *Biomaterials Science* **4**(8), 1244–1251.

Storm, C., Pastore, J., MacKintosh, F., Lubensky, T. and Janmey, P. (2005), 'Nonlinear elasticity in biological gels', *Nature* **435**(7039), 191–194.

Streuli, C. (1999), 'Extracellular matrix remodelling and cellular differentiation', *Current Opinion in Cell Biology* **11**(5), 634–640.

Suki, B., Ito, S., Stamenović, D., Lutchen, K. R. and Ingenito, E. P. (2005), 'Biomechanics of the lung parenchyma: critical roles of collagen and mechanical forces', *Journal of Applied Physiology* **98**(5), 1892–1899.

Sun, K., Li, H., Li, R., Nian, Z., Li, D. and Xu, C. (2015), 'Silk fibroin/collagen and silk fibroin/chitosan blended three-dimensional scaffolds for tissue engineering', *European Journal of Orthopaedic Surgery & Traumatology* **25**(2), 243–249.

Svennersten, K., Berggren, M., Richter-Dahlfors, A. and Jager, E. W. H. (2011), 'Mechanical stimulation of epithelial cells using polypyrrole microactuators', *Lab on a Chip* **11**(19), 3287–7.

Tandon, B., Magaz, A., Balint, R., Blaker, J. and Cartmell, S. (2018), 'Electroactive biomaterials: Vehicles for controlled delivery of therapeutic agents for drug delivery and tissue regeneration', *Advanced Drug Delivery Reviews* **129**, 148–168.

Thompson, B., Murray, E. and Wallace, G. (2015), 'Graphite oxide to graphene. biomaterials to bionics', *Advanced Materials* **27**(46), 7563–7582.

Thrivikraman, G., Boda, S. and Basu, B. (2018), 'Unraveling the mechanistic effects of electric field stimulation towards directing stem cell fate and function: A tissue engineering perspective', *Biomaterials* **150**, 60–86.

Tidball, J. G. (2005), 'Mechanical signal transduction in skeletal muscle growth and adaptation', *Journal of Applied Physiology* **98**(5), 1900–1908.

Toshima, N. and Ihata, O. (1996), 'Catalytic synthesis of conductive polypyrrole using iron (iii) catalyst and molecular oxygen', *Synthetic metals* **79**(2), 165–172.

Trivedi, D., Rahn, C. D., Kier, W. M. and Walker, I. D. (2008), 'Soft robotics: Biological inspiration, state of the art, and future research', *Applied Bionics and Biomechanics* **5**(3), 99–117.

Tzu, J. and Marinkovich, M. P. (2008), 'Bridging structure with function: Structural, regulatory, and developmental role of laminins', *The International Journal of Biochemistry & Cell Biology* **40**(2), 199–214.

Uz, M., Das, S., Ding, S., Sakaguchi, D., Claussen, J. and Mallapragada, S. (2018), 'Advances in controlling differentiation of adult stem cells for peripheral nerve regeneration', *Advanced Healthcare Materials* **7**(14).

Vaitkuviene, A., Kaseta, V., Voronovic, J., Ramanauskaite, G., Biziuleviciene, G., Ramanaviciene, A. and Ramanavicius, A. (2013), 'Evaluation of cytotoxicity of polypyrrole nanoparticles synthesized by oxidative polymerization', *Journal of Hazardous Materials* **250-251**, 167–174.

Vaitkuviene, A., Ratautaite, V., Mikoliunaite, L., Kaseta, V., Ramanauskaite, G., Biziuleviciene, G., Ramanaviciene, A. and Ramanavicius, A. (2014), 'Some biocompatibility aspects of conducting polymer polypyrrole evaluated with bone marrow-derived stem cells', *Colloids and Surfaces A: Physicochemical and Engineering Aspects* **442**, 152–156.

Ventre, M. and Netti, P. (2016), 'Engineering cell instructive materials to control cell fate and functions through material cues and surface patterning', *ACS Applied Materials and Interfaces* **8**(24), 14896–14908.

Vunjak-Novakovic, G., Tandon, N., Godier, A., Maidhof, R., Marsano, A., Martens, T. and Radisic, M. (2010), 'Challenges in cardiac tissue engineering.', *Tissue engineering. Part B, Reviews* **16**(2), 169–187.

Wadhwa, R., Lagenaur, C. and Cui, X. (2006), 'Electrochemically controlled release of dexamethasone from conducting polymer polypyrrole coated electrode', *Journal of Controlled Release* **110**(3), 531–541.

Wallin, T. J., Pikul, J. and Shepherd, R. F. (2018), '3D printing of soft robotic systems', *Nature Reviews Materials* pp. 1–17.

Wang, X., Ding, B., Sun, G., Wang, M. and Yu, J. (2013), 'Electro-spinning/netting: A strategy for the fabrication of three-dimensional polymer nano-fiber/nets', *Progress in Materials Science* **58**(8), 1173–1243.

Wang, X., Gu, X., Yuan, C. et al. (2004), 'Evaluation of biocompatibility of polypyrrole in vitro and in vivo', *Journal of Biomedical Materials Research - Part A* **68**(3), 411–422.

Wang, X., Jiang, M., Zhou, Z., Gou, J. and Hui, D. (2017), '3d printing of polymer matrix composites: A review and prospective', *Composites Part B: Engineering* **110**, 442–458.

Wang, X., Shapiro, B. and Smela, E. (2004), 'Visualizing ion currents in conjugated polymers', *Advanced Materials* **16**(18), 1605–1609.

Wang, X., Shapiro, B. and Smela, E. (2008), 'Development of a Model for Charge Transport in Conjugated Polymers', *The Journal of Physical Chemistry C* **113**(1), 382–401.

Wanjare, M. and Huang, N. (2017), 'Regulation of the microenvironment for cardiac tissue engineering', *Regenerative Medicine* **12**(2), 187–201.

Wells, R. G. (2008), 'The role of matrix stiffness in regulating cell behavior', *Hepatology* **47**(4), 1394–1400.

Westermarck, J. and Kähäri, V.-M. (1999), 'Regulation of matrix metalloproteinase expression in tumor invasion', *FASEB Journal* **13**(8), 781–792.

Willerth, S. and Sakiyama-Elbert, S. (2007), 'Approaches to neural tissue engineering using scaffolds for drug delivery', *Advanced Drug Delivery Reviews* **59**(4-5), 325–338.

Woodfield, T., Guggenheim, M., Von Rechenberg, B., Riesle, J., Van Blitterswijk, C. and Wedler, V. (2009), 'Rapid prototyping of anatomically shaped, tissue-engineered implants for restoring congruent articulating surfaces in small joints', *Cell Proliferation* **42**(4), 485–497.

Yamaura, M., Sato, K. and Hagiwara, T. (1991), 'Effect of counter-anion exchange on electrical conductivity of polypyrrole films', *Synthetic Metals* **41**(1-2), 439–442.

Yan, B., Wu, Y. and Guo, L. (2017), 'Recent advances on polypyrrole electroactuators', *Polymers* **9**(12), 446–20.

Yang, X., Lu, Z., Wu, H., Li, W., Zheng, L. and Zhao, J. (2018), 'Collagen-alginate as bioink for three-dimensional (3d) cell printing based cartilage tissue engineering', *Materials Science and Engineering C* **83**, 195–201.

Yeong, W.-Y., Chua, C.-K., Leong, K.-F., Chandrasekaran, M. and Lee, M.-W. (2007), 'Comparison of drying methods in the fabrication of collagen scaffold via indirect rapid prototyping', *Journal of Biomedical Materials Research - Part B Applied Biomaterials* **82**(1), 260–266.

Yin, T. and Li, L. (2006), 'The stem cell niches in bone', *Journal of Clinical Investigation* **116**(5), 1195–1201.

Yow, S.-Z., Lim, T. H., Yim, E. K. F., Lim, C. T. and Leong, K. W. (2011), 'A 3D electroactive polypyrrole-collagen fibrous scaffold for tissue engineering', *Polymers* **3**(1), 527–544.

Yurchenco, P. D. and Patton, B. L. (2009), 'Developmental and pathogenic mechanisms of basement membrane assembly', *Current Pharmaceutical Design* **15**(12), 1277–1294.

Zein, I., Hutmacher, D., Tan, K. and Teoh, S. (2002), 'Fused deposition modeling of novel scaffold architectures for tissue engineering applications', *Biomaterials* **23**(4), 1169–1185.

Zhang, Y. and Khademhosseini, A. (2017), 'Advances in engineering hydrogels', *Science* **356**(6337).

Zhou, X., Yang, A., Huang, Z., Yin, G., Pu, X. and Jin, J. (2017), 'Enhancement of neurite adhesion, alignment and elongation on conductive polypyrrole-poly(lactide acid) fibers with cell-derived extracellular matrix', *Colloids and Surfaces B: Biointerfaces* **149**, 217–225.

Zhu, S., Jing, W., Hu, X., Huang, Z., Cai, Q., Ao, Y. and Yang, X. (2017), 'Time-dependent effect of electrical stimulation on osteogenic differentiation of bone mesenchymal stromal cells cultured on conductive nanofibers', *Journal of Biomedical Materials Research Part B: Applied Biomaterials* **105**(12), 3369–3383.

Chapter 3

Materials and Methods for DIW AM of Col-PPy constructs

This chapter includes the materials and methods used for the development of DIW Col-PPy constructs. This chapter outlines experimental methods involved in evaluating the performance and physical properties of said constructs. This chapter includes the most influential experimental results of the initial exploratory phase of the research programme, and indicates how the key findings stemming from these initial activities steered the subsequent direction of the research plan. Challenges associated with 3D printing PPy are discussed, and the development of Col-Py inks specially formulated for DIW is outlined. This chapter also includes the specifics associated with the DIW printing process, including: DIW printer configuration, software, substrates and relevant process matters.

3.1 Materials

Collagen type I extracted from bovine Achilles tendon (Sigma-Aldrich, Catalogue# C9879-10G) was solubilized in 0.5 M acetic acid. This concentration of acetic acid

was diluted from glacial acetic acid. 25-gauge needles and 10 CC syringe barrels/cartridges (Nordson EFD). Pneumatic adapter (Optimum, Nordson). Pneumatic controller unit (Ultimus V, Nordson EFD). Py monomer (Sigma-Aldrich, Catalogue# 131709), DBSA (Sigma-Aldrich, Catalogue# 44198), Iron (III) chloride ($FeCl_3$) (Sigma-Aldrich, Catalogue# 157740). Aluminum foil (ALCAN, Foil wrap), FEP paper sheets (McMaster-Carr, Catalogue# 5805T11), 304 stainless steel sheets (McMaster-Carr, Catalogue# 3254K322), parchment paper (PaperChef, Catalogue# 1000294), PVA (Sigma-Aldrich, Catalogue# 341584). Vacuum gauge sensor (Testo 552, Catalogue# 05605522), and Vacuum Pump (Robinair 15150 VacuMaster 1.5 CFM). Methylene blue (MB) (Sigma-Aldrich, Catalogue# M4159). PYREX glass 6-well dishes (CELLSTAR, Catalogue# 07000645). 38-gauge platinum wires (Sigma-Aldrich, Catalogue# 357367). PDMS (DOW, Sylgard 184, Catalogue # 1673921). DMEM culture media solution (Thermofisher, Catalogue# 11885092), 10% fetal bovine serum (Life Technologies, Catalogue # 12483-020), and 1% Penicillin-Streptomycin (Life Technologies, Catalogue # 15140122). 12-well tissue culture plates (Thermofisher, Catalogue# 150628). Hoechst stain (Sigma-Aldrich, Hoechst 33528), ParaFormaldehyde (Fisher, Catalogue # 41678-500), Alexa Fluor 488 Phalloidin (Invitrogen, Catalogue # A12379).

3.2 Experimental Methodology

3.2.1 Preliminary investigations

This section outlines the experimental results of the initial exploratory phase of the research programme that informed the subsequent direction of the research plan. Bovine Achilles tendon Collagen type I was solubilized in 0.5 M acetic acid. This concentration of acetic acid was diluted from glacial acetic acid and chosen as collagen isolates from fish skin, bone and fins were previously shown to be well-solubilized using 0.5 M acetic acid (Nagai and Suzuki, 2000). Solubilization of collagen was performed under constant

stirring at 0–4°C to prevent the evaporation of acetic acid, which is known to be volatile. A decrease in concentration for acetic acid would result in increase in the concentration of collagen in the resultant volume. This holds important consequence as a change in the concentration of collagen leads to variance in the rheological properties of the ink that is to be printed. However, at this point, the initial concern was to evaluate methodologies from scientific tradition for AM feasibility.

Following the solubilization of collagen using 0.5 M acetic acid, concentrations of 100 $mg \cdot mL^{-1}$, 75 $mg \cdot mL^{-1}$, 50 $mg \cdot mL^{-1}$, 25 $mg \cdot mL^{-1}$, 10 $mg \cdot mL^{-1}$, and 5 $mg \cdot mL^{-1}$ were empirically evaluated for continuous extrusion when expelled through a 25-gauge needle at pressures ranging from 15–20 psi using a pneumatic extruder. 25 $mg \cdot mL^{-1}$ collagen solution was observed to be optimal concentration for extruding a steady flow of the collagen ink at low pressures, i.e. 15–20 psi. Higher concentrations, i.e. 100 $mg \cdot mL^{-1}$, 75 $mg \cdot mL^{-1}$, 50 $mg \cdot mL^{-1}$, were observed to be too viscous and required higher pressure to extrude, whereas lower concentrations, i.e. 10 $mg \cdot mL^{-1}$, and 5 $mg \cdot mL^{-1}$, were too fluid to print even at reduced pressures and prone to the aforementioned 'bleeding effect'. However, assessing the 3D printing of collagen inks as stand-alone 3D constructs was not the aim of the present work, as this has been previously reported (Inzana et al., 2014; Rhee et al., 2016; Yang et al., 2018; Lode et al., 2016; Nocera et al., 2018). Rather, the aim of this thesis is to present a novel fabrication method for 3D printing collagen and PPy-based constructs.

The initial investigation for assessing Col-Py DIW feasibility evaluated powder and mould cast protocols developed by Machida et al. (1989); Armes (1987); Li and Khor (1994). As the aim of preliminary investigation was restricted to establishing feasibility for adapting DIW methodology to traditional fabrication methods, factors such as temperature, pH and reaction medium were not optimized, and polymerization of these constructs was conducted at ambient temperatures and humidity.

As shown in Figure 3.1, a 25 $mg \cdot mL^{-1}$ collagen solution was prepared by solubiliz-

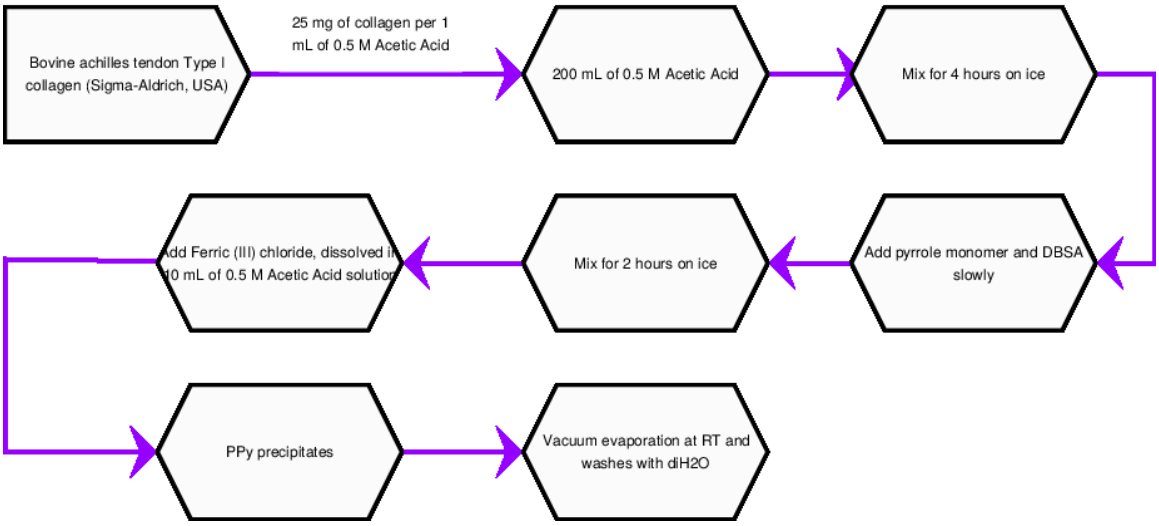

Figure 3.1: The protocol reported by Machida et al. (1989); Li and Khor (1994) was evaluated for DIW potential.

ing the appropriate amount of collagen in 0.5 M acetic acid. 0.5 M Py monomer and 0.3 M DBSA, with respect to Py, were then added after sufficient collagen solubilization (approx. 4 h in an ice bath). The resulting mixture was stirred for 2 h in an ice bath, where the temperature was maintained at 0–4°C. Afterwards, the oxidant, i.e. Iron (III) chloride ($FeCl_3$) was dissolved in 10 mL of 0.5 M acetic acid solution, 3.0 M with respect to Py, and added in a drop-wise manner (Rapi et al., 1988). The polymerization reaction of Py in the solution began immediately after adding the oxidizing $FeCl_3$ solution. Polymerized products subsequently underwent vacuum evaporation at room temperature for 2 h and were washed with copious amounts of deionized water to remove excess $FeCl_3$. Obtained products formed precipitates that were too large to print as a DIW ink. Therefore, the aggregate molecules of Col-PPy were lyophilized, milled and homogenized into 200 mL of the established collagen working solution. However, despite milling and sufficient suspension of PPy precipitates into the collagen or 100% ethanol (EtOH) solutions, DIW cartridges routinely clogged. Making DIW printing difficult. Therefore, another protocol for producing Col-PPy aerogels, reported by Mekonnen et al. (2016), was evaluated for AM potential.

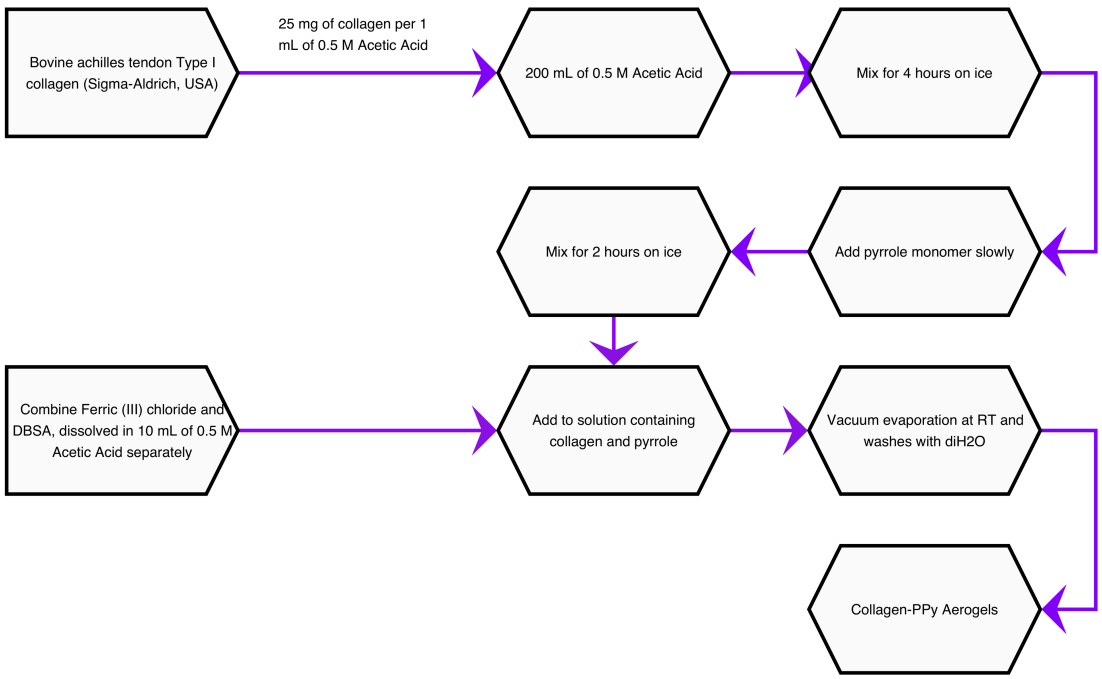

Figure 3.2: The protocol reported by Mekonnen et al. (2016) was evaluated for DIW potential.

As shown in Figure 3.2, a 25 $mg \cdot mL^{-1}$ collagen solution was solubilized in 0.5 M acetic acid and at 1:1 wt% Py monomer was added to solution in a drop-wise manner. The resulting mixture was stirred for 4 h in an ice bath, where the temperature was maintained at 0–4°C. Then the polymerizing solution, $FeCl_3$ and DBSA dissolved in 0.5 M Acetic acid solution, 2.33 M and 0.3 M with respect to Py, were added in a drop-wise manner (Jayamurgan et al., 2013). Fibrous aerogels were produced if the Col-Py-DBSA solution was under constant stirring when the oxidant was added, whereas bulk aerogels (such as those representative of conventional PPy-based aerogels) which adopt the shape of their container formed if the Col-Py-DBSA solution was stationary. Obtained constructs subsequently underwent vacuum evaporation at room temperature for 2 h. Samples were washed with copious amounts of deionized water and freeze-dried. Similar to the initial protocols investigated, the polymerization of Py in the solution began immediately after adding the polymerizing solution, and completed within a few minutes, as evidenced by the colour transition of the Col-Py-DBSA solution from grey-brown to completely black, i.e. PPy formation. This protocol delivered bulk aerogels which occupied the shape of the container, or fibrous strands if the polymerization solution was added as the solution was being mixed. This protocol too could not be adapted for DIW and required further development.

Another aspect of the fabrication process required the selection of the appropriate solvent to contain polymerizing molecules. In order to determine which solvent at hand was most suited to be chosen as the working polymerizing solvent, electrical conductivity (in the form of 4-point probe) tests were performed on samples polymerized in the following solutions, which contained both the dopant and the oxidant: 0.5 M acetic acid, 100% Ethanol (EtOH) and diH_2O. The results of this preliminary investigation are reported in Table 4.1. The solvent of choice would be one that showed fastest polymerizing time, but more importantly, the one which demonstrated highest electrical conductivity. It was observed that samples polymerized in 0.5 M acetic acid and diH_2O

would not always polymerize fully, evident from the lack of colour change. Specifically, the samples were not observed to undergo complete colour change to black, while this was not observed to be the case for 100% EtOH. It also largely took longer for the polymerization reaction to complete for these solvents, in comparison to 100% EtOH; establishing 100% EtOH as the solvent of choice for this composition, which is supported by past literature (Machida et al., 1989). Subsequently, the electrical conductivity of these aerogels is also demonstrated through an LED and battery setup, as shown in Figure 4.5.

3.2.2 Fabrication of Col-Py as a Direct Write Ink

Preliminary investigations established that inclusions of any intervention for the development of a DIW methodology using traditional fabrication protocols for Col-PPy constructs must fit in before the addition of the oxidant. Therefore, a delay aspect was introduced to the developed methodology. This delay capitalizes on the physical properties of the collagen component of this hybrid composition. Although, freezing collagen in moulds has been utilized for creating foams and hydrogels, no one has sought to print collagen and subsequently freeze it to retain geometric properties (Yeong et al., 2007). Using a cold storage chamber to this end seemed most prudent for retaining geometry of 3D printed constructs. This notion was then expanded to the Col-Py blended inks which behaved similar to DIW characteristics of standalone collagen materials. Based on this decision, a fabrication methodology for using Col-Py ink for creating DIW Col-PPy constructs is reported in this section.

As shown in Figure 3.3, a 25 $mg \cdot mL^{-1}$ collagen solution was solubilized in 0.5 M acetic acid. At 1:1 wt% ratio between collagen and Py, the proportionate amount of Py monomer was slowly added to stirring the solution. The resulting mixture was constantly stirred for 4 h in an ice bath, where the temperature was maintained at 0–4°C. This step is performed at 0–4°C to prevent the evaporation of acetic acid from the solution, which is known to be volatile. The resultant mixture was homogenized for 90s on ice, and then centrifuged at 14 000 rpm for 10 min to remove air bubbles introduced during the homogenization step. This Col-Py blend was then used as the ink for DIW purposes.

After successfully 3D printing constructs, samples were stored in containers with dry-ice or -80°C freezers for short-term or long-term storage, respectively. This step in the fabrication process represents the aforementioned delay aspect. It is a deviation from traditional fabrication methods for PPy-based scaffolds.

After samples were sufficiently frozen/solidified, they were transferred to the polymerizing solution and gently agitated. The polymerizing solution contained $FeCl_3$ and

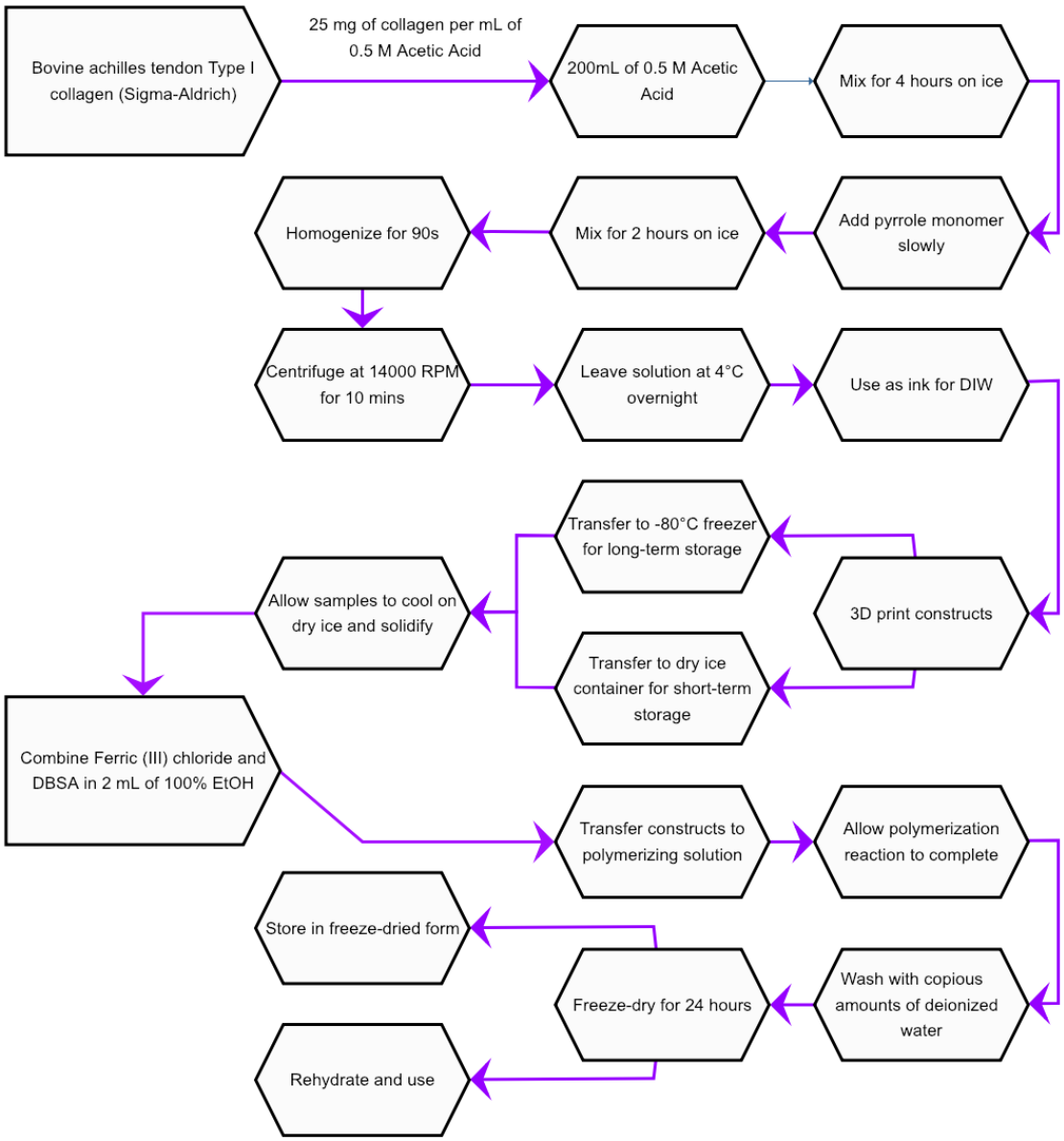

Figure 3.3: The fabrication procedure developed for DIW Col-PPy based scaffolds using chemical oxidative polymerization.

DBSA dissolved in 2 ml of 100% EtOH, 2.33 M and 0.3 M with respect to Py. 3D printed samples were then washed with copious amounts of deionized water to remove excess $FeCl_3$ and subsequently, lyophilized. The development of a freeze-drying unit is detailed in Appendix A.2. Stoichiometric choices were made with previous literature in mind (Bjorklund, 1987; Armes, 1987; Li and Khor, 1994), and are further expanded on in Appendix A.1. In order to conduct experimental evaluations, samples were re-hydrated using fresh deionized water and stored in a 4 °C refrigerator to keep level of dehydration to minimum. The major contribution of this thesis, that is, the development of a fabrication technique for DIW printing PPy-based scaffolds, is demonstrated as constructs retained their 3D printed geometry and underwent complete polymerization, as evidenced by the colour change to black. This colour change is benchmark for indicating formation of PPy.

The duration for samples to undergo complete polymerization for each of the three concentrations of PPy was recorded by observing colour change of the constructs from grey-brown to black, indicative of Col-Py to Col-PPy transition. This is reported in Table 4.2.

3.2.3 Relevant DIW AM Processes and Parameters

The 3D printer used for DIW purposes was a commercially available DeltaMaker printer which was fitted with a paste extrusion system. Its design, associated firmware and framework for the DIW apparatus are reported in detail by Holness and Price (2018).This printer differs from the most common design for 3D printers, that is, the cartesian configuration, as it operates in a delta configuration (ASTM Standard ASTM52900 - 15, 2015). The DeltaMaker printer holds advantage over its competitors due to its open-source nature, easy modifiability, and due to its stationary print bed.

The DIW process is still incumbent on traditional AM processing such as CAD modelling, slicing CAD models to g-codes (in this case, using slicing software Simplify3D)

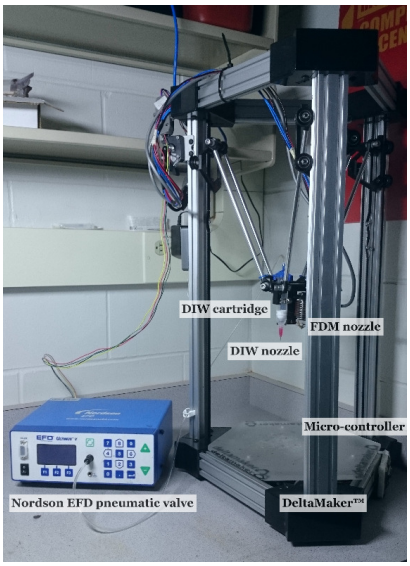

Figure 3.4: A schematic detailing the DIW apparatus.

and assignment of essential print parameters such as print layer heights, infill, speed, temperature and extrusion-widths (as a function of extruder nozzle diameter and nozzle height from the print-bed, in case of DIW). These parameters enable process optimization for the extrusion of any specific material. Of the aforementioned parameters, temperature holds no consequence.

Following the assignment of print parameters, ink materials were loaded into 10 CC syringe barrels, which are closed off with dispensing needles at the nozzle end and include a piston at the end of the barrel to ensure all of the material in the barrel is extruded. The barrels are then attached to an adapter (Optimum, Nordson) which connects to the pneumatic valve. Therefore, creating DIW ready cartridges. These cartridges were then mounted on to the modified extruder compartment and the g-code for select CAD model was run where an auxiliary micro-controller which relays the extrusion signal from the g-code commands to the pneumatic valve to initiate and terminate extrusion cycles. Whereas, extrusion onto the print bed is controlled by the communication between the DeltaMaker, the micro-controller and the pneumatic valve. As the pneumatic valve functions through discrete bursts of pressure, an increase in

the steps-per-mm conversion factor was required to effectively reduce any delay or gap between bursts. This conversion factor was empirically adjusted until the delay between extrusion cycles became indiscernible, and the DIW could be extruded continuously. One shortcoming from the continuous application of pressure is risk of over-extrusion. However, that too can be modulated by increasing print speeds, which deposits less material resulting in decreased trackwidths.

Substrates for DIW printing

The last component of the DIW process, that is, the substrate onto which the Col-Py ink would be printed, was investigated. Initially, aluminum foil was selected because of its ready availability, inexpensiveness and good thermal conductivity. Aluminum foil, irrespective of whether the dull or shiny side was used as substrate surface, allowed quick transference of freezing temperatures when samples printed on this substrate were shifted to a dry-ice container or -80°C freezer for long-term or short-term storage. However, removal of printed structures, especially smaller structures, from the foil required great manoeuvring and the beneficial thermal conductivity proved disadvantageous at this stage as 3D printed structures were seen to return to their solubilized form within 10s of being taken out of the dry-ice container. 3D printed constructs were also prone to breakage if mishandled during the removal from the foil substrate. Due to this reason, other substrates were investigated.

FEP paper sheets were evaluated because of their adhesive back as well as because of their non-adhesive surface that provided low surface energy. The adhesive aspect of this substrate made it difficult to remove 3D printed structures, and transfer to the polymerizing solution. In contrast, structures printed on the non-adhesive surface of the FEP paper sheets were observed to have an increased trackwidths that were observed to be retained on the previously investigated substrate, i.e. aluminum foil. Additionally, transfer from the print bed to freezing container proved difficult as even subtle movement

caused the 3D printed structures to slide on the non-adhesive substrate and lead to loss in print geometry. Thus, FEP paper as the substrate of choice was scrapped.

Next, hardened 304 stainless steel sheets were investigated as they were observed to retain their thermal energy longer than aluminum foil. The stainless sheets were left in dry-ice for 5 min to cool and subsequently transferred to the print bed. The Col-Py ink was printed directly onto these sheets. Although the cold nature of this substrate prevent extruded tracks from bleeding or losing their resolution, it was impossible to remove the printed structures from the sheet without breakage. Thus, 304 stainless steel sheet as the substrate of choice was scrapped.

Next, parchment paper was investigated as it is known for its moisture resistance and non-stick properties. Printing on this substrate failed as the printed areas were affected by the acetic acid presence in the ink and resulted in wrinkling of the substrate. This lead to distortion in the geometry of the prints. Therefore, parchment paper as the substrate of choice was also scrapped.

Lastly, a 10 wt% PVA solution was mixed at 70°C for 3 h, and subsequently spun-coated onto microscope slides at 1 000 rpm for 3 min to create thin films. PVA is known to dissolve in the presence of water (Mallapragada and Peppas, 1996). Col-Py inks were printed directly onto these films. Since, the polymerizing solution of choice selected was 100% EtOH, the PVA dissolution/removal step must necessarily succeed the polymerization step, throughout which structures would have to remain fixed to the substrate. PVA films bearing the printed constructs were cooled on dry-ice, transferred to the polymerizing solution and then to diH_2O for removal of excess oxidant and the PVA substrate. The freezing of PVA and the 3D printed constructs only served to limit the infiltration of oxidant molecules at the bottom face of the printed constructs, as this face of the structure was observed to not always undergo complete polymerization, evidenced by a lack of colour change to black. Additionally, the freezing of the PVA films further increased dissolution time and subsequent recovery of polymerized samples.

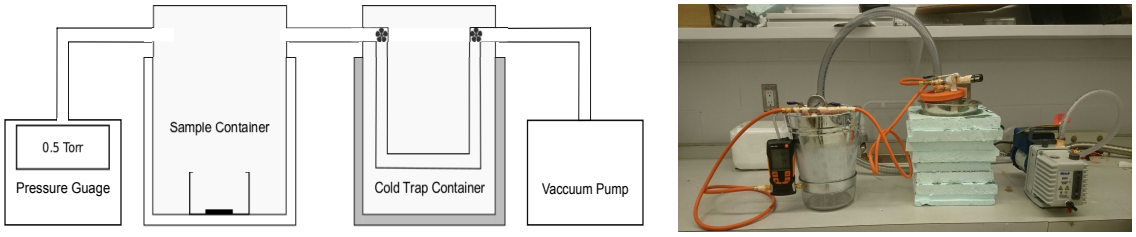

(a) schematic **(b)** physical setup

Figure 3.5: The freeze-drying apparatus is shown as both a (a) schematic and (b) physical setup.

Therefore, aluminum foil was selected as the substrate of choice, begrudgingly, as it still required great skill in manipulation for sample removal. Although the ink could be used to produce 3D structures of any size, removal from the printing substrate remains a limiting factor. Structures printed under 250 μm extruded-width (via 27G needle) presented great difficulty in removal from the substrate of choice. The inability to remove structures essentially represented failed prints, as any attempts at removal resulted in breakage of the extruded structure. Further development of this portion of the AM fabrication process is warranted, with a focus on recovering small and finer printed structures as the printing substrate still limits the resolution at which PPy-based structures can be produced and successfully retrieved, which in turn limits their application.

3.2.4 Freeze-drying Apparatus

The final step in the fabrication process for creating Col-PPy constructs involves freeze-drying 3D printed constructs. Thermally induced phase separation, via freeze-drying, where the cooling and freezing processes imposes formation of hydrogen bonds between collagen fibres and cross-linking via crystallization of solvents and their subsequent removal, in addition to the creation of interconnected network of pores and micro-architecture that can be modulated by controlling the freezing temperatures (Oh et al.,

2012; Annabi et al., 2010; Offeddu et al., 2015). This increases mechanical properties of the construct and pore formation by immobilization in a glassy (chemically inert) matrix, which increases the number of electro-active sites available (Pikal, 1999). Depicted in Figure 3.5 is the freeze-drying system developed for this thesis project. The system includes a vacuum gauge sensor (Testo 552, Catalogue# 05605522) attached to the sample containing stage, which is held at a -10°C using acetone and ice, and a cold trap stage, which serves to freeze vapour solvent molecules and prevent them from damaging the vacuum pump.

3.3 Characterization Methodology

3.3.1 Rheology

For DIW applications, it is vital to achieve proper control over dimension and geometry of extruded material. Therefore, at this point in my thesis, it was important to evaluate the flow characteristics of Col-Py inks for shear thinning behaviour. Understanding the flow properties of the ink allowed adjustment of DIW parameters such as print speed, extrusion pressure and nozzle diameter to enable the fabrication of high-resolution 3D Col-PPy structures. To this end, the rheological properties of 25 $mg \cdot mL^{-1}$ collagen solution with variable concentrations of Py were compared against the base 25 $mg \cdot mL^{-1}$ collagen composition (Figure 4.1).

Rheological experiments were performed using a Rheometrics stress rheometer with parallel plate geometry, by running dynamic strain-rate sweeps from 0.1–100 $rad \cdot s^{-1}$. From this data, a relationship between viscosity and shear rate for 25 $mg \cdot mL^{-1}$ collagen and the various Py concentrations reported in Figure 4.1 was established, using the power law model as shown below:

$$log\,(\eta) = (n-1) \cdot log(\dot{\gamma}) + log(\eta_0), \tag{3.1}$$

where, η, n, $\dot{\gamma}$, and η_0 represent apparent viscosity, power law index, shear rate, and zero viscosity, respectively.

In order to investigate optimal pneumatically controlled extrusion parameters for the DIW process, and whether extruded trackwidths could be predicted, a mathematical model on the resolution of bioprinting bio-inks reported by Suntornnond et al. (2016) was utilized. The model essentially establishes a correlation between the power law model for the viscosity of shear thinning materials and the print process parameters, specifically:

$$d\,(v, \Delta P) = D^2 \sqrt{\frac{1}{32\eta L} \cdot \left(\frac{4n}{3n+1}\right) \cdot \frac{\Delta P}{v}}, \tag{3.2}$$

where d, D, L, η, n, ΔP, and v represent theoretical trackwidth, nozzle diameter, nozzle length, apparent viscosity, power law index, gauge pressure, and print speed, respectively.

Using this model, theoretical values were generated and compared against empirical extrusion width data as a function of pressures applied, at various print speeds for Col-Py 1:4 wt% composition. Results from these investigations are included in Figure 4.2. It was empirically established that the Col-Py inks flowed well at low pressures, ranging from 15–20 psi. However, process refinement was required for increasing print resolution.

For the verification of rheological modelling and extrusion parameters, S-shaped structures (n= 4 samples per condition, 4 measurements per sample) were printed at various speeds and pressures (shown in Appendix A.2). Extruded trackwidths were analyzed using optical microscopy (Dino-lite, AnMo). Obtained images were subsequently analyzed using Fiji and trackwidths were measured and. Mean trackwidths for each condition are reported. Confocal optical imaging was performed on cross-sections of collagen standalone and the Col-PPy 1:4 wt% structures, as shown in Figure 4.4, using a LSM 5 Duo Vario microscope using Zen Software (Zeiss). Additional examples of 3D printed structures are included in Appendix A.2.

3.3.2 Electro-Conductivity

For each of the samples evaluated (n=12 for DIW each concentration of DIW Col-PPy constructs, n=6 for fibrous aerogels, n=6 bulk aerogels), a fixed current of 0.01A was run between two outer probes and voltage is measured between the two inner probes of 2.0 mm spacing in contact with the sample, and consequent resistivity was recorded three times per sample. This constitutes a 4-point probe technique and is primarily performed for the measurement of resistivity, where conductivity is given by taking the reciprocal of measured resistivity.

Electrical conductivity tests were performed using a Keithley 2611 source metre on as synthesized Col-PPy 1:1 wt%, 1:2 wt%, and 1:4 wt% 15 mm $\times$ 10 mm $\times$ 1.5 mm samples, and on Col-PPy 1:1 wt% fibrous aerogels and bulk aerogel samples. Due to the change in dimensions post-freeze drying, subtle changes in sample thickness was measured by using callipers and accounted for in calculations. It is important to note that for the fibrous aerogel and bulk aerogel samples were of indeterminate size due to their irregular dimensions, therefore, electrical conductivity measurements respond to the average size of the constructs produced as the true thickness of the samples measured could not be accurately measured and corrected for. This leads to an underestimation of electrical conductivity values. Electrical conductivity was qualitatively demonstrated by using DIW printed constructs to complete the circuit of power an LED with 9V battery in Figure 4.5 and Figure 4.8. In the 4-point probe experiments reported in this section, electrical conductivity is quantitatively reported (Table 4.4). Resistivity 'p' is given by:

$$p = \frac{V}{I} C_f 2\pi d, \tag{3.3}$$

where C_f, d, V, and I represent the correction factor, probe spacing, voltage and current, respectively. Correction factors were chosen based on the ration between geometric thickness, measured via vernier callipers, of the structures evaluated and probe spacing

between the 4-point probes.

Electrical conductivity of the 3D printed samples was calculated using the following formulas:

$$\sigma = \frac{1}{p}, \tag{3.4}$$

where, σ, p represent conductivity and resistivity, respectively.

3.3.3 Electro-activity: Cyclic Voltammetry

Cyclic voltammetry (CV) experiments were performed with a computer controlled Keithley 2611 source metre. CV was carried out using a 3-electrode cell, 15 mm $\times$ 10 mm $\times$ 1.5 mm samples (n=3 per DIW Col-PPy constructs) were submerged into the working solution using micro-alligator clips to serve as the working electrode, a 50 mm $\times$ 25 mm $\times$ 1 mm a 304 stainless steel sheet was used as the counter electrode, and an Ag/AgCl electrode was used as the reference electrode. Potential cycling was performed at potentials ranging from $\pm$ 0.2 V to $\pm$ 2 V vs Ag/AgCl at a scan rate of 10 m V/s, 20 m V/s, 50 m V/s, 75 m V/s, and 100m V/s in both aqueous 0.1 M $NaDBS_{(aq)}$ solution and DMEM solution. Additionally, to study the lifetime of the constructs, the long-term electro-active capability was examined for 500 cycles of testing. The schematic shown in Figure 3.6 depicts the experimental setup used in CV investigations.

3.3.4 Electro-activity: Spectrometry

A cationic dye, methylene blue, was used to demonstrate bulk electro-active potential of DIW Col-PPy structures produced using the fabrication technique developed in thesis (Cione et al., 1998; Ozdemir et al., 2009). To this end, 3D printed construct were variably electrically stimulated in 100 $mg \cdot mL^{-1}$ MB dye aqueous solutions containing the MB dye for 10 min at the first testing stage. Following electrical stimulation at the first stage, samples were washed twice with fresh diH_2O. Samples were then electrically stimulated

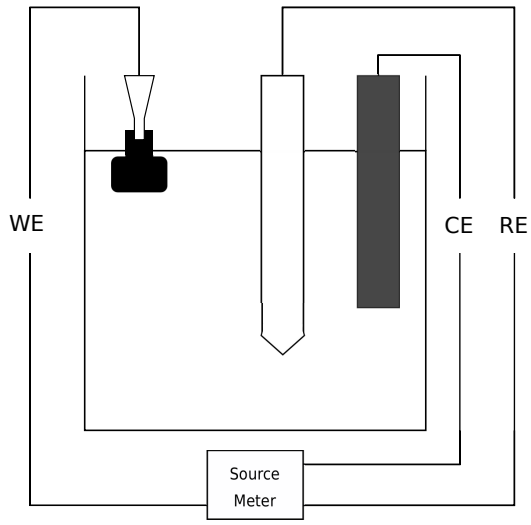

Figure 3.6: The CV experimental setup where a Col-PPy sample is used as the working electrode (WE), a 304 stainless steel sheet was used as the counter electrode (CE). Potential is applied to the WE against an Ag/AgCl reference electrode (RE).

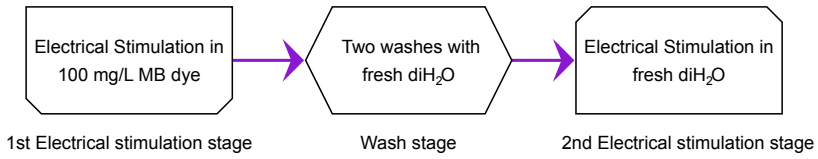

Figure 3.7: The experimental setup where the 1st stage of electrical stimulation was performed in MB dye solution for 10 min, then twice washed in fresh diH_2O, and finally, electrically stimulated at the 2nd in fresh diH_2O for 5 min.

again for 5 min in the opposite potential direction, relative to the applied potential at the first stage of testing, in fresh diH_2O to study the release of MB dye. Adsorption and release of the dye as a result of electrical stimulation in the 2nd stage of the experimental setup is reported in Figure 4.12.

Spectroscopy experiments were performed with a Cary 60 UV-vis (Agilent Technologies) spectrophotometer using Cary WinUV software on 1 cm^2 quartz cuvettes filled with 5 ml solutions. 10 mm $\times$ 10 mm $\times$ 1.5 mm DIW printed Col-PPy 1:4 wt% samples (n=4 per experimental condition) were housed in diH_2O at 4°C prior to any testing, rather than in MB dye solution to ensure no passive capture of the dye would confound results. Samples were subjected to electrical stimulation in PYREX glass

6-well dishes.38-gauge platinum wires were used as both the WE and CE to effectively create a 2-electrode cell which provide direct current (DC) electrical stimulation to 3D printed constructs in MB dye solution, as indicated in Figure 3.8. This setup is similar to the design reported by Mobini et al. (2016) and observed to effectively impart electrical current to individual constructs contained in the wells. Circuit connectivity was confirmed by using a multimeter once electrodes were submerged in dye solution. The range for the absorption spectroscopy was set between 550 nm and 750 nm as the peak absorbance of MB is observed near 665 nm (Ozdemir et al., 2009).

Prior to any absorbance testing, a baseline was established by measuring the absorbance of diH_2O. Subsequently, standards of MB dye ranging from $0.1 - 1.0$ mg/L were measured to provide points of reference against the concentration of MB dye released during the second stage of the experimental setup (as depicted in Figure 3.7).The first batch of experiments involved evaluating the extent of MB dye release as a consequence of electrical stimulation. Samples were submerged in 12 ml of 100 mg/L MB dye solution, electrically stimulated for 10 min at ± 1 V to allow MB dye adsorption, then washed twice with 12 ml of fresh diH_2O to decrease risk of passive MB dye release. Samples were then electrically stimulated again for 5 min at ± 1 V at the second stage in a fresh volume of 12 mlof diH_2O. Post-electrical stimulation at the second stage of testing, samples were removed at 5 ml of the volume was recovered for spectroscopy evaluation. The process noted in Figure 3.7 was held consistently for all experimental conditions.

The second batch of experiments were performed to evaluate the degree of leeching. Samples underwent variable electrical simulation at the first stage, were then washed twice with 12 ml of fresh diH_2O. However, unlike the first batch of experiments, samples did not experience electrical stimulation at the second stage and were left to sit in its absence for 5 min. Subsequent release of the MB dye in this volume as a result of leeching was measured. A third set of experiments for evaluating the degree of passive

adsorption in the absence of electrical stimulation were also performed. Samples were left in 100 mg/L MB dye solution for 10 min, then washed twice with fresh diH_2O. Samples were subsequently placed in a fresh volume of diH_2O for 5 minwhere they did not experience any electrical stimulation. Subsequent release of the MB dye in this fresh volume of diH_2O as a result of passive adsorption was measured. Results from these experiments are summarized in Figure 4.12, additional figures are included in Appendix A.4 to provide further clarification.

Concentrations of MB dye released during each experimental condition were calculated using Lambert-Beer's law:

$$Abs = c \cdot L \cdot \epsilon_x = \log\left(\frac{I_o}{I}\right), \tag{3.5}$$

where Abs, c, L, ϵ_x, I_o, I represent absorbance, analyte concentration, optical path length, the molecular extinction coefficient, incoming light intensity to the sample, and light intensity transmitted across the sample, respectively. The molecular extinction coefficient was appropriated from Prahl (2001). Results from these calculations are reported in Figure 4.13 and Figure 4.14.

3.3.5 Electro-activity: Actuation Profiling

The potential of the composition as a robust electro-actuator was investigated. To this end, the actuation performance of DIW printed Col-PPy structures, i.e. Col-PPy 1:4 wt% monolayer grids and rectangular PDMS-Col-PPy 1:4 wt% bilayers was evaluated.

Actuation performance experiments were performed with a computer controlled a Keithley 2611 source metre. 10 mm $\times$ 10 mm $\times$ 1.5 mm Col-PPy 1:4 wt% monolayer grid samples (n=3 per DIW Col-PPy construct) were 3D printed and initially housed in diH_2O at 4°C prior to any testing. Samples were subjected to electrical stimulation in PYREX glass 6-well dishes. Samples were electrically stimulated in a well using the

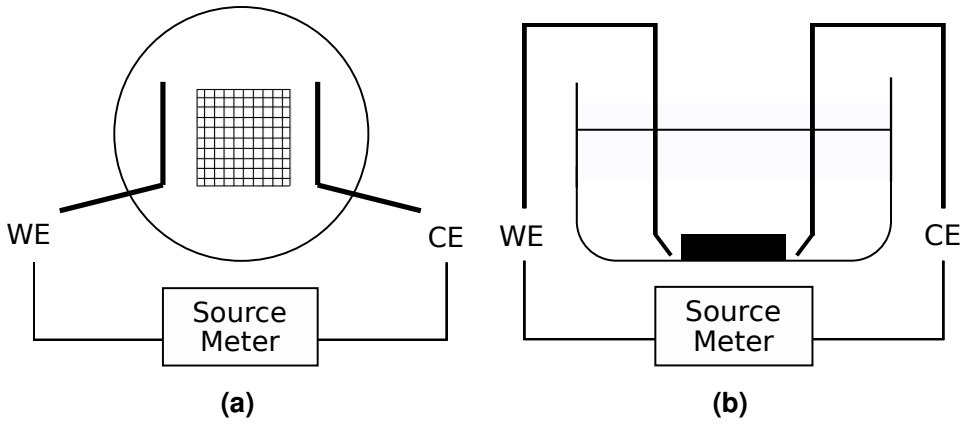

Figure 3.8: A 2-electrode electrical stimulation setup for absorbance and grid actuation experiments is shown. A Col-PPy sample was placed between 38 gauge platinum wires which served as working electrode (WE) and counter electrode (CE) as labelled. This figure includes (a) an upside-view and (b) a sideview of the setup.

same 2-electrode setup outlined in Figure 3.8 using 38 gauge platinum wires, which served as both the WE and CE. DMEM solutions were used to establish how the construct would respond in a solution representative of cell culture media constitution, specifically, establish the actuation profile of the 3D printed constructs was of great significance prior to use in cell culture experiments for electromechanically stimulating cells. The connectivity of the electrodes to create a circuit was confirmed using a multimeter. Observed actuation response of pores is reported as a function of applied potential. All experiments were conducted under an optical microscope, where a Sony 40.1 megapixel camera was mounted onto the ocular lens of an optical microscope to record videos of actuation response at 25$\times$ magnification. Videos were then split into second-by-second still frames, and select pores were analyzed using Fiji software. Additionally for each figure included annotations for the pores corresponding to each sample and experimental condition are included in Appendix B.1).

All % area change measurements reported were determined by manually tracing pores between different images. This was done to reduce any error implicit from using threshold tools available in Fiji. The difference in using internal threshold algorithms and

manual tracing is demonstrated in Figure 5.3. Any error associated with pore expansion and contraction measurements is due to unskilled tracing of the proper, and ascribed to be minimal. Since the traced shape resembles a complex polygon, area is calculated by sectioning off pixels present in the polygon into slices divided into x and y values representative of the simpler shapes such as triangles. The generated values from these calculations are then referenced against a scale set in the beginning and all % area changes are reported after being normalized to the 1s frame from obtained videos. Typical current flow for Col-PPy 1:2 wt% and 1:4 wt% samples from applying $\pm$1 V at 0.00833 Hz is also reported.

Next, 40 mm $\times$ 5 mm $\times$ 1.5 mm DIW Col-PPy 1:4 wt% samples were produced. PDMS slides were spin-coated onto microscope glass slides at 1 000 rpm for achieving uniform thickness. In order to create functional bilayers, dried Col-PPy 1:4 wt% samples were flattened against the slide with PDMS coatings. To cure PDMS against the Col-PPy samples, flattened samples were left at room temperature for 48 h on the spin-coated PDMS slides. Prior to conducting any actuation tests, bilayer samples were hydrated by leaving the samples submerged in the working solution for 30 min under agitation. This was done so that samples may adjust to the new solution's osmolarity. Results from actuation performance evaluations are reported in table 5.2 and table 5.3 for tests conducted in DMEM media solution and 0.1 M NaDBS aqueous solution, respectively. Prior to performing actuation tests, the swelling ratio of the dog bone samples was evaluated and is reported in Table 5.1.

Actuation tests were performed in both 0.1 M $NaDBS_{(aq)}$ solution and DMEM solutions. The $NaDBS_{(aq)}$ solution provided a less complex media to understand how the blended composition of constructs behaved in media of less amounts of present species. Similar to the setup used in CV testing, the sample was clipped above the solution by a micro-alligator clip, while majority of the sample remained submerged in solution and effectively served as the WE. A 38 gauge platinum wire served as the CE.

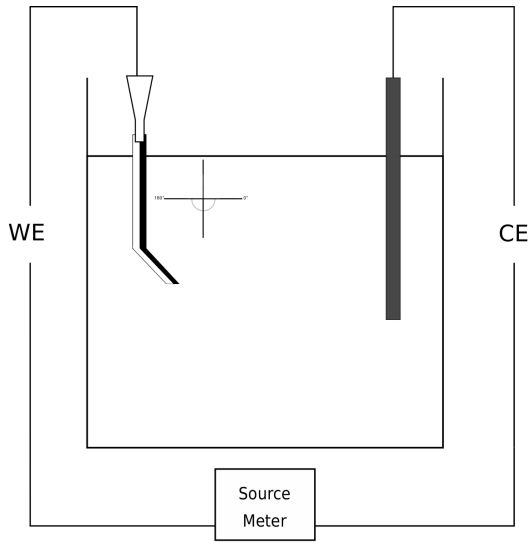

Figure 3.9: The 2-electrode electrical stimulation setup used for conducting bilayer actuation experiments is shown.

Bilayer actuation performance experiments were performed with a computer controlled a Keithley 2611 source metre. All length changes are referenced to the quadrille paper in the background and all angle changes are in reference to the plane shown in Figure 3.9.

3.3.6 SEM

SEM imaging was performed with a Hitachi S-3400N microscope equipped with an Oxford Instruments INCA PentaFETx3 EDAX detector. Col-PPy 1:1 wt%, 1:2 wt%, 1:4 wt% and collagen standalone 3D printed grids underwent imaging at the top surface and cross-sectional levels, and subsequent EDAX elemental mapping.

SEM imaging was initially performed on dry and damp Col-PPy 1:4 wt% samples to determine if SEM imaging under low pressure would adequately capture sample topography and porosity in its semi-hydrated/damp state, as the true state of the sample is represented in its hydrated state. Results of this comparison are shown in Figure 5.13, which show that SEM imaging under variable pressure could be performed and produced sufficient images showcasing macroscopic and microscopic features of the construct.

However, clearer images were produced when samples were sufficiently dehydrated as surfaces features were observed to be out of focus when samples were left damp/hydrated. Additionally, these preliminary images indicated that pore structures and fibres displayed collapse which resulted in an underestimated depiction of porosity and surface topography. Therefore, monolayer Col-PPy 1:1 wt%, 1:2 wt%, 1:4 wt% grid samples were left to dry at room temperature for 48h to remove their water content to prepare for SEM imaging, while freeze-dried collagen standalone grid structures were imaged in their dry state.

Samples (n=1 per condition) were then mounted and imaged. SEM imaging was performed on these dehydrated samples to qualitatively evaluate differences in degree of porosity and morphology between the DIW Col-PPy constructs and collagen standalone structures due to increasing PPy presence. SEM imaging was performed on sample cross-sections to evaluate the consequence of PPy inclusion relative to the scaffolding base composition, i.e. collagen standalone samples. Monolayer grid samples were cry-fractured using liquid N_2 for creating cross-sections along the middle-most row of the grid. SEM imaging of cross-sections was performed to evaluate internal porosity, pore size and homogeneity (Figure 5.15).

Additionally, EDAX elemental mapping was performed on cross-sectioned samples to identify their elemental composition and to clue on the extent of doping of PPy from the inclusion of DBSA in the polymerization step of the fabrication process (Figure 5.16). Table 5.4 reports on results from elemental mapping which implicate iron and sulphur presence corresponding to oxidant and dopant presence, respectively.

3.3.7 Mechanical Evaluation

Assessments of mechanical properties of biological materials have been observed to be dependent on the method of deformation, where reports of elastic behaviour can span several orders of magnitude (McKee et al., 2011; Akhmanova et al., 2015). The most

basic method for mechanical evaluation of materials is the uniaxial tensile test, where the sample undergoes tensile deformation at a fixed displacement rate along a single axis until failure. For the determination of elastic deformation properties of 3D printed Col-PPy constructs, the "Standard Test Method for Tensile Properties of Thin Plastic Sheeting" (ASTM D882) was used and produced thicknesses of specimens were less than the allotted 3.2 mm designation (ASTM Standard ASTM52900 - 15, 2015).

Dogbone shaped samples in accordance with ASTM D1708 were prepared by 3D printing the collagen-Py blended inks at varying concentrations of Py, i.e. 1:1 wt%, 1:2 wt%, 1:4 wt%, as well as DIW printing of collagen standalone ink (ASTM Standard ASTM52900 - 15, 2015). 3D printed ASTM dogbone samples (n=1 per testing condition) underwent the fabrication procedure outlined in section 3.2.2, with the exception of collagen standalone constructs. Samples were left to freeze in dry-ice containers and immediately subjected to freeze-drying for 24h. All freeze-dried samples were rehydrated in DMEM media overnight prior to performing tensile evaluations. This solution was chosen to allow samples to acclimate to physiological osmolarity and swell accordingly. Sample thicknesses were measured by callipers, ranging between 0.95 mm and 1.25 mm after freeze-dried samples were rehydrated in DMEM media overnight. Caliper measurements were performed immediately prior to tensile evaluations, and are included in section B.3. Stretch-break tensile tests were performed for each experimental condition by a CellScale Univert universal tester with a 10 N load cell under a fixed strain rate of 2 $mm \cdot min^{-1}$, at ambient temperature and humidity. The aforementioned load cell was selected due to the next available load cell, i.e. a 1 N load cell, being unable to cover the stress-strain behaviour from implemented deformations. Tensile tests involving electrical stimulation were performed using a Keithley 2611 source metre. Subsequent change in physical properties was assessed by implementing the same stretch-break tests as done for previous samples.

For each experimental condition, the Young's modulus (E), maximum strain before

fracture, ultimate tensile strength (UTS), and the fracture stress values were determined by implementing force versus displacement data as stress versus strain by the following equations:

$$\sigma = \frac{F}{A}, \tag{3.6}$$

where σ, F, A, represent stress, force applied, and cross sectional area of the sponge.

$$\epsilon = \frac{\delta l}{l_o} = \frac{l_f - l_o}{l_o}, \tag{3.7}$$

where ϵ, δl, l_f, l_o, represent strain, change in longitudinal length, final longitudinal length and initial longitudinal length.

$$E = \frac{\sigma}{\epsilon}, \tag{3.8}$$

where E, σ, ϵ, represent Young's modulus of elasticity, stress, and strain.

With the exception of yield strength values which were estimated after yielding of the sample from the stress versus strain curves, rather than applying 0.2% offset rule, as the plastic behaviour of the measured constructs is limited and difficult to discern due to artifacts from the instrument (shown in Appendix B.1). Results from stress versus strain calculations are reported in table 5.5.

3.3.8 Cyto-compatibility Evaluation

Prior to establishing cyto-compatibility for an extended period of time (i.e. 7 days), a preliminary experiment used 10 mm $\times$ 10 mm $\times$ 0.5 mm Col-PPy 1:4 wt% grid samples (n=4) to account any challenges associated with cell culture, immunocytochemical staining and post-staining. Samples were sterilized by in accordance with directions suggested by the provider for Bovine Achilles tendon Collagen type I. Sterilization, and subsequent rehydration, was performed by rinsing samples in an ethanol series protocol

previously reported for chitosan hydrogels (Madihally and Matthew, 1999). Samples were kept in 100% ethanol overnight, then in decreasing amounts of ethanol solutions under agitation and exchanged every 2h, i.e. 100%, 95%, 90%, 80%, 70%, 50% and lastly, 0%.

Following the sterilization protocol, samples were housed in sterile diH_2O until seeding of 25, 000 human BJ fibroblast cells. Samples were submersed with DMEM solution, 10% fetal bovine serum, and 1% Penicillin-Streptomycin with the appropriate volume for 12-well tissue culture plates. Samples were then placed in typical tissue culture incubation conditions (i.e. 95% air, 5% carbon dioxide (CO_2), 37°C). Samples were retrieved for immunocytochemical staining 4 days following initial cell seeding.

Hoechst stain was performed to visualize nuclei of human BJ fibroblast cells proliferating on 3D printed Col-PPy 1:4 samples. Cells were fixed by adding 4% ParaFormaldehyde in 1X PBS buffer, permeabilized with 0.1% solution of Triton 100X dissolved in 1X PBS buffer solution, incubated with 1% BSA (Blocking solution/buffer A) for 30 min and incubated in 1:1000 diluted Hoescht stain for 20 min at room temperature. Stained cells were housed in 1X PBS buffer, protected from light. Subsequently, samples were imaged using an AxioImager.M2m with Zen software (Zeiss) at 20$\times$ magnification as extended depths of view. Results of this preliminary investigation are shown in Figure 5.20.

Preliminary investigations revealed viability for conducting an extended cyto-compatibility experiment. 10 mm $\times$ 10 mm $\times$ 0.5 mm collagen standalone monolayer grid samples ((n=16) were DIW printed to serve as controls against 10 mm $\times$ 10 mm $\times$ 0.5 mm Col-PPy 1:4 wt% grid samples (n=16). Collagen standalone samples were selected to serve as control as collagen was used as the base scaffolding/hydrogel component and because cyto-compatibility and biocompatibility for collagen substrates has been demonstrated repeatedly (Boyce et al., 1988; Chevallay and Herbage, 2000; Gelse, 2003; Zeugolis et al., 2009; Achilli and Mantovani, 2010; Gordon and Hahn, 2010; Gigante et al., 2013;

He and Theato, 2013; Antoine et al., 2014; Chattopadhyay and Raines, 2014). Both sample types underwent the aforementioned ethanol series sterilization and rehydration process.

Two samples from each type were subjected to the same cell culture conditions outlined in section 5.4.1 at two independent occasions (n=8 per sample type for two each set of experiments, and a total of 32 samples per testing batch). 4 sample retrieval and fixation time points post-seeding were chosen for the two sets of 7-day periods relative to initial cell seeding, specifically: 6h, day 1, day 4, day 7.

These experiments were conducted to qualitatively establish extended cyto-compatibility as a consequence of fibroblast cell attachment and survival over the allotted time period. A similar immunocytochemical staining protocol as outlined in section 5.4.1 was utilized. Hoechst staining and Alexa Fluor 488 Phalloidin staining was performed on collagen standalone and 3D printed Col-PPy 1:4 samples to visualize nuclei and actin filaments of human BJ fibroblast cells to evaluate potential changes in cell morphology for each sample type. Cells were fixed by adding 4% ParaFormaldehyde in 1X PBS buffer as samples were retrieved per sample retrieval time points. On the final retrieval day, all samples previously fixed with ParaFormaldehyde were permeabilized with 0.1% solution of Triton 100X dissolved in 1X PBS buffer solution, incubated with 1% BSA (Blocking solution/ buffer A) for 30 min, and then incubated with 1:40 Phalloidin stain for 20 min. After performing Phalloidin actin staining, samples were incubated in 1:1000 diluted Hoescht stain for 20 min at room temperature. Stained cells were housed in 1X PBS buffer, protected from light. Subsequently, samples were imaged using an AxioImager.M2m with Zen software (Zeiss) at 5$\times$ and 20$\times$ magnification. Results of this investigation are shown in Figure 5.21 and Figure 5.22.

3.3.9 Confocal Laser Scanning Microscopy Evaluation

Confocal Laser Scanning Microscopy (CLSM) was conducted on 10 mm $\times$ 10 mm $\times$ 0.5 mm collagen standalone and Col-PPy 1:4 wt% grid samples. A LSM 5 Duo Vario Microscope using Zen Software (Zeiss) was appropriated to provide topographic contrast and to supplement SEM imaging, as SEM imaging required samples to be sufficiently dried which understated topographical properties and surface roughness of constructs. CLSM results are reported in Figure 5.23.

3.4 Chapter Summary

This chapter outlined the materials and methods used in the thesis. This chapter includes the process of the initial exploratory phase of the research programme, which lead to the development of the DIW AM fabrication methodology for Col-PPy constructs. Challenges encountered during the development of the DIW AM methodology for PPy were discussed, and subsequent, successful development of Col-Py inks specially formulated for DIW is outlined. This chapter provided relevant knowledge on the configuration of the DIW printer and associated process matters. Lastly, this chapter outlined the experimental methods and characterization evaluations performed for assessing the functional aspects and physical properties of said constructs.

List of references

Achilli, M. and Mantovani, D. (2010), 'Tailoring mechanical properties of collagen-based scaffolds for vascular tissue engineering: The effects of ph, temperature and ionic strength on gelation', *Polymers* **2**(4), 664–680.

Akhmanova, M., Osidak, E., Domogatsky, S., Rodin, S. and Domogatskaya, A. (2015),

'Physical, spatial, and molecular aspects of extracellular matrix of in vivo niches and artificial scaffolds relevant to stem cells research', *Stem Cells International* pp. 1–35.

Annabi, N., Nichol, J. W., Zhong, X., Ji, C., Koshy, S., Khademhosseini, A. and Dehghani, F. (2010), 'Controlling the porosity and microarchitecture of hydrogels for tissue engineering.', *Tissue Eng Part B Rev* **16**(4), 371–383.

Antoine, E. E., Vlachos, P. P. and Rylander, M. N. (2014), 'Review of collagen i hydrogels for bioengineered tissue microenvironments: characterization of mechanics, structure, and transport.', *Tissue Eng Part B Rev* **20**(6), 683–696.

Armes, S. (1987), 'Optimum reaction conditions for the polymerization of pyrrole by iron(iii) chloride in aqueous solution', *Synthetic Metals* **20**(3), 365–371.

ASTM Standard ASTM52900 - 15 (2015), *Terminology for Additive Manufacturing Technologies*, ASTM International, West Conshohocken, PA.

Bjorklund, R. B. (1987), 'Kinetics of pyrrole polymerisation in aqueous iron chloride solution', *Journal of the Chemical Society, Faraday Transactions 1: Physical Chemistry in Condensed Phases* **83**(5), 1507–1514.

Boyce, S. T., Christianson, D. J. and Hansbrough, J. F. (1988), 'Structure of a collagen-GAG dermal skin substitute optimized for cultured human epidermal keratinocytes', *Journal of biomedical materials research* **22**(10), 939–957.

Chattopadhyay, S. and Raines, R. (2014), 'Review collagen-based biomaterials for wound healing', *Biopolymers* **101**(8), 821–833.

Chevallay, B. and Herbage, D. (2000), 'Collagen-based biomaterials as 3d scaffold for cell cultures: applications for tissue engineering and gene therapy', *Medical and Biological Engineering and Computing* **38**(2), 211–218.

Cione, A., Neumann, M. and Gessner, F. (1998), 'Time-dependent spectrophotometric study of the interaction of basic dyes with clays: Iii. mixed dye aggregates on swy-1 and laponite', *Journal of Colloid and Interface Science* **198**(1), 106–112.

Gelse, K. (2003), 'Collagens—structure, function, and biosynthesis', *Advanced Drug Delivery Reviews* **55**(12), 1531–1546.

Gigante, A., Busilacchi, A., Lonzi, B., Cecconi, S., Manzotti, S., Renghini, C., Giuliani, A. and Mattioli-Belmonte, M. (2013), 'Purified collagen i oriented membrane for tendon repair: An ex vivo morphological study', *Journal of Orthopaedic Research* **31**(5), 738–745.

Gordon, M. and Hahn, R. (2010), 'Collagens', *Cell and Tissue Research* **339**(1), 247–257.

He, L. and Theato, P. (2013), 'Collagen and collagen mimetic peptide conjugates in polymer science', *European Polymer Journal* **49**(10), 2986–2997.

Holness, F. and Price, A. (2018), 'Direct ink writing of 3d conductive polyaniline structures and rheological modelling', *Smart Materials and Structures* **27**(1).

Inzana, J., Olvera, D., Fuller, S., Kelly, J., Graeve, O., Schwarz, E., Kates, S. and Awad, H. (2014), '3d printing of composite calcium phosphate and collagen scaffolds for bone regeneration', *Biomaterials* **35**(13), 4026–4034.

Jayamurgan, P., Ponnuswamy, V., Ashokan, S. and Mahalingam, T. (2013), 'The effect of dopant on structural, thermal and morphological properties of DBSA-doped polypyrrole', *Iranian Polymer Journal* **22**(3), 219–225.

Li, H. and Khor, E. (1994), 'Interaction of collagen with polypyrrole in the production of hybrid materials', *Polymer International* **35**(1), 53–59.

Lode, A., Meyer, M., Brüggemeier, S., Paul, B., Baltzer, H., Schröpfer, M., Winkelmann, C., Sonntag, F. and Gelinsky, M. (2016), 'Additive manufacturing of collagen scaffolds by three-dimensional plotting of highly viscous dispersions', *Biofabrication* **8**(1), 015015.

Machida, S., Miyata, S. and Techagumpuch, A. (1989), 'Chemical synthesis of highly electrically conductive polypyrrole', *Synthetic Metals* **31**(3), 311–318.

Madihally, S. and Matthew, H. (1999), 'Porous chitosan scaffolds for tissue engineering', *Biomaterials* **20**(12), 1133—1142.

Mallapragada, S. K. and Peppas, N. A. (1996), 'Dissolution mechanism of semicrystalline poly (vinyl alcohol) in water', *Journal of Polymer Science Part B: Polymer Physics* **34**(7), 1339–1346.

McKee, C. T., Last, J. A., Russell, P. and Murphy, C. J. (2011), 'Indentation versus tensile measurements of young's modulus for soft biological tissues.', *Tissue Eng Part B Rev* **17**(3), 155–164.

Mekonnen, B. T., Ragothaman, M., Kalirajan, C. and Palanisamy, T. (2016), 'Conducting collagen-polypyrrole hybrid aerogels made from animal skin waste', *RSC Advances* **6**, 63071–63077.

Mobini, S., Leppik, L. and Barker, J. (2016), 'Direct current electrical stimulation chamber for treating cells in vitro', *BioTechniques* **60**, 95–98.

Nagai, T. and Suzuki, N. (2000), 'Isolation of collagen from fish waste material - skin, bone and fins', *Food Chemistry* **68**(3), 277–281.

Nocera, A., Comín, R., Salvatierra, N. and Cid, M. (2018), 'Development of 3d printed fibrillar collagen scaffold for tissue engineering', *Biomedical Microdevices* **20**(2).

Offeddu, G., Ashworth, J., Cameron, R. and Oyen, M. (2015), 'Multi-scale mechanical response of freeze-dried collagen scaffolds for tissue engineering applications', *Journal of the Mechanical Behavior of Biomedical Materials* **42**, 19–25.

Oh, H. H., Ko, Y.-G., Lu, H., Kawazoe, N. and Chen, G. (2012), 'Preparation of porous collagen scaffolds with micropatterned structures', *Advanced materials* **24**(31), 4311–4316.

Ozdemir, F. A., Demirata, B. and Apak, R. (2009), 'Adsorptive removal of methylene blue from simulated dyeing wastewater with melamine-formaldehyde-urea resin', *Journal of applied polymer science* **112**(6), 3442–3448.

Pikal, M. J. (1999), *Mechanisms of protein stabilization during freeze-drying and storage: the relative importance of thermodynamic stabilization and glassy state relaxation dynamics*, Vol. 96, Marcel Dekker Inc., New York.

Prahl, S. (2001), 'Optical absorption of methylene blue', http://omlc.ogi.edu/spectra/mb/index.html.

Rapi, S., Bocchi, V. and Gardini, G. (1988), 'Conducting polypyrrole by chemical synthesis in water', *Synthetic Metals* **24**(3), 217–221.

Rhee, S., Puetzer, J. L., Mason, B. N., Reinhart-King, C. A. and Bonassar, L. J. (2016), '3D Bioprinting of Spatially Heterogeneous Collagen Constructs for Cartilage Tissue Engineering', *ACS Biomaterials Science & Engineering* **2**(10), 1800–1805.

Suntornnond, R., Tan, E. Y. S., An, J. and Chua, C. K. (2016), 'A mathematical model on the resolution of extrusion bioprinting for the development of new bioinks', *Materials* **9**(9), 756.

Yang, X., Lu, Z., Wu, H., Li, W., Zheng, L. and Zhao, J. (2018), 'Collagen-alginate as

bioink for three-dimensional (3d) cell printing based cartilage tissue engineering', *Materials Science and Engineering C* **83**, 195–201.

Yeong, W.-Y., Chua, C.-K., Leong, K.-F., Chandrasekaran, M. and Lee, M.-W. (2007), 'Comparison of drying methods in the fabrication of collagen scaffold via indirect rapid prototyping', *Journal of Biomedical Materials Research - Part B Applied Biomaterials* **82**(1), 260–266.

Zeugolis, D. I., Paul, G. R. and Attenburrow, G. (2009), 'Cross-linking of extruded collagen fibers-A biomimetic three-dimensional scaffold for tissue engineering applications', *Journal of Biomedical Materials Research Part B: Applied Biomaterials* **89A**(4), 895–908.

Chapter 4

Characterization of Direct-ink Write printed Collagen and PPy-based constructs: Part 1

This chapter begins with discussion of the hypothesis which lead to the development of a DIW AM fabrication methodology for Col-PPy constructs. Characterization of the rheological behaviour of ink materials at varying concentrations of Py are reported. Additionally, optical imaging is employed to evaluate the degree of integration between collagen and PPy components within 3D printed constructs at varying PPy concentrations, and to exhibit various structures produced using the DIW methodology. In this chapter, the major functional properties innate to PPy-based constructs, i.e. electro-conductivity and electro-activity, are evaluated to provide insight towards arenas in which the DIW printed hybrid composition can be effectively applied, as well as provide edification on areas which warrant further development.

4.1 Discussion of DIW AM methodology

The lack of development in fabrication methodology has been withstanding motif for PPy-based constructs for some time. Despite the low immunogenicity and the potentially biomimetic topographical, chemical and mechanical cues imparted by a PPy substrate, and modifiable electroactivity, electroconductivity and biodegradability properties that make PPy-based structures promise, such platforms for tissue engineering applications remain gravely limited to fabrication of structures simple and basic in design. This limitation is due to dependence on a fabrication methodology that has remained predominately stagnant since its advent (Li and Khor, 1994; Atala et al., 2012); therefore, limiting application and translation prospects which warrant introduction of feature and geometric complexity to constructs under study.

The nearest claim to be made towards truly 3D printing PPy-based hydrogel structures is the work done by Weng et al. (2011, 2012). Weng *et. al.* inkjet printed collagen droplets on top of pre-produced, patterned and inkjet printed nanoparticles of PPy films. PPy films were produced as PPy nanoparticles dispersed in the ink were pushed through a 25.0 V nozzle head, which served to polymerize PPy aggregates as the ink was ejected from the nozzle in a drop-like manner. Subsequently, these films were seeded with a population of PC12 cells and electrically stimulated (Weng et al., 2011, 2012). Although a unique method of AM is utilized here, produced PPy films are not 3D. Rather these thinly layered films, where the integration between successive layers is a dubious prospect at best as PPy standalone films have not been observed to be self-healing, face the same problems associated with 2D films produced via traditional fabrication methodologies. In addition to the scale issue of produced structures, there exists a risk of the collagen coating (which rests on top of the PPy film) being removed from its inkjet-printed position in a bioreactor or in vivo environment due to friction due to lack of integration or direct interaction between the collagen and PPy components.

Producing PPy-based constructs using AM techniques has been a challenge, and the main reason behind this is PPy's poor processability, in its polymer state (discussed in 2.6.

However, by subjecting the Col-Py ink to freezing temperatures, as printed geometry of constructs is maintained effectively. Examples of this are reported in Figure 4.3. This deviation is at the crux of the novel fabrication methodology for 3D printed PPy-based scaffolds reported in this thesis, because the scaffolding material, i.e. collagen, can now be exchanged for any other naturally derived or synthetically derived hydrophilic materials that freeze and solidify when subjected to cold temperatures, like the ones mentioned in 2.1, namely: dECM, hyaluronic acid, fibrinogen, gelatin, chitosan, etc. In addition to exchanging the scaffolding base component, the dopant-PPy relationship is also open to modulation. Dopant species can dictate topography, morphology, electrical conductivity and other physical properties of PPy-based composites and products (Yan et al., 2017). For instance, large anionic dopant species tend to be immobile within the PPy polymer backbone, forcing the electro-activity response of PPy to be cationic dependent (Otero and Martinez, 2016). This phenomena can be used to sequester drugs or molecules in the vicinity of the construct, allowing the PPy construct to potentially serve as a controlled drug release system or as a biosensor (Edmondson et al., 2014; Entezami and Massoumi, 2006; Koetting et al., 2015; Pillay et al., 2014).

Essentially, the small deviation from traditional fabrication methods now enables researchers with creative freedom in their product design, as a function of DIW AM. It creates room for researchers to tailor important functional properties such as biodegradability, topography, geometric complexity and dimensionality, as well as impart functional electrochemomechanical properties to their scaffolds and constructs (Guo et al., 2013; Asti and Gioglio, 2014). The development of this fabrication technique equips researchers with a versatile and valuable tool which opens up new possibilities in tailoring their *in vitro* constructs to a range of biomedical applications for studying *in vivo* tissue

Table 4.1: Preliminary electrical conductivity measurements using 4-point probe technique were performed on Col-PPy 1:1 wt% bulk aerogel samples (n=1 per concentration) polymerized in varying solvents.

Solvent	**Conductivity** ($S \cdot cm^{-1}$)	**Elapsed polymerization time** (s)
0.5 M Acetic Acid	5.02×10^{-3}	60
100% EtOH	5.46×10^{-3}	45
diH_2O	2.51×10^{-3}	69

response and evaluating *in vitro* cell behaviour following modulation by said constructs.

Table 4.2: Time elapsed for complete polymerization observed for grid structures (n=1 per concentration) produced at varying Py concentrations. Samples were polymerized in 100% EtOH is reported.

Sample	Elapsed polymerization time (s)
DIW Col-PPy 1:1 wt%	45
DIW Col-PPy 1:2 wt%	40
DIW Col-PPy 1:4 wt%	33

4.1.1 Preliminary Empirical Evaluation Results

Table 4.2 reports the variance in time elapsed for complete polymerization, a qualitative measure, which was observed for 1:1 wt% and 1:2 wt% concentrations of Py are attributed to insufficient homogenization as the resultant colour change was not seen to be always reach black, rather a dark brown. Another confounding factor contributing to insufficient polymerization can be attributed to inadequate freezing prior to the polymerization step. During transfer from the cold storage to the polymerization solution, it was observed that inadequate freezing led to loss in structural integrity for 3D printed structures post polymerization as well as incomplete polymerization where structures lacked opacity inherent to PPy constructs. This variability in reproducibility is dependent on operator influence. However, this can be taken care of with the incorporation of a cold-bed and remains one of the limitations of this fabrication methodology at this point. Additionally, these structures were seen to dissolve within a week's time if sufficient polymerization was not observed. This was not observed to be the case for Col-PPy 1:4 wt% DIW printed samples, which were observed to undergo polymerization readily and completely in comparison to other inks. For these reasons, Col-Py 1:4 wt% was chosen as the ink of choice.

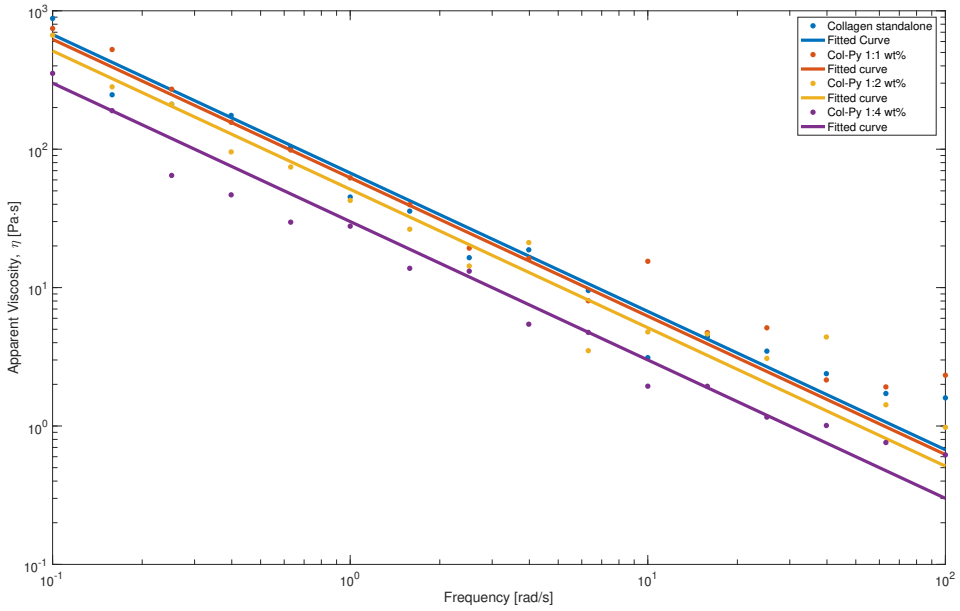

Figure 4.1: Shear-thinning behaviour is observed for all investigated compositions. No drastic decrease in viscosity is observed with increase in Py monomer concentration.

4.2 Rheology Results

All compositions showed favourable shear-thinning behaviour typical of DIW inks as observed in Figure 4.1. Furthermore, print resolution and quality was observed to be majorly controlled by end-process parameters in the DIW process, rather than Col or Py concentrations, such as the paste extruder pressure, nozzle height from print bed and print nozzle diameter. These parameter were then adjusted for optimum paste volume flow.

Comparisons between theoretical values generated using the methodology outlined in 3.3.1 against empirical trackwidth data as a function of applied pressures, at various print speeds for Col-Py 1:4 wt% composition is reported in Figure 4.2. It was empirically established that the Col-Py inks flowed well at low pressures, ranging from 15–20 psi. However, process refinement was required for increasing print resolution.

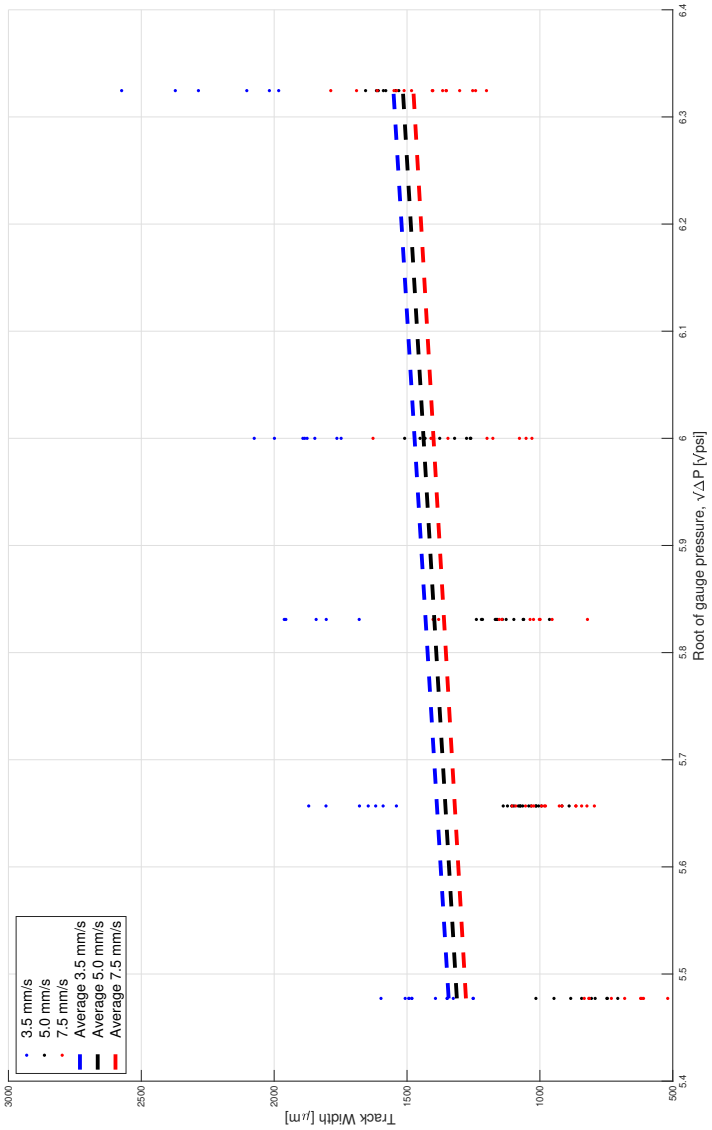

Figure 4.2: Trackwidths for Col-Py 1:4 wt% inks are empirically compared against theoretical values generated using the mathematical model reported by Suntornnond et al. (2016).

4.2.1 Discussion

In accordance with the model presented by Suntornnond et al. (2016), which correlates print process parameters such as print speed, nozzle diameter, nozzle length and applied pressure with track width of material deposited, the power law index (n) for each of the compositions was determined and used to inform on optimum paste volume flow rate. If $n < 1$, the apparent viscosity of the material tends to decrease as shear rate is increased. This behaviour is indicative of a fluid property called shear thinning (Cross, 1979). All compositions demonstrated favourable shear-thinning behaviour which was in line with empirical observations of material extruding more uniformly as applied pressure increased.

Furthermore, in line with work by Suntornnond et al. (2016), print resolution was observed to be controlled by end-process parameters such as the extruder pressure, nozzle diameter and print speed but also nozzle height, relative to the print bed. Simply, if the nozzle was farther away from the print bed, this lead to thinner trackwidths, but a shorter nozzle height produced trackwidths thicker in size. Another factor influencing empirical trackwidth values is the anisotropy of the collagen ink, which remains a limiting factor in achieving uniform trackwidth values. Collagen ink anisotropy from either insufficient homogenization, insufficient solubilization or due to the self-aggregating property of collagen if stored at greater than 4°C for more than two weeks resulted in aggregates which were likely to clog the nozzle. For the aforementioned reasons, a disparity between empirical and expected trackwidths exists and is reflected in Figure 4.2.

The model used in generating theoretical values assumes that deposited material retains its as extruded, cylindrical form and that the deposited material does not bleed out or flatten after deposition. This variability was not observed to be the case for Col-Py ink and was not effectively predicted by by Suntornnond et al. (2016) as structures not transferred to the cold storage units quickly enough led to fused extruded tracks (as shown in Figure A.3).

4.3 Optical Imaging

Depicted in Figure 4.3 are the types of PPy-based structures and features producible using the fabrication methodology reported in this thesis. Limitations associated with the feature resolution for the reported fabrication methodology are similar to those inherent to all DIW processes Zhu et al. (2016). In addition to being limited by components of the DIW printer itself, the low viscosity of the ink can undermine the structural integrity of the printed structures where extruded-widths may be prone to bleeding. Also, structures that require overhang, as such is the case in Figure 4.3 (a-c), are difficult to produce effectively as the curing parameters cannot be introduced fast enough to retain as extruded geometry. This delay in curing parameters is currently without intervention which serves to limit geometric complexities of producible structures. In the case of the Col-Py ink, the onset, duration and other components of curing parameters such as the freezing for collagen and chemical oxidation polymerization for PPy require further development in the DIW apparatus to allow the creation of more complex 3D structures. For instance, the use of a cold-bed that freezes extruded materials as it is deposited could enhance the resolution of printed structures and retention of creation more complex 3D structures such as overhangs or bridges. Lastly, confocal optical imaging was performed on cross-sections of collagen standalone and the Col-PPy 1:4 wt% structures, as shown in Figure 4.4. Additional examples of 3D printed structures are included in Appendix A.2.

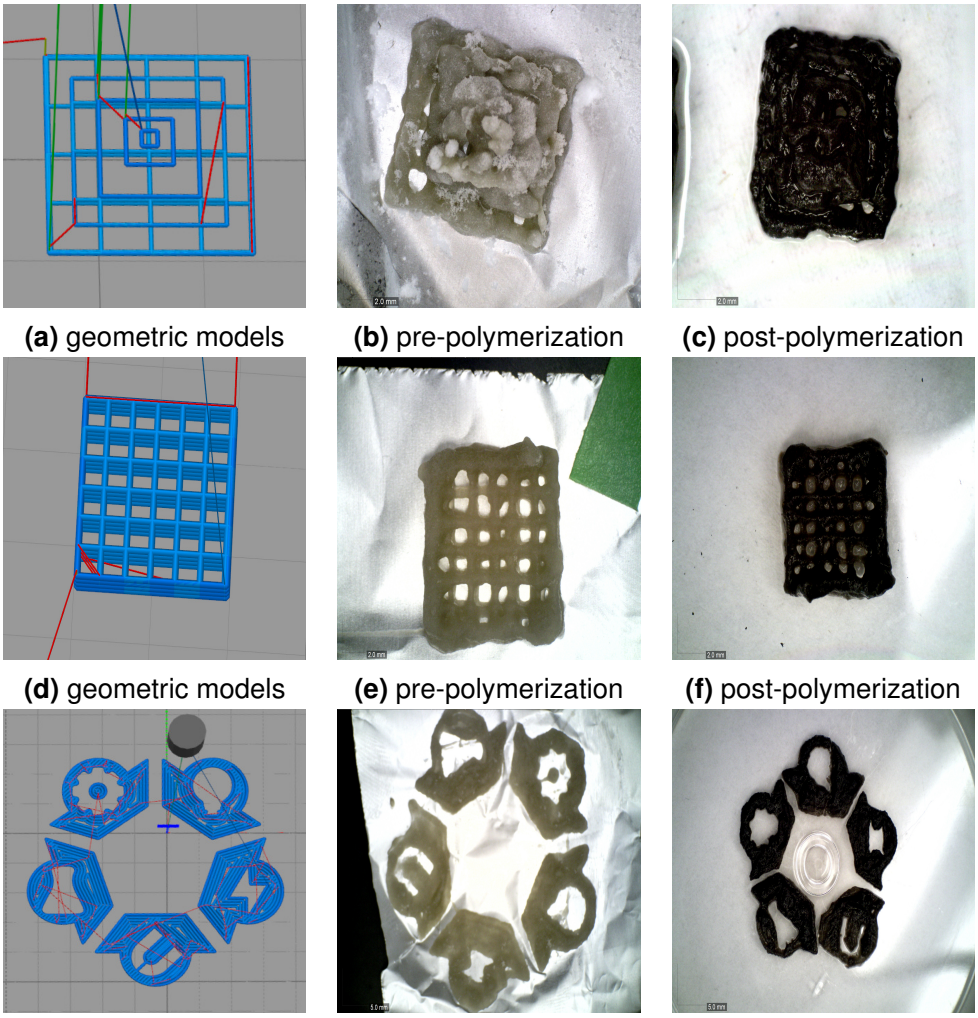

(a) geometric models **(b)** pre-polymerization **(c)** post-polymerization

(d) geometric models **(e)** pre-polymerization **(f)** post-polymerization

(g) geometric models **(h)** pre-polymerization **(i)** post-polymerization

Figure 4.3: Optical images of 3D multilayered Col-PPy 1:4 wt% structures at different stages of the DIW process are depicted here. (a), (d) and (h) depict geometric models of 3D pyramid (20% infill), grid (50% infill) and OMASML logo (100% infill) structures, respectively. (b), (e) and (i) depict optical images of structures as printed, i.e. pre-polymerization of PPy, and (c), (f) and (i) depict optical images of structures post-polymerization.

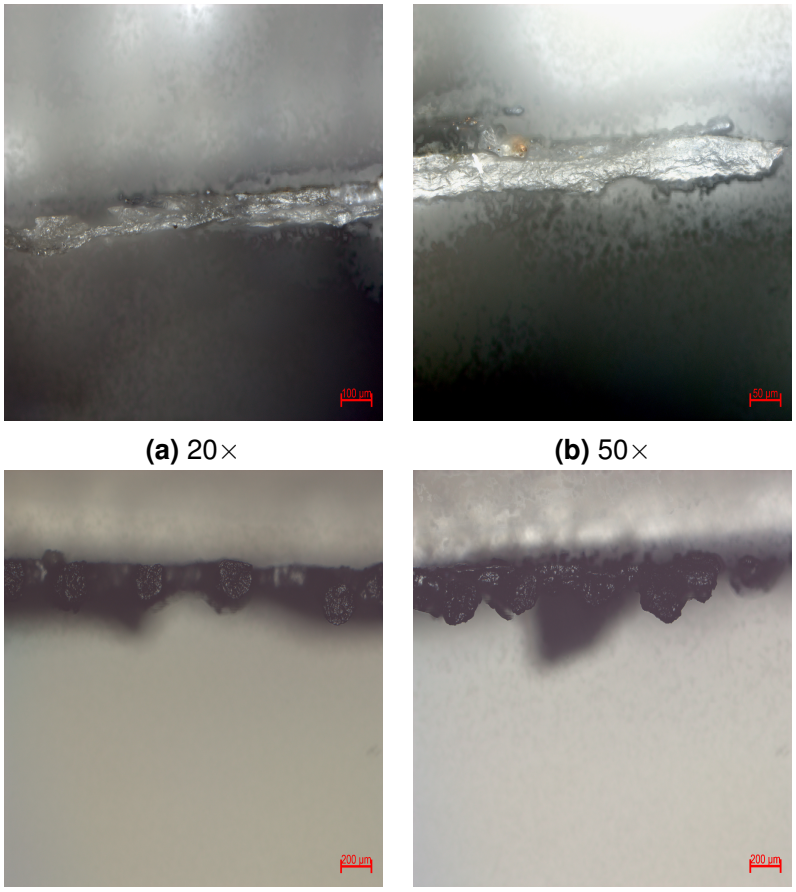

(a) 20× **(b)** 50×

(c) 20× **(d)** 50×

Figure 4.4: Confocal optical imaging was performed at 50× on cryo-fractured monolayer grid cross-sections of 10 mm × 10 mm × 0.5 mm (a) collagen standalone sample pores, (b) collagen standalone sample rows, and along the (c) Col-PPy 1:4 wt% sample pores and (d) Col-PPy 1:4 wt% sample rows to show the degree of polymerization, i.e. collagen and PPy integration in the DIW printed structure, at the cross-sectional level.

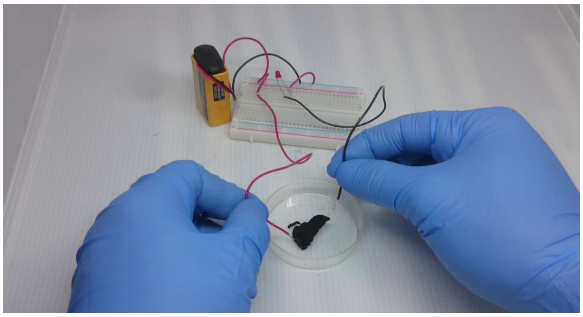

(a) bulk aerogel (Off)

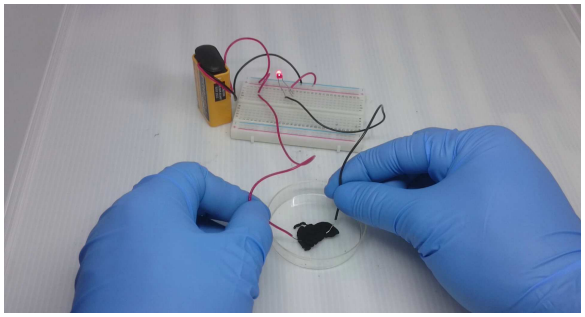

(b) bulk aerogel (On)

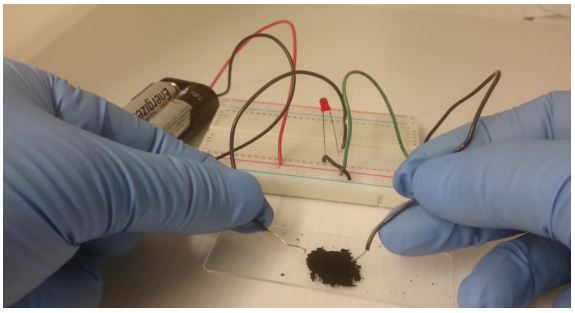

(c) fibrous aerogel (Off)

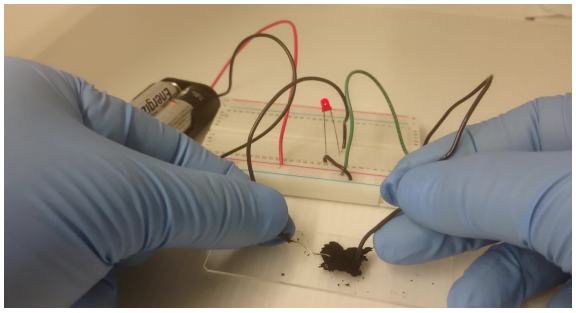

(d) fibrous aerogel (On)

Figure 4.5: Electrical conductivity of Col-PPy 1:1 wt% (a-b) bulk and (c-d) fibrous aerogels is demonstrated using an LED powered by a 9V battery, where the sample completes the circuit.

4.4 Electro-Conductivity Results

Table 4.3: Correction factors (C_f) pertaining to resistivity measurements performed using 4-point probe technique are reported. C_f values are chosen in accordance with the standards set by Topsoe (1986). * denotes that the average C_f, however, as sample thickness varied subtly between 3D printed samples, C_f chosen were specific to each sample's thickness.

Col-PPy sample type	**Standard**	**C_f**
Bulk aerogel 1:1 wt%	Semi-infinite plane sample of finite thickness	0.2686
Fibrous aerogel 1:1 wt%	Infinite plane sample of finite thickness	0.36
DIW constructs	Infinite plane sample of finite thickness	0.446*

Table 4.4: Electrical conductivity measurements for Col-PPy 1:1 wt% bulk and fibrous aerogels, and DIW printed Col-PPy 1:1 wt%, 1:2 wt% and 1:4 wt% samples using 4-point probe technique are reported.

Sample	**Max Conductivity** ($S \cdot cm^{-1}$)	**Min Conductivity** ($S \cdot cm^{-1}$)	**Mean Conductivity** ($S \cdot cm^{-1}$)
Bulk aerogel 1:1 wt%	5.90×10^{-3}	4.46×10^{-3}	$3.82 \times 10^{-3} \pm 9.32 \times 10^{-4}$
Fibrous aerogel 1:1 wt%	2.24×10^{-5}	1.07×10^{-5}	$1.70 \times 10^{-5} \pm 5.89 \times 10^{-6}$
DIW Col-PPy 1:1 wt%	2.50×10^{-5}	1.51×10^{-6}	$4.87 \times 10^{-6} \pm 4.73 \times 10^{-6}$
DIW Col-PPy 1:2 wt%	2.93×10^{-5}	9.09×10^{-7}	$6.04 \times 10^{-6} \pm 5.08 \times 10^{-6}$
DIW Col-PPy 1:4 wt%	2.50×10^{-5}	2.50×10^{-6}	$9.06 \times 10^{-6} \pm 6.50 \times 10^{-6}$

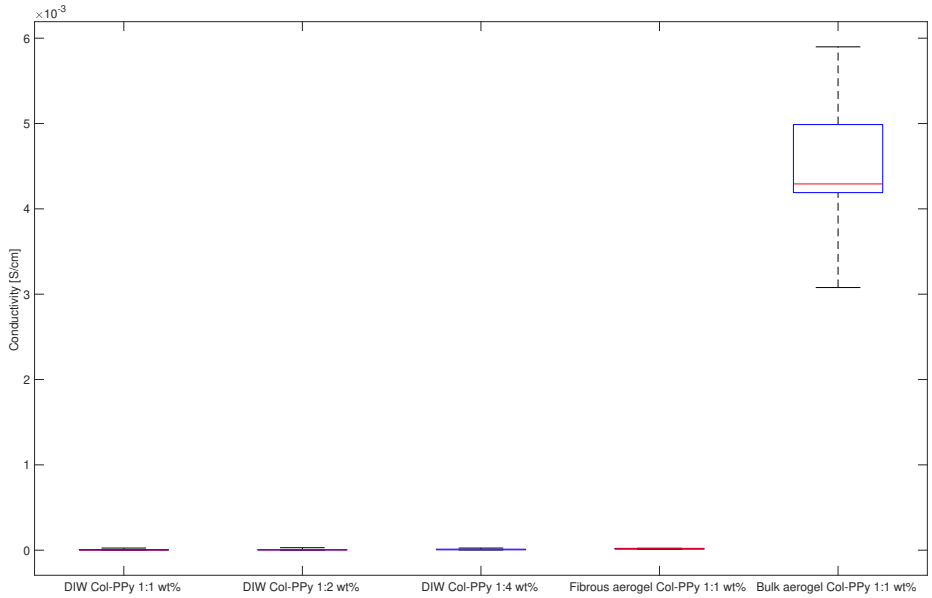

(a)

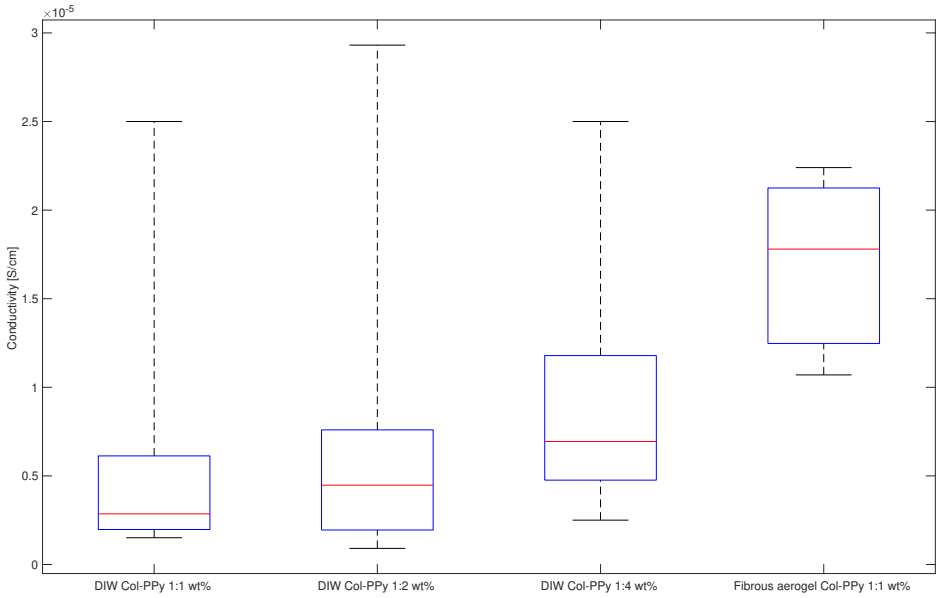

(b)

Figure 4.6: Comparisons for electrical conductivity results between (a) all fabricated structures, i.e. Col-PPy 1:1 wt% bulk and fibrous aerogels, and DIW Col-PPy 1:1 wt%, 1:2 wt% and 1:4 wt%, as well as a comparison between (b) Col-PPy 1:1 wt% fibrous aerogels and DIW Col-PPy 1:1 wt%, 1:2 wt% and 1:4 wt% samples are depicted.

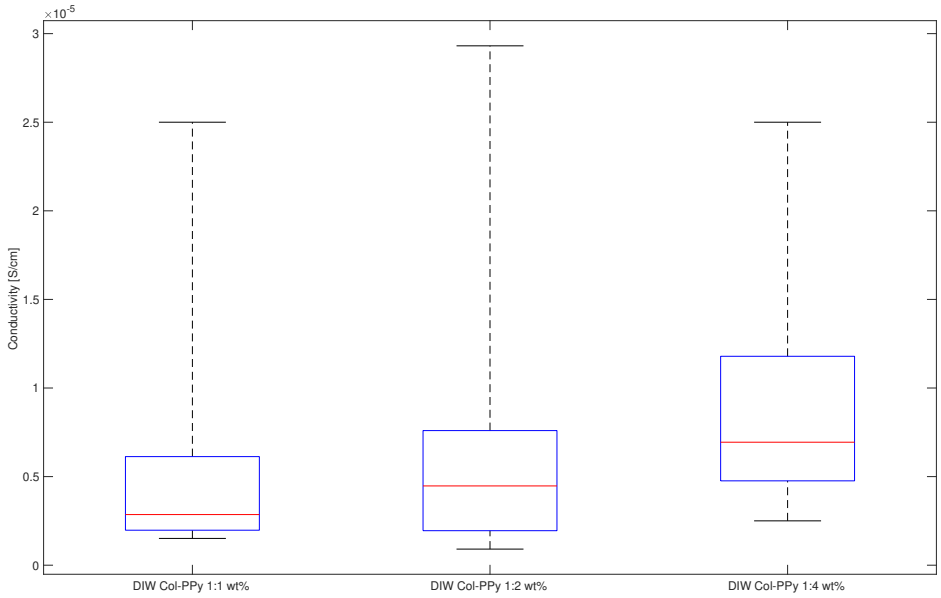

Figure 4.7: A comparison for electrical conductivity results between DIW Col-PPy 1:1 wt%, 1:2 wt% and 1:4 wt% samples are depicted.

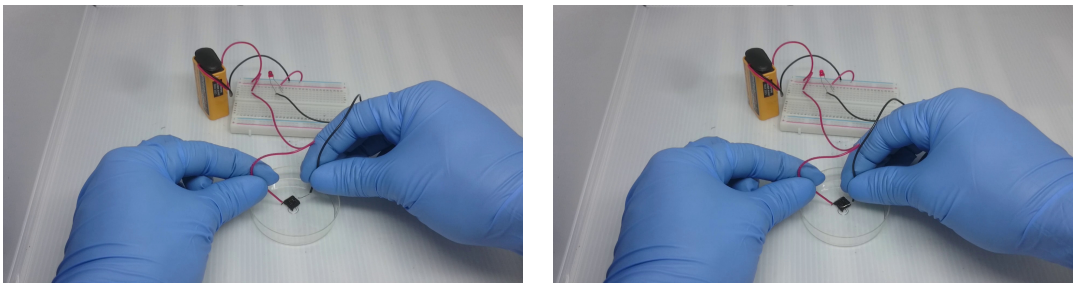

(a) **(b)**

Figure 4.8: Electrical conductivity of Col-PPy1:4 wt% multilayered grids is demonstrated using an LED powered by a 9V battery, where the sample serves to complete the circuit.

4.4.1 Discussion

PPy is electrically conductive due to charge transport occurring along the conjugated polymer chains. Single and double bonds along the polymer chain both contain a chemically strong, localized σ-bond, while double bonds also contain a less strongly localized *p*-bond, where *p*-orbitals overlap, allowing hopping of charge carriers, i.e. holes, polarons, and bipolarons (Khalkhali, 2005; Ansari, 2006). Therefore, electrical conductivity is dependent on the number of charges and their relevant mobility. Since the polymer is chemically oxidatively synthesized in its oxidized, conducting form only the incorporation of dopant molecules (typically, large, negative charged and immobile) stabilizes and neutralizes charge on the polymer backbone (Khalkhali, 2005). The availability of charges is therefore also influenced by the presence of the dopant anions. Increasing dopant levels has been shown to increase in the density of charge carriers and led to the production of conductive PPy films using electrochemical polymerization, for instance, 5×10^{-2} S $\cdot$ cm^{-1} (Kupila and Kankare, 1995; Lee et al., 1995).

Li and Khor (1994) reported an electrical conductivity of 1.4 S $\cdot$ cm^{-1} for their Col-PPy 1:3.35 wt% precipitates, made from a 2 mg $\cdot$ mL^{-1} collagen solution. The maximum conductivity of Col-PPy aerogels reported by Mekonnen et al. (2016) is 3.59×10^{-4} S $\cdot$ cm^{-1} for their Col-PPy-AQSA 1:1 wt% aerogel composition, whereas the maximum conductivity of Col-PPy-DBSA 1:1 wt% bulk aerogels was determined to be 5.90×10^{-3} S $\cdot$ cm^{-1}. This difference in aerogel electro-conductive properties is attributed to dopant choice, as dopants influence the number of charge carriers on the polymer backbone contributing to the construct's electrical conductivity. Interestingly, it is observed that the size of the construct also influences electrical properties, per the results in Table 4.4.

One reason as to why the electrical conductivity of 3D printed Col-PPy constructs does not significantly change as monomer concentration is increased twice-fold or four-fold may be due to the delay aspect included in this DIW AM methodology used to

generate the constructs (Figure 4.7). A natural impedance is imparted by the presence of collagen fibres that may not be sufficiently coated by PPy, i.e. pockets or islands where the oxidant was unable to reach and polymerize pyrrole sufficiently or where pyrrole presence was insufficient, despite best homogenization efforts, resulting in lowered electrical conductivity of the structure.

The aerogels produced using the protocol reported in Mekonnen et al. (2016) exhibit higher electrical conductivity as do the fibrous Col-PPy constructs. Traditional fabrication processes such as the one reported in Mekonnen et al. (2016) involve the production of structures where the scaffolding component blended with Py experiences complete oxidative polymerization, with size restrictions, while excess is washed away. Whereas, in the fabrication methodology presented in this paper, all the collagen-Py ink 3D printed constitutes the entirety of the polymerized scaffold, where polymer chain lengths may be result in fewer electro-conductive islands in areas of insufficient PPy presence. This leads to the number of polymer backbones available and contributing to the PPy structure to not be as well connected as may be the case in the aerogel structures, therefore presenting as lower electrical conductivity despite the smaller construct size of the DIW structures. This relationship is reflected in Figure 4.6 and Table 4.4 where size of the construct seems to influences electrical conductivity.

Although a number of electro-conductive scaffolds and constructs exist in literature, as discussed in section 2.3.3, variance in biologically relevant outcomes such as proliferation and apoptosis is observed between cell types and experiments conducted on the same materials (Love et al., 2018). One reason for why electro-conductive scaffolds have not seen prominence nor renown is due to this variance in response observed under similar stimulation parameters on different substrates, or on the exact same substrate under slightly varied stimulation parameters (Stewart et al., 2015; Merrill et al., 2005; Men et al., 2010; Song et al., 2002). Another reason electrically conductive constructs don't see much light of day is because, as of yet, no gold standard, protocol or plat-

form exists for parameters on electrically stimulating cells, for each electro-conductive scaffold or substrate varies in its degree of electrical conductivity generated across the construct (Love et al., 2018; Shi et al., 2016; Guiseppi-Elie, 2010). This suggests that although electrical conductivity can serve as an instructive construct for directing cell behaviour of select cell types under practical electrical parameters and is an effective means for achieving favourable results such as cell proliferation or stem cell differentiation, dissimilarity between the physical properties and consumed charge of the various electro-conductive constructs lends to confound workable comparisons and replication of those results on another construct under the same parameters. This makes difficult to extrapolate achievements of works investigating electro-conductivity towards translation. A careful selection and tailoring of the stimulation and physical parameters of the substrate for achieving target outcomes combined with a technique which produces uniform structures with uniform physical and electrical stimulation properties, for instance, 3D printing of electro-conductive scaffolds which presently provides uniformity to fabricated constructs. Therefore, providing a suitable answer towards overcoming the seeming variances of current findings in literature.

On the other hand, PPy constructs only consume charge when undergoing redox reactions, i.e. when functioning as an electro-active construct. Despite the decrease in electrical conductivity of the DIW constructs compared to bulk and fibrous Col-PPy aerogels, potential parameters can be appropriately adjusted to generate charge equivalent of past investigations to yield favourable results (Love et al., 2018; Guiseppi-Elie, 2010; Shi et al., 2016; Lee et al., 2018; Arteshi et al., 2018). Unfortunately, the application of the DIW PPy-based constructs as an effective means of achieving electrical stimulation of cells is not addressed in this thesis. This question remains to be answered by future investigations, however, the framework for creating these 3D electro-conductive PPy-based substrates is successfully established by this thesis.

4.5 Electro-activity Characterization Results

4.5.1 Cyclic Voltammetry Results

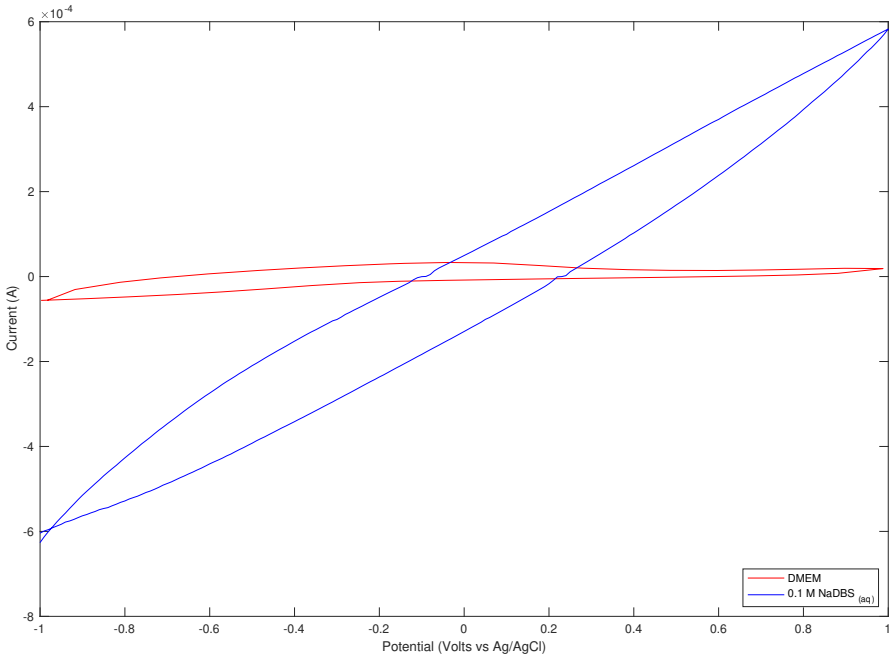

(a)

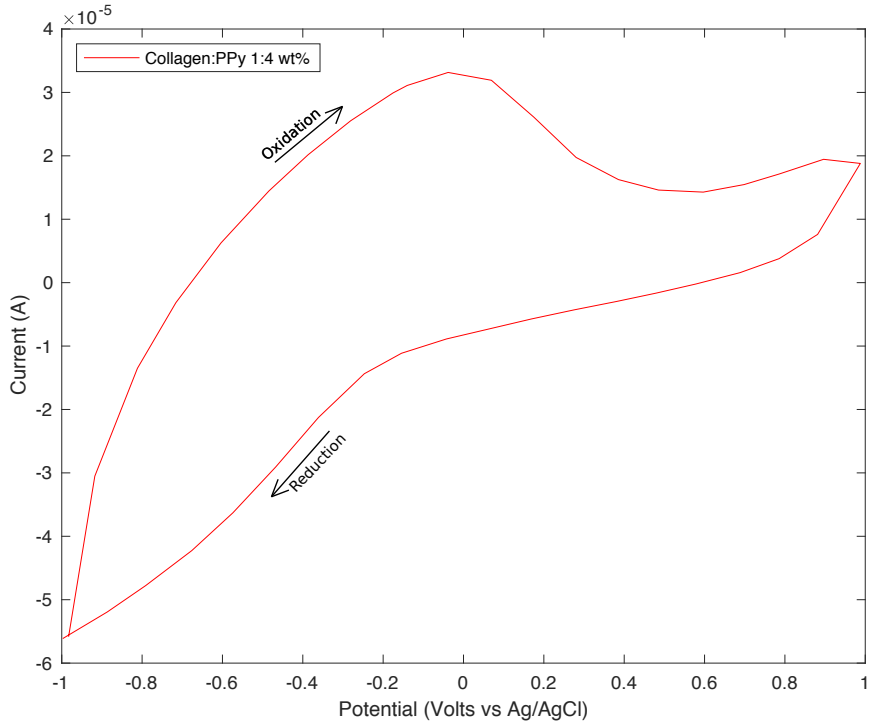

(b)

Figure 4.9: CV performed on 1.5 cm^2 Col-PPy 1:4 wt% samples in (a) DMEM and 0.1 M $NaDBS_{(aq)}$ at 100 mV/s at $\pm$1 V, and (b) DMEM solution at 100 mV/s at $\pm$1 V demonstrates lowered electro-activity in DMEM solution.

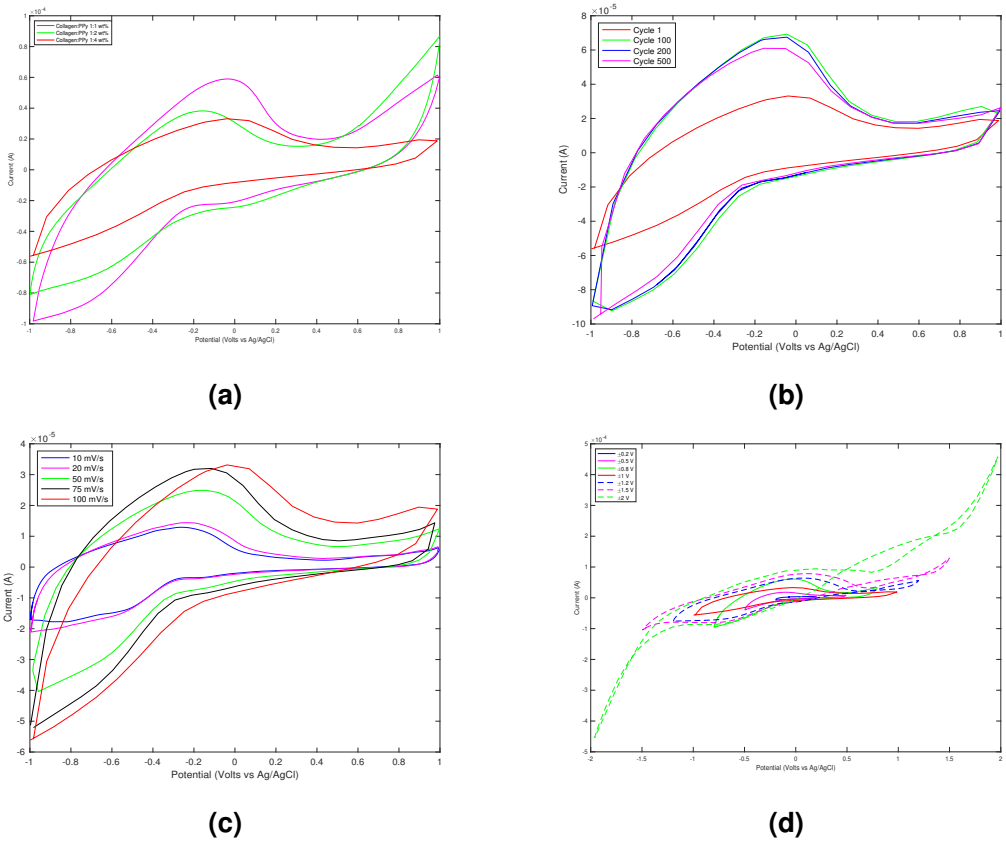

Figure 4.10: CV performed on 1.5 cm^2 samples of (a) Col-PPy 1:1 wt% vs. 1:2 wt% vs. 1:4 wt% in DMEM at 100 mV/s. (b) Col-PPy 1:4 wt% in DMEM at 100 mV/s, up to 500 cycles. (c) Col-PPy 1:4 wt% in DMEM, for various scan rates, at ± 1 V. (d) Col-PPy 1:4 wt% in DMEM for different potentials at 100 mV/s.

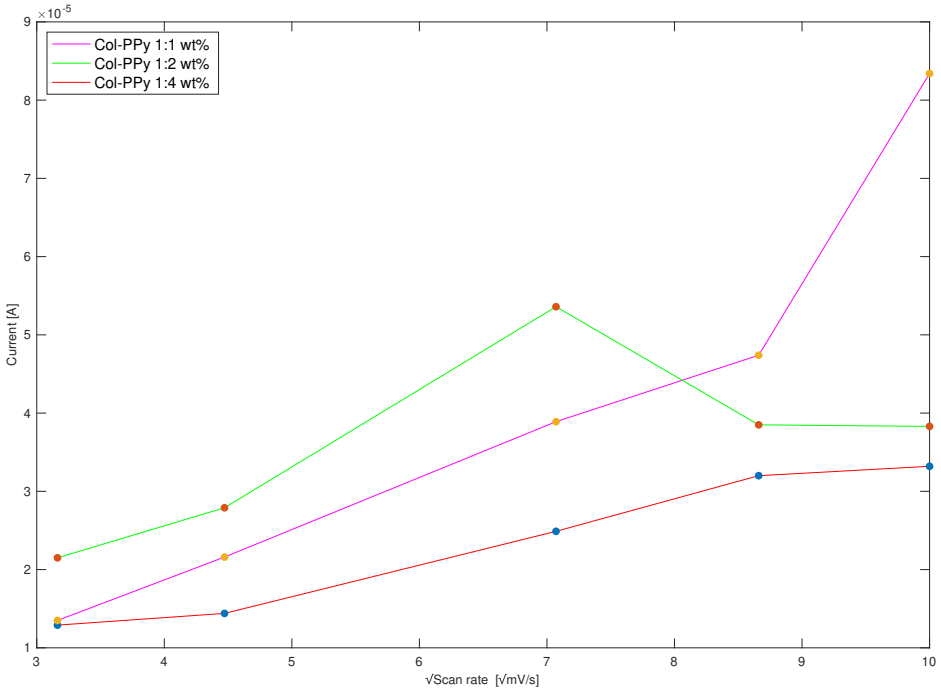

Figure 4.11: Peak anodic potentials for each of the Col-PPy compositions tested reveals the existence of an upper limit to the extent of electro-activity available from each PPy concentration under electrochemical switching.

Discussion

PPy-based constructs are well-suited as electro-active systems as the mechanism underlying this property of PPy allows for incorporation of charged ions during polymerization, and subsequent release of incorporated anionic and cationic molecules under electrical stimulation (Wadhwa et al., 2006; Kulkarni and Biswanath, 2007; Uppalapati et al., 2016; Tandon et al., 2018). This mechanism is outlined in section 2.5.2. Potential of the DIW Col-PPy constructs as vehicles of delivering therapeutic agents and as novel drug-delivery systems capable of directing cell behaviour is established in this section. These systems could serve as therapeutic alternatives where typical drug delivery systems might fail. For instance, traditional drug delivery measures tend to be administered at the tissue level or are administered to select clusters of cells. PPy-based drug delivery systems are currently being investigated for potential in targeting cells via novel substrates that release drugs in a spatiotemporal manner to study individual cellular behaviour in response to local and temporal drug release *in vitro* (Uppalapati et al., 2016). This holds significant applications in arenas of research concerned with disease modelling and drug testing.

Even with the small decrease in the peak currents as the Col-PPy 1:4 wt% sample is run up to 500 cycles, no dramatic loss in peak currents is observed. Additionally, a linear relationship was found for scan rates between 20 m V/s and 75 m V/s and peak currents when the anodic peak current was plotted against the square root of scan rates for Col-PPy 1:1 wt% and Col-PPy 1:4 wt%, but not for Col-PPy 1:2 wt%. This suggests that electrochemical process of the constructs are kinetically controlled and can be manipulated for biosensing applications, however, a working range of electro-activity within the hydrogel-PPy blended constructs serves as a limiting factor, as suggested by Col-PPy 1:2 wt% which observed loss of electro-active capability as scan rate increased (Figure 4.11). Results from CV investigations collectively suggests that electro-activity from DIW Col-PPy materials can be expected, as well as one that can be controlled

under varied potential parameters (as shown in Figure 4.10 (c) and Figure 4.10 (d)). The electro-active properties of DIW Col-PPy constructs can be therefore be applied and designed to function as patterned biosensors or devices capable of drug release (Otero and Martinez, 2016; Ravichandran et al., 2010). Additional figures are included in Appendix A.3 to provide CV results for each of the investigated Col-PPy composition.

CV experiments indicated that each of the three concentrations of Py monomer retained their electro-active properties, with Col-PPy 1:1 wt% reaching the most capacitance. The nearest comparison in literature is the recent work by Liu et al. (2011) where they reported no significant decrease in electro-activity after the inclusion of Type I collagen into their electrochemically polymerized CS-PPy films. The generated capacitance of DIW Col-PPy constructs is greater than that of CS-PPy and CS-Col-PPy films fabricated by Liu et al. (2011) and similar to heparin–PPy composite's developed by Garner et al. (1999).

CV was performed to evaluate the reversibility of the redox reactions occurring in the system and whether switching between redox states was occurring in a repeatable manner. Since these materials are intended for use in biological fluids, DMEM media, was chosen to elucidate the electrochemical activity of this composition under modular electrical stimulation conditions, whereas the NaDBSA solution was chosen to elucidate PPy electrochemical activity in the presence of reduced number of species serving as the active electrolyte in solution. Figure 4.9 suggests that although the capacitance of the Col-PPy constructs is reduced in physiological media, i.e. DMEM, effective charge transport is still present as DMEM serves as the electrolyte solution.

Despite the natural impedance offered by the presence of collagen, CV comparisons between constructs with differing concentrations of Py (Figure 4.10 (a)) at constant potential parameters and scan rates indicate that the no dramatic decrease in polymer electro-activity occurs. However, a reduction in current amplitude is observed as Py concentration in the blend is increased. No drastic decrease in electro-activity is

observed between the three PPy concentrations (Figure 4.10 (a)). However, electro-activity does decrease as PPy concentration in the construct increases. This likely due to a shortening of polymer chain segments serving as electro-active sites on the WE surface, suggesting an upper limit to the strain the hydrogel component of the construct can withstand exists, before PPy chains which serve as electro-active sites could be disconnected or shortened presenting as decreased electro-activity.

Overall, the quasireversible nature of redox reactions associated with PPy is observed to be retained within the DIW printed constructs. Effective electrochemical switching of electro-active sites is demonstrated and seen to increase to a maximum, and subsequently maintained over extended periods of time, specifically for 500 cycles, as depicted in Figure 4.10 (b). As the polymer is reduced, anionic sites form which cause cation ingress or anion egress and charge stabilization, while the opposite phenomena occurs when the polymer is oxidized. The increase in capacitance as a result of extended electrical stimulation as indicated by the change in amplitude of anodic and cathodic peaks after 100 cycles of stimulation suggests that ion mobility increases as the sample is electrically stimulated over an extended period of time. A further breakdown of this evaluation shown in Figure A.3 indicates the DIW Col-PPy 1:4 wt% sample begins to stabilize by the 75^{th} cycle of testing. One reason for this response despite all other parameters being held consistent is that electrical stimulation over longer periods of time leads to the formation or at least exposure of new ion channels in the construct (Price et al., 2012). This presents as enhanced electro-activity and sensing capabilities. Additionally, Figure 4.11 suggests an optimization of the synchrony between collagen and PPy can lead to the development of biosensors of modular sensitivity.

4.5.2 Spectrometry Results

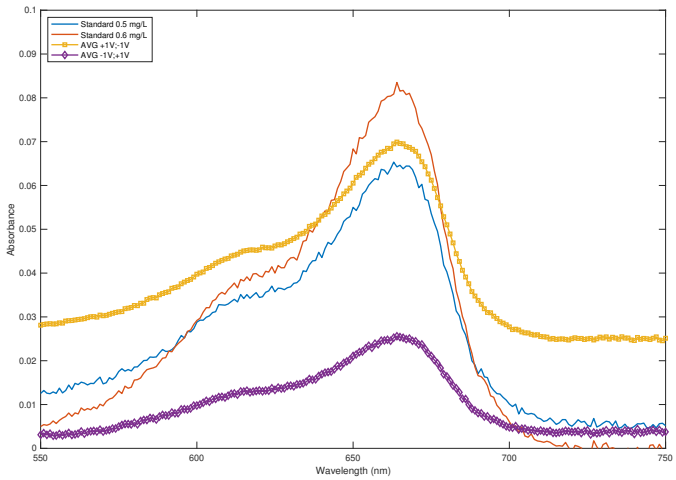

(a)

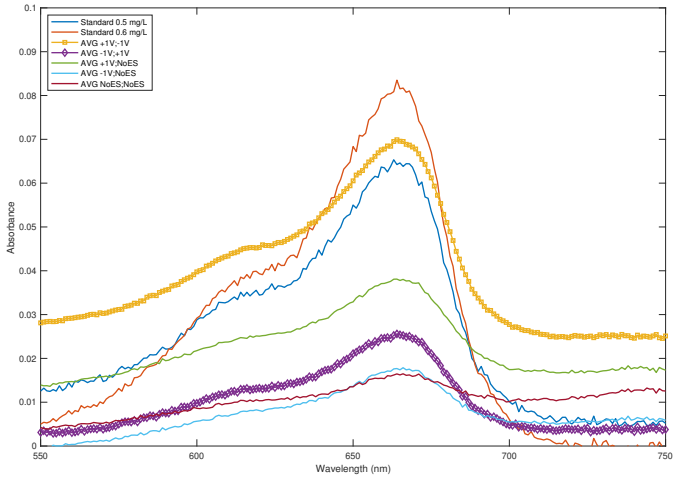

(b)

Figure 4.12: Averaged absorbance profiles for electrically stimulated samples in 100 mg $\cdot$ mL^{-1} MB dye are depicted. (a) depicts the observed effects of applying alternate $\pm$ 1 V electrical stimulation to DIW Col-PPy 1:4 wt% samples, (b) depicts the observed effects of applying alternate electrical stimulation of $\pm$ 1 V and the effects of its absence, in alteration to each or both testing stages, on DIW Col-PPy 1:4 wt% samples.

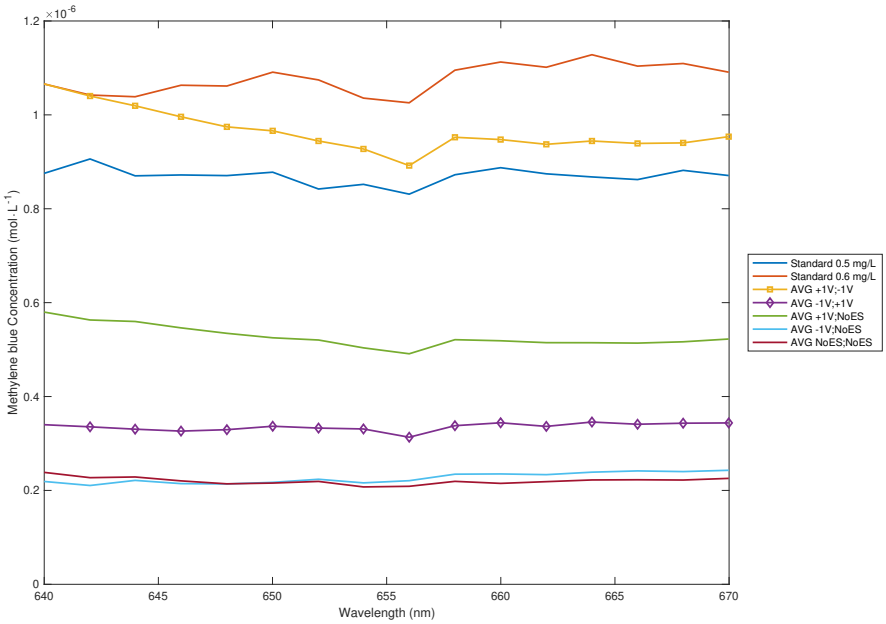

Figure 4.13: Average concentration of MB dye released in response to variable potential parameters is reported.

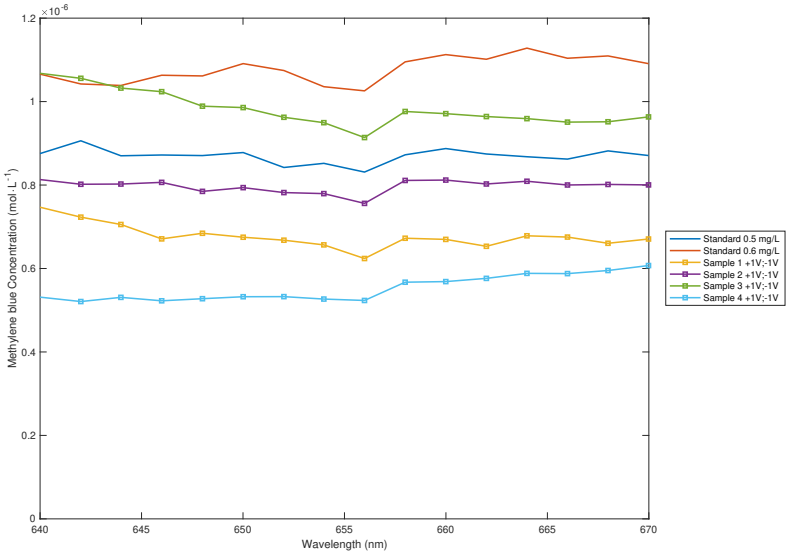

(a) +1V, −1 V

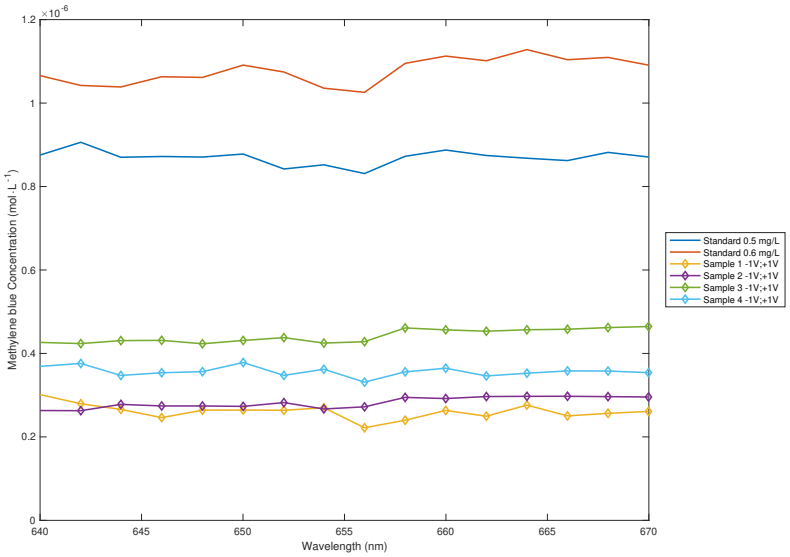

(b) +1V, −1 V

Figure 4.14: Sample deviation for the concentration of MB dye released in response to variable electrical stimulations is reported.

Discussion

The work presented in the previous chapter established the potential of DIW Col-PPy constructs as novel, 3D printed electrochemically controlled drug delivery/release systems, which could effectively serve to emulate the bioactive property of the cellular micro-environment. Consequently, spectrometry experiments were conducted to further demonstrate the application of DIW Col-PPy constructs. Reported concentration values of MB dye are likely underestimated and do not represent the actual amount of MB dye being released upon electrical stimulation. Although the volume between the first stage and the second stage is held constant at 12 ml, results are underestimated as higher volumes at the second stage would serve to dilute any amount of MB dye being released from the Col-PPy sample. Where, use of lower volumes would result in higher absorption spectroscopy measurements, and perhaps more closely represent the amount of MB dye being released. However, sufficient volume to submerge WE and CE and to effectively apply electrical stimulation across the sample is required. Therefore, volume of MB dye and fresh diH_2O at the first and second stage are held consistent.

Since the amount of MB dye being taken up at the first stage of the experiment is not discernible from the current experimental setup, no relationship between potential parameters nor can a claim be made towards the efficacy of the fabricated constructs as electrochemically controlled drug release systems can be made. However, despite the inability to affirm the amount of MB dye being taken up and released, results collectively suggest that application of a positive potential at the first stage results in the greater release of MB dye at the second stage compared to the application of a negative potential (as observed in Figure 4.12 (a)). Results also suggest that leeching in the absence of electrical stimulation at the second stage and passive adsorption in the absence of electrical stimulation at the first stage are about five-fold lower than when electrical stimulation is an applied variable (Figure 4.13).

To overcome the limitations of the experimental setup utilized, future investigations

could employ CV and spectrometry in concert. This would be useful in elucidating the kinetics of the redox reactions involved in MB dye capture and release. Investigations can also be expanded to other molecules of consequence such as therapeutic drugs, glucose or any another species of interest to evaluate the efficacy of the 3D printed constructs as electrochemically controlled drug release systems. Results reported in this section establish that potential for application of the constructs fabricated using the AM technique developed in this thesis as biosensors and as electrochemically controlled drug release systems exists.

4.6 Chapter Summary

This chapter established that all compositions of the Col-Py ink demonstrated favourable shear-thinning behaviour, exist as stable blends and could be DIW printed for creating structures with internal and geometric complexity, as shown by optical imaging, at desired resolution by modulating printing process parameters. Next, potential application of the fabricated DIW PPy-based hydrogels as electro-conductive constructs was established and electro-conductivity was observed to be associated with structure size. Lastly, potential applications of fabricated DIW Col-PPy structures as drug delivery/release systems was established by CV experiments, which demonstrated repeatable electro-activity, and by spectrometry experiments, which demonstrated cationic dye uptake and release.

List of references

Ansari, R. (2006), 'Polypyrrole conducting electroactive polymers: synthesis and stability studies', *Journal of Chemistry* **3**(4), 186–201.

Arteshi, Y., Aghanejad, A., Davaran, S. and Omidi, Y. (2018), 'Biocompatible and

electroconductive polyaniline-based biomaterials for electrical stimulation', *European Polymer Journal* **108**, 150–170.

Asti, A. and Gioglio, L. (2014), 'Natural and synthetic biodegradable polymers: Different scaffolds for cell expansion and tissue formation', *The International Journal of Artificial Organs* **37**(3), 187–205.

Atala, A., Kasper, F. K. and Mikos, A. G. (2012), 'Engineering complex tissues.', *Science Translational Medicine* **4**(160), 160rv12–160rv12.

Cross, M. (1979), 'Relation between viscoelasticity and shear-thinning behaviour in liquids', *Rheologica Acta* **18**(5), 609–614.

Edmondson, R., Broglie, J., Adcock, A. and Yang, L. (2014), 'Three-dimensional cell culture systems and their applications in drug discovery and cell-based biosensors', *Assay and Drug Development Technologies* **12**(4), 207–218.

Entezami, A. and Massoumi, B. (2006), 'Artificial muscles, biosensors and drug delivery systems based on conducting polymers: A review', *Iranian Polymer Journal (English Edition)* **15**(1), 13–30.

Garner, B., Georgevich, A., Hodgson, A. J., Liu, L. and Wallace, G. G. (1999), 'Polypyrrole–heparin composites as stimulus-responsive substrates for endothelial cell growth', *Journal of Biomedical Materials Research* **44**(2), 121–129.

Guiseppi-Elie, A. (2010), 'Electroconductive hydrogels: Synthesis, characterization and biomedical applications', *Biomaterials* **31**(10), 2701–2716.

Guo, B., Glavas, L. and Albertsson, A.-C. (2013), 'Biodegradable and electrically conducting polymers for biomedical applications', *Progress in Polymer Science* **38**(9), 1263–1286.

Khalkhali, R. A. (2005), 'Electrochemical synthesis and characterization of electroactive conducting polypyrrole polymers', *Russian Journal of Electrochemistry* **41**(9), 950–955.

Koetting, M., Peters, J., Steichen, S. and Peppas, N. (2015), 'Stimulus-responsive hydrogels: Theory, modern advances, and applications', *Materials Science and Engineering R: Reports* **93**, 1–49.

Kulkarni, R. and Biswanath, S. (2007), 'Electrically responsive smart hydrogels in drug delivery: A review', *Journal of Applied Biomaterials and Biomechanics* **5**(3), 125–139.

Kupila, E.-L. and Kankare, J. (1995), 'Influence of electrode pretreatment, counter anions and additives on the electropolymerization of pyrrole in aqueous solutions', *Synthetic Metals* **74**(3), 241–249.

Lee, J., Kim, D. and Kim, C. (1995), 'Synthesis of soluble polypyrrole of the doped state in organic solvents', *Synthetic Metals* **74**(2), 103–106.

Lee, S.-J., Zhu, W., Nowicki, M., Lee, G., Heo, D., Kim, J., Zuo, Y. and Zhang, L. (2018), '3d printing nano conductive multi-walled carbon nanotube scaffolds for nerve regeneration', *Journal of Neural Engineering* **15**(1).

Li, H. and Khor, E. (1994), 'Interaction of collagen with polypyrrole in the production of hybrid materials', *Polymer International* **35**(1), 53–59.

Liu, X., Yue, Z., Higgins, M. J. and Wallace, G. G. (2011), 'Conducting polymers with immobilised fibrillar collagen for enhanced neural interfacing', *Biomaterials* **32**(30), 7309–7317.

Love, M., Palee, S., Chattipakorn, S. and Chattipakorn, N. (2018), 'Effects of electrical stimulation on cell proliferation and apoptosis', *Journal of Cellular Physiology* **233**(3), 1860–1876.

Mekonnen, B. T., Ragothaman, M., Kalirajan, C. and Palanisamy, T. (2016), 'Conducting collagen-polypyrrole hybrid aerogels made from animal skin waste', *RSC Advances* **6**, 63071–63077.

Men, J., Deng, X. and Xu, Z. (2010), 'Electrical stimulation enhances viability of osteoblasts on conductive biodegradable material.', *Sheng wu yi xue gong cheng xue za zhi = Journal of biomedical engineering = Shengwu yixue gongchengxue zazhi* **27**(4), 801–805.

Merrill, D., Bikson, M. and Jefferys, J. (2005), 'Electrical stimulation of excitable tissue: Design of efficacious and safe protocols', *Journal of Neuroscience Methods* **141**(2), 171–198.

Otero, T. F. and Martinez, J. G. (2016), 'Electro-chemo-biomimetics from conducting polymers: fundamentals, materials, properties and devices', *Journal of Materials Chemistry B* **4**(12), 2069–2085.

Pillay, V., Tsai, T.-S., Choonara, Y., Du Toit, L., Kumar, P., Modi, G., Naidoo, D., Tomar, L., Tyagi, C. and Ndesendo, V. (2014), 'A review of integrating electroactive polymers as responsive systems for specialized drug delivery applications', *Journal of Biomedical Materials Research - Part A* **102**(6), 2039–2054.

Price, A. D., Gillen, T., Liu, C. C., O'Shaughnessy, C. A. and Naguib, H. E. (2012), 'Evaluation of porous membrane core elasticity and porous morphology for polypyrrole trilayer actuators', *Journal of Cellular Plastics* **48**(1), 25–42.

Ravichandran, R., Sundarrajan, S., Venugopal, J., Mukherjee, S. and Ramakrishna, S. (2010), 'Applications of conducting polymers and their issues in biomedical engineering', *Journal of the Royal Society Interface* **7**(SUPPL. 5), S559–S579.

Shi, Z., Gao, X., Ullah, M., Li, S., Wang, Q. and Yang, G. (2016), 'Electroconductive natural polymer-based hydrogels', *Biomaterials* **111**, 40–54.

Song, B., Zhao, M., Forrester, J. and McCaig, C. (2002), 'Electrical cues regulate the orientation and frequency of cell division and the rate of wound healing in vivo', *Proceedings of the National Academy of Sciences of the United States of America* **99**(21), 13577–13582.

Stewart, E., Kobayashi, N., Higgins, M., Quigley, A., Jamali, S., Moulton, S., Kapsa, R., Wallace, G. and Crook, J. (2015), 'Electrical stimulation using conductive polymer polypyrrole promotes differentiation of human neural stem cells: A biocompatible platform for translational neural tissue engineering', *Tissue Engineering - Part C: Methods* **21**(4), 385–393.

Suntornnond, R., Tan, E. Y. S., An, J. and Chua, C. K. (2016), 'A mathematical model on the resolution of extrusion bioprinting for the development of new bioinks', *Materials* **9**(9), 756.

Tandon, B., Magaz, A., Balint, R., Blaker, J. and Cartmell, S. (2018), 'Electroactive biomaterials: Vehicles for controlled delivery of therapeutic agents for drug delivery and tissue regeneration', *Advanced Drug Delivery Reviews* **129**, 148–168.

Topsoe, H. (1986), *Geometric factors in four point resistivity measurement*, Vol. 472-13, Bulletin.

Uppalapati, D., Boyd, B., Garg, S., Travas-Sejdic, J. and Svirskis, D. (2016), 'Conducting polymers with defined micro- or nanostructures for drug delivery', *Biomaterials* **111**, 149–162.

Wadhwa, R., Lagenaur, C. and Cui, X. (2006), 'Electrochemically controlled release of dexamethasone from conducting polymer polypyrrole coated electrode', *Journal of Controlled Release* **110**(3), 531–541.

Weng, B., Liu, X., Higgins, M. J., Shepherd, R. and Wallace, G. (2011), 'Fabrication and

Characterization of Cytocompatible Polypyrrole Films Inkjet Printed from Nanoformulations Cytocompatible, Inkjet-Printed Polypyrrole Films', *Small* **7**(24), 3434–3438.

Weng, B., Liu, X., Shepherd, R. and Wallace, G. G. (2012), 'Inkjet printed polypyrrole/-collagen scaffold: A combination of spatial control and electrical stimulation of PC12 cells', *Synthetic Metals* **162**(15-16), 1375–1380.

Yan, B., Wu, Y. and Guo, L. (2017), 'Recent advances on polypyrrole electroactuators', *Polymers* **9**(12), 446–20.

Zhu, W., Ma, X., Gou, M., Mei, D., Zhang, K. and Chen, S. (2016), 'ScienceDirect 3D printing of functional biomaterials for tissue engineering', *Current Opinion in Biotechnology* **40**, 103–112.

Chapter 5

Characterization of Direct-ink Write printed Collagen and PPy-based constructs: Part 2

This chapter investigates the retention of other applications pertaining to PPy-based constructs. Potential application of Col-PPy constructs as a bioactuator for studying mechanotransduction effects in 3D cell culture settings is evaluated by assessing actuation performance in response to electrochemical switching. Physical properties of the DIW constructs are evaluated by performing tensile tests, SEM imaging and elemental mapping. Lastly, cyto-compatibility is evaluated by culturing human BJ fibroblast cells on the PPy-based constructs for an extended period of time.

5.1 Actuation Profiling Results

5.1.1 Grid Actuation Performance

Shown in Figure 5.4 are the results from this experiment. In Figure 5.4 (a), positive potential stimulation for 5 min resulted in increase of % area change for two pores, while

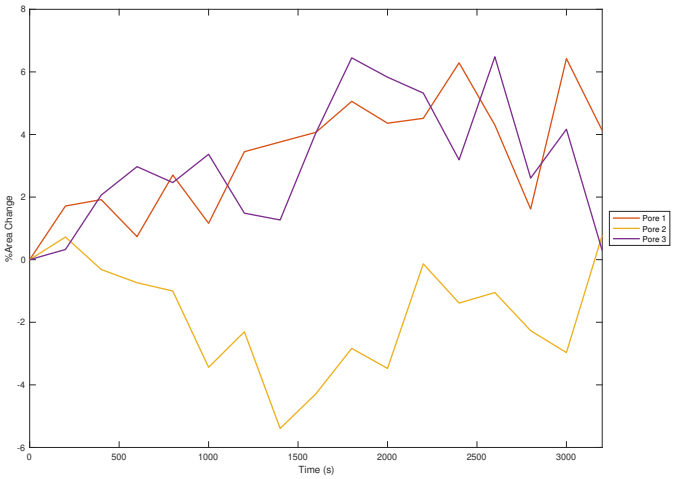

Figure 5.1: Background noise associated solution change is detected in the absence of electrical stimulation.

the opposite effect was seen for the third pore, whereas in the absence of positive potential stimulation % area change was observed to drift and then return almost to 0% area change around 500s after electrical stimulation was halted. In Figure 5.4 (b), negative potential stimulation for 5min predominately resulted in % area change decreasing. Contrary to Figure 5.4 (a), % area change was not observed to drift in the absence of electrical stimulation rather it continued to oscillate in the negative % area change range. These preliminary investigations established that actuation profiles were more representative of the applied electrical stimulation under waveform potential rather than continuous, despite the variable actuation behaviour disparity observed in all experiments between pores of the same sample. At this point, it became impertinent to establish if actuation response could be directed in a controlled manner by manipulating potential parameters.

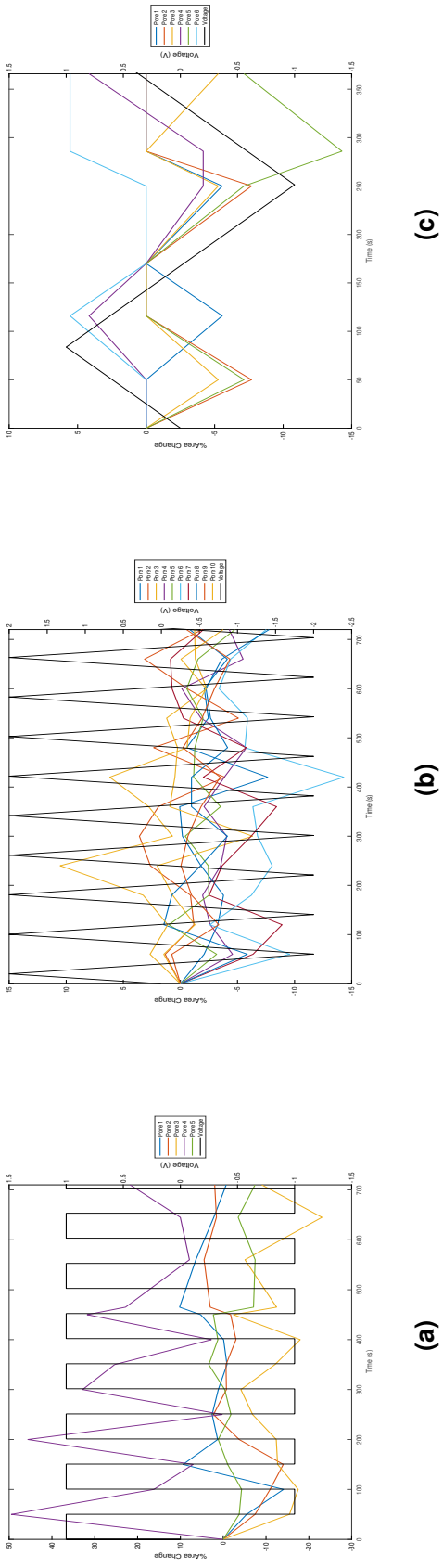

Figure 5.2: DIW Col-PPy 1:4 wt% monolayer grid samples were subjected to electrical stimulation under (a) square waveforms at 0.01 Hz, and triangle waves at (b) 0.0125 Hz and (c) 0.0003 Hz. Square waveforms exhibited greater actuation response and, therefore, were selected as the waveform of choice for subsequent experiments.

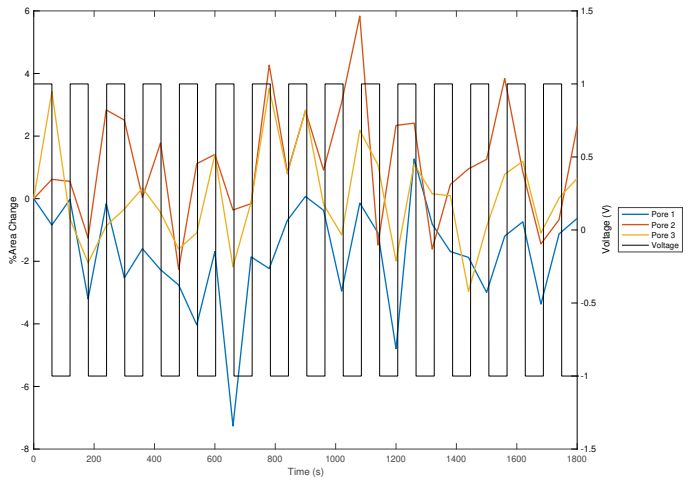

(a)

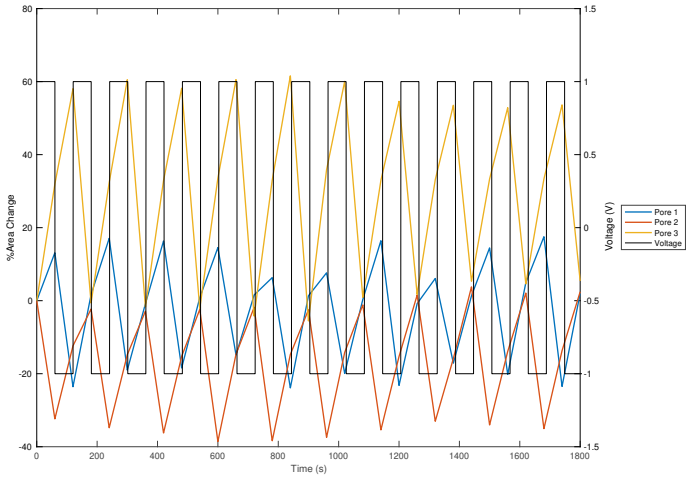

(b)

Figure 5.3: A comparison between (a) manual tracing of grid sample pores, and using (b) internal threshold algorithms within Fiji to determine % area changes for a DIW Col-PPy 1:4 wt% sample, stimulated at 0.00833 Hz frequency, at $\pm$1 V, is reported.

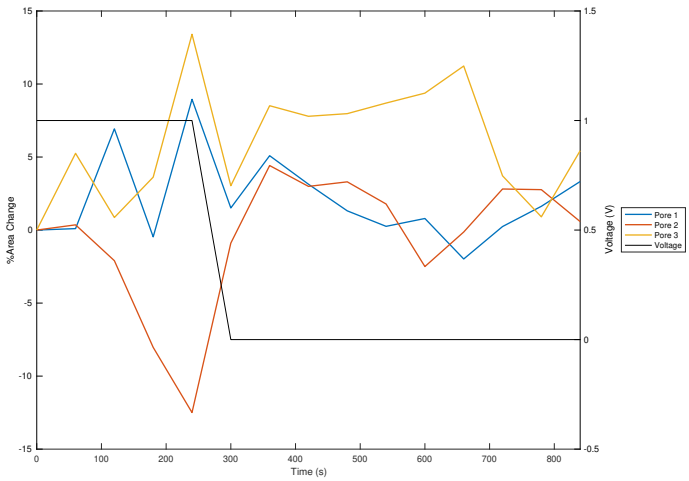

(a)

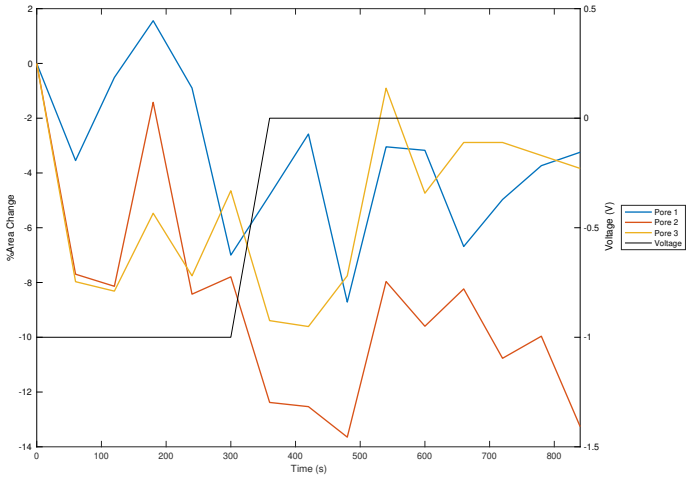

(b)

Figure 5.4: A comparison between continuous electrical stimulation of (a) +1 V (b) −1 V and consequent % area changes for DIW Col-PPy 1:4 wt% samples is reported.

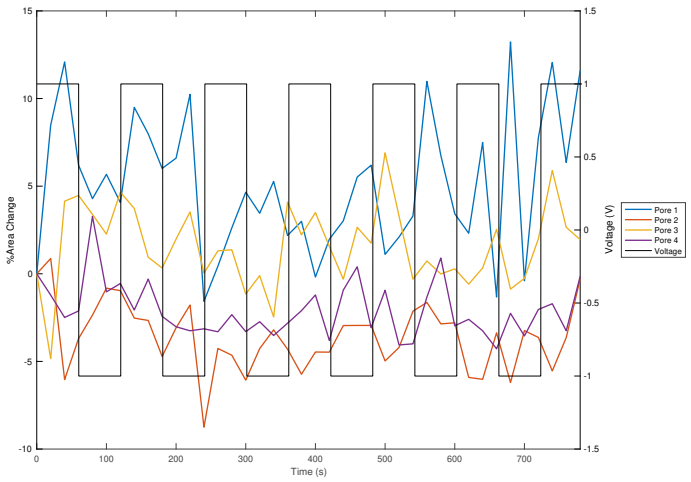

(a)

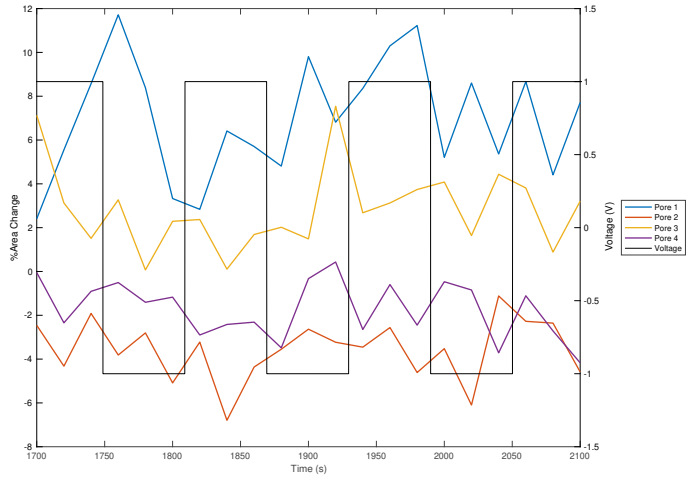

(b)

Figure 5.5: The actuation results of a DIW Col-PPy 1:4 wt% sample are separated to depict (a) the first 13 min, i.e. 0–780s, and (b) 30 min later, i.e. 1700–2100s, at 0.00833 Hz frequency, at ± 1 V.

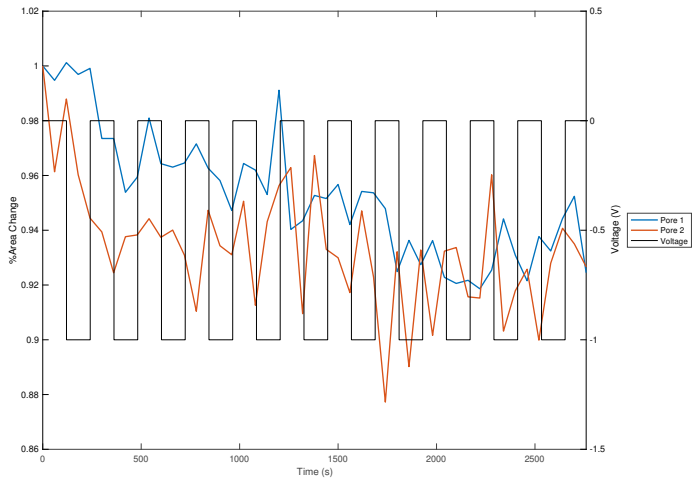

(a) 0V **to** -1 V

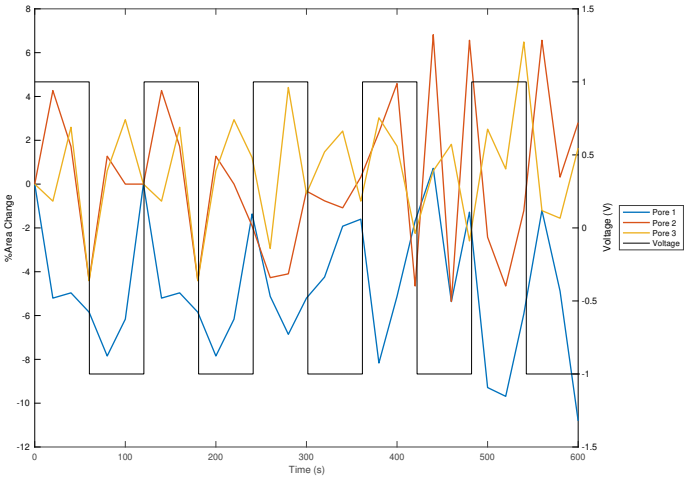

(b)± 1 V

Figure 5.6: A comparison between electrical stimulating DIW Col-PPy 1:4 wt% samples for (a) 0V to -1 V and (b) ± 1 V is presented.

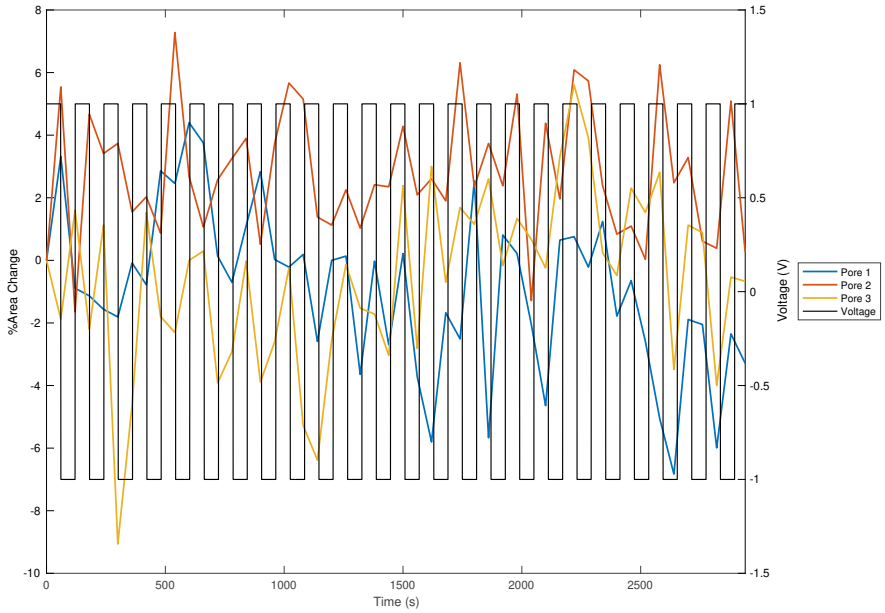

Figure 5.7: The actuation profile of a DIW Col-PPy 1:2 wt% monolayer grid sample electrically stimulated for approx. 1 h is reported.

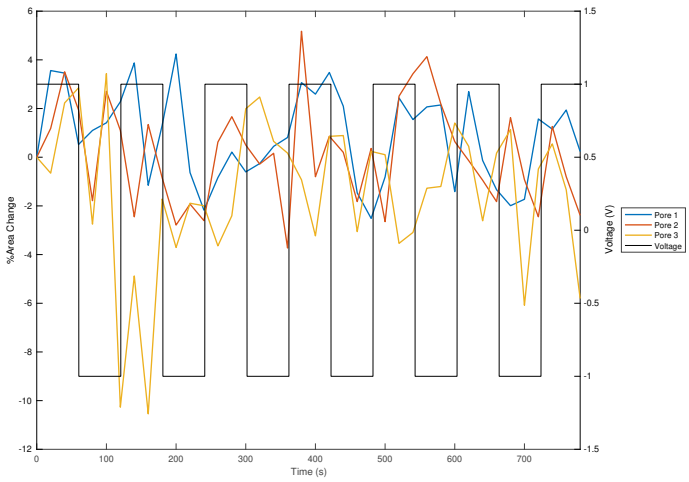

(a) Col-PPy 1:2 wt% sample 1

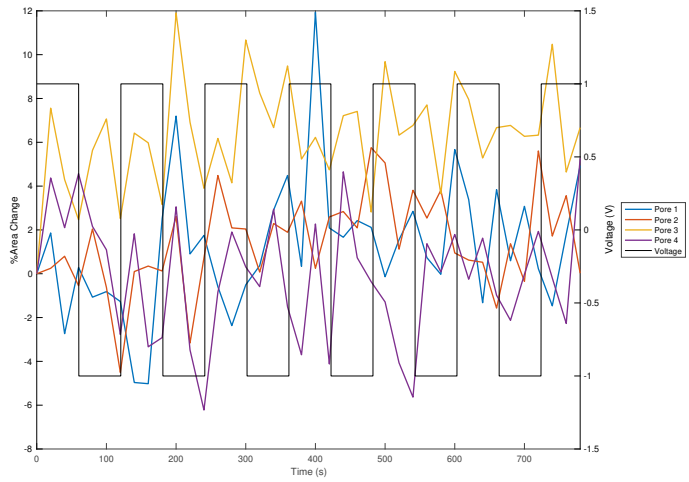

(b) Col-PPy 1:2 wt% sample 2

Figure 5.8: The actuation profiles of a DIW Col-PPy 1:2 wt% monolayer grid samples electrically stimulated for at the same potential parameters as Col-PPy 1:4 wt% samples.

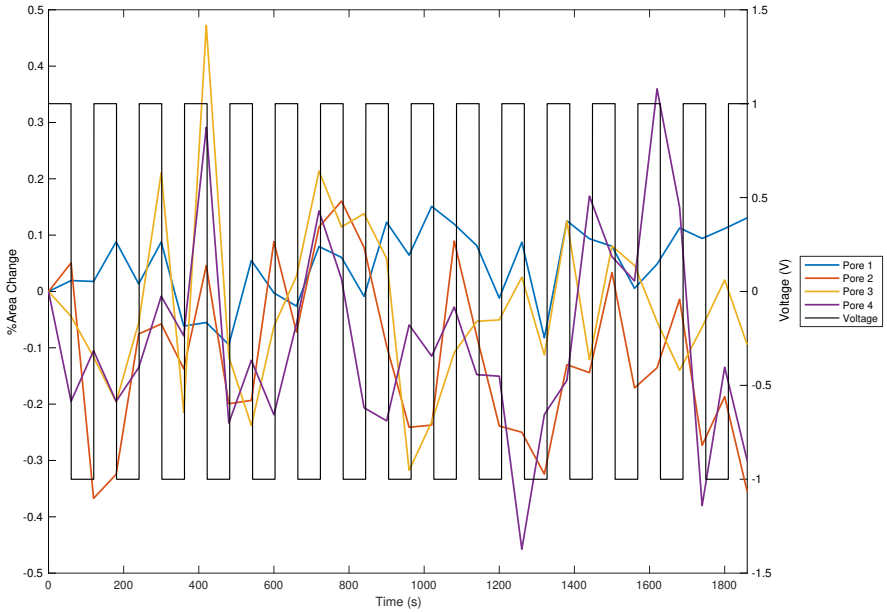

Figure 5.9: The actuation profile of a 25 mg $\cdot$ mL^{-1} collagen standalone DIW grid sample under the working potential parameters.

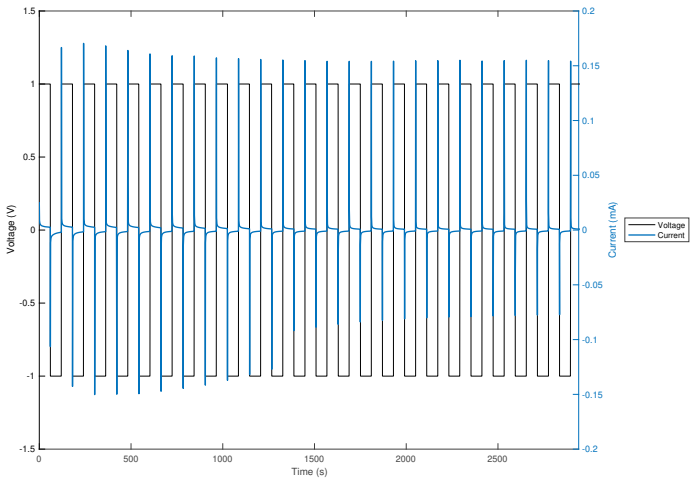

(a) Col-PPy 1:2 wt% sample 1

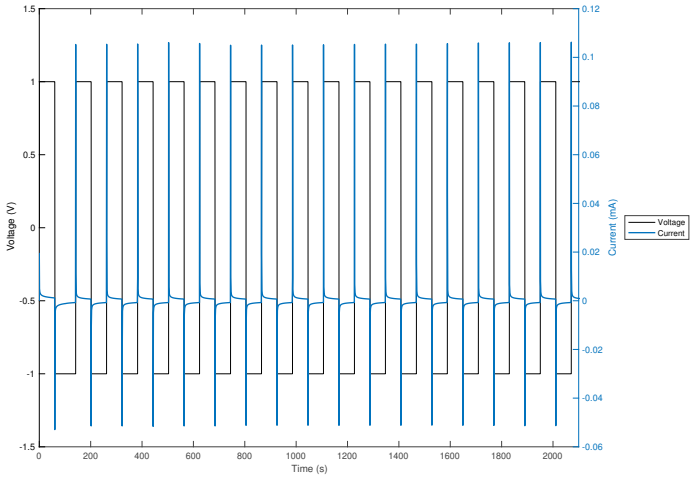

(b) Col-PPy 1:4 wt% sample 1

Figure 5.10: The typical current flow of (a) Col-PPy 1:2 wt% and (b) 1:4 wt% from applying ± 1 V at 0.00833 Hz is depicted.

Discussion

Typical shape-shifting behaviours of actuators in literature presents as changes in the topography and morphology of the constructs, for instance: folding, bending, twisting, and linear or nonlinear expansion and contraction of films or membranes, typically electrochemically polymerized (Svennersten et al., 2011; Jager et al., 1999; Farajollahi et al., 2016; Küttel et al., 2009; Melling et al., 2013; Madden et al., 2004; Hara et al., 2006). PPy-based constructs capitalizes on its ion exchange mechanism to create actuators capable of performing work. This actuation mechanism holds potential as means of imparting mechanical stress and changing a construct's physical properties such as substrate elasticity (Smela and Gadegaard, 2001; Holst et al., 2010; Price et al., 2012; Wu et al., 2007).

The monolayer aspect of Col-PPy 1:4 wt% grids was chosen to simplify assessments on whether detected volume change occurred uniformly throughout the grid construct or whether it was occurring in a spatiotemporal manner, which would present as variable actuation along the internal pores of the construct. A more complex, 3D structure would have made it difficult to assess and model the spatiotemporal aspect of the observed actuation response. The scope of this investigation was limited to assessing actuation ability and resulting potential applications.

Preliminary investigations with Col-PPy 1:4 wt% monolayer grid samples informed subsequent experimental parameters. During these preliminary investigations, irregular actuation response was observed by samples despite being stimulated at variable frequencies, potentials and waveforms. Over the course of investigations, some phenomena were observed to be irregular in terms of actuation response. (1) a delay in sample actuation frequency in response to electrical stimulation frequency is present, and (2) pores seem to respond to electrical stimulation variably, i.e. some pores experience increase in % area change while others experience a decrease. Instances of these phenomena from preliminary investigations are shown in Figure 5.2.

The delay in sample actuation response frequency is expected as it has been previously established that it takes about 30s for PPy electro-active sites to begin respond and presenting bulk behaviour as more electro-active sites are exposed over stimulation time, and subsequently decreasing this delay by responding faster (Otero and Martinez, 2016; Smela and Gadegaard, 2001; Smela, 2003; Wang et al., 2004). However, contrary to other PPy-based electrochemically polymerized films studied for actuation potential, this sample actuation response frequency was not observed to recover nor stabilize over the period of observation. Initially, this irregular actuation response behaviour was attributed to background noise associated with the changing of solutions, i.e. from the diH_2O storage solution to one of greater osmolarity.

Col-PPy 1:2 wt% monolayer grid samples were investigated under the same potential parameters as Col-PPy 1:4 wt% monolayer grids to determine if the irregular actuation response phenomena and its characteristics were restricted to the Col-PPy 1:4 wt% monolayer grids alone. This was not observed to be the case as the irregular actuation response observed during preliminary investigations with Col-PPy 1:4 wt% monolayer grid samples was persisted in Col-PPy 1:2 wt% concentration samples as well (Figure 5.8). Irrespective of location on the sample, pores of the grid were observed to undergo variable expansion and contraction despite electrical stimulation parameters being held consistent across samples, similar to what was observed during preliminary investigations for samples experiencing volume change due to change in osmolarity (Figure 5.1) and despite changes in waveform and frequency (Figure 5.2), as well as for samples under variable applied potential (Figure 5.3 (a) and Figure 5.6 (b)).

For samples undergoing electrical stimulation over extended periods, a shift towards slowed actuation response, when stimulated for extended periods of time. A delay in sample actuation frequency is introduced as stimulating the samples for a longer time periods, which only serves to further the discrepancy between the applied potential frequency and sample actuation response frequency. One possible reasoning behind

this response was referred to the relatively short time frame of observation, i.e. typically 13 min. Therefore, both Col-PPy 1:2 wt% and 1:4 wt% grid and collagen standalone monolayer grid samples were electrically stimulated for greater than 30 min to determine if the actuation response stabilized overtime. This was detected to not be the case, as indicated by Figure 5.5, Figure 5.7 and Figure 5.9.

The next set of experiments connected to test results shown in Figure 4.13. In preliminary experiments, potential was applied as over-potentials and continuously (Figure 5.4). Despite potential being held constant for that allotted time, i.e. in the absence of electrochemical switching, each pore experiences the third phenomena observed to be prevalent in all samples. Specifically, a rebound-like phenomena which presents as oscillatory volume change, contrary to expectations where continued application of electrical stimulation would render PPy electro-active sites less likely to return to their original state (Otero and Martinez, 2016). To assess whether the rebound-like phenomena resulting in oscillatory actuation behaviour would prevail over any and all potential parameters, a square waveform between 0V and -1 V at 0.00833 Hz was applied to a Col-PPy 1:4 wt% monolayer grid sample (Figure 5.6 (a)). Results from this experiment indicate that the rebound-like phenomena presents as slight relaxation ($\pm$2%) of the sample, and cannot be attributed to periods where the sample experiences absence of electrical stimulation as previous investigations where electrical stimulation is held constant also displayed this third phenomena. This third phenomena was observed across all samples, experimental parameters and for each pore of the same sample investigated, even for the time periods for which electrical stimulation is held constant or switched, but one that is not associated in literature with PPy. Therefore, the collagen component of the Col-PPy blend is cited as the most likely guilty constituent of the two.

In addition to observing % area changes in response to potential applied, it was also important to view current changes in response to potential applied, as they reflect the amount of electro-active sites contributing to the observed response and undergoing

redox processes. For all experimental conditions, it was observed that the first cycle of electrical stimulation generated the least current throughout the experiment, however, subsequent cycles quickly established a stabilization of the current which was kept nearly constant from cycle-to-cycle following the stabilization (Figure 5.10). Voltage vs. current vs. time data implies that the bulk number of electro-active sites on the entirety of the sample contributing to the measured current are either held consistently in electro-activity or undergo no drastic changes cycle-to-cycle. However, majority of the % area change vs. voltage vs. time data indicate that for actuation in a spatiotemporal manner is not repetitive, as adjacent pores of the same sample do not demonstrate a homogenous actuation pro-life. Miniaturization of the experimental setup and DIW printed samples perhaps would work to allow a closer examination of the relationship between changes in generated current and volume change. However, at the time of this thesis, this was not accomplished in this study due to unavailability of facilities at hand.

For the grid samples, actuation response as a result of electrical stimulation is occurring; however, it is one that cannot be effectively modelled nor predicted, for it is not occurring in a homogenous nor repeatable manner. The mechanism that underlies actuation response of PPy-based constructs is the same that enables electro-activity. For this composition, the actuation response is postulated to be predominately cationic dependent, as an effect of DBSA inclusion during the polymerization step. Therefore, the polymer contracts in its oxidized state, i.e. when a negative potential is applied, as cations egress, and expands in its reduced state, i.e. when a positive potential is applied, as cations ingress. This is supported by CV, spectroscopy and grid actuation results as bulk response of the structure favours one mode of behaviour over the other. However, the second observed phenomena, that is, pores of the same sample responding to electrical stimulation variably in the form of expansion or contraction resulting in increase or decrease in % area change, suggests that variable actuation direction between adjacent pores of the same sample can be due to inadequate DBSA doping during polymerization.

This notion of inadequate doping is supported by Figure 4.14, where displays select samples (under opposite electrical stimulation of ± 1 V) releasing similar amounts of MB. Inadequate doping would sufficiently explain the irregular actuation response observed for both Col-PPy 1:2 wt% and 1:4 wt% concentrations, at varying potential and frequency parameters. Additionally, as this irregular actuation response is not typical of PPy-standalone constructs, collagen presence in the hydrogel composition may indeed serve as the impeding factor responsible for the rebound-like behaviour. However, the exact mechanism underlying this behaviour requires focused examination. EDAX elemental mapping was also conducted on 3D printed grid constructs to satisfyingly address the question of inadequate doping (section 5.2). At this point, DIW Col-PPy grid structures are not a feasible route for studying mechanotransduction effects.

Table 5.1: The swelling ratios of Col-PPy 1:4 wt% samples 1, 2, and 3 referenced in Table 5.2 were measured prior to performing actuation tests and are reported here.

Sample	**Length (** mm**)**	**Width (** mm**)**	**Cross-section (** mm**)**
1	1.488	2.702	1.442
2	1.966	1.943	1.316
3	3.006	1.438	1.388
Average	1.982$\pm$ 0.7764	1.899$\pm$ 0.6362	1.380$\pm$ 0.0629

Table 5.2: Bilayer actuation performance for Col-PPy 1:4 wt% and PDMS bilayers in DMEM media are reported. These bilayers experienced square waves of varied potentials at 0.00833 Hz. $*$ denotes the samples which did not follow the orientation depicted in Figure 3.9.

Sample number	**Potential parameters**	**Initial angle**	**Final angle**	**Δ angle**
1*	Square $\pm$1 V	53°	57°	4°
2*	Square $\pm$1 V	99°	102°	3°
3	Square $\pm$1 V	87°	74°	13°
4	Square $\pm$2 V	74°	70°	4°
5*	Square $\pm$2 V	115°	126°	11°
6*	Square +1 V, -2 V	112°	118°	6°
7	Square +1 V, -2 V	65°	62°	3°
8*	Square +0.2 V, -0.8 V	98°	103°	5°
9	Square $\pm$3 V	72°	70°	2°
10	Square $\pm$1 V	69°	67°	2°
11	Square $\pm$1 V	78°	75°	3°
12	Square $\pm$1 V	90°	53°	37°
13*	Square $\pm$1 V	53°	55°	2°

5.1.2 Bilayer Actuation Performance

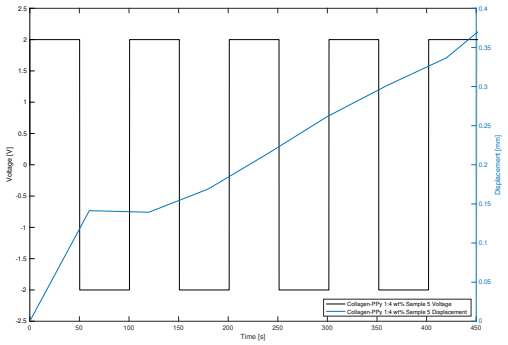

(a) 30.58 mm Sample 5 DMEM

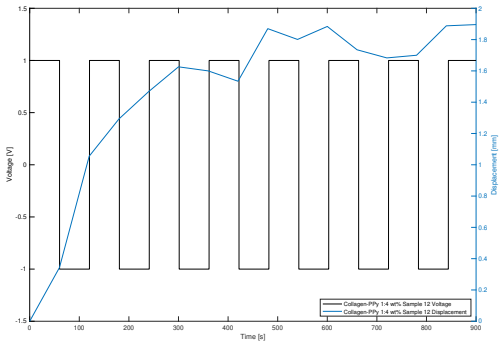

(b) 3.74 mm Sample 12 DMEM

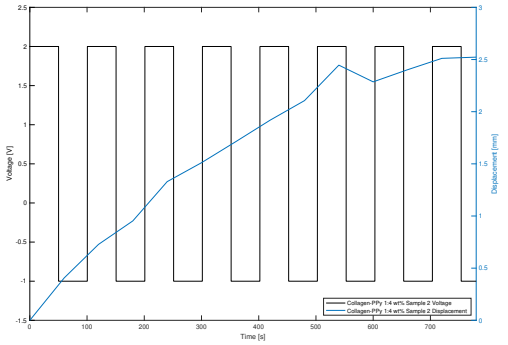

(a) 32.10 mm Sample 2 NaDBS$_{(aq)}$

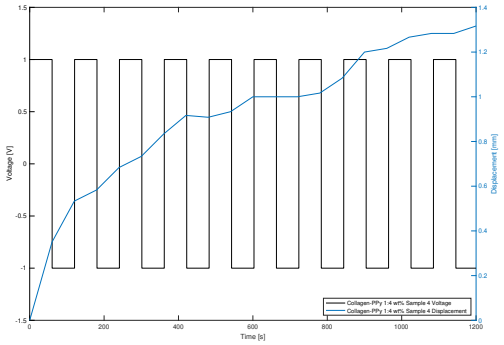

(b) 4.41 mm Sample 4 NaDBS$_{(aq)}$

Figure 5.11: The tip displacement of actuated Col-PPy 1:4 wt% and PDMS bilayers in response to electrical stimulation shows overall increased, sustained displacement over time in both working solutions.

Table 5.3: Bilayer actuation performance for Col-PPy 1:4 wt% and PDMS bilayers in 0.1 M NaDBS$_{(aq)}$ solution are reported. These bilayers experienced square waves of varied potentials at 0.00833 Hz. $*$ denotes the samples which did not follow the orientation showed in Figure 3.9.

Sample number	Potential parameters	Initial angle	Final angle	Δ angle
1*	Square $\pm$ 1 V	107°	110°	3°
2	Square +2 V, -1 V	133°	115°	18°
3	Square $\pm$ 2 V	115°	102°	13°
4	Square $\pm$ 1 V	43°	23°	20°
5	Square +2 V, 0 V	84°	64°	20°

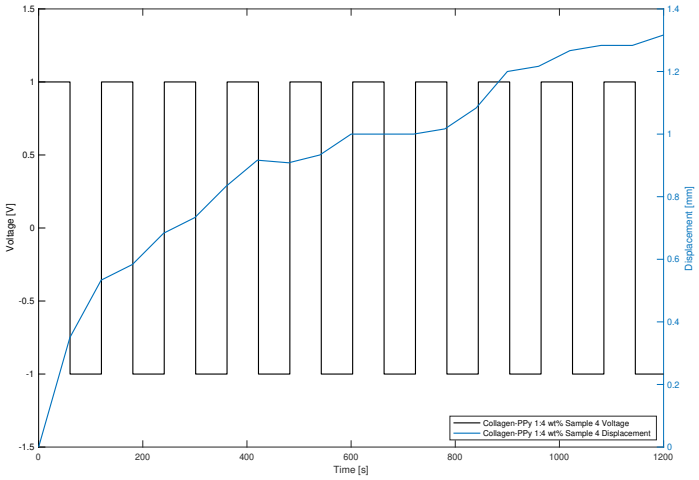

(a) Tip displacement vs. Voltage

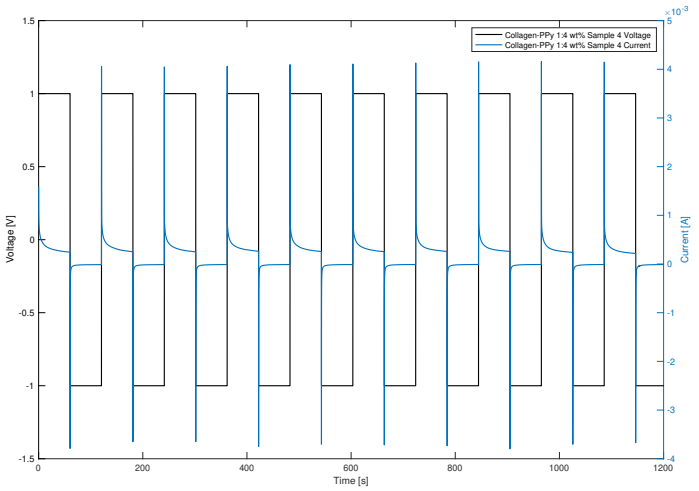

(b) Current vs. Voltage

Figure 5.12: Typical current flow of Col-PPy 1:4 wt% and PDMS bilayers from applying ± 1 V at 0.00833 Hz shows similar current behaviour observed for Col-PPy 1:4 wt% grid structures.

Discussion

For the bilayer, PDMS serves to function as the passive layer while Col-PPy construct serves as the electro-active portion of the bilayer. Expansion or contraction of the electro-active component manifests as bending motion (Jager et al., 1999; Farajollahi et al., 2016; Melling et al., 2013). For evaluations conducted in DMEM media (Table 5.2), application of higher potentials resulted in greater actuation as shown by the difference in angle change (Δ angle) between samples 1 and 2 against sample 3. However, tip displacement measurements in both solutions was observed to respond predominately to oxidizing potentials. Additionally, regardless of amplitude of applied potential, the bending actuation favoured contraction over expansion (Figure 5.11). Samples continued to contract in response to the oxidizing (positive) potential and seemed unaffected for multiple cycles by the reducing (negative) potential which resulted in angle decreasing towards the Col-PPy side of the bilayer, relative to the schematic shown in Figure 3.9.

For DMEM media solution experiments (Table 5.2), it was noticed that potentials above $\pm$ 2.4 V resulted in electrolysis on both the working and counter electrode, as was the case for sample 9,. Therefore, all electrical stimulation parameters for subsequent evaluations remained below $\pm$ 2.4 V. Samples 6 and 7 were subjected to a higher oxidizing potential compared to the reducing potential to determine whether the observed actuation effect would be balanced by applying a higher reducing potential. This parameter was adapted as the bilayers seemed to be entirely unresponsive to oxidizing potentials, and predominately underwent contraction.

Similar to the difference in angle change (Δ angle) observed for bilayers in DMEM media solution, application of higher potentials resulted in greater actuation in the NaDBS $_{(aq)}$ solution as well. This is demonstrated by the difference between samples 1 against sample 2 and 3 (Table 5.3), which represent the same bilayer actuated in both solutions. Similar to the actuation seen in DMEM media solution, regardless of amplitude of applied potential, the bending actuation response also seemed to favour

contraction over expansion. Table 5.3 shows that sample 5 was electrically stimulated only in the oxidative direction. This was done to determine whether applying a higher oxidative potential and subsequent absence of it in succeeding cycles would lead to drift or recovery of the bilayer towards its original state (Figure 5.12 (a)). This was not seen to be the case, rather the bilayer continued to contract and the current (Figure 5.12 (b)) also increases over time. This indicates that the number of electro-active sites available and contributing to the observed effect keep increasing as electrical stimulation is cycled; however, in all likelihood, an upper limit to the number of electro-active sites responding exists. Although sample-to-sample variability exists, anisotropy of collagen fibres in the bilayer may be undercutting bilayer actuation. Another factor confounding results is the length of the bilayer, which varied from sample-to-sample.

Although constructs when 3D printed and even post-polymerization retained their uniformity/as-printed morphology, fabricated samples were dried over a 48 h period to allow adequate PDMS to cure onto Col-PPy 1:4 wt% samples used to fabricate the bilayers. This lead to variable drying of samples resulted in varying sample sizes. For smaller samples in DMEM, the degree of bending averaged at 2–6°, whereas larger constructs underwent angle change (Δ angle) greater than 10° and in one case up to 37°. Samples in NaDBS solution managed greater degrees of expansion for almost all samples, regardless of bilayer length, compared to actuation tests conducted in DMEM solution. This behaviour is attributed to the presence of the dopant in the working solution, which increases doping of the construct and therefore increasing cation-dependent actuation. The relationship between Δ angle, bilayer length and potential parameters is shown in Figure B.1, which in concert with the inadequate doping hypothesis suggests no direct relationship between angle change and bilayer length exists.

The one-sided preference, that is, contraction for the Col-PPy portion of the bilayer, is similar to an effect observed for some ionic polymer-metal composites (IPMC) where

the composite quickly bends towards the anode or cathode and experiences slow back-relaxation, i.e. return to neutral position, irrespective of potential (Nemat-Nasser, 2002). As discussed by Nemat-Nasser (2002), in IPMCs this effect is dependent on the chemical properties of ionic polymer, the size of ions that form a boundary layer near the anode or cathode during electrochemical switching and degree of hydration. In the case of Col-PPy constructs, samples were sufficiently hydrated prior to testing. The behaviours observed in these bilayers, i.e. continuous expansion and no back relaxation, suggest that the polymer is not sufficiently releasing cationic species from the polymer backbone once potential is cycled in the opposite direction or that osmotic pressure as a consequence of PPy's actuation mechanism is no longer the dominant force in these structures. Another possible reason for the lack of back-relaxation is attributed to the presence of collagen fibres in the construct, which serve to function as an impedance and have minimal electrical conductivity and piezoelectric properties but in this case may be deformed by the electrostatic forces stimulating PPy (Fukada and Yasuda, 1964; Ahn and Grodzinsky, 2009). The scale of the construct also seems to have an influence on the actuation capabilities of the fabricated constructs where grid samples were observed to undergo unrepeatable volume change, but volume change as expansion and contraction, while the bilayers are predominately experiencing contraction. Therefore, further vigorous investigations toward studying the mechanical actuation response associated with PPy-based hydrogel constructs is warranted. Consequently, one method for compensating lack of back-relaxation in this Col-PPy composition would be to create patterned actuators that function in an antagonistic manner, therefore, effectively cancelling out this limitation (Fleming et al., 2012).

5.2 SEM Results

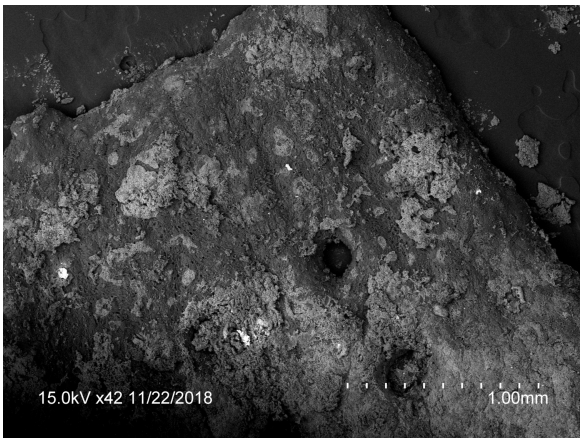

(a) damp, 42× magnification

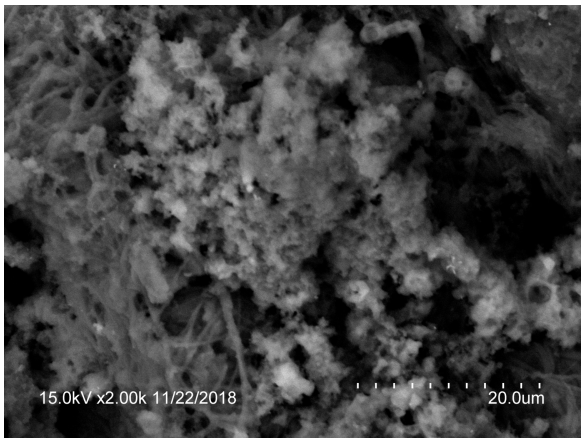

(b) damp, 2 000× magnification

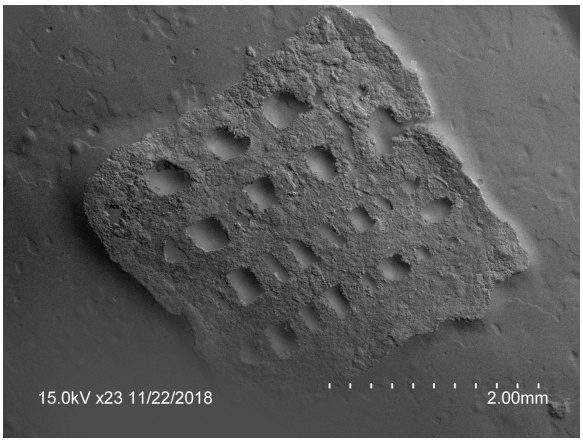

(c) dry, 23× magnification

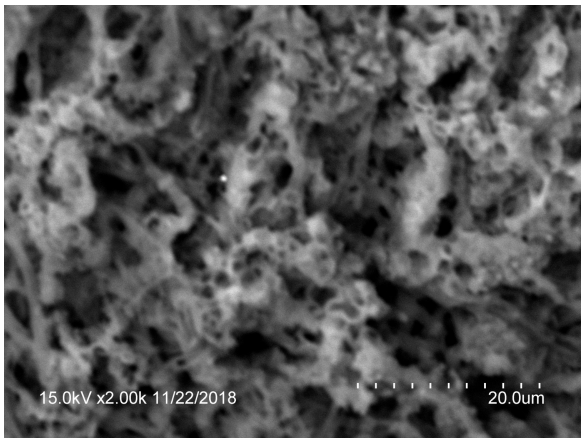

(d) dry, 2 000× magnification

Figure 5.13: SEM of DIW Col-PPy 1:4 wt% grid structures conducted at low magnifications for (a) damp and (c) dried shows the collapse of topographical features upon dehydration. Adequate retention of porosity is observed when samples were compared under (b) damp conditions and (d) dry conditions at 2 000× magnification.

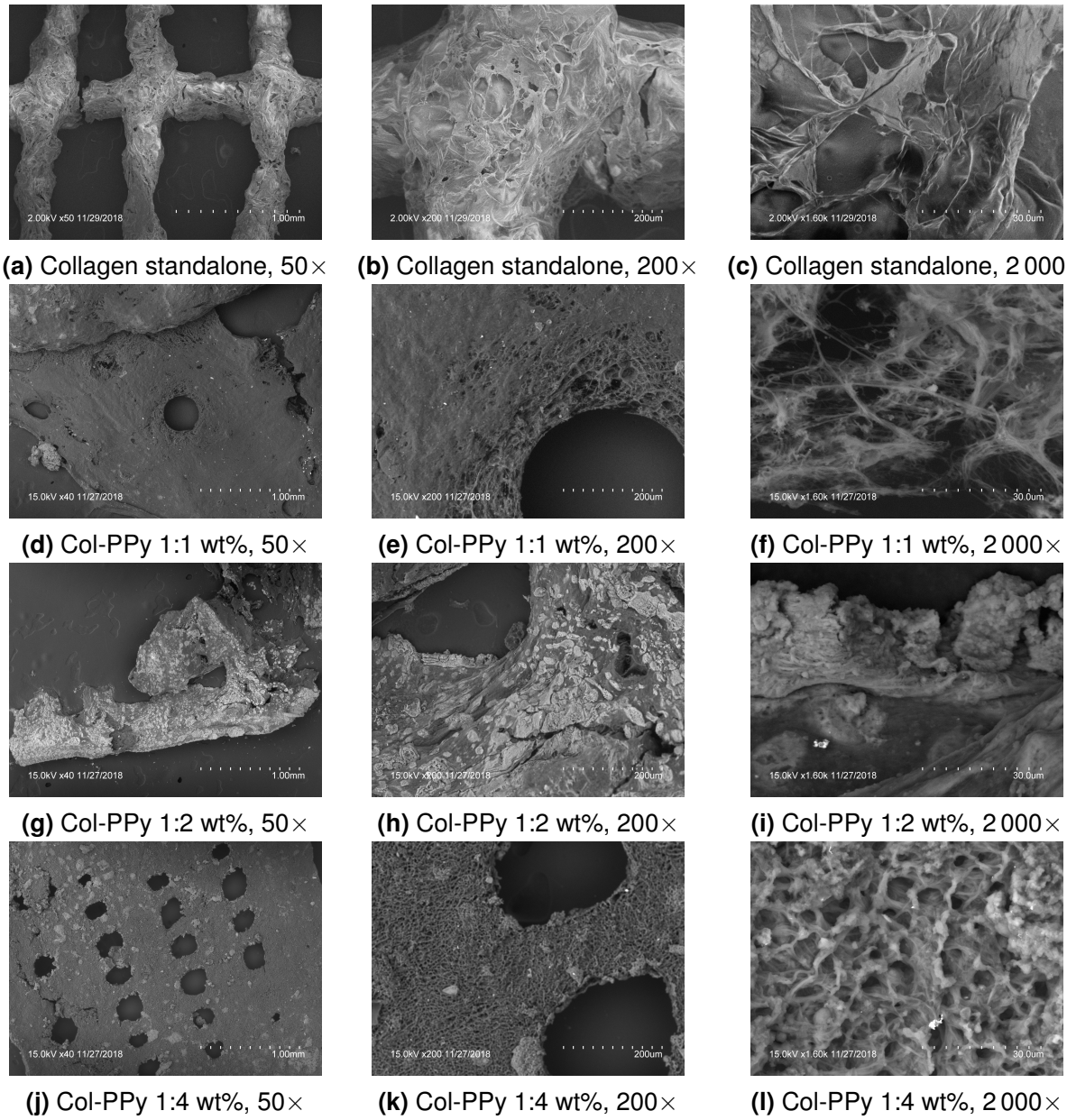

(a) Collagen standalone, 50× **(b)** Collagen standalone, 200× **(c)** Collagen standalone, 2 000×

(d) Col-PPy 1:1 wt%, 50× **(e)** Col-PPy 1:1 wt%, 200× **(f)** Col-PPy 1:1 wt%, 2 000×

(g) Col-PPy 1:2 wt%, 50× **(h)** Col-PPy 1:2 wt%, 200× **(i)** Col-PPy 1:2 wt%, 2 000×

(j) Col-PPy 1:4 wt%, 50× **(k)** Col-PPy 1:4 wt%, 200× **(l)** Col-PPy 1:4 wt%, 2 000×

Figure 5.14: SEM of dehydrated DIW collagen standalone and DIW Col-PPy 1:1 wt%, 1:2 wt%, 1:4 wt% structures reveals retention of collagen's fibrillar nature, whereas increasing PPy concentration indicates increased porosity.

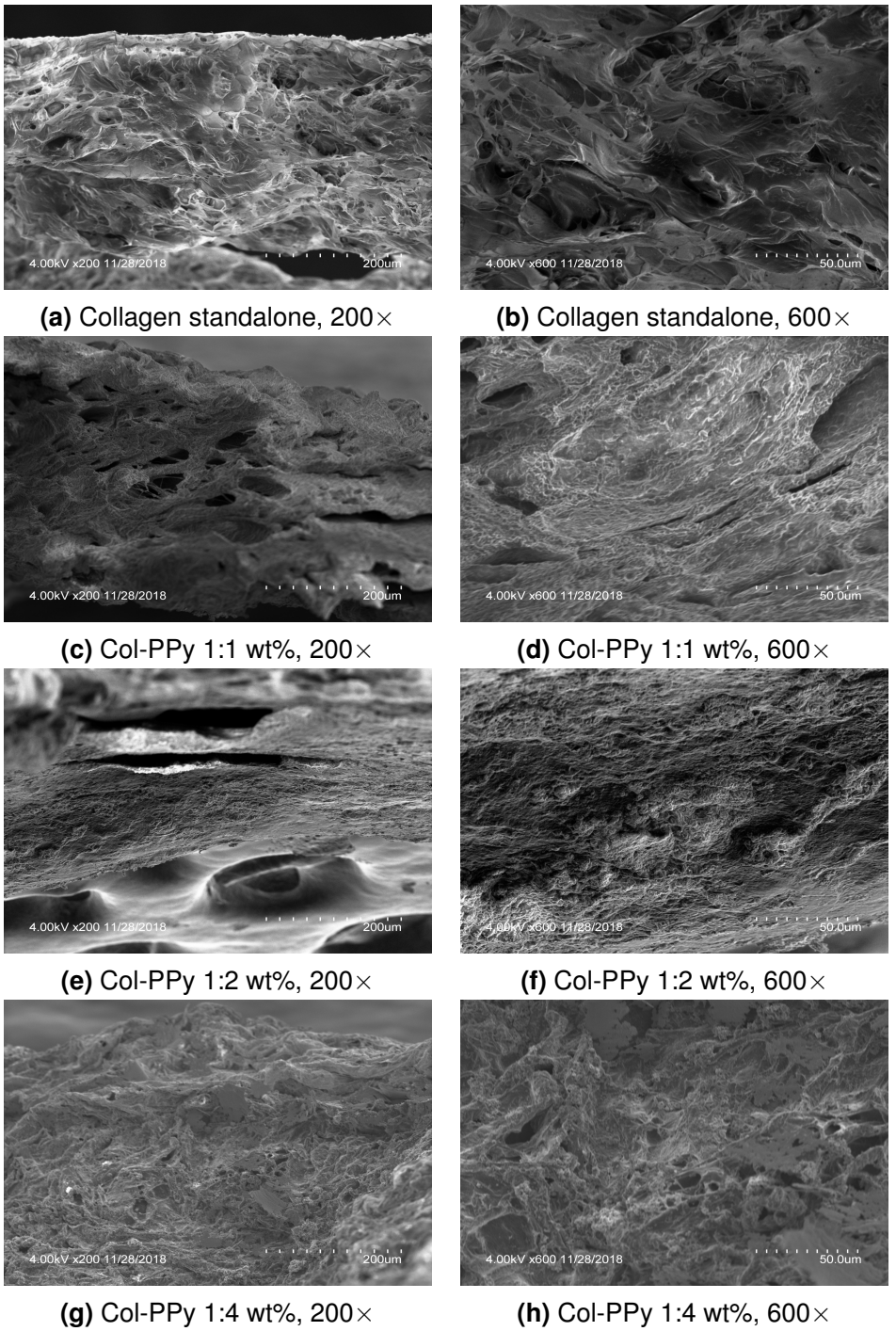

(a) Collagen standalone, 200×

(b) Collagen standalone, 600×

(c) Col-PPy 1:1 wt%, 200×

(d) Col-PPy 1:1 wt%, 600×

(e) Col-PPy 1:2 wt%, 200×

(f) Col-PPy 1:2 wt%, 600×

(g) Col-PPy 1:4 wt%, 200×

(h) Col-PPy 1:4 wt%, 600×

Figure 5.15: SEM of cross-sections of DIW collagen standalone constructs and Col-PPy 1:1 wt%, 1:2 wt%, 1:4 wt% structures reveal the PPy blends with collagen, while no drastic loss in internal porosity is observed.

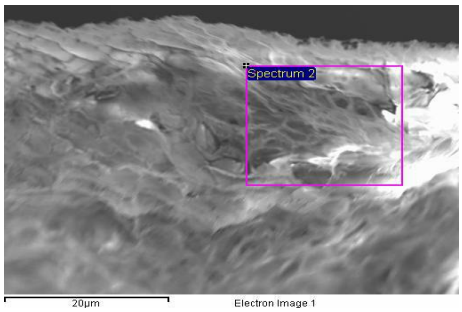

(a) Collagen standalone, 16 000×

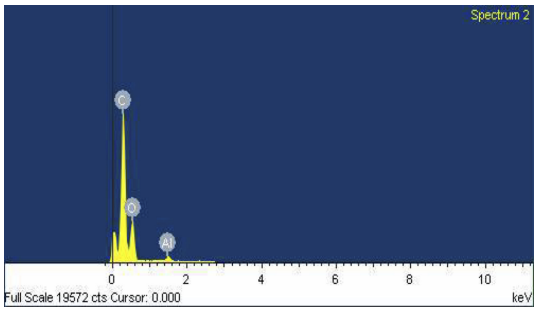

(b) Collagen standalone EDAX

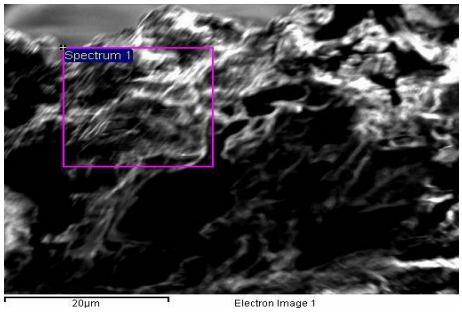

(c) Col-PPy 1:1 wt%, 16 000×

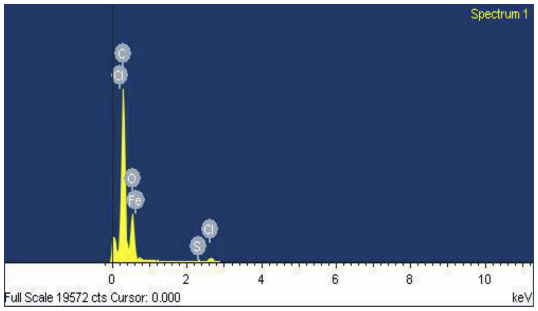

(d) Col-PPy 1:1 wt% EDAX

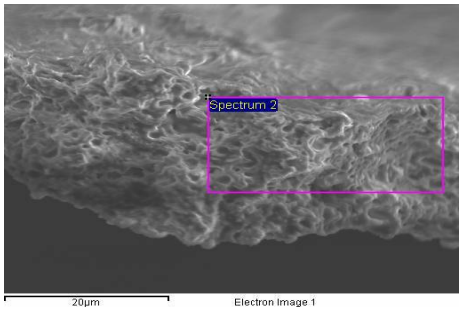

(e) Col-PPy 1:2 wt%, 600×

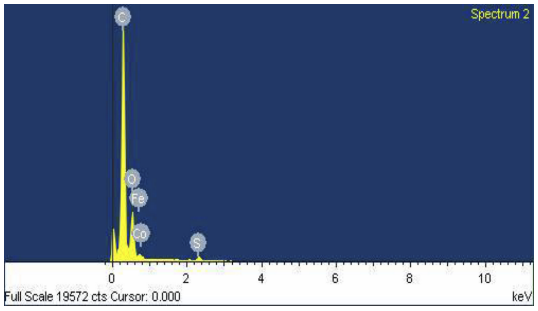

(f) Col-PPy 1:2 wt% EDAX

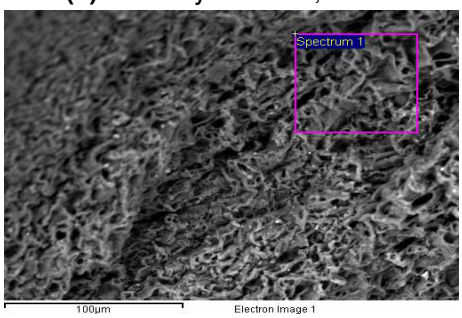

(g) Col-PPy 1:4 wt%, 500×

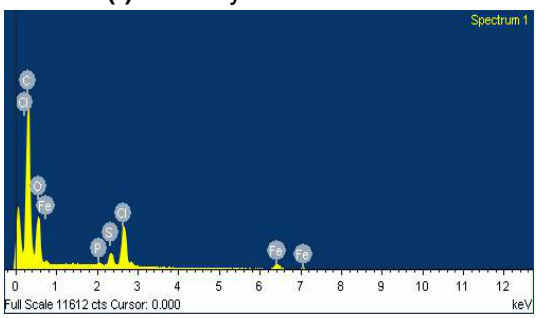

(h) Col-PPy 1:4 wt% EDAX

Figure 5.16: Elemental mapping of cross-sections of collagen standalone and Col-PPy 1:1 wt%, 1:2 wt%, 1:4 wt% structures suggests insufficient dopant presence.

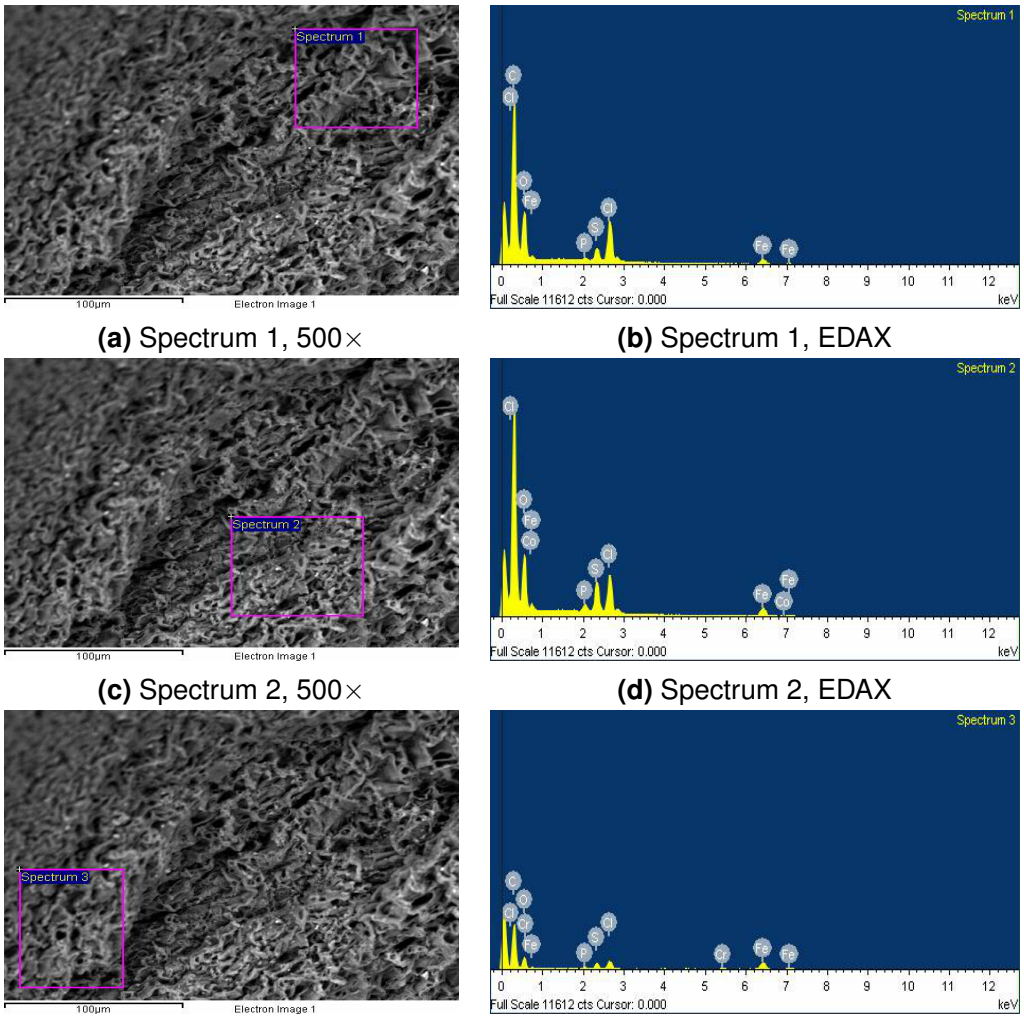

(a) Spectrum 1, 500× **(b)** Spectrum 1, EDAX

(c) Spectrum 2, 500× **(d)** Spectrum 2, EDAX

(e) Spectrum 3, 500× **(f)** Spectrum 3, EDAX

Figure 5.17: Elemental mapping of cross-sections of Col-PPy 1:4 wt% samples suggests variance in dopant presence for adjacent areas of the same sample.

Table 5.4: Collagen standalone and Col-PPy DIW printed constructs were evaluated for their elemental composition via EDAX for sites shown in Figure 5.16 and Figure 5.17. Cross-sections of Col-PPy 1:4 wt% and collagen standalone were specifically evaluated for iron presence and sulphur presence corresponding to oxidant and dopant presence, respectively.

	Composition [wt%]			
Site	C	O	Fe	S
Collagen standalone (Spectrum 2)	63.77	34.16	0.00	0.00
Col-PPy 1:1 wt% (Spectrum 1)	63.38	31.14	2.58	0.66
Col-PPy 1:2 wt% (Spectrum 2)	68.96	24.99	2.78	0.92
Col-PPy 1:4 wt% (Spectrum 1)	61.91	26.23	3.65	1.59
Col-PPy 1:4 wt% (Spectrum 2)	NA	52.29	16.31	10.86
Col-PPy 1:4 wt% (Spectrum 3)	58.68	15.75	17.79	2.37

5.2.1 Discussion

SEM imaging was performed on these dehydrated samples to qualitatively evaluate differences in degree of porosity and morphology between the hybrid and collagen standalone structures due to increasing PPy presence. Greater porosity was observed for the PPy-based structures, relative to the collagen sample, despite flattening of the Col-PPy constructs once the samples were dried (Figure 5.14). With the exception of the Col-PPy 1:2 wt% sample, which was observed to have undergone greater dehydration than other samples, resulting in considerable flattening which is reflected in decreased topography and porosity compared to collagen standalone and Col-PPy 1:1 wt% or 1:4 wt%.

EDAX results suggest that although sulfur (indicative of the DBSA molecule) is present in the Col-PPy 1:1 wt%, 1:2 wt% and 1:4 wt%, it is not nearly enough to reflect the concentration used during the polymerization step of the fabrication process. Additionally, Figure 5.17 suggests large degree of variance even in adjacent areas. EDAX elemental mapping results are inconsistent with elemental analysis results reported by Jayamurgan et al. (2013) who observed approximately 5% sulfur presence when the same concentration of DBSA was used during the chemical oxidative PPy polymerization process.

One possible reason for this discrepancy is attributed to the difference in scale of structures produced which influences inclusion of the dopant molecules. Jayamurgan et al. (2013) were able to produce powder particles of varied sizes, typically 200nm, which held smaller surface area and also greater infiltration of dopant molecules solvated in the solution into fabricated structures, therefore greater inclusion of the dopant in the nano-particles is reported. Whereas, the structures produced in this study are 1000$\times$ larger in scale. Specifically, convection and diffusion forces govern oxidant and dopant interaction with pyrrole monomers and oligomer chains embedded with the collagen fibres during the polymerization step of the fabrication process. Obtaining uniform

dopant-levels throughout the structures warrants additional investigation.

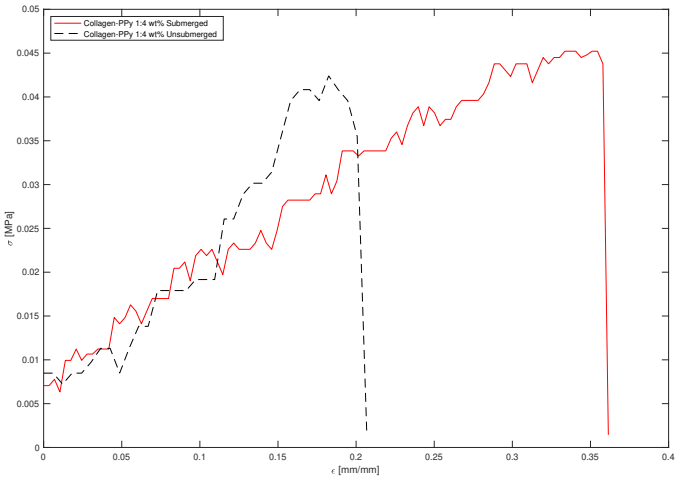

Figure 5.18: Stress versus strain curves of samples tested in wet/submerged and unsubmerged conditions are reported.

5.3 Mechanical Characterization Results

As the aim of the previous section was to establish whether the 3D printed constructs held potential for stimulating mechanotransduction effects, this section studies the effects of varying Py monomer concentration in the DIW ink, the effect of hydration and the effect of electrical stimulation on the 3D printed constructs' elasticity and stiffness.

Table 5.5: Calculations pertaining to tensile testing performed on (a-c) samples with increasing PPy concentration, (d) unsubmerged samples, (e-f) samples under electrical stimulation are reported.

Sample	***E* (KPa)**	**Max Strain**	**UTS (KPa)**	**Fracture Stress (KPa)**	**Yield Strength (KPa)**
(a) 1:1 wt %	114.5	296.6	21.7	32.9	32.9
(b) 1:2 wt %	115.1	359.1	37.5	41.8	37.5
(c) 1:4 wt %	120.0	360.0	43.8	45.2	43.8
(d) 1:4 wt % Unsubmerged	203.9	200.7	35.5	42.4	40.8
(e) 1:4 wt % Oxidized	78.5	320.0	31.6	32.4	31.6
(f) 1:4 wt % Reduced	79.1	291.2	50.0	53.2	48.4

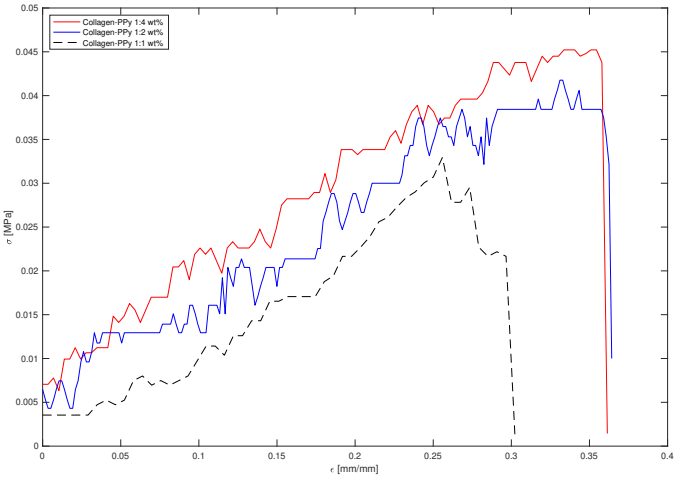

(a) Col-PPy 1:1 wt% vs. 1:2 wt% vs. 1:4 wt%

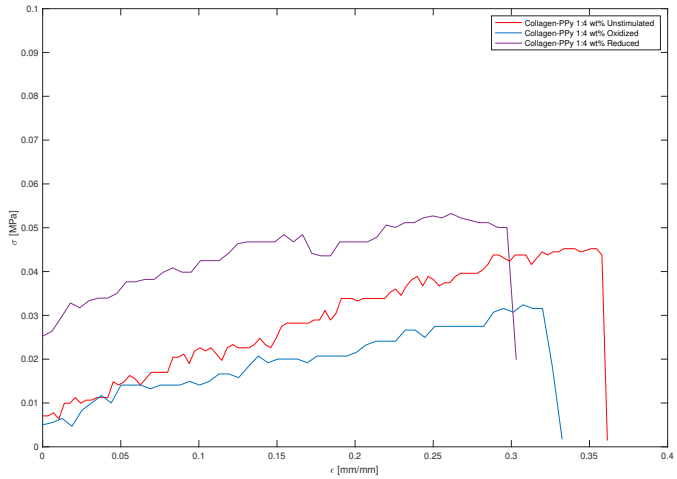

(b) Col-PPy 1:4 wt% vs. electrical stimulation

Figure 5.19: Stress versus strain curves demonstrating the effect of (a) increasing PPy concentration and (b) applying electrical stimulation are reported.

5.3.1 Discussion

For collagen-like hydrogels, curing method, either physical or chemical, and conditions of the hydrogel's curing process, such as concentration of the scaffolding material and environmental parameters as pH, temperature and ionic strength of the working solution, majorly influence elastic properties of the fabricated construct. Achilli and Mantovani (2010) reported that mechanical properties such as microstructure, degree of gelation and size of fibrils of the collagen hydrogel can be influenced by interchanging the three aforementioned fabrication conditions, however, such changes only elicited $\pm$ 0.2 to 0.05 MPa change in the *E* value.

In addition to the influence of the method of mechanical evaluation, another impactful factor is the curing agent, or simply, the method of inducing collagen cross-linking. Chemical cross-linkers such as glutaraldehyde, microbial transglutaminase (MTGase), PEG succinimidyl glutarate, and genipin have been reported to greatly influence collagen hydrogel stiffness as *E* values ranged from 20 MPa to 0.6 MPa. However, freeze-drying was the curing method opted for the collagen portion of the Col-PPy construct in this thesis as chemical cross-linking agents have been observed to induce cyto-toxicity effects, host immunogenicity and high resistance to collagenase enzymatic digestion (Delgado et al., 2015, 2017). In addition to the fabrication parameters that can be modulated to control the physical properties of collagen constructs, the inclusion of PPy indicates an increase in mechanical integrity and material toughness (Figure 5.19 (a)). The retention of the electro-active properties of PPy which work to change the bulk physical properties of the construct as a result of electrical stimulation is demonstrated in Figure 5.19 (b).

It is important to note that collagen standalone constructs, which were fabricated to serve as the control against Col-PPy constructs and inform on the effect of Py inclusion to the collagen scaffolding base material, were observed to collapse under their own weight after rehydration. Collagen standalone dog bone samples were prone

to bending and doubling over which necessitated repositioning and manual flattening prior to mounting on to the Univert tester. However, this manoeuvring resulted in tearing of the sample and made impotent any efforts for evaluating tensile properties of the fabricated samples, without exception. This behaviour is attributed to the thickness of the 3D printed construct, but one that was observed not to be a problem for Col-PPy constructs.

Results from tensile testing corroborate empirical observations from sample handling that weakening of the mechanical properties of construct presents as PPy concentration decreases. Results demonstrate the tailor-ability and dynamic nature of the 3D printed constructs fabricated using the protocol presented in this thesis. The bulk physical properties of 3D printed constructs can now be adapted for tissue engineering applications *in vitro* and beyond. By changing scaffolding material (collagen, in this case) concentration, PPy concentration or by simply applying variable electrical stimulation, the physical properties of the construct are apt to changing in concert with its shape as established by Figure 5.2. However, additional studies are required to further understand and profile the extent of influence PPy imparts, under electrical stimulation, to change volume and elasticity/stiffness of the 3D printed hybrid structures.

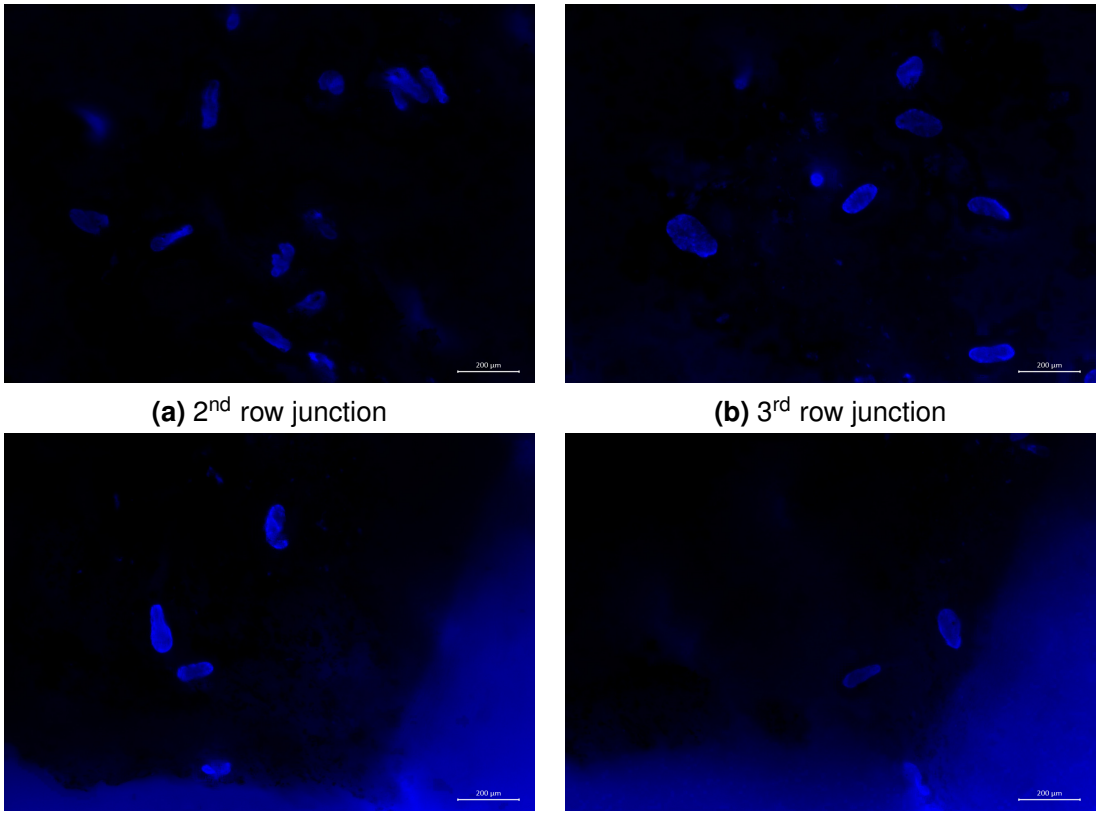

(a) 2nd row junction **(b)** 3rd row junction

(c) corner at Z-height-1 **(d)** corner at Z-height-2

Figure 5.20: Hoescht stained human BJ fibroblast on DIW printed Col-PPy 1:4 wt% grid samples imaged demonstrated cell attachment and cell survival at 96h following initial cell seeding, at 20× magnification.

5.4 Cyto-compatibility Results

5.4.1 Preliminary evaluation

A pilot study to evaluate cyto-compatibility was performed where human BJ fibroblast cells cultured on 3D printed Col-PPy 1:4 wt% samples underwent immunocytochemical staining of Hoechst stain to visualize cell nuclei. Cels were observed to survive up to 4 days of culture. During the imaging process, fibroblasts were observed to occupy multiple Z-heights even in the same visual field, suggesting that sizeable deviations in topography must exist for hydrated constructs as this feature quality is not detectable using SEM imaging. This phenomena is depicted in Figure 5.20 (c) and (d).

5.4.2 Extended cyto-compatibility evaluation

Figure 5.21: Initial experiment with human BJ fibroblast cells cultured on DIW collagen standalone and Col-PPy 1:4 wt% grid structures demonstrate cell attachment 6h post-cell seeding and continued cell survival up to day 7. Immunocytochemical staining indicates Col-PPy constructs fabricated using the novel DIW methodology are cyto-compatible.

Figure 5.22: Second cyto-compatibility experiment with human BJ fibroblast cells cultured on DIW collagen standalone and Col-PPy 1:4 wt% grid structures demonstrate cell attachment 6h post-cell seeding and continued cell survival up to day 7. Immunocytochemical staining indicates Col-PPy constructs fabricated using the novel DIW methodology are cyto-compatible.

5.4.3 Confocal Laser Scanning Microscopy Results

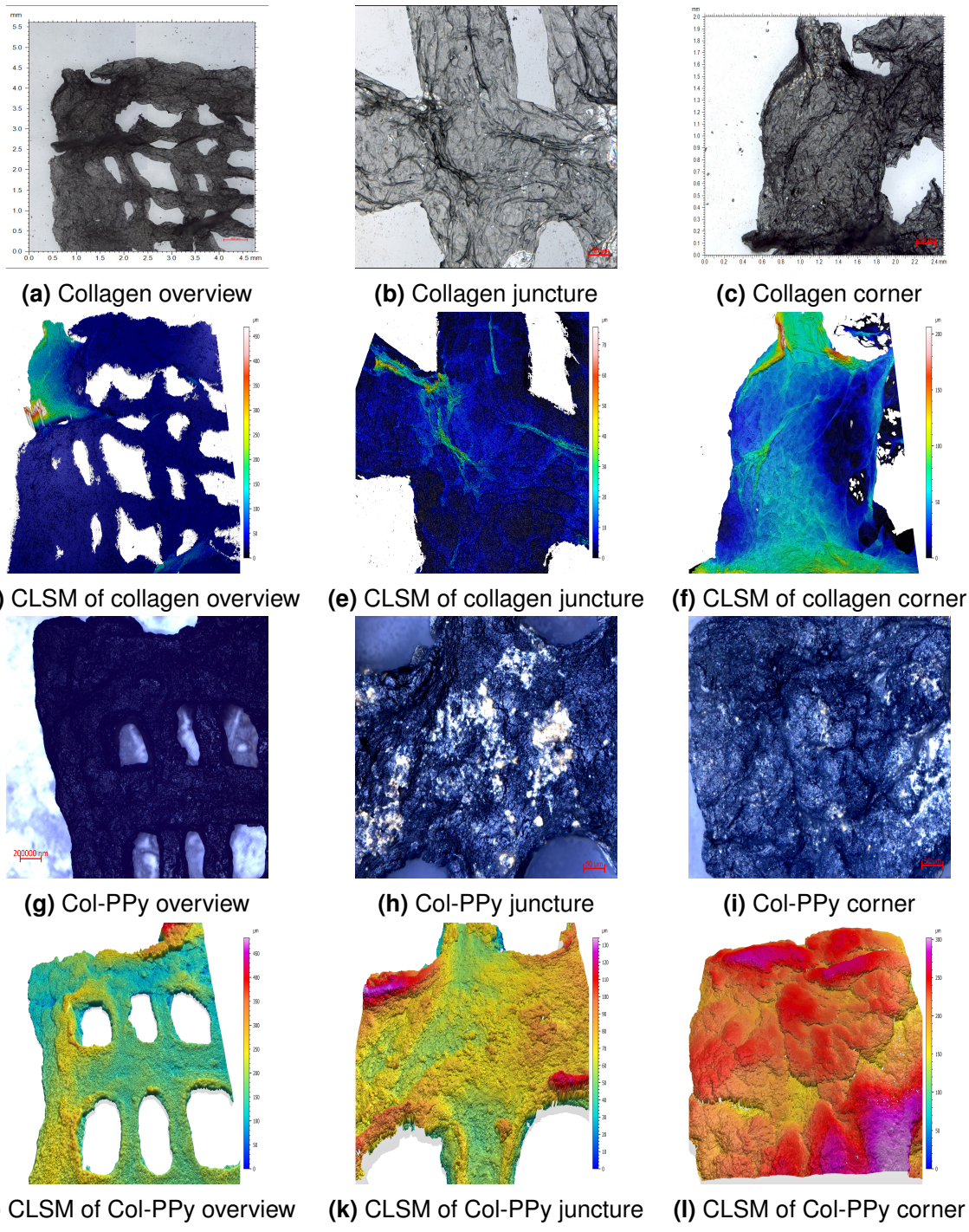

(a) Collagen overview **(b)** Collagen juncture **(c)** Collagen corner

(d) CLSM of collagen overview **(e)** CLSM of collagen juncture **(f)** CLSM of collagen corner

(g) Col-PPy overview **(h)** Col-PPy juncture **(i)** Col-PPy corner

(j) CLSM of Col-PPy overview **(k)** CLSM of Col-PPy juncture **(l)** CLSM of Col-PPy corner

Figure 5.23: Confocal imaging of (a-c) collagen standalone and (g-i) Col-PPy 1:4 wt% samples, and CLSM topographic analysis of (d-f) collagen standalone and (j-l) Col-PPy 1:4 wt% samples is depicted.

5.4.4 Discussion

With the DIW printing Col-PPy fabrication methodology presented in this thesis, PPy-based hydrogel constructs are now no longer restricted in feature and geometric complexity. Therefore, adding design-ability to the list of attributes associated with favourable properties of PPy-based constructs. Extended cell culture experiments established that the novel DIW fabrication methodology developed in this thesis produces Col-PPy constructs which retains the cyto-compatible aspect associated with Col-PPy constructs fabricated using traditional methodologies.

As evidenced by continued fibroblast confluence at each measured time point, for both sets of experiments. One observed phenomena differentiating collagen standalone and Col-PPy constructs is a clumping feature of actin fibres on Col-PPy samples, present at each of fixation/imaging time points. Whereas, collagen standalone samples observed an elongation of actin fibres over time. This stark difference in behaviour is attributed to the natural epitopes present on collagen constructs contributing to observed difference in fibroblast behaviour (Boyce et al., 1988; Chattopadhyay and Raines, 2014; Aziz et al., 2016). Another explanation for said behaviour of actin filaments may be due to mismatching of the physical properties to that of the fibroblast's tissue of origin, that is, skin. In contrast, PPy inclusion to collagen samples was observed to increase material stiffness (section 5.3). A deviation from the physical properties of the construct to one that would keep fibroblasts proliferating and explorative is attributed to this phenomena (Peyton and Putnam, 2005; Skardal et al., 2012; Nam et al., 2016). Additionally, the combined use of high concentrations of both PPy at 1:4 wt% and collagen at 25 $mg \cdot mL^{-1}$ compared to that of most investigations which utilize collagen as standalone or collagen with Py at $2 - 3$ $mg \cdot mL^{-1}$ may serve to explain observed clumping behaviour on constructs containing PPy (Achilli and Mantovani, 2010; Delgado et al., 2015, 2017; Sung et al., 2004; Weng et al., 2012; Mekonnen et al., 2016; Ketabat et al., 2017; Ravichandran et al., 2018).

Additional investigation to study effects of modulating scaffolding base and PPy concentration on consequent physical properties of constructs to provide edification for parameter under which cells of interest are geared towards biologically relevant outcomes such as proliferation and anoikis. Findings from said investigation would inform future researchers, who aspire to implement functional properties of PPy to static constructs, to the limits of the hybrid construct as a function of PPy inclusion, as well as inform them of the range to which the hybrid PPy-based construct's physical properties can be modulated under electrical stimulation.

Similar to observations of the preliminary investigation, cells were observed to occupy multiple Z-heights in the same visual field, implicating topographical deviations which must be contributing to increased surface roughness, more so near the internal junctions and corners of the construct. This was not observed to be the case for collagen standalone samples during imaging, however, the lack of opacity of collagen standalone samples could be a confounding factor. In collagen standalone samples, fibroblasts were observed to infiltrate into the substrate during imaging. The degree of infiltration was not quantified. However, qualitatively, this infiltration is apparent in collagen samples as translucency of the sample allows fluorescent cells to be adequately captured via imaging. Increased diffusion of stain fluorescence over time is attributed to the assertion of infiltration, as imaging parameters of the microscope were held consistent.

In the case of the Col-PPy samples, infiltration could not be observed as it would require fibroblasts to display motility, which requires an exercise of actin filaments. Although actin elongation is not observed, topographical features of the Col-PPy construct are observed to be well-occupied as fibroblast cells confound the same visual field by taking up residence at different Z-heights. For this reason, obtaining clear images at higher magnifications for Col-PPy samples presented a challenge, as stained cells above and below the imaged area, for any one Z-height, would confound image capture by increasing fluorescence diffusion. This notion was observed to be present but

marginally less impactful for image acquisition for the collagen standalone samples at the same magnification. Additional studies which exploit the functional properties of PPy, for instance, electro-activity/volumetric change, would provide interesting edification on how electrical stimulation can impart mechanical changes in material stiffness and consequent effect on cell morphology and behaviour. For instance, eliciting changes in behaviour that transition cells from extant/homeostatic to anoikis or back to homeostasis before anoikis onset (Humphrey et al., 2014; Kollmannsberger et al., 2018).

Lastly, CLSM was used to provide topographic contrast and to supplement SEM imaging, as SEM imaging required samples to be sufficiently dried which understated topographical properties and surface roughness of constructs. As well as corroborate empirical observations of image acquisition post-immunocytochemical staining of collagen standalone and Col-PPy 1:4 wt% samples. Empirical observations during image acquisition suggested Col-PPy 1:4 wt% samples held greater surface roughness and topographical features compared to collagen standalone samples, especially at the junctures. This is confirmed by CLSM results shown in Figure 5.23.

5.5 Chapter summary

This chapter investigated cyto-compatibility and the physical properties of DIW Col-PPy constructs. The capability of constructs as a bioactuators for studying mechanotransduction effects in 3D cell culture settings as 3D printed structures and bending bilayers was assessed and deemed to warrant further investigation before actuation performance can be realized for applications. Physical properties of the DIW constructs were measured by tensile tests, SEM imaging and elemental mapping and are reported in this chapter. Lastly, cyto-compatibility is qualitatively established by culturing human BJ fibroblast cells on the PPy-based constructs for an extended period of time. In this chapter, potential of the 3D printed Col-PPy constructs as another addition to the library of materials

and methods employable to study and evoke biologically relevant cellular responses and behaviour is established.

List of references

Achilli, M. and Mantovani, D. (2010), 'Tailoring mechanical properties of collagen-based scaffolds for vascular tissue engineering: The effects of ph, temperature and ionic strength on gelation', *Polymers* **2**(4), 664–680.

Ahn, A. C. and Grodzinsky, A. J. (2009), 'Relevance of collagen piezoelectricity to "wolff's law": a critical review', *Med Eng Phys* **31**(7), 733–741.

Aziz, J., Shezali, H., Radzi, Z., Yahya, N., Abu Kassim, N., Czernuszka, J. and Rahman, M. (2016), 'Molecular mechanisms of stress-responsive changes in collagen and elastin networks in skin', *Skin Pharmacology and Physiology* **29**(4), 190–203.

Boyce, S. T., Christianson, D. J. and Hansbrough, J. F. (1988), 'Structure of a collagen-GAG dermal skin substitute optimized for cultured human epidermal keratinocytes', *Journal of biomedical materials research* **22**(10), 939–957.

Chattopadhyay, S. and Raines, R. (2014), 'Review collagen-based biomaterials for wound healing', *Biopolymers* **101**(8), 821–833.

Delgado, L. M., Bayon, Y., Pandit, A. and Zeugolis, D. I. (2015), 'To cross-link or not to cross-link? cross-linking associated foreign body response of collagen-based devices.', *Tissue Eng Part B Rev* **21**(3), 298–313.

Delgado, L. M., Fuller, K. and Zeugolis, D. I. (2017), 'Collagen cross-linking: Biophysical, biochemical, and biological response analysis', *Tissue Engineering Part A* **23**(19-20), 1064–1077.

Farajollahi, M., Woehling, V., Plesse, C., Nguyen, G. T. M., Vidal, F., Sassani, F., Yang, V. X. D. and Madden, J. D. W. (2016), 'Self-contained tubular bending actuator driven by conducting polymers', *Sensors & Actuators: A. Physical* **249**, 45–56.

Fleming, M. J., Kim, K. J. and Leang, K. K. (2012), 'Mitigating ipmc back relaxation through feedforward and feedback control of patterned electrodes', *Smart Materials and Structures* **21**(8), 085002.

Fukada, E. and Yasuda, I. (1964), 'Piezoelectric effects in collagen', *Japanese Journal of Applied Physics* **3**(2), 117.

Hara, S., Zama, T., Takashima, W. and Kaneto, K. (2006), 'Tris(trifluoromethylsulfonyl)methide-doped polypyrrole as a conducting polymer actuator with large electrochemical strain', *Synthetic Metals* **156**(2-4), 351–355.

Holst, J., Watson, S., Lord, M. S., Eamegdool, S. S., Bax, D. V., Nivison-Smith, L. B., Kondyurin, A., Ma, L., Oberhauser, A. F., Weiss, A. S. and Rasko, J. E. J. (2010), 'Substrate elasticity provides mechanical signals for the expansion of hemopoietic stem and progenitor cells', *Nature Biotechnology* **28**(10), 1123–1128.

Humphrey, J. D., Dufresne, E. R. and Schwartz, M. A. (2014), 'Mechanotransduction and extracellular matrix homeostasis', *Nature Reviews Molecular Cell Biology* **15**(12), 802–812.

Jager, E., Smela, E., Inganäs, O. and Lundström, I. (1999), 'Polypyrrole microactuators', *Synthetic Metals* **102**(1-3), 1309–1310.

Jayamurgan, P., Ponnuswamy, V., Ashokan, S. and Mahalingam, T. (2013), 'The effect of dopant on structural, thermal and morphological properties of DBSA-doped polypyrrole', *Iranian Polymer Journal* **22**(3), 219–225.

Ketabat, F., Karkhaneh, A., Aghdam, R. M. and Tafti, S. H. A. (2017), 'Injectable conductive collagen/alginate/ polypyrrole hydrogels as a biocompatible system for biomedical applications', *Journal of Biomaterials Science, Polymer Edition* pp. 0–0.

Kollmannsberger, P., Bidan, C., Dunlop, J., Fratzl, P. and Vogel, V. (2018), 'Tensile forces drive a reversible fibroblast-to-myofibroblast transition during tissue growth in engineered clefts', *Science Advances* **4**(1).

Küttel, C., Stemmer, A. and Wei, X. (2009), 'Strain response of polypyrrole actuators induced by redox agents in solution', *Sensors & Actuators: B. Chemical* **141**(2), 478–484.

Madden, P. G. A., Madden, J. D. W., Anquetil, P. A., Vandesteeg, N. A. and Hunter, I. W. (2004), 'The Relation of Conducting Polymer Actuator Material Properties to Performance', *IEEE Journal of Oceanic Engineering* **29**(3), 696–705.

Mekonnen, B. T., Ragothaman, M., Kalirajan, C. and Palanisamy, T. (2016), 'Conducting collagen-polypyrrole hybrid aerogels made from animal skin waste', *RSC Advances* **6**, 63071–63077.

Melling, D., Wilson, S. and Jager, E. W. H. (2013), 'The effect of film thickness on polypyrrole actuation assessed using novel non-contact strain measurements', *Smart Materials and Structures* **22**(10), 104021–30.

Nam, S., Hu, K. H., Butte, M. J. and Chaudhuri, O. (2016), 'Strain-enhanced stress relaxation impacts nonlinear elasticity in collagen gels', *Proceedings of the National Academy of Sciences* .

Nemat-Nasser, S. (2002), 'Micromechanics of actuation of ionic polymer-metal composites', *Journal of Applied Physics* **92**(5), 2899–2915.

Otero, T. F. and Martinez, J. G. (2016), 'Electro-chemo-biomimetics from conducting polymers: fundamentals, materials, properties and devices', *Journal of Materials Chemistry B* **4**(12), 2069–2085.

Peyton, S. and Putnam, A. (2005), 'Extracellular matrix rigidity governs smooth muscle cell motility in a biphasic fashion', *Journal of Cellular Physiology* **204**(1), 198–209.

Price, A. D., Gillen, T., Liu, C. C., O'Shaughnessy, C. A. and Naguib, H. E. (2012), 'Evaluation of porous membrane core elasticity and porous morphology for polypyrrole trilayer actuators', *Journal of Cellular Plastics* **48**(1), 25–42.

Ravichandran, R., Martinez, J., Jager, E., Phopase, J. and Turner, A. (2018), 'Type i collagen-derived injectable conductive hydrogel scaffolds as glucose sensors', *ACS Applied Materials and Interfaces* **10**(19), 16244–16249.

Skardal, A., Mack, D., Atala, A. and Sokern, S. (2012), 'Substrate elasticity controls cell proliferation, surface marker expression and motile phenotype in amniotic fluid-derived stem cells', *Journal of the Mechanical Behavior of Biomedical Materials* **17**, 307–316.

Smela, E. (2003), 'Conjugated polymer actuators for biomedical applications', *Advanced Materials* **15**(6), 481–494.

Smela, E. and Gadegaard, N. (2001), 'Volume change in polypyrrole studied by atomic force microscopy', *The Journal of Physical Chemistry B* **105**(39), 9395–9405.

Sung, W., Park, K. and Lee, K. (2004), A novel extracellular matrix based on polypyrrole/-collagen composites, *in* 'Australian Society for Biomaterials', p. 1280.

Svennersten, K., Berggren, M., Richter-Dahlfors, A. and Jager, E. W. H. (2011), 'Mechanical stimulation of epithelial cells using polypyrrole microactuators', *Lab on a Chip* **11**(19), 3287–7.

Wang, X., Shapiro, B. and Smela, E. (2004), 'Visualizing ion currents in conjugated polymers', *Advanced Materials* **16**(18), 1605–1609.

Weng, B., Liu, X., Shepherd, R. and Wallace, G. G. (2012), 'Inkjet printed polypyrrole/-collagen scaffold: A combination of spatial control and electrical stimulation of PC12 cells', *Synthetic Metals* **162**(15-16), 1375–1380.

Wu, Y., Alici, G., Madden, J. D. W., Spinks, G. M. and Wallace, G. G. (2007), 'Soft Mechanical Sensors Through Reverse Actuation in Polypyrrole', *Advanced Functional Materials* **17**(16), 3216–3222.

Chapter 6

Concluding Remarks

6.1 Summary of conclusions

This thesis explored issues inherent to traditional fabrication methods of PPy-based constructs which made it difficult to adapt AM methods. This thesis effectively combined PPy with an ECM protein using a DIW AM method for the development of novel designable, electro-active and electro-conductive Col-PPy 3D structures. Produced structures were evaluated for their electrical conductivity for potential as electro-conductive hydrogel constructs, for their electro-active capabilities for potential as drug delivery release systems and their actuation performance and cyto-compatibility for potential as bioactuators and as platforms for studying mechanotransduction effects in cell culture settings. The knowledge ascertained from these activities has prompted the following conclusions:

1. Traditional fabrication methods, specifically chemical oxidative polymerization, for creating PPy-based structures were explored for integration with AM techniques, specifically DIW 3D printing. Traditional fabrication methods for PPy-based hydrogel constructs were observed to produce structures of limited form, i.e. aggregates, and fibrous or bulk hydrogel constructs. Therefore, traditional fabrication methods for creating PPy-based hydrogel constructs were not compatible with AM

technology.

2. A novel DIW AM fabrication methodology which adapts traditional fabrication methods was developed. This process entailed the use of collagen and Py as a monomer as the DIW ink and evaluation of favourable shear-thinning characteristics. The major revision to traditional fabrication methods is the inclusion of a delay aspect, that is, by subjecting produced structures to freezing temperatures, to effectively retain pre-meditated geometrical features of 3D printed structures.

3. Col-PPy structures produced from this fabrication methodology were evaluated for the retention of favourable properties associated with PPy structures produced via traditional fabrication methodologies. Properties such as electrical conductivity, electro-activity, actuation capability, and cyto-compatibility were evaluated.

4. The potential of 3D printed PPy-based constructs as a designable, 3D multifaceted, dynamic platform capable of imparting modifiable electrical, mechanical and chemical stresses to its environment, for the purpose of emulating the native cellular micro-environment's unique properties in a combinatory manner and observing concurrent cell behaviour, is established.

6.2 Summary of contributions

This research makes a contribution to scientific knowledge in the form of new methodology and new evidence. The most significant research contributions presented in this thesis are summarized as follows:

- The first-ever study to characterize the rheological properties of Col-Py blend as a DIW ink. This thesis demonstrates that Col-Py DIW inks, at varying concentrations of Py, exist as stable blends presenting shear-thinning behaviour as a function of increasing shear rates.

- Development of a novel DIW fabrication methodology for producing PPy-based structures is reported. This is the first ever-study to ameliorate traditional fabrication methods of PPy-based hydrogel constructs with an AM technique.

- An apparatus for the freeze-drying of 3D printed PPy-based constructs was developed to serve the final step in the fabrication methodology reported in this thesis. Not only does this freeze-dryer increase the mechanical properties of the hydrogel construct by inducing cross-linking of the scaffolding constituent, it also removes trapped polymerizing oxidant/solvent particles that would otherwise have remained constricted within the construct. By effectively increasing porosity of the freeze-dried DIW printed PPy-based constructs, the number of sites available and contributing to the construct's electro-activity are increased.

- The first-ever study to show that DIW printed Col-PPy constructs exhibit all of the properties inherent to standalone PPy constructs, i.e. cyto-compatibility, mechanical stability, electro-activity and electro-conductivity; properties that are open to modulation by incorporation of different dopants, and scaffolding components. Tailoring of these synthesis parameters will lead to the fabrication of novel DIW printed PPy-based constructs with practical applications in biomedicine and tissue engineering.

- The first-ever study to suggest the favourable properties of 3D printed ECM-protein and PPy-based constructs can be used in concert, i.e. in a combined manner, to impart electrochemomechanical stimulation. The efficacy of the DIW printed constructs to potentially study and modulate biologically relevant outcomes such as proliferation, apoptosis, anoikis, stem cell differentiation and disease pathophysiology using the favourable properties discussed and demonstrated in this thesis in future studies is demonstrated.

6.3 Recommendations for future research

It is important to keep in mind the endgame goals for the specific type of technology being presented in this thesis. The DIW fabrication methodology presented in this thesis provides the framework for producing 3D PPy-based hydrogel structures. That is, an instructive platform cells of any type of to be cultured onto in an *in vitro*, extended cell culture setting. Rather than in an isolated manner, future projects which build on the work presented in this thesis can now evaluate the effect of combinatory electrochemomechanical stimulation. The platform introduced in this thesis is shown to be capable of allowing future researchers to capitalize on the electro-conductive and electro-active properties of PPy-based constructs. Cells of interest to tissue engineers and researchers, ranging from stem cells to cancerous cell types, can be cultured onto the said platform, then stimulated in a manner which utilizes on the electro-conductive and/or electro-active properties of the PPy-based constructs, followed by observing and profiling consequent cell behaviour. Building a library of such profiles of cell behaviour in response to stimulation on the DIW printed PPy-based constructs on a standardized cell culture platform effectively tackles the variability in cell behaviour attributed to changing the materials used to build instructive platforms capable of directing cell behaviours, differentiation, migration, apoptosis, etc. The formation of such a library would lead future researchers to realize aforementioned biologically relevant outcomes and design constructs to support clinically relevant outcomes.

A key advantage of this methodology is the design freedom it enables the researcher via AM workflow. With DIW printing, in addition to rheological properties of the DIW ink, the resolution of printable structures is also limited by the 3D printing apparatus. Future work focused towards initiating ink curing as material is deposited on the print bed, for instance, in the form of a cold print-bed, would provide valuable contribution towards further increasing the resolution and complexity of printable structures, while

decreasing operator-based variance. Although DIW printed structures were observed to undergo complete polymerization, under the right conditions, the semi-frozen state of the structure during chemical oxidation polymerization, one that is fundamental to the polymerization process, is attributed to be serving as the limiting factor to dopant infiltration. Therefore, limiting PPy presence in the final construct. A future study focused on optimizing the polymerization process parameters would provide valuable edification on the maximum yield of electro-active and electro-conductive capabilities of DIW structures, fabricated using the developed AM methodology.

Additionally, PPy-based constructs have been demonstrated to be capable of modulating cellular behaviours such as proliferation and maturation via integration with both naturally-derived and synthetically derived polymers. The DIW fabrication methodology reported in this thesis allows exchange of the scaffolding base/hydrogel component of the PPy-based construct with any of the materials PPy has been demonstrated to be well-integrated with, including but not limited to: HA, CS, silk, PLGA, chitosan, alginate, PLA, PLLA, PLGA, chitin, and agarose (Donderwinkel et al., 2017; Romero et al., 2014; Di Felice et al., 2015; Park et al., 2015; Gudapati et al., 2016; Kim et al., 2016; Hur et al., 2014; Yang et al., 2018; Elieh-Ali-Komi and Hamblin, 2016; Jia et al., 2013). In addition to adapting materials that have been successfully combined with PPy, it would be interesting to investigate the integration of dECM with PPy, as most constituents of native ECM (i.e. collagen, HA, CS, etc.) have been successfully combined with PPy to provide favourable stimulus responsive constructs. It would be interesting to evaluate the integration of a material so close in constitution to native ECM and observe its electro-conductive and electro-active properties of PPy.

Second to the hydrogel component in importance to the fabrication process is the dopant. Dopant choice directly impacts the functional properties of PPy and PPy-based constructs, but also their biodegradability, immunogenicity, topographic, chemical and mechanical properties (Babensee et al., 1998; Mattioli-Belmonte et al., 2003;

Armentano et al., 2010; Wang et al., 2004, 2017; Fonner et al., 2008; Ramanaviciene et al., 2010; Kunzmann et al., 2011; Yen et al., 2010; Tandon et al., 2018; Shi et al., 2014). Investigations with dopants of interest would yield in tailorable electro-conductivity and electro-activity profiles for constructs, which while maintaining similar composition would allow constructs to be tailored to the specific application at hand, as dopant inclusion can be mediated via electrochemical switching post-polymerization.

For DIW fabricated Col-PPy grid structures, actuation was observed to be present, but not in repeatable manner. Therefore, at this point, actuation mechanism of Col-PPy cannot be modelled or applied in a predictable manner. This response was attributed to the impedance imparted by the hydrogel component, that is, collagen. Other materials may not observe the same restriction. Investigations with other hydrophilic polymers such as those that directly interact and PPy can be doped with, such as CS, may not exhibit such behaviour and can be evaluated as an effective means for studying mechanotransduction effects using designable, DIW printed constructs on various cell types (Björninen et al., 2014; Lee et al., 1995).

Another interesting application of PPy-based actuators involves depositing PPy on one site of a hydrogel to serve as the functional coating, and collectively as a bilayer actuator (Ismail et al., 2011). A future study which compares the actuation profile of hydrogel structures, 3D printed or fabricated using traditional methods, with PPy coatings against 3D printed hydrogel-PPy blended structures would inform which methodology results in higher actuation capability, or whether the observed actuation response is confounded when 3D printed hydrogel-PPy blended structures are augmented with PPy coating.

One of the interesting properties of PPy is its intrinsic electro-conductivity. At the conclusion of this thesis, DIW printed 3D Col-PPy structures can be evaluated for practical applications as designable, electro-conductive substrates and studying cell behaviour in response to varied electrical stimulation and varied substrate composition.

DIW printed 3D Col-PPy structures can be used as a platform for studying the effects of electrical stimulation on electrically responsive cell types, including: cardiac cells, smooth muscle cells, neural cell types, as well as neuroprogenitor cells. Although, Col-PPy constructs as means for imparting mechanical stimulation was not established, potential for expecting such stimulation from 3D printed PPy-based constructs was established. Future studies should investigate materials from which actuation mechanism can be better modelled. After achieving this, future researches should study changes in cell behaviour and phenotype as a consequence of applying electrical stimulation (as a result of PPy's electro-conductivity), mechanical stimulation or chemical stimulation (as a result of PPy's electro-activity), or in a combinatory manner, including but not limited to stem cell lineage committance.

List of references

Armentano, I., Dottori, M., Fortunati, E., Mattioli, S. and Kenny, J. (2010), 'Biodegradable polymer matrix nanocomposites for tissue engineering: A review', *Polymer Degradation and Stability* **95**(11), 2126–2146.

Babensee, J., Anderson, J., McIntire, L. and Mikos, A. (1998), 'Host response to tissue engineered devices', *Advanced Drug Delivery Reviews* **33**(1-2), 111–139.

Björninen, M., Siljander, A., Pelto, J., Hyttinen, J., Kellomäki, M., Miettinen, S., Seppänen, R. and Haimi, S. (2014), 'Comparison of Chondroitin Sulfate and Hyaluronic Acid Doped Conductive Polypyrrole Films for Adipose Stem Cells', *Annals of Biomedical Engineering* **42**(9), 1889–1900.

Di Felice, V., Serradifalco, C., Rizzuto, L., De Luca, A., Rappa, F., Barone, R., Di Marco, P., Cassata, G., Puleio, R., Verin, L., Motta, A., Migliaresi, C., Guercio, A. and Zummo,

G. (2015), 'Silk fibroin scaffolds enhance cell commitment of adult rat cardiac progenitor cells', *Journal of Tissue Engineering and Regenerative Medicine* **9**(11), E51–E64.

Donderwinkel, I., van Hest, J. C. M. and Cameron, N. R. (2017), 'Bio-inks for 3D bioprinting: recent advances and future prospects', *Polymer Chemistry* **8**(31), 4451–4471.

Elieh-Ali-Komi, D. and Hamblin, M. R. (2016), 'Chitin and chitosan: Production and application of versatile biomedical nanomaterials.', *Int J Adv Res (Indore)* **4**(3), 411–427.

Fonner, J. M., Forciniti, L., Nguyen, H., Byrne, J. D., Kou, Y.-F., Syeda-Nawaz, J. and Schmidt, C. E. (2008), 'Biocompatibility implications of polypyrrole synthesis techniques', *Biomedical Materials* **3**(3), 034124–13.

Gudapati, H., Dey, M. and Ozbolat, I. (2016), 'A comprehensive review on droplet-based bioprinting: Past, present and future', *Biomaterials* **102**, 20–42.

Hur, J., Im, K., Kim, S. W., Kim, J., Chung, D.-Y., Kim, T.-H., Jo, K. H., Hahn, J. H., Bao, Z., Hwang, S. and Park, N. (2014), 'Polypyrrole/Agarose-Based Electronically Conductive and Reversibly Restorable Hydrogel', *ACS Nano* **8**(10), 10066–10076.

Ismail, Y. A., Martínez, J. G., Harrasi, A. S. A., Kim, S. J. and Otero, T. F. (2011), 'Sensing characteristics of a conducting polymer/hydrogel hybrid microfiber artificial muscle', *Sensors and Actuators B: Chemical* **160**(1), 1180 – 1190.

Jia, L., Prabhakaran, M., Qin, X. and Ramakrishna, S. (2013), 'Stem cell differentiation on electrospun nanofibrous substrates for vascular tissue engineering', *Materials Science and Engineering C* **33**(8), 4640–4650.

Kim, J., Kim, S. and Jung, Y. (2016), 'Current status of three-dimensional printing

inks for soft tissue regeneration', *Tissue Engineering and Regenerative Medicine* **13**(6), 636–646.

Kunzmann, A., Andersson, B., Thurnherr, T., Krug, H., Scheynius, A. and Fadeel, B. (2011), 'Toxicology of engineered nanomaterials: Focus on biocompatibility, biodistribution and biodegradation', *Biochimica et Biophysica Acta - General Subjects* **1810**(3), 361–373.

Lee, J., Kim, D. and Kim, C. (1995), 'Synthesis of soluble polypyrrole of the doped state in organic solvents', *Synthetic Metals* **74**(2), 103–106.

Mattioli-Belmonte, M., Giavaresi, G., Biagini, G., Virgili, L., Giacomini, M., Fini, M., Giantomassi, F., Natali, D., Torricelli, P. and Giardino, R. (2003), 'Tailoring biomaterial compatibility: In vivo tissue response versus in vitro cell behavior', *International Journal of Artificial Organs* **26**(12), 1077–1085.

Park, S., Kang, Y. J. and Majd, S. (2015), 'A Review of Patterned Organic Bioelectronic Materials and their Biomedical Applications', *Advanced Materials* **27**(46), 7583–7619.

Ramanaviciene, A., Kausaite, A., Tautkus, S. and Ramanavicius, A. (2010), 'Biocompatibility of polypyrrole particles: an in-vivo study in mice', *Journal of Pharmacy and Pharmacology* **59**(2), 311–315.

Romero, I. S., Bradshaw, N. P., Larson, J. D., Severt, S. Y., Roberts, S. J., Schiller, M. L., Leger, J. M. and Murphy, A. R. (2014), 'Biocompatible Electromechanical Actuators Composed of Silk-Conducting Polymer Composites', *Advanced Functional Materials* **24**(25), 3866–3873.

Shi, Z., Gao, H., Feng, J., Ding, B., Cao, X., Kuga, S., Wang, Y., Zhang, L. and Cai, J. (2014), 'In situ synthesis of robust conductive cellulose/polypyrrole composite aerogels and their potential application in nerve regeneration', *Angewandte Chemie - International Edition* **53**(21), 5380–5384.

Tandon, B., Magaz, A., Balint, R., Blaker, J. and Cartmell, S. (2018), 'Electroactive biomaterials: Vehicles for controlled delivery of therapeutic agents for drug delivery and tissue regeneration', *Advanced Drug Delivery Reviews* **129**, 148–168.

Wang, X., Gu, X., Yuan, C. et al. (2004), 'Evaluation of biocompatibility of polypyrrole in vitro and in vivo', *Journal of Biomedical Materials Research - Part A* **68**(3), 411–422.

Wang, X., Jiang, M., Zhou, Z., Gou, J. and Hui, D. (2017), '3d printing of polymer matrix composites: A review and prospective', *Composites Part B: Engineering* **110**, 442–458.

Yang, X., Lu, Z., Wu, H., Li, W., Zheng, L. and Zhao, J. (2018), 'Collagen-alginate as bioink for three-dimensional (3d) cell printing based cartilage tissue engineering', *Materials Science and Engineering C* **83**, 195–201.

Yen, W., Baosong, L., Changkui, F. and Hongxu, Q. (2010), 'Electroactive conducting polymers for biomedical applications', *Acta Polymerica Sinica* **12**, 1399–1405.

Appendices

Appendix A

Expanded Results from Chapter 4

A.1 Stoichiometry of the oxidant and dopant

Stoichiometry of the oxidizing agent, i.e. ferric (III) chloride ($FeCl_3$), was acquired from seminal work done by (Armes, 1987). They reported that the optimum reaction conditions for the polymerization of Py by $FeCl_3$ in aqueous solutions is 2.38 ± 0.04, at pH$>$1.5. Conjugating polymers only consume current when undergoing structural change, and due to poor electrical to mechanical energy conversion they have very low actuating speed and efficiency (Smela (2003)). However, the incorporation of dopants is known to modulate topographical, electrical and mechanical properties. DBSA was chosen for as the dopant because the PPy-DBSA actuation mechanism has been well-reported in literature to be representative of oxidation (p-doping) with exchange of cations (Carpi, 2016; Wang and Smela, 2008; George et al., 2005). In addition to being shown to be cyto-compatible, the actuation strain of PPy-DBS films of $150 - -300$ nm thickness and bilayers was shown to reach 2–10% (Yan et al. (2017); Kivilo et al. (2016); Smela and Gadegaard (2001); Wang et al. (2004)). This matches well with the strain collagen fibers can handle (Dong and Lv (2016)). Others have reported that although higher concentrations of DBSA increased surface roughness, thermal stability and PPy solubility in inorganic solvents (such as m-cresol), it also been shown to decrease the electrical conductivity of PPy-DBSA constructs (Jayamurgan et al., 2013; Fahlgren et al., 2015). Therefore, dopant concentration was chosen in accord with well-established works reported by Bjorklund (1987).

A.2 Additional collagen and PPy-based structures

(a) bulk aerogel

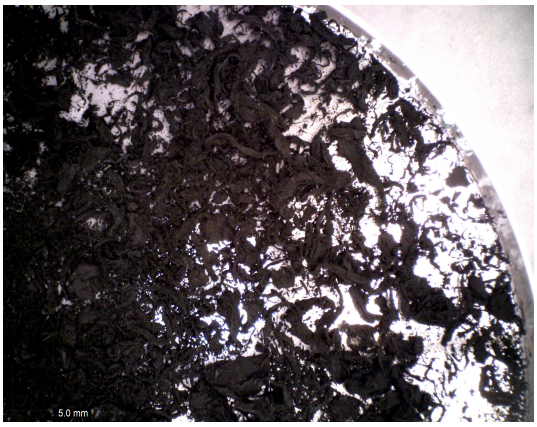

(b) fibrous aerogel

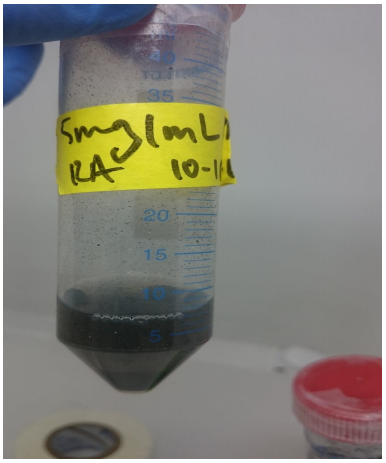

(c) powder aggregates at 5 mg · mL^{-1}

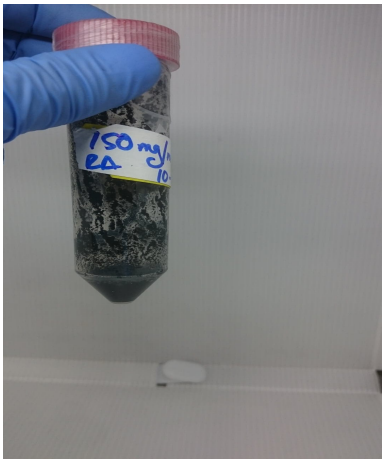

(d) powder aggregates at 150 mg · mL^{-1}

Figure A.1: Optical imaging was performed on structures evaluated for DIW AM feasibility (as outlined in section 3.2.1) produced using traditional chemical oxidative polymerization fabrication methods, including (a) Col-PPy 1:1 wt% Bulk aerogels of 6 mm diameter, (b) Col-PPy 1:1 wt% fibrous aerogels of indeterminate size, and Col-PPy 1:1 wt% powder aggregates dispersed using ultra-sonication at (c) 5 mg · mL^{-1} and (d) 150 mg · mL^{-1}. Said structures demonstrated incompatibility of traditional fabrication methods with DIW AM.

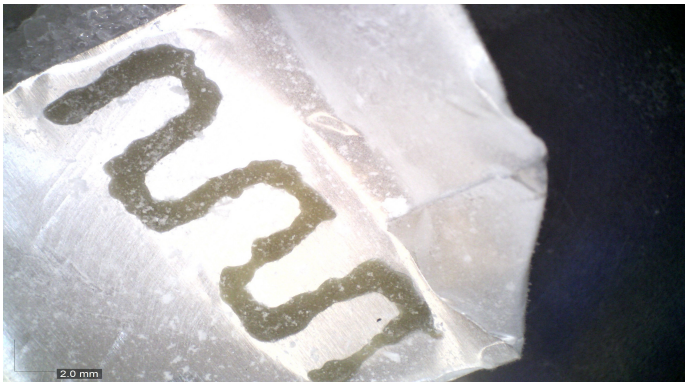

(a) 3.5 mm · s^{-1} at 15 psi

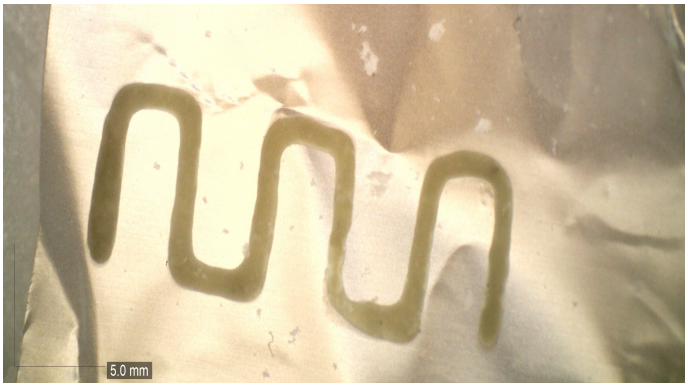

(b) 5.0 mm · s^{-1} at 15 psi

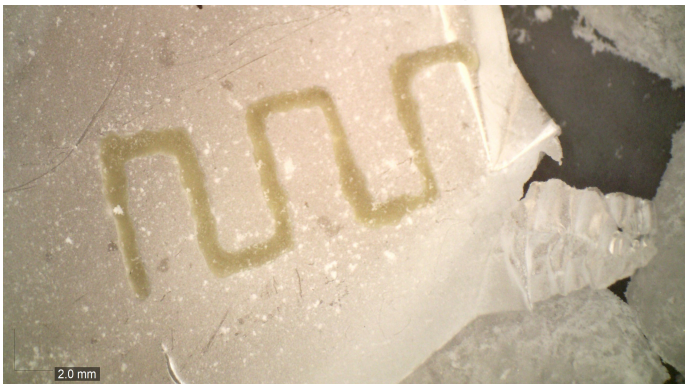

(c) 7.5 mm · s^{-1} at 15 psi

Figure A.2: Examples of S-shaped structures DIW printed relating to Figure 4.2 for verification of rheological modelling and optimization of extrusion parameters are shown using optical imaging.

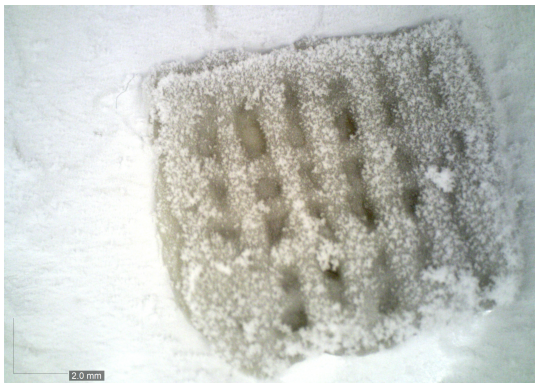

(a) overview of 2-layered grid structure

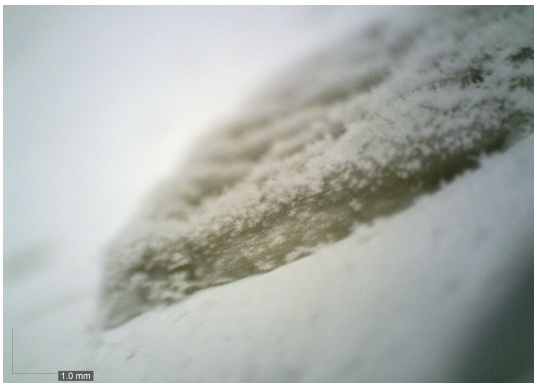

(b) side-view of 2-layered grid structure

(b) 2-layered grid post-polymerization

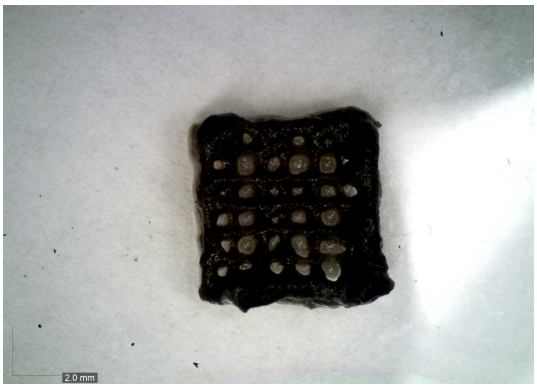

(c) 4-layered grid post-polymerization

Figure A.3: The consequences of delayed curing of the Col-Py DIW ink is demonstrated via a comparison of Col-PPy 1:4 wt% (50% infill) 2-layered grid structure (50% infill) at (a, b) pre-polymerization, and (c) post-polymerization, with (d) a Col-PPy 1:4 wt% (50% infill) 4-layered grid post-polymerization using optical imaging.

(a) **(b)** **(c)**

Figure A.4: The degree of polymerization, i.e. in terms of collagen and PPy integration, in the DIW printed Col-PPy 1:4 wt% 4-layered structure (50% infill) evaluated using optical imaging reveals no layering artifacts nor the presence of un-polymerized areas at the cross-sectional level.

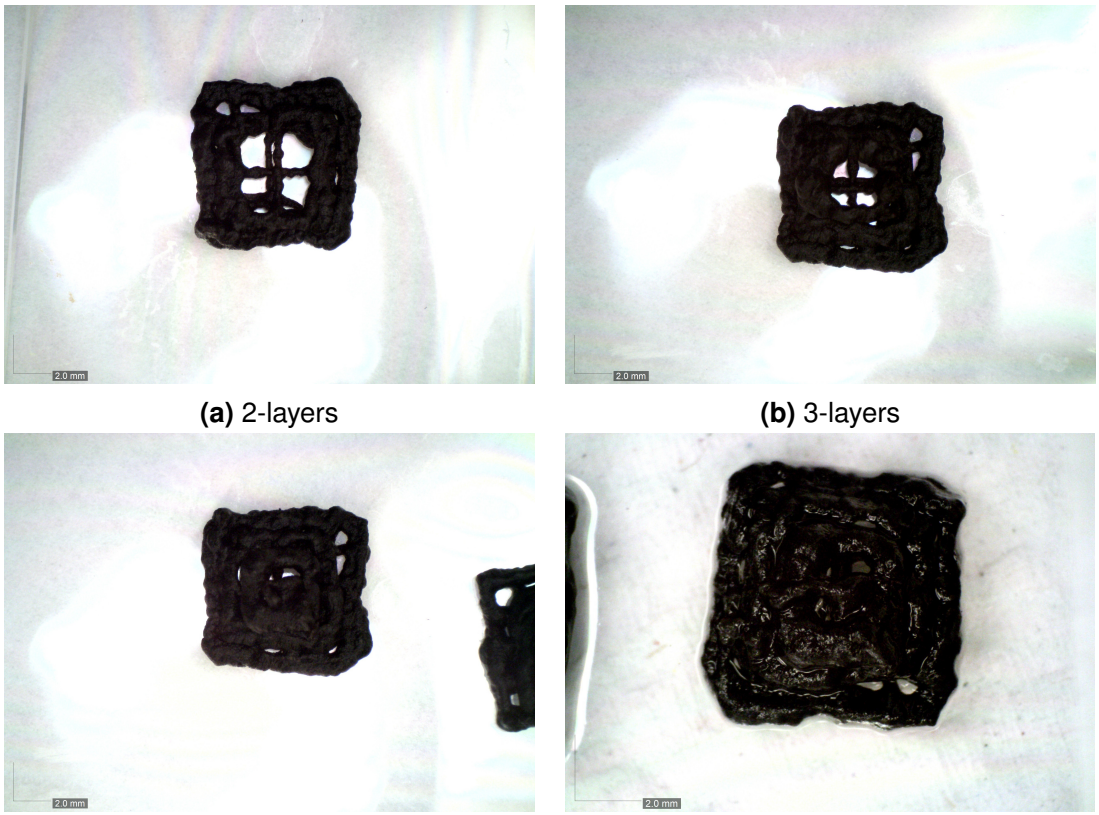

(a) 2-layers **(b)** 3-layers

(c) 4-layers **(d)** 5-layers

Figure A.5: Optical imaging was performed on a Col-PPy 1:4 wt% 5-layered pyramid structures (20% infill, 20% reduction of area per additional layer) to evaluate feasibility of DIW printing structures with overhang and bridges.

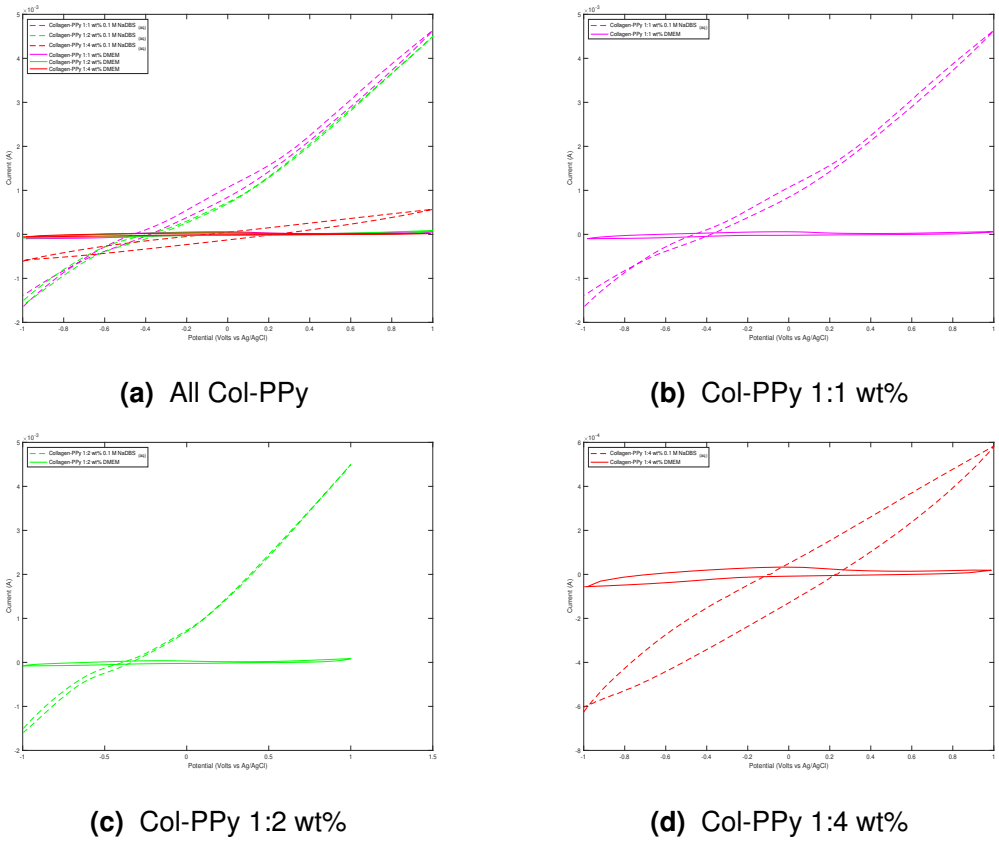

(a) All Col-PPy

(b) Col-PPy 1:1 wt%

(c) Col-PPy 1:2 wt%

(d) Col-PPy 1:4 wt%

Figure A.6: CV comparisons performed in DMEM and 0.1 M NaDBS$_{aq}$ solutions reveal the effect of dopant inclusion in the working solution on sample electro-activity, where Col-PPy 1:1 wt% observe greatest capacitance.

A.3 Expanded results on Cyclic voltammetry

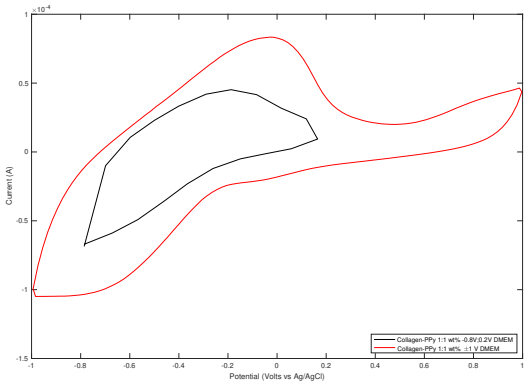

(a)

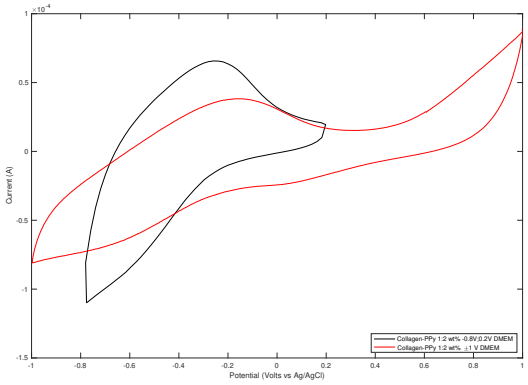

(b)

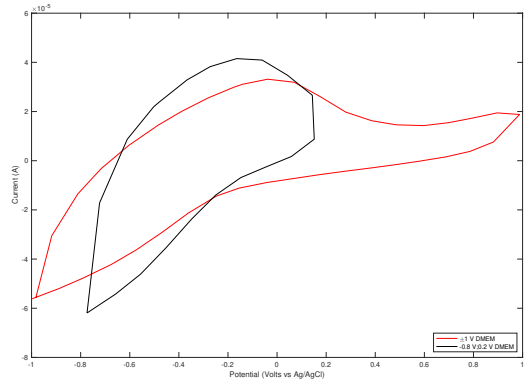

(c)

Figure A.7: CV comparisons between $\pm$ 1 V and -0.8 V; 0.2 V in DMEM for (a) Col-PPy 1:1 wt%, (b) Col-PPy 1:2 wt%, (c) Col-PPy 1:4 wt% reveal electro-activity can be controlled acutely by potential parameters.

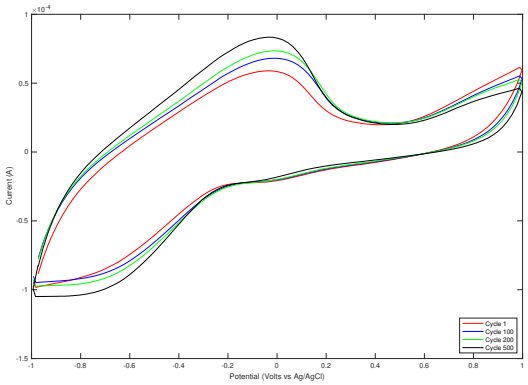

(a)

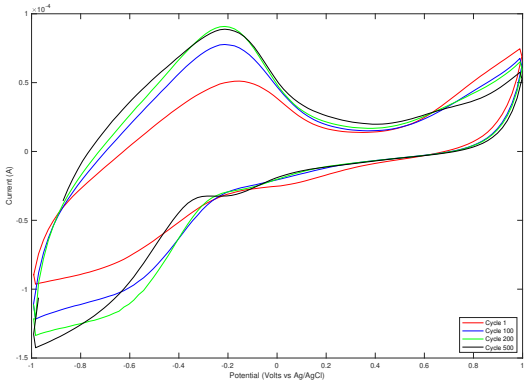

(b)

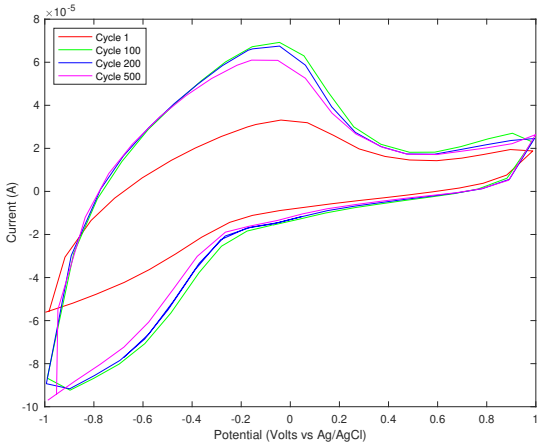

(c)

Figure A.8: 500 cycles of CV were run on (a) Col-PPy 1:1 wt%, (b) Col-PPy 1:2 wt%, (c) Col-PPy 1:4 wt% in DMEM at 100 mV/s for $\pm$ 1 V.

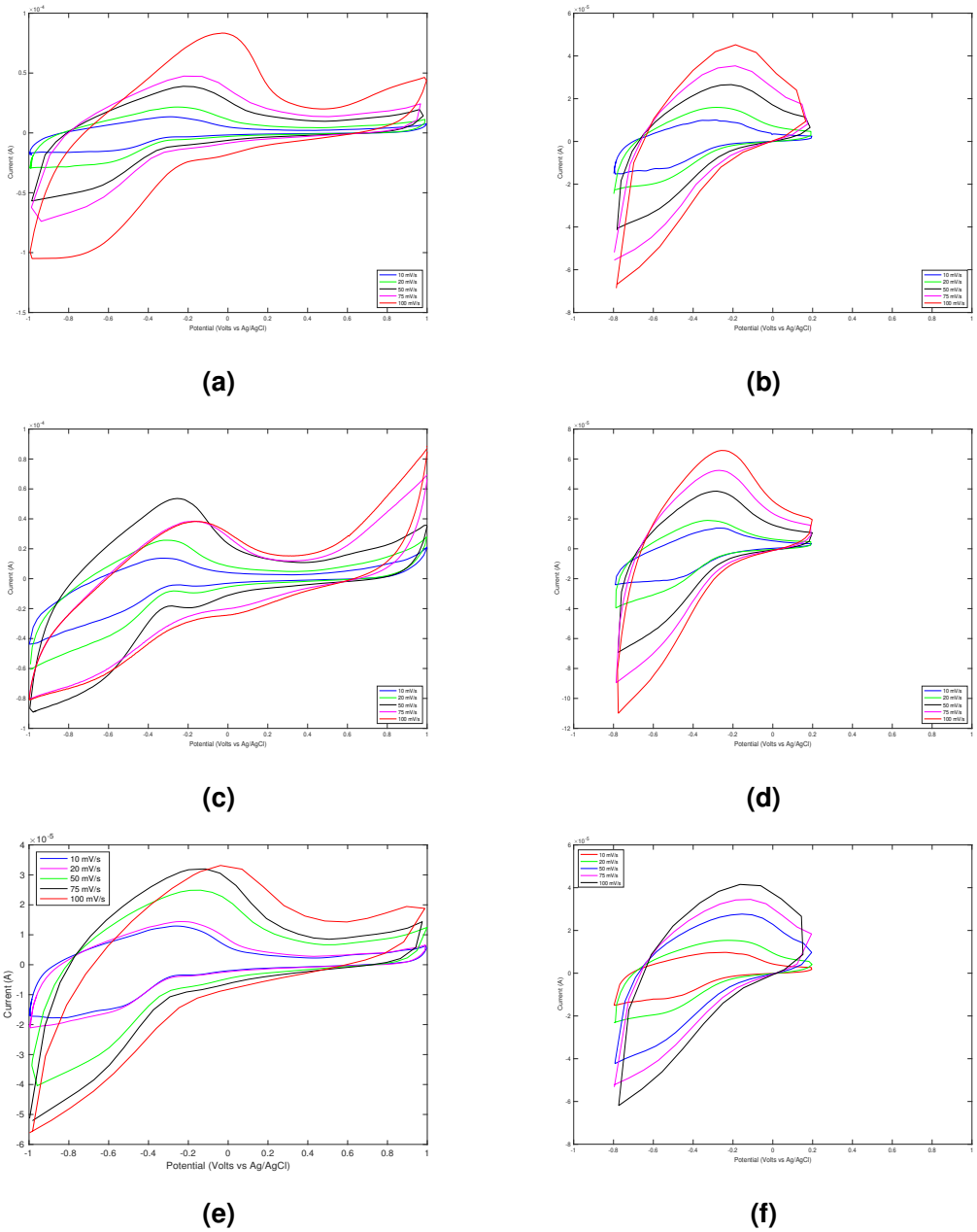

Figure A.9: CV comparisons between Col-PPy samples in DMEM run at (a, c, e) $\pm$ 1 V and (b, d, f) -0.8 V; 0.2 V potentials at different scan rates reveals highest capacitance is observed by (a, b) Col-PPy 1:1 wt% samples as scan rate increases.

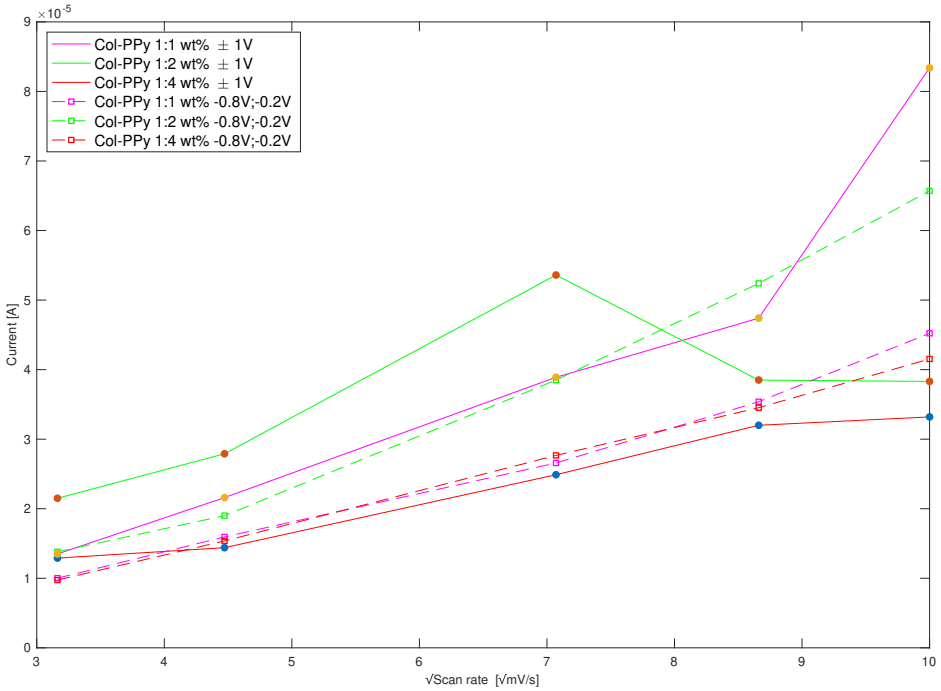

Figure A.10: Peak anodic potentials for each of the Col-PPy compositions for $\pm$ 1 V and -0.8 V; 0.2 V reveals potential parameters influence the activation of electro-active sites contributing to bulk capacitance during electrochemical switching.

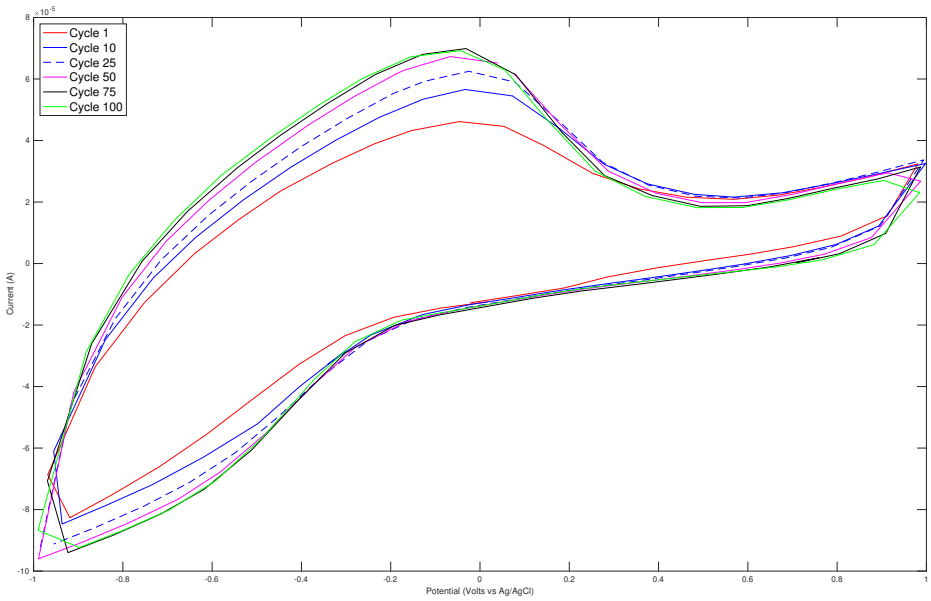

Figure A.11: CV performed on 1.5 cm^2 samples of Col-PPy 1:4 wt% in DMEM at 100 mV/s was observed to stabilize within 75 cycles of evaluation and to maintain electro-activity for up to 500 cycles of testing (Figure 4.10).

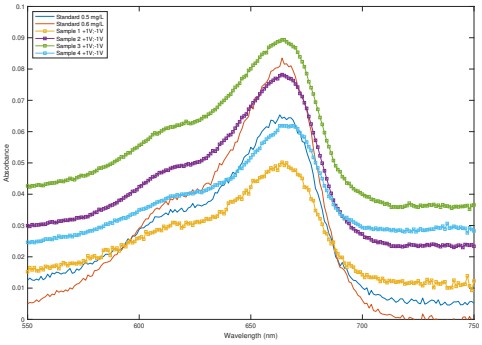

(a) Absorbance for +1 V, −1 V

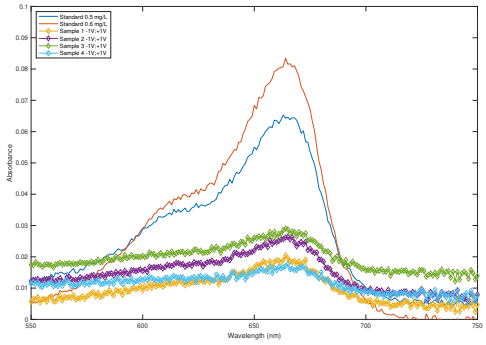

(b) Absorbance for −1 V, +1 V

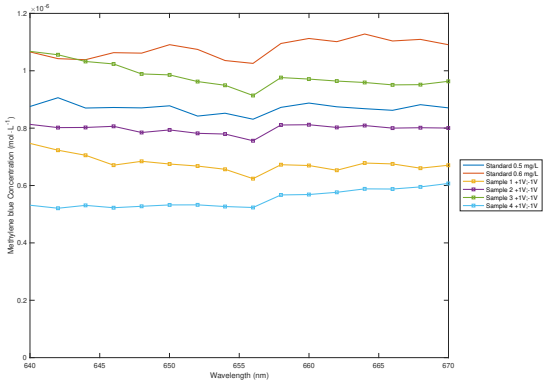

(c) Concentrations for +1 V, −1 V

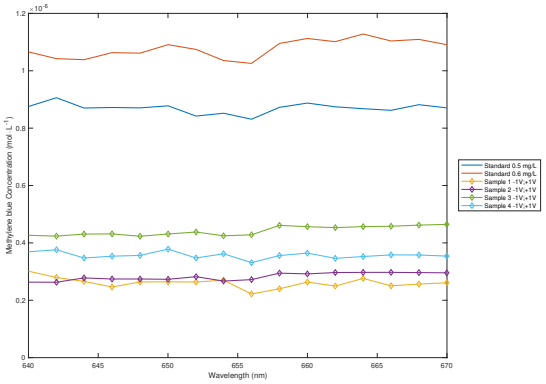

(d) Concentrations for −1 V, +1 V

Figure A.12: Individual samples forming (a, b) absorbance results and (c, d) concentration calculations of Col-PPy 1:4 wt% sample MB dye adsorption and release in response to electrical stimulations for noted potential parameters are reported.

A.4 Expanded results on Spectrometry analysis

List of references

Armes, S. (1987), 'Optimum reaction conditions for the polymerization of pyrrole by iron(iii) chloride in aqueous solution', *Synthetic Metals* **20**(3), 365–371.

Bjorklund, R. B. (1987), 'Kinetics of pyrrole polymerisation in aqueous iron chloride solution', *Journal of the Chemical Society, Faraday Transactions 1: Physical Chemistry in Condensed Phases* **83**(5), 1507–1514.

Carpi, F., ed. (2016), *Electromechanically active polymers*, Springer.

Dong, C. and Lv, Y. (2016), 'Application of collagen scaffold in tissue engineering: Recent advances and new perspectives', *Polymers* **8**(2), 42–20.

Fahlgren, A., Bratengeier, C., Gelmi, A., Semeins, C. M., Klein-Nulend, J., Jager, E. W. H. and Bakker, A. D. (2015), 'Biocompatibility of polypyrrole with human primary osteoblasts and the effect of dopants', *PLoS ONE* **10**(7), e0134023–17.

George, P., Lyckman, A., Lavan, D., Hegde, A., Leung, Y., Avasare, R., Testa, C., Alexander, P., Langer, R. and Sur, M. (2005), 'Fabrication and biocompatibility of polypyrrole implants suitable for neural prosthetics', *Biomaterials* **26**(17), 3511–3519.

Jayamurgan, P., Ponnuswamy, V., Ashokan, S. and Mahalingam, T. (2013), 'The effect of dopant on structural, thermal and morphological properties of DBSA-doped polypyrrole', *Iranian Polymer Journal* **22**(3), 219–225.

Kivilo, A., Zondaka, Z., Kesküla, A., Rasti, P., Tamm, T. and Kiefer, R. (2016), 'Electrochemo-mechanical deformation properties of polypyrrole/dodecylbenzenesulfate linear actuators in aqueous and organic electrolyte', *RSC Advances* **6**(99), 96484–96489.

Smela, E. (2003), 'Conjugated polymer actuators for biomedical applications', *Advanced Materials* **15**(6), 481–494.

Smela, E. and Gadegaard, N. (2001), 'Volume change in polypyrrole studied by atomic force microscopy', *The Journal of Physical Chemistry B* **105**(39), 9395–9405.

Wang, X., Shapiro, B. and Smela, E. (2004), 'Visualizing ion currents in conjugated polymers', *Advanced Materials* **16**(18), 1605–1609.

Wang, X. and Smela, E. (2008), 'Experimental studies of ion transport in PPy(DBS)', *The Journal of Physical Chemistry C* **113**(1), 369–381.

Yan, B., Wu, Y. and Guo, L. (2017), 'Recent advances on polypyrrole electroactuators', *Polymers* **9**(12), 446–20.

Appendix B

Expanded Results from Chapter 5

B.1 Expanded results on grid actuation

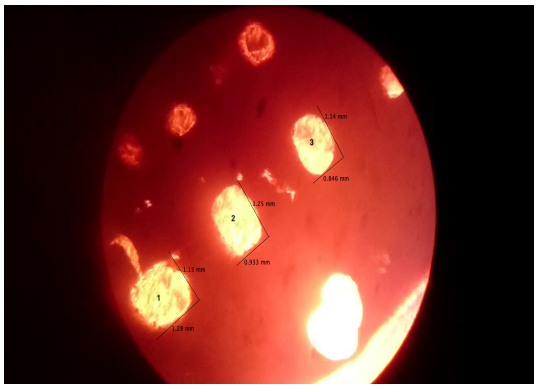

(a) Figure 5.1

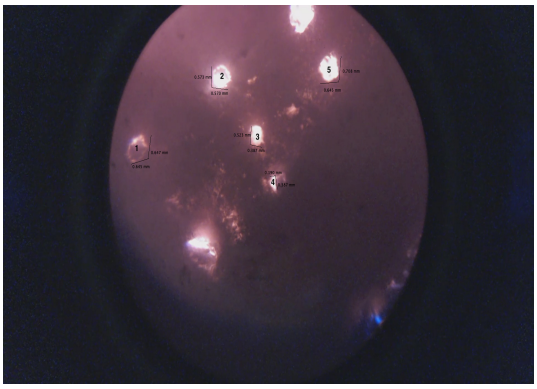

(b) Figure 5.2 (a)

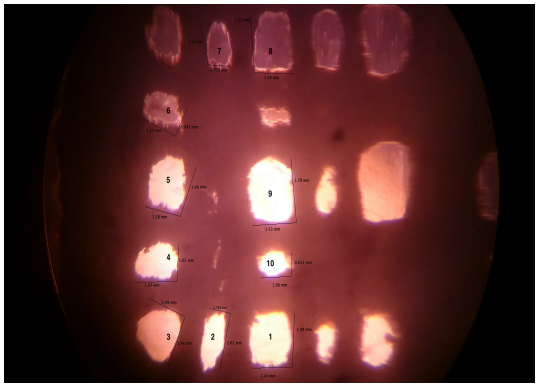

(c) Figure 5.2 (b)

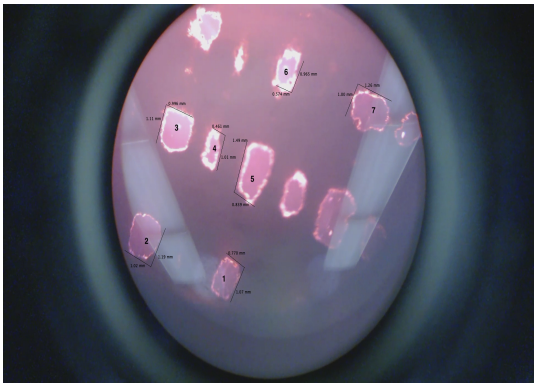

(d) Figure 5.2 (c)

Figure B.1: Annotations of Col-PPy 1:4 wt% grid sample pores corresponding to % area change evaluations conducted in section 5.1.1 are shown for (a) Figure 5.1 and (b, c, d) Figure 5.2.

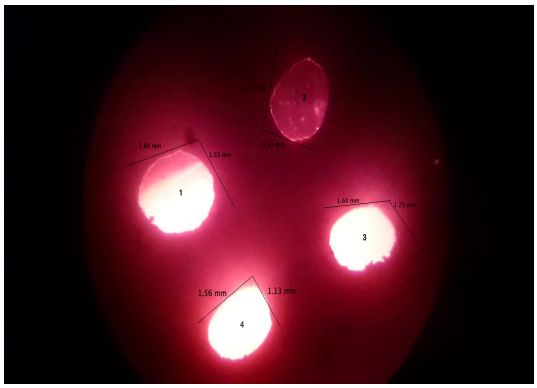

(a) Figure 5.3

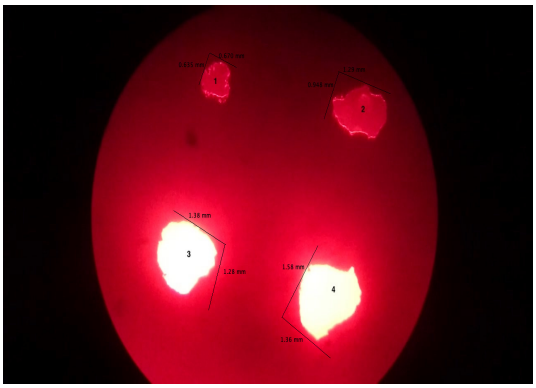

(b) Figure 5.5

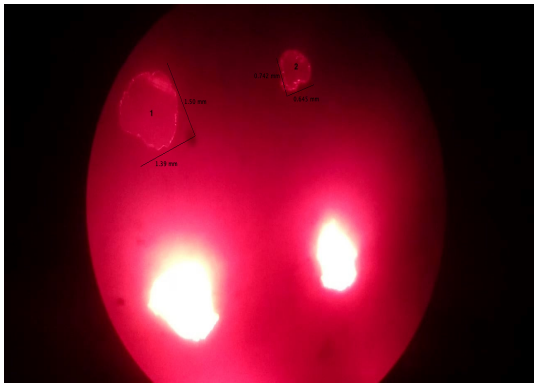

(c) Figure 5.6 (a)

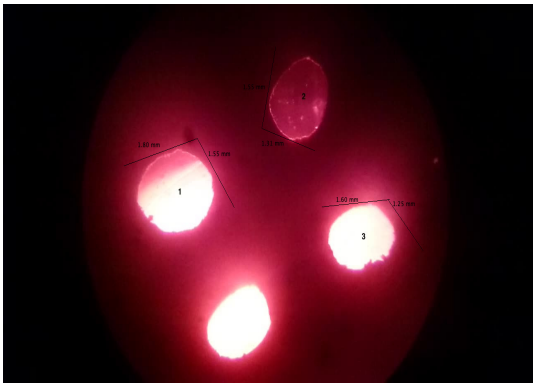

(d) Figure 5.6 (b)

Figure B.2: Annotations of Col-PPy 1:4 wt% grid sample pores corresponding to % area change evaluations, as indicated, conducted under varying potential parameters are reported.

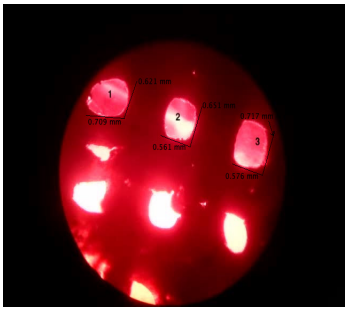

(a) Figure 5.7

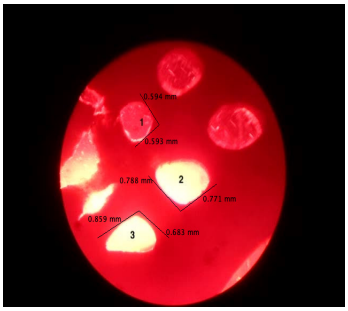

(b) Figure 5.8 (a)

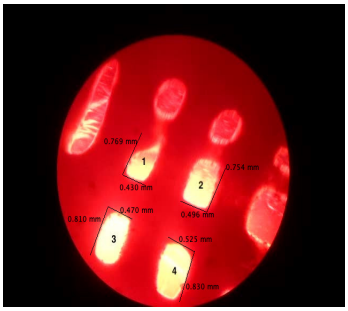

(c) Figure 5.8 (b)

Figure B.3: Annotations of Col-PPy 1:2 wt% grid sample pores corresponding to % area change evaluations, as indicated, conducted under varying potential parameters are reported.

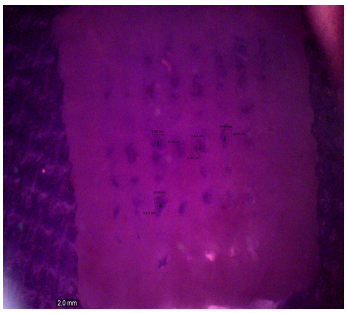

(a) Figure 5.9

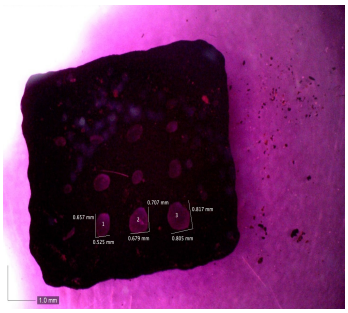

(b) Figure 5.4 (a)

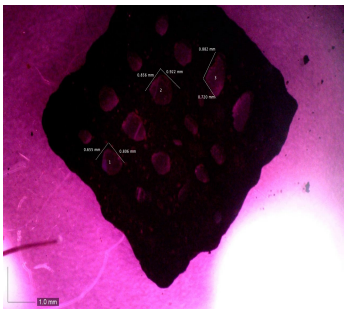

(c) Figure 5.4 (b)

Figure B.4: Annotations of (a) collagen standalone grid samples and (b, c) Col-PPy 1:4 wt% grid sample pores corresponding to % area change evaluations, as referenced, conducted under varying potential parameters are reported.

Table B.1: Bilayer actuation performance results for Col-PPy 1:4 wt% and PDMS bilayers in DMEM media are reported. These bilayers experienced square waves of varied potentials at 0.00833 Hz.* denotes the samples which did not follow the orientation showed in Figure 3.9.

Sample	**Potential parameters**	**Initial angle**	**Final angle**	**Initial length (mm)**	**Final length (mm)**	**Δ Length (mm)**	**Δ angle**
1*	Square $\pm$ 1 V	57°	53°	12.26	12.28	0.02	4°
2*	Square $\pm$ 1 V	99°	102°	2.84	12.89	0.05	3°
3	Square $\pm$ 1 V	115°	126°	30.58	31.59	1.01	11°
5*	Square $\pm$ 2 V	65°	62°	12.8	12.7	0.1	3°
6*	Square +1 V, -2 V	112°	118°	25.92	25.76	0.16	6°
7	Square +1 V, -2 V	100°	106°	8.9	8.4	0.5	6°
8*	Square +0.2 V, -0.8 V	87°	74°	7.14	7.14	0	13°
10	Square $\pm$ 1 V	69°	67°	6.18	6.3	0.12	2°
12	Square $\pm$ 1 V	90°	53°	3.74	3.53	0.21	37°

B.2 Expanded results on bilayer actuation

Table B.2: Bilayer actuation performance results for select Col-PPy 1:4 wt% and PDMS bilayers in 0.1 M $NaDBS_{(aq)}$ solution are reported. These bilayers experienced square waves of varied potentials at 0.00833 Hz.* denotes the samples which did not follow the orientation showed in Figure 3.9.

Sample number	**Potential parameters**	**Initial angle**	**Final angle**	**Initial length (mm)**	**Final length (mm)**	**Δ Length (mm)**	**Δ angle**
1*	Square $\pm$ 1 V	107°	110°	14.27	14.13	0.14	3°
2	Square +2 V, -1 V	133°	115°	33.24	32.1	1.14	18°
3	Square $\pm$ 2 V	115°	102°	29.97	29.8	0.17	13°
4	Square $\pm$ 1 V	43°	23°	3.85	4.41	0.56	20°
5	Square +2 V, 0 V	84°	64°	8.86	9.17	0.31	20°

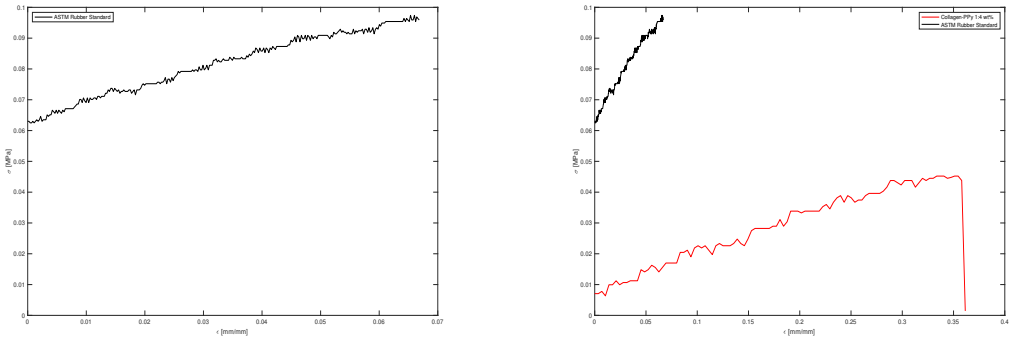

(a) Silicone Rubber **(b)** Silicone Rubber versus Col-PPy 1:4 wt%

Figure B.5: Tensile stretch with CellScale Univert tester on a SHORE 10A silicone rubber (McMaster-Carr, catalog# 9010K13) revealed instrument artifacts contributing to tensile data measurements.

B.3 Expanded results on tensile testing

Table B.3: Caliper measurements and regression details corresponding to tensile testing performed on (a-c) samples with increasing PPy concentration, (d) unsubmerged samples, (e-f) samples under electrical stimulation are reported. These evaluations pertain to the samples shown in Figure 5.5.

Sample	X-Area (mm^2)	L_o (mm)	Regression equation	r^2 value	*E* (KPa)	Max Strain	UTS (KPa)	Fracture Stress (KPa)	Yield Strength (KPa)
(a) 1:1 wt %	5.02	23.3	y = 0.1145x - 0.0002	0.9624	114.5	296.6	21.7	32.9	32.9
(b) 1:2 wt %	5.10	19.1	y = 0.1151x + 0.0049	0.9555	115.1	359.1	37.5	41.8	37.5
(c) 1:4 wt %	6.94	28.8	y = 0.120x + 0.008	0.9857	120.0	360.0	43.8	45.2	43.8
(d) 1:4 wt % Unsubmerged	3.18	16.4	y = 0.2039x + 0.0027	0.9384	203.9	200.7	35.5	42.4	40.8
(e) 1:4 wt % Oxidized	5.90	16.6	y = 0.0785x + 0.0071	0.9623	78.5	320.0	31.6	32.4	31.6
(f) 1:4 wt % Reduced	9.01	16.8	y = 0.0791x + 0.032	0.8769	79.1	291.2	50.0	53.2	48.4

Appendix C

Copyright Permissions

The following pages provide confirmation of acquired copyright permissions for the appropriate referenced figures in this thesis. Included is a table summarizing the copyright information, followed by excerpts of the relevant emails. The table presents the figure permissions as they appear in the thesis. The excerpts are provided as figures. They are cropped to remove any personal information and only outline the copyright permission. Note that copyright permission from The Royal Society of Chemistry publications is provided based on the conditions outlined in the relevant statement below.

Many thanks for sending the permissions request below. The Royal Society of Chemistry hereby grants permission for the use of the material specified below in your thesis.

Please note that if the material specified below or any part of it appears with credit or acknowledgement to a third party then you must also secure permission from that third party before reproducing that material.

Please ensure that the published article carries a credit to The Royal Society of Chemistry in the following format:

[Original citation] – Reproduced by permission of The Royal Society of Chemistry

and that any electronic version of the work includes a hyperlink to the article on the Royal Society of Chemistry website.

Figure C.1: Copyright permission statement from The Royal Society of Chemistry publications.

Table C.1: Summary of Copyright Permission Information.

Figure #	Reference Title	Page #	Reference Figure #	1st Author	Publication	Publisher	License Confirmation #
2.1 (a)	3D-printing methods based on photopolymerization	33	Figure 3 (a)	A. Ambrosi	2015 Chemical Society Review	Royal Society of Chemistry	RSC Statement
2.1 (b)	Schematic diagram of laminated object manufacturing (LOM)	33	Figure 6	A. Ambrosi	2015 Chemical Society Review	Royal Society of Chemistry	RSC Statement
2.1 (c)	Schematic diagram of binder jetting 3D-printing	33	Figure 5 (b)	A. Ambrosi	2015 Chemical Society Review	Royal Society of Chemistry	RSC Statement
2.2 (a,b)	Schematic diagram of fused deposition modeling (FDM)	33	Figure 4 (a,b)	A. Ambrosi	2015 Chemical Society Review	Royal Society of Chemistry	RSC Statement
2.3	Schematic of a normal cell and its mechanical interaction with extant extracellular matrix (ECM) that is stressed or strained due to native applied forces (top row, centre)	43	Figure 3	J.D. Humphrey	2014 Molecular Cell Biology	Nature Reviews	4461490307459
2.4	Chart diagramming natural (red) and synthetic (blue) polymer distributions for use as bioinks compiled from relevant literature	50	Figure 13.2	J.K. Carrow	2015 Polymers for bioprinting	Elsevier	4506450572163
2.5	A more detailed look at PPy formation	59	Figure 2.1	G.G. Wallace	2002 Conductive Electroactive polymers	CRC Press LLC	11763538
2.6	Oxidation/Reduction of the polymer	61	Equation 2.2	G.G. Wallace	2002 Conductive Electroactive polymers	CRC Press LLC	11763538
2.7	Volume variations during redox reactions	62	Figure 1	T.F. Otero	2016 Electromechanically Active Polymers	Springer International Publishing	11762270

Your confirmation email will contain your order number for future reference.

printable details

License Number	4506450572163
License date	Jan 12, 2019
Licensed Content Publisher	Elsevier
Licensed Content Publication	Elsevier Books
Licensed Content Title	Essentials of 3D Biofabrication and Translation
Licensed Content Author	James K. Carrow,Punyavee Kerativitayanan,Manish K. Jaiswal,Giriraj Lokhande,Akhilesh K. Gaharwar
Licensed Content Date	Jan 1, 2015
Licensed Content Pages	20
Type of Use	reuse in a thesis/dissertation
Portion	figures/tables/illustrations
Number of figures/tables/illustrations	1
Format	both print and electronic
Are you the author of this Elsevier chapter?	No
Will you be translating?	No
Original figure numbers	Chapter 13 of Polymers for Bioprinting (Academic Press), FIGURE 13.2 Chart diagramming natural (red) and synthetic (blue) polymer distributions for use as bioinks compiled from relevant literature. Hybrid systems split into polymer constituents for consid
Title of your thesis/dissertation	BME graduate student
Publisher of new work	University of western ontario
Expected completion date	Dec 2018
Estimated size (number of pages)	1
Requestor Location	university of western ontario 1511 richmond street london, ON N6A 3K7\ Canada

Figure C.2: Copyright permission information for license number 4506450572163.

License Number	4461490307459
License date	Nov 03, 2018
Licensed Content Publisher	Springer Nature
Licensed Content Publication	Nature Reviews Molecular Cell Biology
Licensed Content Title	Mechanotransduction and extracellular matrix homeostasis
Licensed Content Author	Jay D. Humphrey, Eric R. Dufresne, Martin A. Schwartz
Licensed Content Date	Oct 22, 2014
Licensed Content Volume	15
Licensed Content Issue	12
Type of Use	Thesis/Dissertation
Requestor type	academic/university or research institute
Format	print and electronic
Portion	figures/tables/illustrations
Number of figures/tables/illustrations	1
High-res required	no
Will you be translating?	no
Circulation/distribution	<501
Author of this Springer Nature content	no
Title	BME graduate student
Institution name	University of western ontario
Expected presentation date	Dec 2018
Portions	Figure 3

Figure C.3: Copyright permission information for license number 4461490307459.

Electromechanically Active Polymers : A Concise Reference

Billing Status: **N/A**

Order detail ID:	71646929
ISBN:	9783319315294
Publication Type:	Other
Volume:	
Issue:	
Start page:	
Publisher:	Springer International Publishing

Permission Status: Granted

Permission type: Republish or display content
Type of use: Thesis/Dissertation
Order License Id: 4462131007825

Hide details

Requestor type	Academic institution
Format	Print, Electronic
Portion	chart/graph/table/figure
Number of charts/graphs/tables/figures	1
The requesting person/organization	rooshan arshad
Title or numeric reference of the portion(s)	Chapter 11, figure 1
Title of the article or chapter the portion is from	Conducting Polymers as EAPs: Fundamentals and Materials
Editor of portion(s)	NA
Author of portion(s)	Toribio F. Otero and José G. Martínez
Volume of serial or monograph	NA
Page range of portion	239
Publication date of portion	2016
Rights for	Main product
Duration of use	Current edition and up to 5 years
Creation of copies for the disabled	no
With minor editing privileges	no
For distribution to	Worldwide
In the following language(s)	Original language of publication
With incidental promotional use	no
Lifetime unit quantity of new product	Up to 499

Figure C.4: Copyright permission information for confirmation number 11762270.

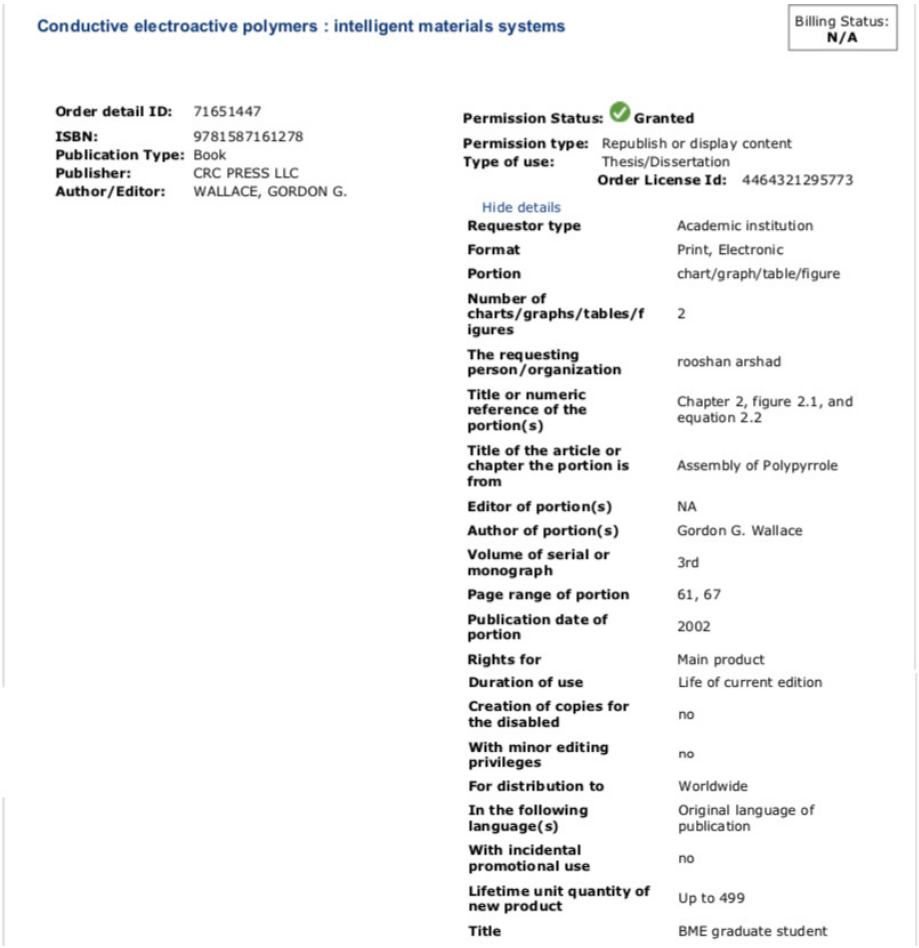

Conductive electroactive polymers : intelligent materials systems

Billing Status: N/A

Order detail ID: 71651447
ISBN: 9781587161278
Publication Type: Book
Publisher: CRC PRESS LLC
Author/Editor: WALLACE, GORDON G.

Permission Status: Granted
Permission type: Republish or display content
Type of use: Thesis/Dissertation
Order License Id: 4464321295773

Hide details

Requestor type	Academic institution
Format	Print, Electronic
Portion	chart/graph/table/figure
Number of charts/graphs/tables/figures	2
The requesting person/organization	rooshan arshad
Title or numeric reference of the portion(s)	Chapter 2, figure 2.1, and equation 2.2
Title of the article or chapter the portion is from	Assembly of Polypyrrole
Editor of portion(s)	NA
Author of portion(s)	Gordon G. Wallace
Volume of serial or monograph	3rd
Page range of portion	61, 67
Publication date of portion	2002
Rights for	Main product
Duration of use	Life of current edition
Creation of copies for the disabled	no
With minor editing privileges	no
For distribution to	Worldwide
In the following language(s)	Original language of publication
With incidental promotional use	no
Lifetime unit quantity of new product	Up to 499
Title	BME graduate student

Figure C.5: Copyright permission information for confirmation number 11763538.

Curriculum Vitæ

Name:	Rooshan Arshad
Post-Secondary Education and Degrees:	University of Windsor Ontario Windsor, Ontario, Canada 2012 – 2014 B.Sc. in Biological Sciences (Transferred) Wayne State University Detroit, Michigan, USA 2014 – 2016 B.Sc. in Biological Sciences (Minored in Philosophy)
Honours and Awards:	CMHR Bone and Joint Institute Trainee 2017 – 2018 Wayne State University Dean's Honour List 2015 – 2016
Related Work Experience:	Teaching Assistant The University of Western Ontario 2017 – 2018 Research Assistant Children's Hospital of Michigan, Department of Neurosurgery Detroit, Michigan, USA 2016 – 2017

Publications:

1. **R. Arshad**, A. D. Price. Fabrication of Direct-Ink Write printed Col-PPy hybrid constructs. *In preparation*.

2. L.I. Grossman, N. Purandare, **R. Arshad**, S. Gladyck, M. Somayajulu, M. Hüttemann, and S. Aras. MNRR1, a bi-organellar regulator of mitochondria. *Oxidative Medicine and Cellular Longevity*, vol. 2017, pp., 2017.

3. M.C. Maroun, L.I. Grossman, **R. Arshad**, W.D.L̃ancaster, F. Fernández-Madrid. Mitochondrial Encoded Targets of Breast Cancer Anti-Mitochondrial Antibodies Implications of Mitochondrial Autoimmunity for Breast Cancer Progression. *Open J Biotechnol Bioeng Diagn.*, vol. 1 (1), pages 001 – 008, 2017.

Conference Presentations

1. **R. Arshad** and A.D. Price. Fabrication of novel 3D printed Collagen and Polypyrrole constructs for cell stimulation. *Canadian Bone and Joint Conference*, May 11, 2018. London, Ontario, Canada.

2. M.C. Maroun, L.I. Grossman, **R. Arshad**, F. Fáernndez-Madrid. Autoimmunity preferentially targets the RNA-protein synthesizing machinery in breast cancer. *10th International Congress of Autoimmunity*, April 10, 2016, Leipzig, Saxony, Germany.